Gene expression profiling and functional studies of astrocytes in SOD1-related amyotrophic lateral sclerosis

David Baker

Department of Neuroscience (SITraN)

Supervisors: Dr Janine Kirby, Dr Daniel Blackburn and Prof. Dame Pamela Shaw

PhD Thesis

Submitted March 2015

Abstract

Amyotrophic Lateral Sclerosis (ALS) is the most common adult onset motor neuron (MN) disorder, characterised by muscle wasting due to MN death. Astrocytes play an important role in disease progression in the $SOD1^{G93A}$ transgenic mouse model and patients of ALS. Although astrocytes display a selective toxicity to MN, the toxic factor(s) have not been identified. We hypothesise that differential gene expression in SOD1-ALS astrocytes will reveal targets for therapeutic intervention. Microarray analysis was performed upon Laser Capture Microdissected astrocytes isolated from spinal cord of symptomatic (90 day) and late-stage (120 day) $SOD1^{G93A}$ mice and non-transgenic (NTg) littermates, and from *post-mortem* human SOD1-ALS and control spinal cord. Functional studies were performed using enzymatic activity assays and immunohistochemistry upon spinal cord and *in vitro* validation studies were performed using murine neonatal cultures of astrocytes, microglia and embryonic MNs and "i-astrocytes" directly converted from human ALS fibroblasts. In murine astrocytes annotation clustering analysis showed increased expression of lysosomal transcripts which were validated by qPCR . Using functional experiments, we have found significantly higher activity of the lysosomal enzyme β-hexosamindase in the spinal cord of $SOD1^{G93A}$ mice. Immune response and phagocytic pathways are also enriched within both datasets, and phagocytosis assays using fluorescently labelled NSC34 cell debris show that $SOD1^{G93A}$ astrocytes engulf significantly higher amounts of neuronal debris compared to NTg controls, highlighting an increased reactivity of astrocytes at symptom onset. Human SOD1-astrocytes show down-regulation of transcripts involved in tight junction formation such as ZO-2, Claudin-5 and Occludin, and we hypothesise that ALS-astrocytes contribute to the breakdown in blood-brain-barrier (BBB) integrity seen in ALS. qPCR confirmed differential expression of BBB-influencing genes such as claudin-5, junctional adhesion molecule 2 and transforming growth factor beta-2. Model BBBs made with i-astrocytes from human patients co-cultured with endothelia show significantly lower transendothelial electrical resistance and dextran-permeability values pointing to an astrocyte role in increased BBB permeability during disease. These studies show the breadth of behaviours displayed by astrocytes during ALS disease progression and will provide an important guide for future therapeutic intervention.

Statement of contribution

All of the work in this thesis is my own apart from where stated.

Acknowledgments

First of all, I would like to thank my supervisors (who were numerous!): Dr Laura Ferraiuolo, Dr Daniel Blackburn, Dr Janine Kirby and Professor Pamela Shaw. Your help, along with many of the researchers and PIs present in SITraN, has been greatly appreciated, never less so than in the writing of this thesis. I would also like to thank Dr Brian Kaspar of Ohio State University for allowing me to work in his lab for 3 months of my PhD. It was a once in a lifetime experience and I am extremely grateful to the entire Kaspar lab for their continuing help and friendship.

I thank my parents and sister, who have always supported me in whatever I do, even if they do not understand what I am doing! It is no coincidence that I have managed to achieve a PhD after being brought up in such a loving and supportive environment.

Finally, and most importantly, I would like to thank my fiancée Nicole, who has been a crutch to me whenever I have needed, and has accepted my travel to America and endless hours spent in the lab and office writing my thesis. Thank you for keeping me grounded.

I only have two words left to say: never again.

Contents

List of Figures

List of Tables

Abbreviations

AbA cells	Aberrant astrocytes
ACM	Astrocyte conditioned medium
AD	Alzheimer's disease
ALDH1L1	Aldehyde dehydrogenase 1 like 1
ALS	Amyotrophic lateral sclerosis
ALSFRS-R	ALS functional rating scale –revised
ANLS	Astrocyte neuron lactate shuttle
BBB	Blood brain barrier
BDNF	Brain derived neurotrophic factor
BMDM	Bone marrow derived macrophage
BSCB	Blood spinal cord barrier
C9ORF72	Chromosome 9 open reading frame 72
cDNA	Complementary deoxyribonucleic acid
CNS	Central nervous system
CNTF	Ciliary neurotrophic factor
CSF	Cerebro-spinal fluid
DAVID	Database for annotation, visualisation and integrated discovery
DMEM	Dulbecco's modified eagles medium
DNA	Deoxyribonucleic acid
EAAT2	Excitatory amino acid transporter 2
ECS	Extracellular space
EB	Embryoid body
ER	Endoplasmic reticulum
ESC	Embryonic stem cell
fALS	Familial amyotrophic lateral sclerosis
FC	Fold change
FTD	Fronto-temporal dementia
GABA	Gamma aminobutyric acid
GCSF	Granulocyte colony stimulating factor
GDNF	Glial derived neurotrophic factor
GFAP	Glial fibrillary acidic protein
GFP	Green fluorescent protein
GLUR2	Metabotropic glutamate receptor 2
GO	Gene ontology
GRP	Glial restricted precursor
HBSS	Hanks balanced salt solution
HBSS-TD	Hanks balanced salt solution with trypsin and DNAse
HD	Huntington's disease
HUVEC	Human umbilical vein endothelial cell
iACM	i-astrocyte conditioned medium
IFNγ	Interferon gamma
IHC	Immunohistochemistry
IL	Interleukin
IκB	Inhibitor of kappa B
LCM	Laser capture microdissection
LPS	Lipopolysaccharide
MAC	Membrane attack complex
MAO-B	Monoamine Oxidase-B

MHC	Major histocompatibility complex
MEF	Mouse embryonic fibroblast
MMGMOS	Multi-chip modified gamma model for oligonucleotide signal
MOI	Multiplicity of infection
mSOD1	Mutant form of SOD1
NF-κB	Nuclear factor kappa B
NGF	Nerve growth Factor
NMJ	Neuromuscular junction
NMJ	Neuromuscular junction
NO	Nitric oxide
NRF2	Nuclear factor erythroid 2-related factor 2
NTg	Non-transgenic
NUSE	Normalised unscaled standard error
PAMP	Pathogen associated molecular pattern
PBS	Phosphate buffered saline
PCR	Polymerase chain reaction
PD	Parkinson's disease
PLS	Primary lateral sclerosis
PMA	Progressive muscular atrophy
QC	Quality control
qPCR	Quantitative polymerase chain reaction
RAGE	Receptor for advanced glycation products
RLE	Relative log expression
RNA	Ribonucleic acid
ROS	Reactive oxygen species
sALS	Sporadic amyotrophic lateral sclerosis
SMA	Spinal muscular atrophy
SOD1	Superoxide dismutase 1
TBS	Tris-buffered saline
TDP-43	TAR DNA-binding protein 43
TIMP	Tissue inhibitor of metalloproteinase
TLR	Toll-like receptor

CHAPTER 1

Introduction

1. Introduction

1.1 Motor neuron disease

Motor neurons are cells which convey electrical information from the motor cortex to the musculature to bring about movement. Motor neurons can be divided into upper and lower motor neurons, depending upon which part of the central nervous system (CNS) their cell bodies are contained within. In general, information regarding movement is sent along upper motor neurons which originate in the motor cortex, through the brainstem and into the spinal cord via the corticospinal tract. These neurons communicate with lower motor neurons which originate in the brainstem and the ventral horn of the spinal cord and project to the musculature.

Motor neuron disease encompasses a group of neurodegenerative conditions which feature a progressive loss of motor neurons leading to loss of muscular movement. Several conditions exist, dependent upon the site of onset and subsequent neurodegeneration (Al-Chalabi and Hardiman, 2013). For example, degeneration of upper motor neurons with unaffected lower motor neurons is termed primary lateral sclerosis (PLS); degeneration of lower motor neurons with unaffected upper motor neurons is termed progressive muscular atrophy (PMA) and degeneration of both upper and lower motor neurons is termed amyotrophic lateral sclerosis (ALS). These disorders exist on a spectrum whereby PLS and PMA exist at the extremes and ALS features differing proportions of upper and lower motor neuron involvement. Motor neuron disease also includes progressive bulbar palsy (a.k.a. bulbar ALS), which features degeneration of upper and/or lower motor neurons supplying the muscles responsible for speech and swallowing.

1.2 Amyotrophic lateral sclerosis

Amyotrophic lateral sclerosis was first described by Jean Martin Charcot in 1869 and is the most common of the motor neuron diseases (Cooper-Knock et al., 2013). The progressive loss of motor neurons and thus muscular movement leads to death, typically from respiratory muscle failure, within 2-3 years of symptom onset. ALS occurs in approximately 2 per 100,000 population with incidence enhanced by factors

such as: increasing age; gender (~1.5:1 male to female ratio); and genetic susceptibility – where ~5-10% of ALS cases are caused by genetic mutations (Table 1.1) (Al-Chalabi and Hardiman, 2013). ALS caused by these genetic mutations is termed familial ALS (fALS) whereas the remaining ~90-95% of ALS cases have no known family history and are known as sporadic ALS (sALS). sALS patients may also have mutations in some of the key causative genes, but their disease occurrence may also be due to environmental factors such as smoking, exercise and exposure to certain toxins (Al-Chalabi and Hardiman, 2013). Currently, the drug riluzole (trade name Rilutek) is the only treatment which exerts a neuroprotective effect in ALS, and extends life by 2-3 months on average (Miller et al., 2007).

ALS is classified using the El Escorial criteria (Brooks, 1994) which lay down the disease symptoms that are required, supportive, compatible or that rule out disease diagnosis (Ince et al., 1998a). For example, the required symptoms for ALS diagnosis are the presence of upper and lower motor neuron signs and evidence of disease progression. The El Escorial criteria have been updated since they were first established. For example the Awaji-Shima recommendations proposed a larger involvement of electrophysiology data in diagnosis, and have subsequently led to a more consistent set of patients entering clinical trials (Costa et al., 2012). ALS progression is measured using the revised ALS functional rating scale (ALSFRS-R) which consists of 12 questions regarding the regions of the body that might be affected by the disease (Rutkove, 2015). Although 2-3 years is the median survival of patients with ALS, the speed of disease progression is variable. Rapid progression is predicted by bulbar site of onset and asymmetrical (i.e. predominantly left or right-sided) degeneration with mixed upper and lower motor neuron involvement (Wijesekera et al., 2009). Other factors associated with rapid disease progression are: higher age of onset, short duration from first symptom to diagnosis and whether or not there is cognitive impairment (Al-Chalabi and Hardiman, 2013).

With reference to cognitive impairment, ALS is now known to exist on a spectrum with fronto-temporal dementia (FTD), with variable cognitive involvement depending upon the ALS subtype (Giordana et al., 2011). FTD is the second most common form of dementia after Alzheimer's disease (AD) leading to neuronal death in the frontal and

temporal lobes of the brain. FTD shares pathological features with ALS such as protein inclusions and also shares some of the same causative genes.

1.3 Genetic Subtypes of ALS

Although 90-95% of ALS cases have no known hereditary cause, mutations or expansions in several genes are now known to cause or increase vulnerability to ALS (Table 1.1). The first discovered gene which when mutated gave rise to ALS was the gene coding for Cu/Zn superoxide dismutase 1 (*SOD1*) (Rosen et al., 1993). The most common ALS-linked genes include *FUS* (Kwiatkowski et al., 2009, Vance et al., 2009) and *TARDBP* (Sreedharan et al., 2008) which encode proteins involved in RNA processing. In 2011, a non-coding expansion consisting of GGGGCC repeats in chromosome 9 open reading frame 72 (*C9ORF72)* was identified as accounting for up to 50% of fALS and a significant proportion of sALS (up to 8%) cases (Renton et al., 2011, DeJesus-Hernandez et al., 2011). The involvement of cognitive deficits is variable depending upon the genetic subtype of ALS, for example SOD1-ALS features nearly no involvement of FTD whereas C9ORF72-ALS cases feature up to 50% FTD involvement (Byrne et al., 2012).

Table 1.1 Major genes conferring susceptibility to ALS. FTD = fronto-temporal dementia. Data obtained from the ALSoD database (http://alsod.iop.kcl.ac.uk/)

ALS subtype	Gene affected	Gene symbol	Chromosomal locus	Proportion of fALS (approx.)	Reference
ALS1	superoxide dismutase 1	*SOD1*	21q22	20%	(Rosen et al., 1993)
ALS2	alsin	*ALS*	2q33	Rare	(Yang et al., 2001)
ALS3	Unknown		18q21		(Hand et al., 2002)
ALS4	senataxin	*SETX*	9q34	Rare	(Chen et al., 2004)
ALS5	spatacsin	*SPG11*	15q15-q21	Rare	(Orlacchio et al., 2010)
ALS6	fused in sarcoma	*FUS*	16p11.2	4%	(Kwiatkowski et al., 2009, Vance et al., 2009)
ALS7	Unknown		20-ptel-p13	Rare	(Sapp et al., 2003)
ALS8	vesicle associated membrane protein 2B	*VAPB*	20q13.3	<1%	(Nishimura et al., 2004)
ALS9	angiogenin	*ANG*	14q11.2	1%	(Greenway et al., 2006)
ALS10	TAR DNA binding protein	*TARDBP*	1p36.2	5%	(Sreedharan et al., 2008)
ALS11	Polyphosphoinositide phosphatase	*FIG4*	6q21	<1%	(Chow et al., 2009)
ALS12	optineurin	*OPTN*	10p13	<1%	(Maruyama et al., 2010)
ALS 13	ataxin 2	*ATXN2*	12q23-q24.1		(Elden et al., 2010)
ALS 14	valosin-containing protein	*VCP*	9p13		(Johnson et al., 2010)
ALS 15	ubiquilin 2	*UBQLN2*	Xp11.21		(Deng et al., 2011)
ALS 16	sigma non-opioid intracellular receptor 1	*SIGMAR1*	9p13		(Al-Saif et al., 2011)
ALS 17	chromatin modifying protein 2B	*CHMP2B*	3p12.1	<1%	(Skibinski et al., 2005, Cox et al., 2010)
ALS 18	profilin 1	*PFN1*	17p13.3		(Wu et al., 2012a)
ALS 19	v-erb-b2 avian erythroblastic leukemia viral oncogene homolog 4	*ERBB4*	2q33.3-q34		(Takahashi et al., 2013)
ALS 20	heterogeneous nuclear ribonucleoprotein A1	*HNRNPA1*	12q13.1		(Kim et al., 2013)
ALS 21	matrin 3	*MATR3*	5q31.2		(Johnson et al., 2014)
ALS-	chromosome 9 open reading frame 72	*C9ORF72*	9q21-22	40-50%	(Renton et al., 2011, DeJesus-Hernandez

ALS subtype	Gene affected	Gene symbol	Chromosomal locus	Proportion of fALS (approx.)	Reference
FTD1					et al., 2011)
ALS-FTD2	coiled-coil-helix-coiled-coil-helix domain containing 10	*CHCHD10*	22q11.23		(Bannwarth et al., 2014)

1.3.1 Superoxide dismutase 1

Superoxide dismutase 1 (*SOD1*), mutations in which are the cause of ~20% of familial ALS (fALS) (Rosen et al., 1993), was the first and is therefore the most well-characterised of the ALS-linked genes. Mutant SOD1 is widely used for transgenic animal models of the disease such as the $SOD1^{G93A}$ mouse (Gurney et al., 1994) and the $SOD1^{G93R}$ zebrafish (Ramesh et al., 2010). These models allow for detailed study of motor neurons and the surrounding glia during disease progression. At least 150 different mutations in *SOD1* are known to cause ALS, with all mutations being dominant apart from the N86S and D90A mutations which are also found to be recessive in Scandinavia (Turner and Talbot, 2008). Toxicity from mutant SOD1 is assumed to be through a toxic gain of function, rather than a loss of enzyme activity, as knockdown or inactivation of the enzyme does not result in motor neuron death (Reaume et al., 1996). In addition mutations that confer 100% disumutase activity such as G37R and those that confer no dismutase activity such as H46D/H48Q both lead to motor neuron loss (Wong et al., 1995, Wang et al., 2002). The dismutase-inactive mice also showed ubiquitinated inclusions in the spinal cord and aggregates containing high-molecular weight SOD1. This supports hypotheses that SOD1 misfolding and aggregation may play a role in ALS pathogenesis (Hart, 2006). However the motor neurons in SOD1 knockout mice are more sensitive to injury and SOD1 null mice also display increased amounts of denervation (Shefner et al., 1999), meaning that a loss of activity cannot be completely dismissed.

Interestingly, disease course is variable dependent upon the SOD1 mutation, with the A4V mutation (the most common in the U.S.A.) showing an aggressive disease course (Cudkowicz et al., 1997) whereas the D90A mutation (the most common in the world) shows a slow disease course (Andersen et al., 1995). Correspondingly, animal models based upon different SOD1 mutations show phenotypically different disease progressions (Lobsiger et al., 2007, Turner and Talbot, 2008, Pan et al., 2012). Nevertheless, these models have provided invaluable insights into the mechanisms that lead to motor neuron death during ALS. Finally, there is evidence to suggest that wild-type SOD1 is involved in non SOD1-ALS. The knockdown of wild-type SOD1 in astrocytes derived from sALS patients is protective to co-cultured neurons (Haidet-

Phillips et al., 2011), and misfolded SOD1 is seen in cases of familial ALS containing *TARDBP* and *FUS* mutations (Pokrishevsky et al., 2012).

1.3.1.1 Mouse models of ALS based upon mutations in SOD1

Mouse models containing mutations in *SOD1* have been the most common model of ALS since mutations in the gene were found to cause disease. Gurney et al. (1994) were the first to develop a mouse model of ALS based upon a glycine to alanine substitution at position 93 of SOD1. To date this has been the most used model within ALS, however models based upon other mutations in SOD1 also exist. Commonly used models include the $SOD1^{G37R}$ model, which has full dismutase activity and an aggressive disease course (Wong et al., 1995), and the $SOD1^{G85R}$ and $SOD1^{H46R}$ models which show no dismutase activity (Bruijn et al., 1997, Wang et al., 2002). Despite being the most common mutations amongst SOD1-ALS patients, the $SOD1^{A4V}$ and $SOD1^{D90A}$ models are rarely used relative to the aforementioned mutations. When initially developed $SOD1^{A4V}$ mice did not show a phenotype and conversion to an ALS-like phenotype only occurs when the $SOD1^{WT}$ is also expressed in mice, suggesting that there may be a toxic effect of $SOD1^{A4V}$ upon $SOD1^{WT}$ (Deng et al., 2006). The $SOD1^{D90A}$ mouse model leads to a late-onset disease at around 12 months (Jonsson et al., 2006), in comparison to the 3 month disease onset of the $SOD1^{G93A}$ model, making it less amenable for experimentation. However the less aggressive disease course in this model may better represent the human condition.

Although there are slight variations in disease onset and duration between models, this is representative of the heterogeneity in human SOD1-ALS already described, and all models display an ALS-like disease characterised by motor neuron degeneration and muscle wasting. These models have proven invaluable in the elucidation of the pathological mechanisms of ALS and the isolation of primary cells from these animals have allowed *in vitro* testing and drug-screening studies to be performed. Recent progress has been made in improving the consistency of disease onset and duration between $SOD1^{G93A}$ mice by inbreeding mice to remove background variability (Mead et al., 2011). This consistency in disease course means that fewer animals are now needed to model specific time points of disease.

1.4 Pathology of ALS

The pathology of ALS is complex and consists of several disease mechanisms, most of which are able to influence one another. The situation is made more unclear due to different mechanisms being more or less important dependent upon the subtype of ALS. In addition to motor neurons, other cell types in the CNS known collectively as glia play important roles in disease pathogenesis. Some of the key pathological features of ALS are given below.

1.4.1 ALS is a dying back axonopathy with impairment of axonal transport

Evidence suggests that motor neuron death in ALS first begins at the distal end, i.e. towards the synaptic end of the axon, rather than at the cell body. Motor neurons in the $SOD1^{G93A}$ mouse model of ALS show a loss of synapses at the neuromuscular junction (NMJ) before symptom onset (Frey et al., 2000). Further studies revealed that denervation of the NMJ and loss of axons from the ventral root precede loss of motor neuron cell bodies in $SOD1^{G93A}$ mice (Fischer et al., 2004). In addition to a loss of synapses at NMJs preceding motor neuron death, this innervation is selectively lost at sites of fast-twitch muscle fibre innervation relative to slow-twitch muscle fibres (Hegedus et al., 2007).

A contributing factor to the dying back aspect of neuronal death may be impairment in axonal transport. The so called “slow transport” of large structural components such as neurofilament proteins and cytoskeletal components is disrupted in mSOD1 mice long before symptomatic disease begins (Williamson and Cleveland, 1999) suggesting that axonal defects are an early part of the disease process. Real time i*n vivo* imaging of axonal transport of the C-terminal fragment of tetanus toxin has also shown deficits in transport beginning at the pre-symptomatic point of disease (Bilsland et al., 2010). Surprisingly, when *Legs at odd angles* (Loa) mice containing a mutation in the microtubule binding protein dynein were crossed with $SOD1^{G93A}$ mice, a significant improvement in retrograde axonal transport was observed, along with an increase in motor neuron survival (Kieran et al., 2005). This counter-intuitive finding may mean that mutant $SOD1^{G93A}$ mediates its effects through interference with axonal transport.

1.4.2 Inclusions

The majority of ALS cases are characterised by protein inclusions or aggregates occurring within the cytoplasm of both motor neurons and glial cells. The presence of ubiquitin within these inclusions is common (Leigh et al., 1988, Lowe et al., 1988) and ubiquitinated inclusions occur in different shapes such as compact inclusions or the more fibrous skein-like inclusions (Ince et al., 1998a). Ubiquitin is a small 8kDa protein which when added to other proteins targets them for degradation via the proteasome. In most genetic sub-types of ALS, the ubiquitinated protein within the inclusions is TAR-DNA binding protein 43 (TDP-43, endoded by the *TARDBP* gene) (Neumann et al., 2006), which normally resides within the nucleus and plays a role in RNA processing. Another protein, optineurin, is also a common constituent of ubiquitinated and TDP-43-containing inclusions in ALS (Maruyama et al., 2010).

Mislocalisation of TDP-43 from the nucleus to the cytoplasm and its presence in protein aggregates is seen in nearly all ALS sub-types but is not found in SOD1-related ALS, where TDP-43-negative ubiquitinated hyaline inclusions are seen (Mackenzie et al., 2007, Robertson et al., 2007). Additionally, ALS caused by mutations in SOD1 or FUS contain inclusions of SOD1 or FUS respectively (Bruijn et al., 1997, Kwiatkowski et al., 2009, Vance et al., 2009).

As well as inclusions containing these disease-linked proteins, the majority of ALS cases also contain inclusions known as bunina bodies. Bunina bodies are negative for TDP-43 and ubiquitin in most cases that have been examined, and to date only the lysosomal cysteine protease inhibitor cystatin C and and the iron transport protein transferrin have been identified as bunina body constituents (Okamoto et al., 2008). Finally, ALS cases may contain inclusions of neurofilament protein (Ince et al., 1998b), which may have detrimental effects on neuronal structural integrity. The presence of inclusions in different genetic subtypes of ALS highlights the heterogeneity of disease mechanisms that can lead to a common disease course. As a further indication that ALS and FTD occur on a spectrum of disease pathology, TDP-43 aggregation is also a hallmark of FTD (Arai et al., 2006).

1.4.3 Excitotoxicity

Glutamate is the excitatory neurotransmitter used by motor neurons of the CNS. A classic pathological mechanism in ALS is over-stimulation of motor neurons by glutamate, known as excitotoxicity. Glutamate may build up in the synaptic cleft through loss or altered expression of glutamate transport mechanisms or through excessive glutamate release (Van Den Bosch et al., 2006) (see section 1.5.2.1). The two key glutamate receptors present upon motor neurons are N-methyl-d-aspartate receptor (NMDAr) and the α-amino-3-hydroxy-5-methyl-4-isoxazole propionic acid receptor (AMPAr). Motor neurons are thought to be especially susceptible to excitotoxic damage due to the low level expression of the AMPAr subunit GluR2, which normally confers a high level of calcium impermeability (Williams et al., 1997). In addition, motor neurons contain relatively low levels of calcium binding proteins which may lead to a lower calcium buffering capacity (Ince et al., 1993). Thus, excess glutamate stimulation can lead to calcium influx and disruption of calcium homeostasis, disrupting many signalling pathways within the cell (Ferraiuolo et al., 2011b). The resulting influx of calcium leads to neuronal production of reactive oxygen species (ROS) from mitochondria and a feed-forward excitotoxic loop (Rao and Weiss, 2004). This interaction is also seen in other neurodegenerative diseases; Aβ, the major component of amyloid plaques in Alzheimer's disease, is seen to increase cellular ROS and decrease glycolysis, a driver of glutamate uptake (Schubert et al., 2009).

To compound the damage from excitotoxicity, motor neurons in mSOD1 mice have intrinsically increased excitability upon depolarisation (Meehan et al., 2010). Interestingly, motor neurons of $SOD1^{G93A}$ mice show an increased amount of inhibitory synapses relative to excitatory synapses, suggesting that these cells are trying to limit excitotoxic damage (Avossa et al., 2006). With relevance to ALS being a dying back axonopathy, excitotoxic stimulation of motor neurons in culture leads to distal axonal swelling, accumulation of neurofilament proteins and loss of axons, suggesting that excitotoxicity is a key driver of motor neuron loss (King et al., 2007).

1.4.4 Oxidative stress and reactive oxygen species (ROS)

Oxidative stress is caused by a build up of ROS within the cell. Sources of ROS can include the electron transport chain of mitochondria and ROS generation by reactive glial cells. Markers of oxidative stress are increased in patients with ALS; increased levels of 3-nitrotyrosine, a marker of peroxynitrite, is seen in the spinal cord and cerebrospinal fluid (CSF) (Beal et al., 1997, Tohgi et al., 1999). In addition, modification of proteins such as the astrocyte glutamate transporter EAAT2 by lipid peroxidation products is also seen (Pedersen et al., 1998), linking oxidative stress and excitotoxicity. Superoxide, nitric oxide, peroxynitrite, membrane lipid peroxidation and mitochondrial reactive oxygen species are all increased significantly over non-transgenic motor neurons in cultured murine $SOD1^{G93A}$ motor neurons (Kruman et al., 1999). ROS accumulation results in damage to mRNA (Chang et al., 2008), DNA (Fitzmaurice et al., 1996) and protein (Shaw et al., 1995, Ferrante et al., 1997). Among the mRNA species particularly affected by ROS are those involved in the electron transport chain, providing a link to the mitochondrial dysfunction also commonly seen in ALS (Wong et al., 1995, Wiedemann et al., 2002, Chang et al., 2008). To compound this further, the expression of nuclear erythroid factor 2-related factor 2 (Nrf2), a regulator of genes involved in the oxidative stress response, is reduced in murine $SOD1^{G93A}$ cells and human ALS tissue (Kirby et al., 2005, Sarlette et al., 2008).

Oxidative stress has received great attention due to the normal function of the SOD1 enzyme as a remover of ROS. However, as previously mentioned, mutations in *SOD1* that lead to inactivation of dismutase activity still result in motor neuron degeneration, suggesting oxidative stress may be a secondary effect. Nevertheless, mouse models based upon mutations in *TARDBP*, which encodes the TDP-43 protein that is the major component of inclusions seen in the majority of ALS cases, have also been demonstrated to show markers of oxidative stress such as increased lipid peroxidation and decreased mitochondrial membrane potential (Duan et al., 2010). Thus oxidative stress is a feature of several genetic sub-types of ALS rather than just SOD1-ALS.

1.4.5 Mitochondrial damage

Metabolic, and in particular mitochondrial, dysfunction is a key part of several neurodegenerative diseases including ALS. Mitochondria are the energy production machinery of the cell, but also play important roles in calcium buffering (linking mitochondrial stress and excitotoxicity) and apoptosis via the release of the pro-apoptotic factor cytochrome c (Duffy et al., 2011).

In ALS, mitochondrial degeneration and respiratory chain dysfunction is seen in human tissue and mutant SOD1 mouse models (Wiedemann et al., 2002, Wong et al., 1995). SOD1 is found associated with mitochondria *in vivo* (Higgins et al., 2002) and mutant SOD1 accumulates with high affinity at the outer mitochondrial membrane (Vande Velde et al., 2008). Mutant SOD1, but not $SOD1^{WT}$, binds to the anti-apoptotic protein Bcl2 within mitochondria of the spinal cord, potentially increasing the vulnerability of neurons to apoptosis (Pasinelli et al., 2004). Mutant SOD1 selectively associates with mitochondria within the spinal cord and not in tissues such as muscle, liver and brain, providing another reason for selective motor neuronal vulnerability relative to other cell-types (Liu et al., 2004).

Within neurons, mitochondria are highly motile, and move on microtubules along the neuronal axon (Ligon and Steward, 2000). In ALS, a breakdown in mitochondrial transport is observed, where there is a reduction in anterograde transport (away from the cell body) of mitochondria, leading to a lack of mitochondria in more distal parts of the axon (De Vos et al., 2007). Mitochondria are heavily concentrated at synapses to meet energy demands (Chang et al., 2006), thus the impaired trafficking of mitochondria could lead to faulty synaptic function and contribute to the dying back of motor neurons. Due to their role in many of the disease mechanisms already mentioned, mitochondria may be a good target for therapeutics. However, the small molecule drug olexisome, which previously extended survival in the $SOD1^{G93A}$ mouse (Bordet et al., 2007), failed phase III clinical trials in 2011, meaning that other therapeutic avenues will need to be explored.

1.4.6 Inflammation and immune response

An aberrant immune response and inflammation are recognised as key features of ALS and include immune cell infiltration (Henkel et al., 2004), increased levels of chemokines (Kuhle et al., 2009), increased complement activity (Grewal et al., 1999, Goldknopf et al., 2006) and glial activation (Sargsyan et al., 2005, Hensley et al., 2006)(see section 1.5). Whether these responses are beneficial or detrimental for motor neurons is not clear. Knockout of the pro-inflammatory cytokine IL-1β in $SOD1^{G93A}$ mice leads to increased survival time and decreased inflammation (Meissner et al., 2010), indicative of the negative role that inflammation can play. In contrast, the phagocytic activity of activated immune cells can clear debris allowing neuronal regeneration (Neumann et al., 2009). In further support of a beneficial role for inflammation, mice with a genetic background that leads to a slower, more benign disease course feature increased expression of immune transcripts in motor neurons (Nardo et al., 2013). Furthermore, knockdown of proliferating microglia, the immune cell of the CNS, using the thymidine kinase-ganciclovir system to conditionally ablate $Cd11b^{+}$ cells, does not affect motor neuron survival in $SOD1^{G93A}$ mice indicating that dysregulated immune and inflammatory responses may not be a prime cause of motor neuron death in ALS (Gowing et al., 2008).

1.4.7 RNA processing

Several ALS causing genes are involved in the processing of RNA or disrupt RNA processing during disease, including *TARDBP* (which encodes TDP-43)*, FUS,* and *C9ORF72*. TDP-43, the main component of the inclusions seen in ALS, is a heterogeneous nuclear ribonucleoprotein (hnRNP) containing RNA recognition motifs (Buratti and Baralle, 2001) and binds to over 4000 RNA targets including those involved in the synaptic function, RNA processing and neuronal development (Sephton et al., 2011). Similar to TDP-43, FUS contains an RNA binding motif and both mutated FUS and TDP-43 mislocalise to the cytoplasm instead of the nuclear localisation seen in control cases with wild-type TDP-43 and FUS (Kwiatkowski et al., 2009, Vance et al., 2009). Such mislocalisation would lead to dysregulated expression of many genes. In contrast to TDP-43 and FUS, which have direct roles in mRNA processing, intronic expansions within *C9ORF72* interfere with RNA species by direct binding and sequestration of RNA binding proteins within RNA foci (Walsh et al., 2014). This can result in abnormal splicing of the target mRNAs of these binding proteins. In addition, the presence of the C9ORF72 expansion upon one allele may lead to lower levels of functional C9ORF72 protein. The fact that TDP-43/FUS and C9ORF72 feature different mechanisms of disrupting normal RNA-processing increases its importance as a disease mechanism.

Spinal muscular atrophy (SMA), another motor neuron disorder, is caused by mutations in the *SMN1* gene (Lefebvre et al., 1995) which is involved in the construction of RNA processing proteins (Burghes and Beattie, 2009), again indicating that abnormal RNA processing is detrimental for motor neuron survival. Even, SOD1-ALS, which does not contain mislocalisation of TDP-43, features transcriptional repression as seen in the NSC34 motor neuron like cell line expressing $SOD1^{G93A}$ (Kirby et al., 2005) and in laser captured motor neurons from the late-stage $SOD1^{G93A}$ mouse (Ferraiuolo et al., 2007).

1.5 Non-cell autonomy in ALS

Not only do the above-mentioned pathological processes affect neurons, they also affect their glial neighbours. The CNS is comprised of multiple cell types, which can be subdivided into neurons and glia. Glia are by far the most numerous of these cells making up ~90% of human brain (He and Sun, 2007) and comprise three main cell-types: astrocytes, oligodendrocytes and microglia. Astrocytes and oligodendrocytes are derived from a neural progenitor population which is ectodermal in origin whereas microglia, the immune effector cells of the CNS, are derived from mesoderm and are thought to develop from peripheral macrophages (Kettenmann and Ransom, 2005).

The ALS disease process appears to affect all of the major cell types within the CNS, and all cells play a role in the eventual death of motor neurons. The process by which a diseased cell-type causes damage to another cell-type is termed non-cell autonomy. Non-cell autonomy is an important part of ALS, for example the expression of mutant SOD1 (mSOD1) in neurons alone is not sufficient for disease initiation (Pramatarova et al., 2001) suggesting that other CNS cells are essential for damage. It is now known that astrocytes, microglia and oligodendrocytes all play a role in motor neuron death and in multiple ALS pathogenic processes (Figure 1.1).

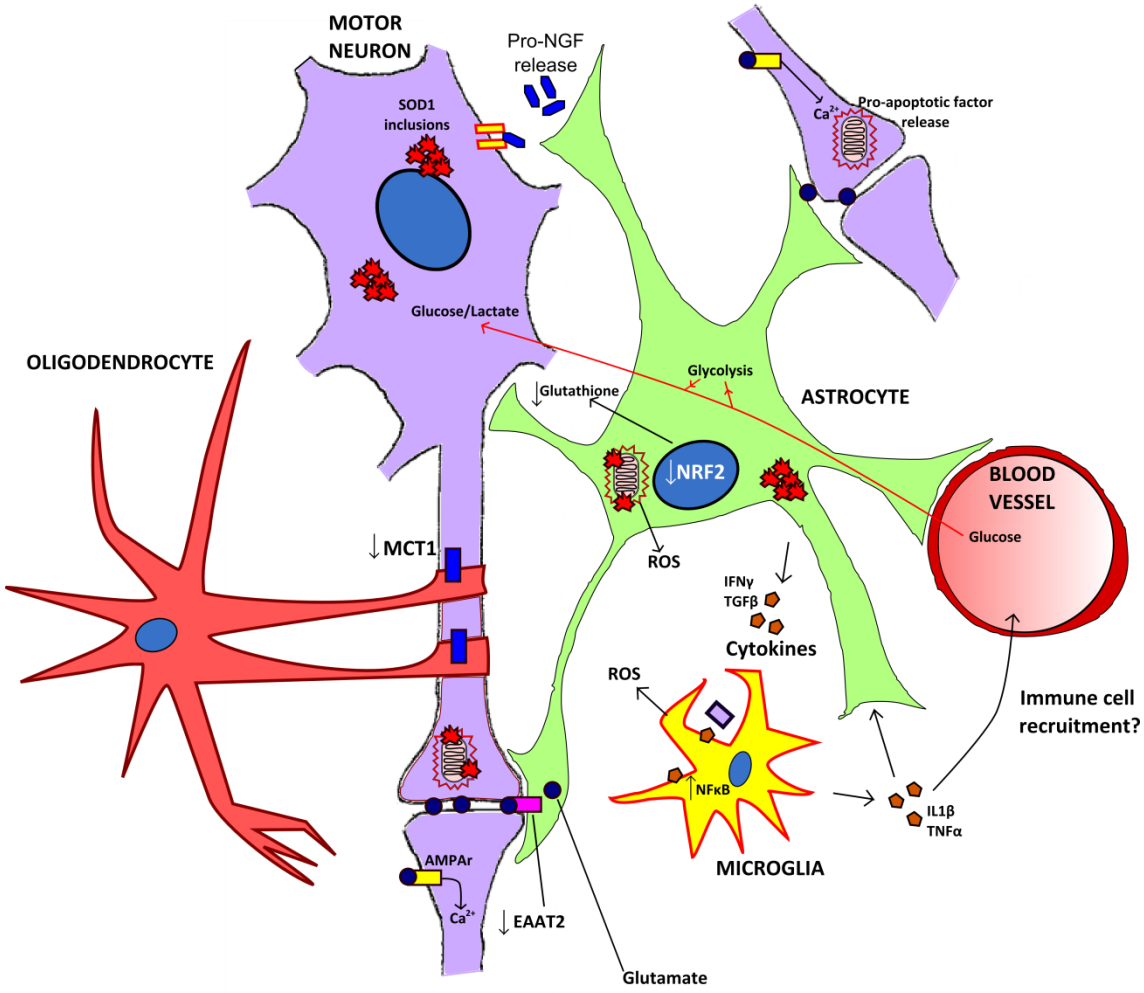

Figure 1.1 Key non-cell autonomous processes in SOD1-ALS. All glial cells undergo increased proliferation during disease progression. ROS are produced by dysfunctional mitochondria through mSOD1 association with the mitochondrial membrane. Normally, astrocytes respond to ROS by activation of the NRF2 transcription factor, its translocation to the nucleus, and subsequent transcription of antioxidant genes such as those involved in glutathione biosynthesis. However NRF2 is down-regulated in ALS. Astrocytes provide metabolic support to neurons through provision of glucose or lactate, the latter produced by glycolysis which may be affected by mitochondrial dysfunction. Glutamate is taken up by astrocytes from the extracellular space (ECS) and converted to glutamine for transport back to neurons (not shown). Astrocytic glutamate uptake through EAAT2 is fuelled by the aforementioned disrupted mitochondrial glycolysis, leading to lower glutamate uptake and increased glutamate concentrations in the ECS which cause excitotoxic damage via Ca2+ influx through ionotropic receptors. In ALS, EAAT2 expression is reduced, exacerbating excitotoxic damage. Microglial activation by mSOD1, heat shock proteins or other cellular breakdown products leads to secretion of TNF-α and IL1β and pro-inflammatory migroglial and astrocytic phenotypes. Oligodendrocytes lose the expression of MCT1, a lactate transporter important in providing metabolic support to the axon, and disruptions are seen in the myelin sheath.

1.5.1 Astrocytes

Astrocytes are the most abundant cell in the central nervous system (CNS) and fulfil diverse roles including: maintenance of neuronal homeostasis, metabolic support, regulation of synaptic plasticity, clearance of neurotransmitters from synapses, interaction with microglia, and protection of nervous tissue when injury occurs. Astrocytes are characterised by a ramified morphology with many fine processes essential for performing the many functions listed above. Astrocytes are characterised by expression of proteins such as glial fibrillary acidic protein (GFAP), the calcium binding protein S100b, the cell surface glycoprotein CD44, aldehyde dehydrogenase 1 family member L1 (ALDH1L1) and aquaporin 4 (AQP4), the expression of which varies according to astrocyte location and function. For over a decade, astrocytes have been regarded as part of "the tripartite synapse", playing an essential role in synaptic signalling along with the pre-synaptic and post-synaptic neuron (Araque et al., 1999). Astrocytes form vast gap-junction connected syncitial networks through which they can dissipate signals and metabolites, and are integral parts of the blood brain barrier (BBB) and blood-spinal-cord-barrier (BSCB) (Blackburn et al., 2009).

1.5.1.1 The provision and recycling of neurotransmitter

Of particular importance to motor neurons, which use glutamate as the main excitatory neurotransmitter, astrocytes are important in removal of glutamate from the synaptic cleft. The two main astrocyte glutamate transporters are excitatory amino acid transporter 1 (EAAT1, a.k.a. GLAST in mice and rats) and EAAT2 (a.k.a. GLT-1 in mice and rats) (Pines et al., 1992, Storck et al., 1992). When GLAST and GLT1 were knocked down in wild-type rats, a severe deficit was seen with an excess of extracellular glutamate whereas knock down of the neuronal glutamate transporter EAAC1 did not alter extracellular glutamate levels (Rothstein et al., 1996). The imported glutamate is converted within astrocytes to the precursor glutamine by the astrocyte-specific enzyme glutamine synthetase (Norenberg and Martinez-Hernandez, 1979). This glutamine is then safe to transport back to neurons without provoking excitation via glutamate receptors. Once inside the neuron, glutamine can be converted back to glutamate for use in neurotransmission (Bak et al., 2006). Astrocytes

are also involved in the recycling of the inhibitory neurotransmitter γ-aminobutyric acid (GABA), which is also derived from glutamine (Schousboe et al., 2004).

1.5.1.2 Provision of energy substrate to neurons

Perhaps the most important role of astrocytes is the provision of substrate to neurons for energy production. Since the suggestion that neurons use lactate generated through astrocytic glycolysis, termed the astrocyte-neuron lactate-shuttle (ANLS) (Pellerin and Magistretti, 1994), there has been considerable debate surrounding the preferred fuel source of neurons (Figure 1.2). Pellerin and Magistretti (1994) found that increased glutamate concentrations stimulated astrocytic Na^+/glutamate co-transport powered by aerobic glycolysis, demonstrated by increased lactate production by astrocytes *in vitro*. They hypothesised that this lactate could be utilised by neurons as an energy source through conversion to pyruvate and subsequent use in oxidative phosphorylation. This argument is not without controversy however; arguments against lactate as the preferential neuronal fuel source centre on findings that astrocytes are capable of higher rates and higher amounts of lactate uptake than neurons, whilst the opposite applies for glucose, and that modelling the ANLS requires using values not supported by the current literature (Simpson et al., 2007, Mangia et al., 2009).

There now exist two different hypotheses of neuronal glucose metabolism: the classical pathway and the ANLS (Figure 1.2). The classical pathway proposes glucose to be taken up from the blood stream either into astrocytes through the glucose transporter GLUT-1 or directly into neurons from the extracellular space (ECS) through a neuronal glucose transporter such as GLUT-3. Glucose is then used in respiration and the lactate by-product is transported from neurons into astrocytes via monocarboxylate transporters (MCT-2 on neurons and MCT1 and 4 on astrocytes) where it diffuses through the syncytial network to the bloodstream. Lactate may also be transported into the ECS where it diffuses along its concentration gradient to the bloodstream. In the ANLS, glucose is taken up from the blood into astrocytes where it is used in glycolysis, a process which also fuels uptake of glutamate from the synaptic cleft. The lactate by-product is then transported to neurons where it can be converted to pyruvate and used in oxidative phosphorylation. Note that in the ANLS, glucose and

lactate may also diffuse directly between the bloodstream and neurons, however this process is thought to be secondary to the ANLS (Pellerin et al., 2007).

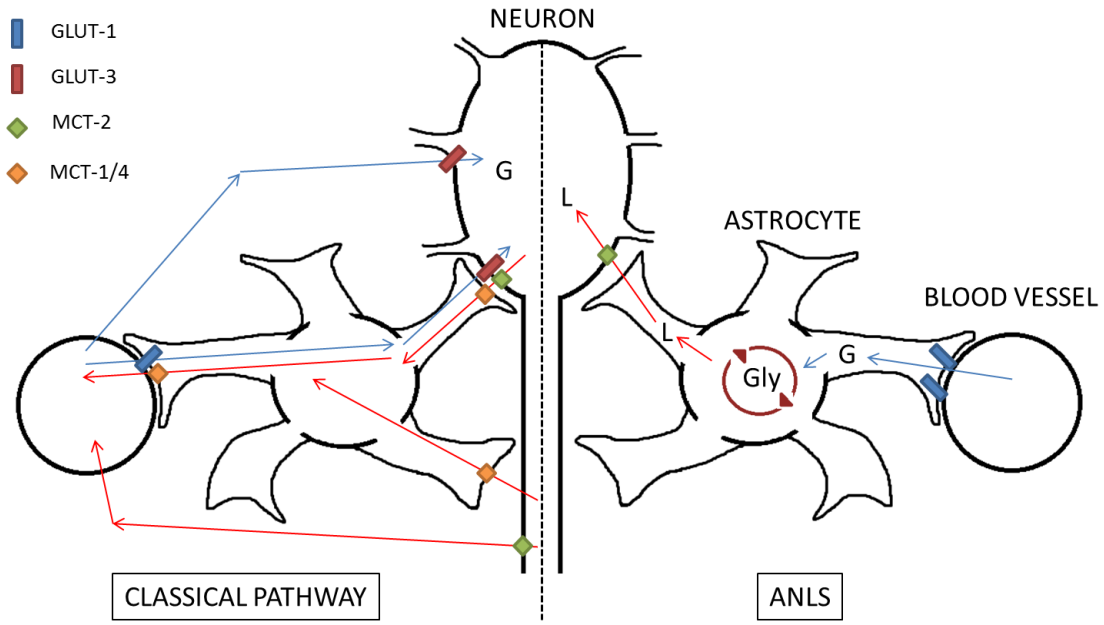

Figure 1.2 The two competing hypotheses of neuronal glucose metabolism. The classical pathway proposes glucose to diffuse directly from the blood stream to neurons and through astrocytes. Neuronal lactate is then taken up by the astrocytic lactate transporters MCT1/4. In the ANLS, glucose is first metabolised in astrocytes to lactate and transported into neurons via the neuronal lactate transporter MCT-2. Blue arrows: Glucose movement; Red arrows: lactate movement; G: Glucose; L: Lactate; Gly: Glycolysis.

1.5.1.3 Astrocytes are a key part of the blood brain barrier and blood spinal cord barrier

The BBB is the cellular network lining the brain microvasculature, consisting of an endothelial cell lining surrounded by a layer of extracellular matrix known as the basal lamina (which contains pericytes and smooth muscle cells) onto which astrocytic endfeet project (Abbott et al., 2006). In contrast to endothelial cells of the periphery, the endothelia of the BBB and BSCB are joined by tight junctions, such that diffusion of most substances takes place transcellularly (i.e. through the cells rather than between them). Much transport of substrates is performed through endothelial transport proteins and astrocytes have been shown to modulate transport capabilities of the

endothelial network e.g. through up-regulating the glucose transporter GLUT-1 on endothelial cells in response to glucose deprivation (Regina et al., 2001). Astrocytes are able to signal across the syncytial network by the propagation of calcium waves (Cornell-Bell et al., 1990) which could signal neuronal metabolic demands to endothelial cells with resultant increase in substrate transport (Abbott et al., 2006).

1.5.1.4 Heterogeneity of astrocytes in the CNS

The generalisation of astrocytes as one group of cells is much too simplistic, as these cells appear to be as functionally heterogeneous as neurons. Ramon y Cajal, who first described astrocytes, noted the different morphologies of these cells from different brain regions (Zhang and Barres, 2010). An obvious morphological difference is that seen between white matter (a.k.a. fibrous) and grey matter (a.k.a. protoplasmic) astrocytes, where white matter astrocytes have clearly defined processes with little branching and grey matter astrocytes possess many fine processes with multiple branch points (Matyash and Kettenmann, 2010). The most commonly used marker of astrocytes, GFAP, is highly expressed in white matter astrocytes but much less in those of the grey matter (Cahoy et al., 2008), and is usually associated with astrocytic activation.

The functional heterogeneity seen may reflect the different regions in which astrocytes develop. White matter astrocytes in the spinal cord show expression of different transcription factors based upon their location, perhaps reflecting their localisation with different neuronal subtypes (Hochstim et al., 2008). Oligodendrocyte transcription factor (OLIG2) is a transcription factor essential for oligodendrocyte and motor neuron development (Lu et al., 2002). In the P2 region of the developing spinal cord, the transcription factor T-Cell Acute Lymphocytic Leukemia 1 (TAL1 a.k.a. SCL) is required for the development of astrocytes rather than oligodendrocytes or interneurons via its repression of OLIG2 (Muroyama et al., 2005). However, *OLIG2* ablation only seems important for white matter astrocyte development but not for grey matter astrocytes (Cai et al., 2007), showing that astrocyte heterogeneity arises early in development.

Despite many similarities between astrocytes from rodents and humans, human astrocytes are much more complex and have been found to propagate calcium waves three times faster than those of the mouse (Han et al., 2013). Further, this study found that engraftment of human astrocytes into the mouse brain led to improved memory and learning when compared to non-engrafted mice. Thus it is important to bear in mind that human astrocytes may play more complex roles in disease processes than those of rodents.

1.5.2 Astrocytes in ALS

There is much evidence showing astrocytes to be affected by, and effectors of, the ALS disease process. Much of this information has come from the use of mutant SOD1 (mSOD1) mouse models. The mutant SOD1-containing inclusions seen within motor neurons in the $SOD1^{G85R}$ mouse are also present in astrocytes of the $SOD1^{G85R}$ mouse (Bruijn et al., 1997) and human cases (Forsberg et al., 2011). Neuron-specific expression of mSOD1 did not lead to motor neuron degeneration (Pramatarova et al., 2001). Similarly, expression of SOD^{G37R} in motor neurons and oligodendrocytes did not lead to disease onset in chimaeric mice (Yamanaka et al., 2008a). In addition, motor neurons of $SOD1^{G93A}$ mice do not up-regulate gene expression associated with cell death (Perrin et al., 2005) and if anything up-regulate genes involved in re-entry to the cell-cycle (Ferraiuolo et al., 2007), whereas motor neurons of human sALS cord do up-regulate cell-death genes (Jiang et al., 2005), leading to confusion as to whether death signals may come from other cell types. The generation of chimaeric mice featuring mSOD1 expression in select groups of cells has shown wild-type glia to improve viability of mSOD1 motor neurons (compared to mSOD1 glia) (Clement et al., 2003). Astrocyte-specific expression of mSOD1 does not cause motor neuron death (Gong et al., 2000). However, transplantation of $SOD1^{G93A}$ glial restricted precursors into healthy rat spinal cord induced death of nearby motor neurons (Papadeas et al., 2011). An astrocytic role in disease has been further clarified using Cre-lox knockdown of mSOD1 specifically in astrocytes in the $SOD1^{G37R}$ mouse model, which showed no effect upon disease onset, but a significant increase in survival time (Yamanaka et al., 2008b). In support of this, the knockdown of mutant SOD1 predominantly in astrocytes and motor neurons using adeno-associated virus 9 significantly increased lifespan in

SOD1^{G93A} and SOD1^{G37R} mice (Foust et al., 2013). In contrast to the study by Yamanaka et al (2008b) showing no astrocyte effect upon disease onset, knockdown of the SOD1^{G85R} mutation in astrocytes of the SOD1^{G85R} mouse did lead to a delay in both the onset and progression of disease (Wang et al., 2011). SOD1^{G37R} has full dismutase activity, whereas SOD1^{G85R} has no activity, and thus a different disease mechanism may be operating in this model. This further highlights the heterogeneity in SOD1-ALS mentioned previously (Section 1.3.1.1).

Data from *in vitro* experiments reinforce *in vivo* findings and highlight astrocytes as key players in the disease progression. Expression of mSOD1 *in vitro* in mouse primary motor neurons alone did not lead to significant differences in survival between non-transgenic and transgenic cells (Nagai et al., 2007). However, conditioned medium from astrocytes expressing mSOD1 was significantly more toxic to motor neurons than that from non-transgenic astrocytes, and was also significantly more toxic than that from transgenic microglia (Nagai et al., 2007). Additionally, treatment of motor neuronal precursors with conditioned medium from mSOD1-astrocytes had a significantly negative effect upon precursor proliferation and differentiation compared to wild-type, suggesting that disease-causing mutations cause detrimental effects at very early stages of life (Christou et al., 2013).

In addition to these conditioned medium experiments, astrocytes derived from murine SOD1^{G93A} embryonic stem cells (ESCs) are significantly more toxic to murine and human ESC derived motor neurons than astrocytes derived from wild-type SOD1 ESCs and the toxic effect is compounded when both cell types express SOD1^{G93A} (Di Giorgio et al., 2007, Di Giorgio et al., 2008). Astrocyte toxicity seems to be motor neuron specific, as human ESC-derived inter-neurons are not affected in co-culture with SOD1^{G93A} glia. Also, fibroblasts harbouring the SOD1^{G93A} mutation do not cause ESC-derived-motor neuron death (Di Giorgio et al., 2008). In the rat SOD1^{G93A} model, a highly proliferative and highly toxic aberrant astrocytic-phenotype is observed, which has lead to the description of AbA (for aberrant astrocyte) cells in this model (Diaz-Amarilla et al., 2011). In humans, Haidet-Phillips et al (2011) successfully differentiated neural progenitor cells from sALS and fALS patients into astrocytes, and showed these cells to be toxic to motor neurons *in vitro*. With reference to their role as metabolic

partners of motor neurons, astrocytes from pre-symptomatic $SOD1^{G93A}$ mice show reduced lactate provision for motor neurons and increased secretion of pro-NGF (nerve growth factor), the latter of which coincided with an increase in the pro-NGF receptor p75 on motor neurons and increased apoptosis. Replenishment of lactate and blockade of the p75 receptor led to complete rescue of motor neurons co-cultured with $SOD1^{G93A}$ astrocytes (Ferraiuolo et al., 2011a).

It is important to recognise that most work on the non-cell autonomous effect of astrocytes has been performed in SOD1-ALS. More recent studies using mutant TDP-43 models has cast doubt upon the role of non-cell autonomy in that particular subtype of ALS. Unlike SOD1-ALS models (Pramatarova et al., 2001), mutant TDP-43 expression in motor neurons alone is enough to lead to an ALS phenotype (Huang et al., 2012). Separate studies have found astrocytes to be toxic/non-toxic in *TARDBP*-related ALS. Haidet-Phillips et al (Haidet-Phillips et al., 2013) have found that glial restricted precursors (GRP) isolated from $TDP\text{-}43^{A315T}$ mice do not give rise to astrocytes that cause toxicity to motor neurons *in vitro*. When these $TDP\text{-}43^{A315T}$ GRPs were transplanted into the spinal cord of wild-type rats they did not cause motor neuron death, in contrast to GRPs derived from $SOD1^{G93A}$ mice (Papadeas et al., 2011).

In support of the studies by Haidet-Phillips et al. (2013) and Papdeas et al. (2011) , iPS derived TDP-43 astrocytes were not toxic to iPS derived motor neurons (WT or TDP-43) (Serio et al., 2013). Additionally, $SOD1^{G93A}$ astrocytes are known to be very toxic, and express the mutant transgene at a level of around 11-fold more activity compared to the 3-fold increase in expression seen by Haidet-Phillips et al. (Haidet-Phillips et al., 2013). Care must be taken in the analysis of GRP transplantation experiments before excluding mutant TDP-43 astrocytes as contributors to disease. The transplantation of GRPs will only lead to a small proportion of astrocytes in the spinal cord possessing the mutant gene, and previous studies have shown wild-type glia to be neuroprotective (Clement et al., 2003). In addition, the inability of astrocytes to cause disease on their own does not mean that they are not involved in the disease progression. Indeed Huang et al. (2012) showed that mutant TDP-43 expression in motor neurons alone produced an ALS phenotype, with profound astrocytic and microglial activation. Furthermore, expression of mutant TDP-43 or FUS in motor neurons alone has been

found to induce the expression of lipocalin 2 in astrocytes, which acts as a toxic factor (Bi et al., 2013). Finally, Tong et al. (Tong et al., 2013) did see MN degeneration in models with TDP-43^{M337V} expression solely in astrocytes, indicating that further work in this area is needed. Finally, fibroblasts from C9ORF72-ALS and sALS patients that are directly converted to astrocytes are toxic to co-cultured motor neurons *in vitro* (Meyer et al., 2013), indicating that astrocyte toxicity is common mechanism amongst ALS genetic sub-types.

1.5.2.1 Astrocytes are key players in excitotoxicity and oxidative stress in ALS

The contribution of oxidative stress and glutamate excitotoxicity and the interconnectivity between these processes is a key feature of astrocytes in ALS. Under normal homeostatic conditions, glutamate is co-transported from the synaptic cleft into astrocytes with Na^+ and H^+ (in exchange for K^+) through the glutamate transporters EAAT1 and EAAT2 (Bak et al., 2006). Astrocytic glutamate uptake is an energy intensive process often occurring far away from the cell body; the glutamate transporter GLT-1 has recently been demonstrated to co-localise with mitochondria and glycolytic enzymes in astrocyte processes (Genda et al., 2011), a process which requires co-culture with neurons *in vitro* (Ugbode et al., 2014). Astrocytes are able to influence glutamatergic activity by the release of ATP which acts to inhibit neurotransmission (Zhang et al., 2003). In ALS, mSOD1 associates with the mitochondrial membrane causing disruption of mitochondrial energy metabolism and increased ROS in SOD1^{G93A} astrocytes (Mattiazzi et al., 2002, Cassina et al., 2008), which would therefore lead to lower ATP production and exacerbation of excitotoxic damage.

To compound the vulnerability of motor neurons to glutamate through their lack of the GluR2 subunit, the expression of the glutamate transporter EAAT2 is reduced in astrocytes during ALS (Howland et al., 2002). Thus a key glutamate removal mechanism is lost. In rat models, astrocytes modulate neuronal GluR2 subunit expression via a secreted protein factor, whilst in the same study rats transgenic for SOD1^{G93A} were shown to have reduced GluR2 expression (Van Damme et al., 2007). The authors conclude that astrocytes protect against excitotoxicity both by glutamate uptake and modulation of GluR2 protein levels and that this protection is lost during

ALS. Crossing of SOD1^{G93A} mice with mice over-expressing *EAAT2* (a.k.a. *GLT1*) improved the motor outcomes but did not significantly delay disease onset or progression in these mice, suggesting that excitotoxicity is not the main mechanism in disease progression (Guo et al., 2003). In contrast, the astrocyte glutamate transporter GLT1 was increased in expression upon β-lactam treatment in SOD1^{G93A} mice and this correlated with significant increases in motor neuron survival and overall survival time (Rothstein et al., 2005). This difference may be due to timing, where treatment in the study by Rothstein et al. (Rothstein et al., 2005) was started at disease onset rather than over-expression operating from birth. In support of the importance of glial modulation of excitotoxicity, GRPs injected into the spinal cord of SOD1^{G93A} rats differentiated into astrocytes with retention of GLT-1 at end stage disease which led to decreased motor neuron loss (Lepore et al., 2008), emphasising the importance of astrocyte glutamate uptake for neuronal health. In addition, Riluzole, which is thought to mediate some of its protective effects through protection against excitotoxic damage, increases the expression of GLT-1 upon astrocytes *in vitro* (Carbone et al., 2012).

Excitotoxicity, oxidative stress and mitochondrial damage are intimately linked in SOD1-ALS. ROS, produced through processes such as mitochondrial oxidative phosphorylation, inflammation or through mSOD1 itself, leads to decreased expression of astrocytic glutamate transporters and a build up of glutamate in the synaptic cleft (Bush, 2002, Valentine and Hart, 2003). The toxicity of astrocytes towards motor neurons may be mediated through ROS; reduced oxygen consumption in astrocytic mitochondria, as shown in SOD1^{G93A} rat astrocytes (Cassina et al., 2008), leads to enhanced ROS production. Murine SOD1^{G93A} astrocytes have also been seen to cause defects in mitochondria of wild-type motor neurons when co-cultured (Bilsland et al., 2008). In keeping with their role in the inflammatory response (Section 1.5.2.2), astrocytes have been found to increase expression of iNOS and neuronal NOS (nNOS) during neurodegeneration (Almer et al., 1999, Sasaki et al., 2000, Anneser et al., 2001), resulting in increased amounts of nitric oxide stress to neurons.

Astrocytes are able to withstand higher amounts of oxidative stress than neurons. The nuclear factor erythroid 2-related factor 2 (NRF2) transcription factor has a major role

in the protective response to oxidative stress; astrocytes have much higher levels of Nrf2 induction than neurons upon oxidative insult in a mouse model (Kraft et al., 2004). In a $SOD1^{G93A}$ related cellular model of ALS, the down-regulation of Nrf2 and glucose-6-phosphate dehydrogenase expression in the NSC34 neural cell line lead to weakened defences against oxidative stress (Kirby et al., 2005). Further, NRF2 expression in motor neurons is reduced in post-mortem tissue of ALS patients compared to controls (Sarlette et al., 2008). Astrocytes are an attractive target to compensate for this neuronal NRF2 reduction; activation of NRF2 with fibroblast growth factor-1 (FGF-1), thought to be released upon motor neuron damage, leads to increased production of haem oxygenase-1 (HO1) in astrocytes and increased motor neuron survival in co-culture (Vargas et al., 2005). Astrocytes also produce more antioxidant glutathione upon activation of the NRF2 pathway which protects neurons from glutamate-induced toxicity (Shih et al., 2003). Neurons are incapable of glutathione uptake, therefore glutathione is metabolised to cysteine in the extracellular space (ECS) and taken up by neurons for neuronal glutathione synthesis (Dringen, 2000). Recently, NRF2 has been shown to regulate the expression of the EAAT3 transporter on neurons, responsible for increased cysteine uptake and subsequent glutathione synthesis upon stimulation by ROS (Escartin et al., 2011). Thus, NRF2 activation during oxidative stress leads to increased astrocytic glutathione secretion, increased cysteine levels in the ECS, and corresponding increased levels of neuronal EAAT3 to take up cysteine for neuronal glutathione synthesis and protection. This protective mechanism is lost during ALS progression.

1.5.2.2 Astrocyte-mediated inflammation in CNS injury and ALS

In contrast to acute or sub-acute CNS injury, ALS involves a much slower activation of astrocytes and the role of inflammation is less well established. Nevertheless, inflammation is a key feature of ALS progression, involving glial and immune cell proliferation, release of ROS and pro-inflammatory cytokines and induction of cell death. Injury to the CNS induces reactive astrogliosis, an increase in astrocyte proliferation and migration around the site of injury, which in acute injury cases may form a glial scar (Sofroniew, 2009). Astrogliosis may be preceded by de-differentiation to an earlier developmental stage, as seen in stab injury to the neocortex (Buffo et al.,

2008). The increased astrocytic presence serves to form a tight separation between the damaged and healthy tissue, but the consequence of this is scar tissue which is inhibitory to axonal regrowth (see Fawcett and Asher (1999)). However, knock down of reactive astrogliosis leads to increased leakiness of the BBB, greater migration of systemic inflammatory cells and more neuronal death (Faulkner et al., 2004). This demonstrates a positive role of inflammation and highlights the complexities that will be faced in controlling the inflammatory response.

Astrogliosis, precedes behavioural defects in mice transgenic for mutant TDP-43 (Swarup et al., 2011). Recent experiments using mice transgenic for both TDP-43 and GFAP-luciferase (to allow *in vivo* imaging of astrogliosis) showed higher astrocytic expression of pro-inflammatory cytokines (transgenic vs. control) when stimulated with bacterial LPS *in vitro*, and found evidence for interaction between TDP-43 and p65 resulting in amplified inflammatory responses (Swarup et al., 2011). Furthermore, the use of a super-inhibitor of the NF-κB complex led to decreased astrogliosis and motor neuron death in mutant TDP-43 transgenic mice (Swarup et al., 2011). IFNγ production by astrocytes increases with disease stage in $SOD1^{G93A}$ mice and induces motor neuron cell death (Aebischer et al., 2011), and increased TGFβ signalling is concurrent with astrogliosis, however TGFβ may act as a protective mechanism (Phatnani et al., 2013).

A master regulator of inflammatory gene expression, NF-κB, plays a key role in the up-regulation of 35-60% of tested pro-inflammatory genes in fALS and sALS-astrocytes compared to non-diseased controls (Haidet-Phillips et al., 2011). In contrast to these findings, astrocyte-specific knockdown of NF-κB has been shown not to affect disease initiation and progression in a $SOD1^{G93A}$ mouse model of ALS (Crosio et al., 2011, Frakes et al., 2014). However, ALS is a non-cell autonomous process, therefore NF-κB activation in other cells may supply the required pro-inflammatory factors, and the aforementioned study by Haidet-Phillips *et al.* (2011) found only 35-60% of pro-inflammatory genes to be influenced by NF-κB, which implies a level of redundancy is present in the inflammatory response.

1.5.2.3 Toxicity or loss of support?

A key question regarding astrocytes in ALS is whether they are toxic to motor neurons or whether motor neurons die due to a loss of astrocyte support. Given the evidence described in the previous sections, it seems that a combination of both factors is most likely. In terms of toxicity, astrocytes secrete lipocalin 2 (Bi et al., 2013), increased amounts of nitric oxide (Anneser et al., 2001) and pro-inflammatory cytokines (Haidet-Phillips et al., 2011). At the same time, there is down-regulation of astrocytic glutamate transporters leading to excitotoxicity (Howland et al., 2002), and a lower amount of lactate provision by astrocytes to neurons for energy production (Ferraiuolo et al., 2011a). Given that the latter study saw this lactate deficit at the pre-symptomatic stage, perhaps loss of support is an early feature which follows through to a toxic phenotype as the disease progresses. Indeed, if supportive factors such as IGF1 or GNDF are delivered pre-symptomatically to $SOD1^{G93A}$ mice there is a significant delay in disease onset (Kaspar et al., 2003).

1.5.3 Microglia

The macrophages of the CNS are called microglia, which differ from archetypal macrophages in appearance and behaviour; being extremely sessile and possessing a ramified morphology at rest (Stollg and Jander, 1999). Nevertheless microglia are highly immune competent and possess multiple immune receptors such as toll-like receptors (TLR) 1-9 and receptors for pathogen associated molecular patterns (PAMPs) (Xavier et al., 2014). They produce multiple different cytokines and up-regulate MHC II expression in response to TLR ligation (Olson and Miller, 2004), and secrete increased amounts of superoxide upon activation (Colton and Gilbert, 1987). Lastly, microglia are capable phagocytes involved in the clearance of cell debris and dying cells (Raff et al., 1979). Microglia are in a constant state of surveillance with each cell moving and covering a certain area and as such, are dominant at sites of acute CNS injury (Kigerl et al., 2009).

As with macrophages of the peripheral immune system, microglia exist on a spectrum of activation. Classical activation of macrophages occurs in the presence of pro-inflammatory factors such as bacterial lipopolysaccharide (LPS) or interferon-γ (IFNγ) secreted in a typical Th1-type immune response (Schroder et al., 2004). This pro-

inflammatory activation state is characterised by antigen presentation, high expression of the transcription factor IRF5, increased nitric oxide production, and a cytokine expression profile consisting of high amounts of Interleukin (IL)-12 and IL-23 and low amounts of IL-10 (Mantovani et al., 2004, Krausgruber et al., 2011). In contrast to this pro-inflammatory state, macrophages also exist in an alternatively activated phenotype, induced by Th2-type cytokines such as IL-4 (Stein et al., 1992). Alternatively activated macrophages are characterised as immunosuppressive and involved in tissue repair and secrete high amounts of IL-10 and IL-1 receptor antagonist (IL1RA) (Mosser, 2003). These two ends of the macrophage activation spectrum have been designated M1 for classically activated macrophages and M2 for alternatively activated macrophages (Mosser, 2003). Initial differentiation into M1 or M2 cells can be stimulated by granulocyte-macrophage colony stimulating factor (GM-CSF) or macrophage colony stimulating factor (M-CSF) respectively (Gordon and Martinez, 2010). IFNγ then primes classically activated (M1) macrophages (Mosser, 2003) whilst interleukin 4 (IL4) and interleukin 13 (IL13) prime the alternatively activated phenotype (Stein et al., 1992). This binary categorisation of macrophages is overly simplistic, for instance another population of macrophages is seen to develop in response to IgG-opsonised cells and classical activation signals that induces a Th2-type humoral immune response (Anderson and Mosser, 2002). M2 macrophages can therefore be subdivided into: M2a, which develop in response to IL-4 and IL-13; M2b, an IL-10 high, IL-12 low expressing cell-type that develops in response to FCγ receptor ligation and activation of toll-like receptors or Interleukin-1 receptors (Sutterwala et al., 1997, Sutterwala et al., 1998); and M2c cells that develop in response to IL-10 (Mantovani et al., 2004). Central to the two ends of the activation spectrum are IRF5, a transcription factor which polarises towards the M1 phenotype (Krausgruber et al., 2011), and Krüppel like factor 4 (KLF4) which in combination with STAT6 regulates polarisation toward an M2 phenotype and is important in the repression of pro-inflammatory genes (Liao et al., 2011). The inflammatory gene suppression by KLF4 is postulated to occur through competition for p300 and PCAF, which are co-activators of NFκB (Liao et al., 2011).

1.5.4 Microglia in ALS

Similar to astrocytes, microglial proliferation (microgliosis) is a hallmark of ALS from the symptomatic stage onwards (Alexianu et al., 2001). mRNA transcripts for markers of microglia are significantly increased over controls and there is increased levels of the chemoattractant MCP-1 in ALS spinal cord (Henkel et al., 2004, Henkel et al., 2006). Microgliosis per se may not lead to motor neuron death. As previously mentioned in section 1.4.6, depletion of proliferating microglia did not affect motor neuron degeneration even though it did affect number of activated cells in $SOD1^{G93A}$ mice (Gowing et al., 2008).

Microglia transition between activation states during ALS. Levels of pro-inflammatory cytokines such as TNFα were increased in the $SOD1^{G93A}$ spinal cord with disease progression and treatment of a microglial cell line with these cytokines *in vitro* led to increased levels of nitrite production (Hensley et al., 2003). Treatment of microglial cells with mutant SOD1 (mSOD1) leads to M1 polarisation, through interaction with toll-like receptors 2 and 4 and CD14, and subsequent toxicity towards motor neurons when placed in co-culture (Zhao et al., 2010). Interestingly mSOD1 treatment of motor neurons in the absence of microglia does not lead to cell death, suggesting that the mutant protein is not toxic to motor neurons in isolation. The PU.1 knockout mouse, which lacks B and T cells and cells of the myeloid lineage such as macrophages and microglia, has shown that mSOD1 prompts neurons to signal to microglia and induce a toxic phenotype. When $PU.1^{-/-}$ and $SOD1^{G93A}$ mice were crossed to produce $SOD1^{G93A}/PU.1^{-/-}$ mice and were then given bone marrow transplants, wild type bone marrow led to significantly increased survival time over $SOD1^{G93A}$ bone marrow (Beers et al., 2006). In this study, injection of $SOD1^{G93A}$ bone marrow into the singly transgenic $PU.1^{-/-}$ strain did not lead to motor neuron death, therefore it was only when $SOD1^{G93A}$ was present in all cells that $SOD1^{G93A}$ microglia became toxic, suggesting a neuronal signal is the cause of microglial activation in this disease (Beers et al., 2006).

In keeping with a toxic role of mSOD1-expressing microglia in disease, knockout of mSOD1 specifically in microglia significantly extends survival of $SOD1^{G37R}$ mice but does not affect onset (Boillee et al., 2006). This is concordant with the aforementioned study which performed the same knockout in astrocytes (Yamanaka et al., 2008b).

With further similarity to the studies performed upon astrocytes, knockdown of $SOD1^{G85R}$ in microglia alone did significantly affect both onset and survival, again showing the importance of disease mutation (Wang et al., 2009). Meissner (2010) show that mutant SOD1 treatment of microglia leads to caspase 1 and IL1β activation. The knockout of caspase 1 or IL1β leads to increased survival time in $SOD1^{G93A}$ mice. Non-transgenic microglia are neuroprotective when transplanted into $SOD1^{G93A}$ animals lacking any endogenous microglia (Beers et al., 2006). Finally, the proinflammatory transcription factor NF-κB increases with disease progression in the $SOD1^{G93A}$ mouse and knock-down of NF-κB in microglia but not astrocytes ameliorates inflammatory damage and extends survival in $SOD1^{G93A}$ mice (Frakes et al., 2014).

In contrast to M1 polarisation, M2 microglia are thought to be neuroprotective. M2 microglia promote differentiation of oligodendrocyte precursor cells and subsequent remyelination following damage to the corpus callosum (Miron et al., 2013). Miron et al (2013) also found M2 microglia to decrease with age in mice, a factor that might explain the positive correlation between age and neurodegenerative diseases. In the $SOD1^{G93A}$ model of ALS, M2 microglia are most abundant at disease onset whereas at end-stage disease markers of the M1 phenotype dominate (Liao et al., 2012). An increased amount of M2 microglia in cervical vs. Lumbar spine may contribute to the decreased pathology seen in cervical spine in early disease (Beers et al., 2011).

Microglia can also be supplemented by macrophages derived from the bone marrow in the periphery; Lewis et al (2009) found that CX_3-CR1 macrophages labelled with GFP were present in the CNS of the mSOD1 mouse model of ALS. Similarly, Butovsky et al. (2012) found that peripheral monocytes had a pro-inflammatory phenotype prior to disease onset and that these cells infiltrated the spinal cord as the disease progressed. In contrast to the above studies, a recent study by Chiu et al (2013) in which flow cytometry was used to characterise cell populations present in the spinal cord of the $SOD1^{G93A}$ mouse at different time-points suggests that microglia in the CNS are not supplemented by peripheral macrophages. In addition, a dual RNA-sequencing and microarray approach was used to show that microglia in the CNS of the $SOD1^{G93A}$ mouse have a distinct activation profile from the classic M1 and M2 datasets. This profile is characterised by increased expression of neurotrophic genes such as *Igf1* but

also of neurotoxic genes such as *Nox2*. However, the comparisons made by Chiu et al (2013) were drawn between ALS microglia and LPS-treated RAW 264.7 macrophages (the M1 dataset) and IL-4 stimulated human bone marrow derived macrophages (the M2 dataset). Such singular stimuli would produce large-scale and highly polarised gene expression changes which would not reflect the multitude of factors acting upon a microglial cell during ALS progression. Thus, there may still be a subtle skewing of ALS-microglia toward the M1 or M2 end of the spectrum during disease progression. Nikodemova (2013) show decreased expression of both M1 and M2 markers with disease progression, perhaps showing a decreased reactivity of the cells for either phenotype.

The separation into "bad" M1 cells and "good" M2 cells is not so clear cut and is dependent upon the disease concerned. In experimental autoimmune encephalitis (EAE), a model of the neuroinflammatory disease multiple sclerosis, injection with IL-4 conditioned bone-marrow-derived macrophages (BMDM) (Vaknin et al., 2011) or IL-10 and IL-13 activated peripheral blood monocytes (Mikita et al., 2011) ameliorated symptoms whereas injection of the $SOD1^{G93A}$ mouse with IL-4-conditioned BMDMs from an early disease stage led to an acceleration of the disease which was not seen with IFNγ-conditioned BMDMs (Vaknin et al., 2011).

1.5.4.1 Astrocytes and microglia are partners in inflammation

Given the similarity of astrocytes and microglia in their response and toxicity during ALS progression, it is not surprising that they act in a synergistic way during inflammatory events. In the previously mentioned study by Yamanaka et al. (2008b) astrocyte-specific knockdown mSOD1 in a mouse model reduced microgliosis and microglial production of nitric oxide but did not affect astrogliosis (Yamanaka et al., 2008a), suggesting that microglial activation by astrocytes is due to dysregulated communication between astrocytes and microglia rather than just increased astrocyte proliferation. In the non-diseased state, astrocytes synthesise the inhibitory neurotransmitter γ-aminobutyric acid (GABA), which reduces microglial activation during inflammatory cues (Lee et al., 2011).

Microglia are also able to signal to astrocytes; treatment of $SOD1^{G93A}$ mice with granulocyte colony stimulating factor (GCSF) decreased both micro- and astrogliosis despite astrocytes being deficient in the GCSF receptor (Pollari et al., 2011). Microglial TNFα release was decreased in this study, suggesting TNFα as a microglial signal for astrocyte activation. Indeed, TNFα can hyper-stimulate $SOD1^{G93A}$ astrocytes leading to increased production of pro-apoptotic factors such as caspase-8 and pro-inflammatory prostaglandin E2 (Hensley et al., 2006).

In line with this large amount of glial crosstalk, astrocytes express a multitude of receptors for different cytokines. Increased expression of the IFNγ receptor has been suggested for multiple neurodegenerative diseases and conditioned media from IFNγ treated astrocytes is toxic to neuronal cell lines (Hashioka et al., 2009). Increased astrocytic expression of Toll-like receptor 4 (TLR4) and the receptor for advanced glycation products (RAGE) in human sALS post-mortem tissue supports the inflammatory role that these cells play in human disease (Casula et al., 2011). These findings contradict earlier results from Lenhardt *et al.* (2002, 2008), which showed TLR-4 to be expressed exclusively upon microglia and not astrocytes, and which interestingly found TLR-4 to be bound by a heat shock protein (HSP60) (Lehnardt et al., 2008), which have also been found to induce inflammatory factor production by astrocytes in Alzheimer's Disease (Bruinsma et al., 2011). These inconsistent findings for glial TLR-4 expression may be due to the use of different tissue types; non-diseased rat cells were used *in vitro* by Lehnardt *et al.* whilst human post-mortem sALS tissue was used by Casula *et al.* This suggests that during the disease process astrocytes, perhaps through de-differentiation, can express markers more typical of microglia such as TLR-4 leading to amplification of a local neurogenic inflammatory state. There is also evidence that microglia start to express markers more typical of astrocytes during disease progression in the $SOD1^{G93A}$ rat (Trias et al., 2013), though this may be a feature of the highly aggressive disease course in this model.

Despite the focus upon the harmful inflammatory reaction during neurodegeneration, glial inflammation has a positive effect at least in the initial stages of disease. Phase III trials of minocycline, an inhibitor of proinflammatory enzymes and microglial activation which has previously proven beneficial in the MPTP mouse model of

Parkinson's Disease (Du et al., 2001, Investigators, 2006), led to worse scores on the ALS functional rating scale than placebo (Gordon et al., 2007). Similarly, $SOD1^{G93A}$ rats receiving transplants of glial restricted precursors plus minocycline treatment showed reduced microgliosis but an initial deterioration in motor function (Papadeas et al., 2011). Welser-Alves *et al.* (2011) have recently found microglial stimulation with lipopolysaccharide (LPS) to induce tissue inhibitor of metalloproteinase-1 (TIMP-1) expression in astrocytes through an IL-1β dependent manner, and microglia are also important in clearance of cellular debris for subsequent regeneration (Neumann et al., 2009).

1.5.5 Oligodendrocytes

In addition to astrocytes and microglia, oligodendrocytes are the third glial cell-type that plays a role in ALS. Oligodendrocytes are important in the CNS as they produce the myelin which ensheathes the axonal compartment of neurons and allows fast saltatory conduction of nerve signals. Due to their close contact with long axons, these cells are also vital for metabolic support of the axon (Philips and Rothstein, 2014). NG2 cells, also known as oligodendrocyte precursor cells (OPCs), are abundant cells in the CNS that were originally thought to give rise to neurons, astrocytes and oligodendrocytes (Nishiyama et al., 2009). It has been suggested that NG2 cells specifically give rise to oligodendrocytes in the CNS (Kang et al., 2010). However, NG2 cells in cerebellar slices express GFAP, suggesting that they are also capable of differentiating into astrocytes *in vivo* (Leoni et al., 2009). NG2 cells may play a role at the synapse as they have been seen to receive synaptic inputs (Bergles et al., 2000), and are now considered a cell-type in their own right (Trotter et al., 2010).

1.5.5.1 Oligodendrocytes in ALS

In comparison to astrocytes and microglia there is relatively little data on the role of oligodendrocytes and their precursors in ALS. The main role of these cells, myelin production, appears compromised during disease progression. Myelin sheathes of axons show progressive disorganisation and loss from the symptomatic stage onwards in the $SOD1^{G93A}$ rat (Niebroj-Dobosz et al., 2007). In ALS patients, there is significantly less myelin in the motor cortex and ventral horn of the spinal cord at end-stage (Kang et al., 2013). In addition to myelin loss, TDP-43, the major constituent of protein

aggregates in ALS, localises with cells of oligodendrocyte morphology in cases of FTD (Neumann et al., 2007) and ALS (Philips et al., 2013), which may impair oligodendrocyte function.

During disease progression in the $SOD1^{G93A}$ mouse the proliferation of OPCs significantly increases with most new oligodendrocytes produced in the ventral horn grey matter, the site of motor neuron degeneration (Magnus et al., 2008, Philips et al., 2013, Kang et al., 2013). Despite this increased production of OPCs, the number of oligodendrocytes in the spinal cord of these mice at end-stage is not increased, suggesting that oligodendrocyte death is also a feature of the disease process. As with astrocytes and microglia, mutant SOD1 has been selectively excised from oligodendrocytes in the $SOD1^{G37R}$ mouse. Excision of $SOD1^{G37R}$ led to a significant delay in the onset of disease and a significantly increased lifespan, however disease progression appears to be unaffected (Kang et al., 2013).

Recently, it has been suggested that oligodendrocytes affect neuron survival in ALS through perturbed lactate provision (Lee et al., 2012). MCT1 (a.k.a. SLC16A1), a lactate transporter highly expressed by oligodendrocytes is lost from the motor cortex of human ALS tissue and progressively from the ventral horn of symptomatic $SOD1^{G93A}$ mice (Philips et al., 2013, Lee et al., 2012). Furthermore, MCT1 expression is increased upon knockout of $SOD1^{G37R}$ solely in oligodendrocytes (Kang et al., 2013).

1.5.6 The involvement of other cell types in ALS

Although motor neurons and the three main forms of glia described above are key players in ALS pathogenesis, other cell types in the CNS and peripheral nervous and immune systems are also affected and involved. Due to ALS featuring a dying back phenomenon of motor neurons from the neuromuscular junction to the cell body, skeletal muscle cells could be a site of neurotoxicity. However, deletion of mSOD1 from skeletal muscle tissue of $SOD1^{G37R}$ mice does not affect the disease onset or progression and increasing the muscle mass also does not improve motor symptoms (Miller et al., 2006). Similarly, endothelia of the blood brain barrier (BBB) also have a very close association with astrocytes and neurons in the CNS, and the BBB is seen to breakdown during disease progression in the $SOD1^{G93A}$ mouse (Zhong et al., 2008,

Miyazaki et al., 2011) and ALS patients (Leonardi et al., 1984, Winkler et al., 2013). As with muscle cells, selective depletion of $SOD1^{G37R}$ within endothelia did not affect disease onset or survival in $SOD1^{G37R}$ mice (Zhong et al., 2009). In addition to endothelial cells, another important cell at the BBB, pericytes, are significantly reduced in ALS subjects versus controls, so perhaps this also leads to BBB disruption (Winkler et al., 2013). Lastly, another study featuring knockdown of mSOD1 within Schwann cells, the myelinating cells of the peripheral nervous system (PNS), actually led to a more aggressive disease course with accelerated disease progression (Lobsiger et al., 2009). Therefore a blanket approach targeting all cell types may not prove effective in ALS.

In addition to cells located within the central and peripheral nervous systems, cells of the peripheral immune system are also involved in ALS pathogenesis. T-helper cells and T-cytotoxic cells are present in the ventral horns of patients with ALS (Engelhardt et al., 1993). Evidence suggests that T-cells are important modulators of astrocyte and microglial behaviour. Crossing of $SOD1^{G93A}$ mice with mice deficient in T helper cells leads to a faster disease progression (Beers et al., 2008). Surprisingly, astro- and microgliosis is decreased in these animals whilst transcript levels of the inflammatory cytokines TNFα and NOX2 are increased. This phenotype was rescued by a bone marrow transplant from wild-type mice which restored functional T-cells. Support for this neuroprotective role of T-cells comes from Chiu et al (2008) who found that $CD4^+$ and $CD8^+$ T-cells infiltrated the spinal cord during disease progression and promoted a neuroprotective phenotype in microglia. When crossed with a T-cell deficient mouse strain, $SOD1^{G93A}$ mice showed decreased amounts of microgliosis but microglia had also lost their neuroprotective phenotype (Chiu et al., 2008). The type of T-cell is important for disease progression. As with M1 and M2 microglia, T-helper cells can be divided into pro-inflammatory Th1 cells and anti-inflammatory Th2 cells. In the $SOD1^{G93A}$ mouse motor symptoms first occur in the hindlimbs rather than the forelimbs, due to more intense motor neuron death in the lumbar versus cervical cord. There is greater expression of neurotrophic factors such as BDNF and GDNF and anti-inflammatory cytokines in the cervical cord of these mice coupled to a greater expression of Th2 genes compared to the lumbar cord where Th1 genes dominate (Beers et al., 2011). Another class of T-cell, T-regulatory cells (T-regs), suppress the

expression of microglial NOX2 and ROS to a greater extent than cytotoxic T-effector (Teff) cells, through the secretion of anti-inflammatory cytokines IL-4, IL10 and TGFβ (Zhao et al., 2012). T-regs are reduced in the peripheral blood of patients with rapidly progressing ALS compared to slow progressing and non-ALS controls (Henkel et al., 2013). Treatment of peripheral T-cells may hold promise for disease progression. Activation of Natural Killer T-cells with a ligand that promotes an anti-inflammatory phenotype led to an extension in survival of $SOD1^{G93A}$ mice and an increase of T-cells within the spinal cord, again providing evidence of the beneficial effects of T-cells (Finkelstein et al., 2011).

1.6 Gene expression profiling identifies dysregulated pathways in ALS

As discussed, much is already known regarding the pathogenic mechanisms operating in ALS and the effect that astrocytic manipulation can have. From these broader disease concepts gene expression profiling using microarray technology has been used to delineate specific pathways that may serve as therapeutic targets.

1.6.1 Microarray technology

Microarray is a powerful tool for analysing the expression of thousands of genes at the same time. In essence, many thousands of probes are fixed to a solid surface and bind to complementary cDNA or cRNA targets within a sample. Fluorescent labelling of the target allows quantification and thus estimation of gene expression (Allison et al., 2006). The use of photolithography for production of microarray chips was pioneered in 1991 (Fodor et al., 1991), and proof that gene expression measurements could be multiplexed came using a slightly different method involving the attachment of 48 cDNA probes to a glass slide to identify differential gene expression in *Arabidopsis thaliana* (Schena et al., 1995). Today, microarray technology allows comparisons based upon factors such as disease status, treatment status, transgene expression and time series data (Gresham et al., 2008).

Two main types of microarray platform exist: cDNA microarrays and oligonucleotide microarrays such as those produced by Affymetrix, the latter of which are now the major microarray platform. In cDNA microarrays, cDNA probes are attached to the support surface and are then used to probe a sample containing cDNA species,

produced by reverse transcription of sample mRNA. In oligonucleotide arrays, probes are designed from genomic sequences and used to interrogate a sample of complementary RNA (cRNA). On Affymetrix oligonucleotide microarrays, there is a 25-nucleotide probe which perfectly matches the target mRNA species which sits next to a probe which is identical apart from the 13^{th} nucleotide. This second probe acts as a mismatch probe to control for non-specific binding. Sample mRNA is first reverse transcribed to cDNA using primers containing a T7 promoter sequence. T7 polymerase then binds to these sites and reverse transcribes the cDNA into cRNA whilst also incorporating a biotin label. This biotinylated cRNA is then fragmented so as to allow more efficient binding to probes and is then hybridised to the probes on the array. The arrays are washed to remove unbound cRNA, and a streptavidin-phycoerythrin stain is then used to visualise the bound biotinylated cRNA on the arrays and allow quantification of gene expression (Figure 1.3).

In general, cDNA microarrays are conducted using a two-colour method and oligonucleotide microarrays by a one-colour method. In the two colour method the two samples to be compared are reverse-transcribed in the presence of different dyes, which are incorporated into the cDNA product. Equal amounts of both samples are then hybridised onto the same microarray and the fluorescence read. If a gene has a higher expression in one condition over another then its corresponding dye will dominate at that probe position, however if a gene is equally expressed in both conditions then the dyes will merge to give a different colour (e.g. red and green to give yellow). In the single colour method samples from each condition are kept separate and are hybridised onto different arrays. The expression level on each chip is then calculated using internal standards and these levels compared between conditions. Both methods have shown consistency in the results they produce (Patterson et al., 2006).

1.6.2 Chip manufacture

For oligonucleotide arrays such as those produced by Affymetrix, microarray chips are synthesised using a process called photolithography. In this process a solid support such as a glass slide or a nylon membrane is coated with photolabile protection groups (Fodor et al., 1991). Light is then shone through a mask such that only specific areas of

the support lose protection. Nucleotides are added to the support and only adhere where this protection has been removed. These nucleotides also contain photolabile protection groups meaning that subsequent nucleotide addition can only occur if the protection group is removed by light. The successive use of different masks results in the targeting of desired nucleotides to desired locations on the array (Fodor et al., 1991). This method allows the synthesis of thousands of 25-nucleotide long probes, each specific to a region of a target mRNA.

1.6.3 Competing technologies

Microarrays have developed beyond simply being able to measure gene expression and are now able to measure the abundance of different splice-forms of a gene by probing different exons within an mRNA (Affymetrix, 2005). Such exon arrays have been found to produce results in keeping with conventional IVT arrays in analysis of stimulated T cells, with the added benefit of information regarding alternative transcript abundance (Whistler et al., 2010).

Another development in the field of large-scale gene expression profiling is next generation sequencing (NGS). Using this technique, the whole transcriptome of a cell can be sequenced giving information on expression level, transcript variants, single nucleotide polymorphisms etc. The process works by fragmenting the starting sample into small fragments of 90 base pairs (in the Illumina system) which then bind to a flow cell. The fragments are sequenced one base at a time using a PCR method and fluorescent nucleotides and are then joined back into continuous sequences using computer software (Mardis, 2008). The technique is expensive relative to microarray technologies and also requires a lot of computing power, such that data analysis can take days at a time.

1.6.4 Application to ALS

Microarray analysis in ALS first focused upon whole tissue homogenates from the motor cortex and spinal cord. In homogenates from patient spinal cord the analysis of ~6800 genes identified increased expression of pro-inflammatory transcripts and dysregulated expression of mitochondrial transcripts and transcripts involved in excitotoxicity (Dangond et al., 2004). In another study of whole spinal cord from ALS

patients, increased lysosomal enzyme and cholesterol transport transcript expression was seen (Offen et al., 2009), with common gene expression between ALS patients and $SOD1^{G93A}$ mice. Microarray analysis of whole tissue from the motor cortex of ALS patients shows an increased expression of immune transcripts and impairment of ion homeostasis and glycolysis (Lederer et al., 2007).

These initial experiments, though providing valuable information, did not identify cell specific gene expression and therefore the contribution of different cell-types to disease. To tackle this problem, microarray analysis was performed upon the NSC34 neuronal cell line transfected with human $SOD1^{G93A}$ (Kirby et al., 2005). $SOD1^{G93A}$ dysregulated the antioxidant response of NSC34 cells, with Nrf2, the master regulator of anti-oxidant gene expression, down-regulated by 3.14 fold in comparison to cells transfected by vector only (Kirby et al., 2005). Other studies have focused upon isolation of primary cell-types from the mSOD1 mouse model. Vargas et al. (2008b) cultured astrocytes from neonatal $SOD1^{G93A}$ rats and performed gene expression profiling, showing a phenotype with decreased trophic support. However the time spent in culture may mean that gene expression profiling of *in vitro* astrocytes does not accurately reflect the *in vivo* situation (Blackburn, 2010).

Another method of analysing the gene expression of a specific cell type is to identify and remove it from tissue *post mortem*. Several microarray studies in ALS have utilised the laser capture microdissection (LCM) technique. LCM is a technique in which a laser is fired through a thermo-reactive film onto a tissue section. Consequently, the film adheres to the tissue in the targeted region, which can then be removed. The combination of this technique with immunohistochemistry allows the identification and capture of specific cell types, and is as close as possible at capturing the gene expression profile of a cell *in vivo*. This technique has been successfully used to capture motor neurons from: sALS spinal cord for use on conventional microarrays (Jiang et al., 2005); sALS spinal cord for use on exon-level arrays which identified aberrant splicing in sALS versus control motor neurons (Rabin et al., 2010); and SOD1-ALS human spinal cord motor neurons (Kirby et al., 2011). In this latter study, the PI3K/PTEN pathway was identified as altered in a direction favouring cell survival in those motor neurons which had survived the disease course. PTEN knockdown led to increased survival in

NSC34 and primary motor neurons expressing $SOD1^{G93A}$ in *in vitro* validation studies (Kirby et al., 2011).

LCM has allowed longitudinal studies to be performed using the mSOD1 mouse model, allowing gene expression to be characterised at different stages of the disease. Laser capture microdissected motor neurons from the $SOD1^{G93A}$ mouse model at pre-symptomatic (~60 day), symptomatic (~90 day) and late-stage (~120 day) has been performed (Ferraiuolo et al., 2007). In this analysis: pre-symptomatic motor neurons showed an up-regulation of genes involved in transcription and translation, carbohydrate metabolism and mitochondrial respiratory chain components; symptomatic motor neurons showed a dysregulated expression of transcription, signalling and cell cycle activity genes; and late-stage motor neurons showed dysregulated expression of immune response, axonal transport genes, a repression of transcription, and up-regulation of genes encoding proteins involved in the cell cycle (Ferraiuolo et al., 2007). This correlates with the laser captured motor neuron microarray data from human SOD1-linked ALS cases in which transcriptional repression was identified (Kirby et al., 2011).

In addition to motor neurons, LCM-microarray studies are now being performed upon astrocytes and have revealed a key role for astrocytes in metabolic homeostasis in early disease. A reduction in lactate provision is seen in pre-symptomatic $SOD1^{G93A}$ astrocytes (Ferraiuolo et al., 2011a), which when re-supplied exogenously leads to motor neuron rescue. This provides an example of the power of microarray to identify therapeutic targets. In a different approach, de Oliveira et al. (2013) performed microarray of whole tissue from two pre-symptomatic time points and then confirmed whether genes were differentially expressed in astrocytes using subsequent LCM and qPCR.

Again, it is important to remember the heterogeneity of ALS; mutations in several other genes cause ALS through apparently different pathological mechanisms to SOD1 and this is evident in gene expression data. For example, expression analysis of human motor neurons from patients with a mutation in *CHMP2B* (charged multivesicular protein 2B) showed perturbations in MAPK and calcium signalling and also in

autophagic activity (Cox et al., 2010), whilst mice with a deletion in the hypoxia response element in the promoter of *VEGF,* which causes an ALS-like disorder, display differential expression of genes involved in cholesterol metabolism as well as nervous system development (Brockington et al., 2010).

Further investigation of microarray data using functional *in vitro* and *in vivo* studies is now common. The field of gene therapy offers an opportunity to correct the dysregulated gene expression seen in microarray studies. Gene therapy has already proved effective in treatment of the $SOD1^{G93A}$ mouse. For example, viral delivery of *IGF-1* has been shown to be protective in the $SOD1^{G93A}$ mouse (Kaspar et al., 2003) and delivery of short hairpin RNA to knock down *SOD1* expression has been performed by Foust et al. (2013). Certain viral sub-types, such as adeno-associated virus 9 (AAV9), preferentially target astrocytes and neurons (Foust et al., 2009), making the modulation of neuronal and astrocyte gene expression a reality.

1.7 Summary of the current situation

Astrocytes play a fundamental part in almost every aspect of neuronal health. The oxidative stress, excitotoxic and inflammatory reactions that occur during ALS are mediated by complex interactions between astrocytes, microglia and neurons and there is promise that modification of these cells' behaviour may modulate the disease course.

As previously mentioned, riluzole, a drug which counteracts glutamate excitotoxicity, is the only approved drug for ALS and extends life by approximately three months on average (Miller et al., 2007). This demonstrates the significance of excitotoxicity, a process which astrocytes are a key part of, in disease progression. A major problem in finding effective therapeutic strategies for the treatment of ALS is the multifaceted and non-cell autonomous disease process (Figure 1.2). In addition to inflammation, metabolic support, oxidative stress and excitotoxicity, disruptions in processes such as ion regulation and neurogenesis also occur. All of these processes are heavily interconnected such that the targeting of one element may not ameliorate disease progression. Knockdown of mSOD1 in multiple different cell types of mSOD1 transgenic mice shows a differential contribution of each cell type to the onset and the

duration of disease progression, thus understanding the contributions of each affected cell type is also important for therapeutic intervention.

The definitive mechanism that starts the ALS disease process remains elusive. This highlights a major obstacle in the study of ALS in that the long time-course of disease means that many homeostatic functions are dysregulated by the time symptoms appear. In ALS, genetic mutations in fALS patients allow causal links to be established, however for the remaining ~90% of sALS patients pinpointing the cause of disease remains difficult. Due to the complexity of the disease process a top-down approach is needed so that interactions between different disease mechanisms can be identified. This approach can then be used to study the specific changes that occur in astrocytes during ALS and how these affect their interaction with motor neurons. Work with animal models is vital, allowing different time-points of disease and specific cell types to be investigated. The development of a $SOD1^{G93A}$ mouse model which has a highly consistent disease course (Mead et al., 2011) has allowed for the separation of the disease course into pre-symptomatic (60 day), symptomatic (90 day) and late-stage (120 day) disease. This robust disease model gives strength to microarray studies of the various time-points, and has already led to the previously mentioned important findings at the pre-symptomatic time point (Ferraiuolo et al., 2011a).

1.8 Hypothesis and aims

Astrocytes have been laser-capture microdissected and RNA extracted from symptomatic and late-stage time points of the $SOD1^{G93A}$ mouse and non-transgenic controls. Microarray has been performed, however these data are still to be analysed. This analysis will investigate astrocyte behaviour throughout the disease time-course and also compare toxicity and loss of support as potential astrocyte-mediated disease mechanisms in ALS. Importantly as stated earlier, although the $SOD1^{G93A}$ mouse-model recapitulates the human pathology, differences are still observed between murine and human SOD1-ALS. In addition, human astrocytes have greater complexity than mouse astrocytes. Thus, it is important to conduct similar studies of human astrocytes. Therefore, human SOD1-ALS patient and healthy control astrocytes will be laser capture microdissected *post-mortem* and microarray analysis performed. This will create the first microarray analysis of human astrocytes in SOD1-ALS.

Two hypotheses will be tested by this project.

1.8.1 Microarray of astrocytes from the $SOD1^{G93A}$ mouse model

The hypothesis tested in this part of the project will be:

Astrocytes in symptomatic and late-stage $SOD1^{G93A}$ transgenic mice possess dysregulated gene expression that reveals the contribution of astrocytes to motor neuron death throughout the disease course.

The initial aims of this project are as follows:

1. To conduct an analysis of microarray data from symptomatic and late-stage $SOD1^{G93A}$ astrocytes isolated from murine spinal cord by LCM.
2. To conduct validation studies to investigate pathways discovered through microarray analysis.
3. To evaluate how the symptomatic and late-stage microarray data fits in with data obtained from pre-symptomatic $SOD1^{G93A}$ astrocytes so as to build a picture of the role of astrocytes over the course of the disease.

1.8.2 Microarray of astrocytes from SOD1-ALS human subjects

The hypothesis of this part of the project is:

Astrocytes in SOD1-ALS human subjects possess dysregulated gene expression that reveals the contribution of astrocytes to motor neuron death.

The aims of this part of the project are as follows:

1. To isolate astrocytes from human spinal cord of SOD1-ALS subjects and controls by LCM for use in microarray analysis.
2. To conduct an analysis of microarray data from isolated astrocytes.
3. To conduct validation studies to investigate pathways discovered through microarray analysis.
4. To evaluate how the data from human SOD1-ALS cases compares to that seen in microarray analysis of $SOD1^{G93A}$ astrocytes.

CHAPTER 2

Materials and methods

2 Materials and methods

2.1 Materials

The SOD1^{G93A} mouse model, staining, laser capture microdissection (LCM) and microarray analysis were performed as in Ferraiuolo et al. (2011a) and are summarised below.

2.1.1 SOD1^{G93A} transgenic mouse model

Mice used were male high copy number B6SJL-Tg (SOD1^{G93A}) 1 Gur/J, which had been backcrossed onto C57Bl/6 J Ola/Hsd (Harlan) for over 20 generations, and their non-transgenic littermates. All procedures were performed according to UK Home Office regulations. Symptomatic and late-stage mice were euthanised by Dr Laura Ferraiuolo by intraperitoneal injection of Pentobarbital (supplied by University veterinary services) and transcardially perfused with PBS containing 30% sucrose. The CNS was removed and snap-frozen in liquid nitrogen, and then stored at -80˚C. Subsequent staining and LCM of symptomatic and late-stage astrocytes performed by Mr Paulius Viskaitis and Dr Dilraj Sokhi respectively.

For primary motor neuron culture, embryos of C57Bl/6 J Ola/Hsd (Harlan) mice were used at gestational day 13.

2.1.2 Cases for human microarray study

Cases for the microarray analysis of human SOD1-astrocytes and controls were obtained from the Sheffield MND Brain Tissue Bank and according to local research ethics committee (LREC) regulations and were stored as frozen blocks at -80˚C (Table 2.1).

2.1.3 Chemicals and reagents

General reagents were sourced from either Fisher Scientific or Sigma unless otherwise stated. Plastics for tissue culture were obtained from Sigma unless otherwise stated.

Table 2.1 Details of the human cases and controls from which astrocytes were obtained. Mutations are described based upon the recommendations of the Human Genome Variation Society (www.hgvs.org). sALS = sporadic-ALS.

ID	Disease status	Mutation	Disease duration (months)	Date of death	Post mortem interval	Age (death)	Gender	Reason for death
Tissue for human array studies								
2JK4	Control				24	80	Female	Pulmonary embolism
2JK3	Control				25	71	Male	Burst aortic aneurysm
2JK7	Control				24	54	Female	Ovarian cancer
135.34	Control				24	89	Female	Unknown
2JK10	Control				12	82	Male	Pulmonary fibrosis
20/07	Control				32	77	Male	Lobar pneumonia
34/92	SOD1-ALS	p.E101G	41		23	40	Female	ALS
37/04	SOD1-ALS	p.I114T	13		27	60	Female	ALS
49/94	SOD1-ALS	p.I114T	14		50	66	Female	ALS
Cells for tissue culture studies								
155	Control							
AG	Control							
170	Control							
210	SOD1-ALS	p.D77Y						
295	SOD1-ALS	p.D91A						
009	sALS	Unknown						

2.2 Methods

2.2.1 Gene expression profiling of murine SOD1^{G93A} astrocytes

2.2.1.1 Rapid staining procedure of murine astrocytes

Rapid staining of astrocytes for LCM was performed as in Ferraiuolo et al (2011a). This protocol allows rapid isolation of astrocytes so as to preserve RNA quality. Sections (10µm) of frozen mouse lumbar spinal cord or human cervical spinal cord were placed on microscope slides and fixed in 4˚C acetone for 3 mins. Sections were then incubated in goat serum blocking solution for 3 mins at room temperature. For the mouse study, the primary antibody used was rabbit polyclonal anti-ALDH1L1 (Abcam, #ab 79727) at 1:50 dilution whereas for the human study anti-GFAP (DAKO # Z0334) at 1:150 was used. Primary antibody was added to the slides and left for 3 mins at room temperature. Slides were washed 3 times in Tris-buffered saline (TBS) for 10 secs and incubated with secondary antibody (1:200 in TBS) for 3 mins. Slides were washed 3 times in TBS for 10 secs then incubated in ABC solution for 3 mins at room temperature. Goat serum, secondary antibody and ABC solution were from the Vectastain rabbit IgG kit (Vector Labs # PK-6101). Slides were washed 3 times in TBS for 3 mins and incubated in diaminobenzidene for 3 mins in the dark. The reaction was stopped in water for 15 secs and dehydrated in a graded alcohol series: 70%, 95% and 100% for 15 secs followed by xylene for 5-10 mins. Slides were then allowed to dry at room temperature for 30 mins.

2.2.1.2 Laser capture microdissection of murine astrocytes

In the mouse study, laser capture of ~1500 astrocytes from the ventral horn of the lumbar spinal cord was performed using the Arcturus Pixcell II microdissection instrument (Life Technologies, Carlsbad, CA) with Arcturus Capsure Macro LCM Caps (Life Technologies #LCM0211) (Figure 2.1). LCM of symptomatic and late-stage astrocytes was performed by Mr Paulius Viskaitis and Dr Dilraj Sokhi respectively. For qPCR validation one of the non-transgenic littermates had astrocytes laser captured using the Arcturus Veritas microdissection instrument (Life Technologies). RNA was extracted from captured cells using the Arcturus Picopure RNA Isolation kit (Life Technologies #12204-01) and tested for RNA quantity using the Agilent Nanodrop

spectrophotometer ND-1000 (Agilent Technologies, Santa Clara, CA) and for quality using the RNA 6000 PicoChip kit (Agilent # 5067-1513).

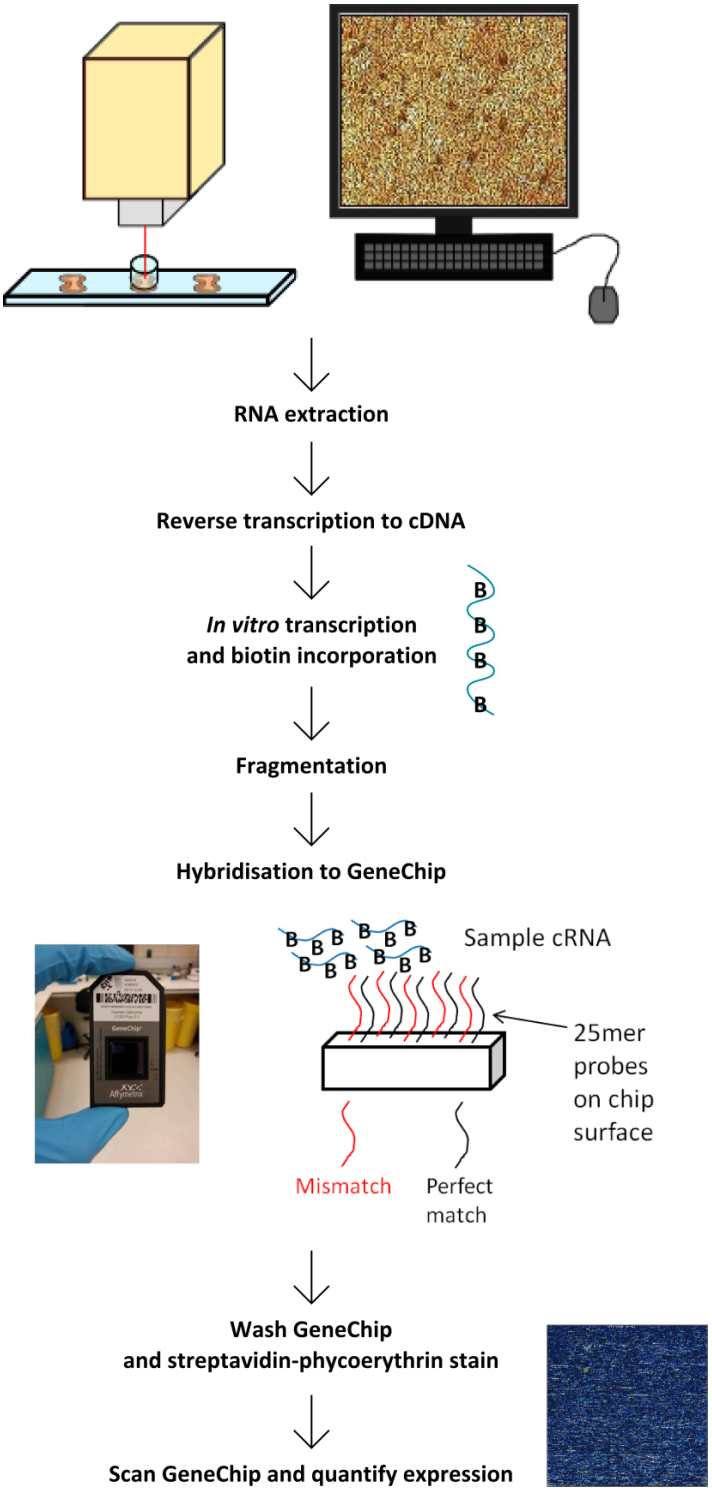

Figure 2.1 The process of capturing cells using LCM through to gene expression profiling by microarray analysis using the Affymetrix platform. Cells are labelled with specific antibody and captured using LCM equipment (top). The RNA is extracted, reverse transcribed and then *in vitro* transcription performed with biotin-labelling of the resultant cRNA. cRNA is then fragmented and hybridised to the GeneChip, which contains perfectly matching probes and mismatch probes containing a non-matching base at the 13th nucleotide position, which control for non-specific binding. Following wash and stain steps, presence of mRNA species is visualised using a scanner, whereby increased signal is reflective of increased expression of the target transcript.

2.2.1.3 Microarray analysis

RNA was linearly amplified using the Genechip two-cycle cDNA synthesis kit (Affymetrix #900432). cRNA was generated using the GeneChip Expression 3' Amplification Reagents for IVT labelling (Affymetrix). 15µg of cRNA for each of 3 x $SOD1^{G93A}$ and 3 x NTg mice was fragmented and hybridised onto Mouse Genome 430 2.0 Genechips (Affymetrix #900495).

2.2.1.4 Data processing and analysis

Quality control checks were performed using the Affymetrix Expression Console software and the packages "simpleaffy" (Miller), "affyqcreport" (Parman et al.) and "affyPLM" (Bolstad) within Bioconductor (Gentleman et al., 2004) and R (R-Core-Team, 2014) following the script in Appendix 1. Initial GeneChip analysis for determination of differentially expressed transcripts was performed using Genespring GX (Agilent) and the Probe Logarithmic Intensity Error (PLIER) algorithm, as in the analysis of 60 day astrocytes by Ferraiuolo et al. (2011a). Transcripts with fold change ≥ 2 and $p \leq 0.05$ were defined as differentially expressed as in Ferraiuolo et al. (2011a). Due to an *n* number of 3 in the mouse study, multiple testing correction was not used on microarray data. Probesets were filtered from the dataset using MAS5 present call in Bioconductor, whereby a probeset was excluded if it was called absent in all samples (see Filter section of Appendix 1).

2.2.1.5 Gene Ontology categorisation

For Gene Ontology categorisation, the Database for Annotation, Visualisation and Integrated Discovery (DAVID) v6.7 was used (http://david.abcc.ncifcrf.gov/) in combination with NetAffx Analysis Centre (www.affymetrix .com) and Genecards V3 (www.genecards.org). All DAVID analyses were run using the functional annotation clustering tool with the Gene Ontology terms for biological process, cellular compartment and molecular function selected, and using the highest stringency settings. Enrichment of pathways in the Kyoto Encyclopedia of Genes and Genomes (KEGG) was also performed using DAVID. These databases were chosen for investigation in DAVID due to the clarity of the annotations provided.

2.2.2 Quantitative PCR (qPCR) validation

2.2.2.1 cDNA synthesis

The Quantitect Reverse Transcription Kit (Qiagen # 205311) was used for all cDNA synthesis. Primers were optimised using either Universal cDNA which had been synthesised from Universal Mouse Reference RNA (Agilent #740100), or cDNA obtained from cultured cells, at a concentration of 12.5ng/µl. Amplified RNA from $SOD1^{G93A}$ and NTg astrocytes (from which aliquots had also been taken for the arrays) was synthesised to cDNA for qPCR validation of microarray results.

2.2.2.2 Primer design and optimisation

Genes were chosen for validation from categories that were enriched in both the symptomatic and the late-stage time-points. Primers were designed for genes of interest using the Primer Blast tool from NCBI (http://www.ncbi.nlm.nih.gov/tools/primer-blast/). Accession numbers for each gene were entered and primers designed within or near to the region of the corresponding probe on the Affymetrix Mouse Genome 430 2.0 GeneChip. Primer pairs were chosen that did not bind to non-specific targets and that detected all transcripts of a gene (if multiple transcripts were present). Primers were designed to produce amplicons of 50-150bp in length and to overlap an exon boundary. If an exon boundary could not be overlapped controls were used which had received no reverse transcriptase enzyme during cDNA synthesis, thus checking for the presence of genomic DNA. Primers were ordered from Sigma Aldrich at a synthesis scale of 0.025µmol and desalt purification and were kept at a stock concentration of 100µM at -20°C according to manufacturers instructions. A range of primer concentrations were tested (Table 2.2) and the optimum primer concentration was chosen as the concentration that produced the best replicates and the cleanest dissociation curve. Agarose gel electrophoresis was performed to confirm that products were the correct size. Primer sensitivity was then tested using a serial 1:2 dilution of cDNA from 12.5ng/µL to 0.2ng/µL with subsequent generation of a standard curve. Primers were taken forward to qPCR validation if they had an r^2 value of 0.98 or above and were between 90 and 110% efficiency. For primer optimisation and validation, reactions were performed in 20µL reaction volumes containing 10µL Brilliant III Ultra Fast SYBR®Green qPCR mastermix (Agilent # 600882),

1µL cDNA (12.5ng/µL), forward and reverse primers (concentrations indicated in Table 2.2) and the reaction volume completed with nuclease free water. qPCR was run at 95˚C for 10 mins followed by 40 cycles of 95˚C for 30 secs and 60˚C for 1 min, this was then followed by 95˚C for 1 min, 55˚C for 30 secs and 95˚C for 30 secs.

2.2.2.3 qPCR of samples

qPCR was performed on a Stratagene MX3000p qPCR instrument (Stratagene, CA) with analysis performed using the MXPro software v4.10 build 389 by Stratagene. To calculate relative concentration differences between $SOD1^{G93A}$ astrocytes and NTg controls the 2(-Delta Delta Ct) method was used (Livak and Schmittgen, 2001). *Gapdh* was chosen as the housekeeping gene due to a consistent expression level across all GeneChips. Genes were tested for statistical significance using a one-tailed independent samples t-test in Graphpad Prism v 6.05 (Graphpad Software Inc.).

Table 2.2 Primer concentrations used in primer optimisation for qPCR. Primers were first tested at concentrations in the range 150/150nM to 600/600nM. However if spurious products were observed (indicative of non-specific product amplification) then concentrations in the range 50/50nM to 150/150nM were tested.

Forward primer concentration (nM)	Reverse primer concentration (nM)
50	50
100	50
50	100
100	100
150	100
100	150
150	150
150	300
300	150
300	300
600	300
300	600
600	600

Table 2.3 Primers and primer concentrations used in qPCR validation of mouse microarray data and subsequent microglial phenotype studies.

Gene category	Gene name	Gene symbol	Primers (5' – 3')	Conc. Used (nM)
Lysosome	Cathepsin D	*Ctsd*	FW:TGCTGCCCTCTGCCTGTCTGA	150
			RV:AGGGCGGCAGGACAAGACAA	150
	Cathepsin S	*Ctss*	FW:CGACGCCAGCCATTCCTCCTT	150
			RV:AGAGTCCCATAGCCAACCACAAGA	150
	Hexosaminidase A	*Hexa*	FW:TCGCTGAGAGACTGTGGAGCAGTA	150
			RV:GGCCTGGATTCCTCTCCTCACCA	150
	Lysosomal-associated protein transmembrane 5	*Laptm5*	FW:AGCACCTGGAGGCTGGGAAGTC	150
			RV:TTGCCATCAGAGCAGTGGCTCAT	150
Complement components	C1qb	*C1qb*	FW:CACCAACGCGAACGAGAACT	150
			RV:GGCCAGGCACCTTGCA	150
Immune response	C-X-C motif chemokine 10	*Cxcl10*	FW: TAGCTCAGGCTCGTCAGTTCTA	300
			RV: TGGGAAGATGGTGGTTAAGTTC	150
	Chemokine (C-C motif) ligand 6	*Ccl6*	FW: GCAGGCATTGTCACCCACTT	50
			RV: AGGCGGAGTCCACATGAATAC	100
Extracellular Matrix	Matrix metalloproteinase 9	*Mmp9*	FW: TGGGCCCCAGGAGTCTGGATAAG	150
			RV: CGAATCTCCAGACACGCCCCTTG	150
	Tissue Inhibitor of Metalloproteinase 1	*Timp1*	FW: CTGTGGGAAATGCCGCAGAT	150
			RV: GTTCTGGGACTTGTGGGCATA	300
	Lipoprotein Lipase	*Lpl*	FW: CGGCATCCCCATTATTGCTA	300
			RV: CTTTCCAGTGTTTACAAGCATTC	300
	Chondrolectin	*Chodl*	FW: ACACGTGCCTTACAATTATTCTT	150
			RV: ACCTGTGATTTGTACTGCAGATG	150
Other	Insulin-like growth factor binding protein 5	*Igfbp5*	FW:CCCCGCCTCTCTTCCCTGTTAG	50
			RV:GGCCAGAGTCTGTGAAGTGGTGA	50
	Activating transcription factor 3	*Atf3*	FW:TTCTGAGAGTCTGGGGATCTGCCAT	100
			RV:TCCCCTGGTGCCAGCCAGTTC	100

Gene category	Gene name	Gene symbol	Primers (5' – 3')	Conc. Used (nM)
M1 microglial marker	Nitric Oxide synthase 2	*Nos2*	FW:TGGAGACTGTCCCAGCAATG	300
			RV: GCGCAGAACTGAGGGTACAT	150
	Prostaglandin-endoperoxide synthase 2	*Cox2 (Ptgs2)*	FW: CCCATGGGTGTGAAGGGAAATA	300
			RV: AAGTGCTGGGCAAAGAATGC	150
M2 microglial marker	Arginase 1	*Arg1*	FW:CTCCAAGCCAAAGTCCTTAGAG	300
			RV:AGGAGCTGTCATTAGGGACATC	300
	Chitinase, acidic	*Ym1*	FW:TCACTTACACACATGAGCAAGAC	300
			RV: CGGTTCTGAGGAGTAGAGACCA	300
House keeping	Glyceraldehyde-3-phosphate dehydrogenase	*Gapdh*	FW: GCTACACTGAGGACCAGGTTGTCT	300
			RV: AGCCCCGGCATCGAA	300

2.2.3 Functional studies of murine astrocytes

2.2.3.1 Isolation of astrocytes from neonatal animals

$SOD1^{G93A}$ and NTg littermate neonatal mouse pups up to a maximum of 2 days old were euthanised by cervical dislocation. The head was removed and kept on ice and tail clips taken for genotyping (Section 2.2.3.2) Under sterile conditions, the skull was cut dorso-ventrally along the midline and peeled back, and the brain removed in one piece. The brain was placed in Hanks Balanced Salt Solution (HBSS) without Calcium or Magnesium (HBSS-/-) and the hindbrain, diencephalon, and meninges removed to leave the cortical hemispheres. The cortical hemispheres were transferred into minimal amounts of HBSS -/- and finely chopped with a scalpel. The resulting tissue was then taken up in a P1000 pipette with a pre-cut tip (tips were cut with sterile scissors to give a larger aperture) and placed in a falcon tube with 6mL of HBSS-/- (Lonza #BE10-547F) on ice to settle. Once settled the HBSS-/- was replaced with 6mL of HBSS containing Calcium and Magnesium (HBSS+/+) and 100µL 2.5% Trypsin with Versene (Lonza, #BE17-160E), 30µL 10mg/mL Collagenase (Sigma, #C6885) and 30µL 10mg/mL DNAse (Sigma #D5025-15KU) added. Each falcon was placed at 37˚C for 15 minutes, with gentle mixing performed every five minutes, and the tissue was then triturated 10 times using a 10mL stripette (where one trituration equals a movement up and down the stripette). This step was repeated and 6mL of Dulbecco's Modified Eagles Medium (Lonza, #BE12-741F) containing 10% Foetal Bovine Serum (Biosera, #S1900-500) and 1% Penicillin/Streptomycin (Lonza, #DE17603E) added to neutralise

the trypsin (this medium formulation is hereafter called “DMEM complete”). Falcons were then spun at 400g for 4mins to pellet the cells. Pellets were re-suspended in 4mL DMEM complete and plated in T25 flasks (Greiner one bio #609175).

2.2.3.2 Genotyping of neonatal animals

Tail clips from neonatal animals were taken and placed in 0.5mL eppendorf tubes. 30µL of QuickExtract DNA Extraction Solution (Epicentre # QE09050) was added to each tube, making sure that the clip was submerged. Tubes were vortexed and briefly centrifuged to make sure contents were at the bottom, and were then placed onto a heat-block at 65˚C for 30 minutes, with brief vortexing and centrifugation halfway through the incubation period. When the 30 minutes had elapsed, tubes were incubated at 98˚C for 2 minutes, giving DNA extract ready for use in PCR. For each animal, 1µL of DNA extract was then added to a 0.2mL eppendorf tube containing 4.5µL nuclease free water, 2µL FIREPol 5x PCR Mix RTL 7.5 (Solis Biodyne # 04-12-00115). Primers were added at a concentration of 400nM for human *SOD1* (FW: 5’ CATCAGCCCTAATCCATCTGA 3’, RV: 5’ CGCGACTAACA ATCAAAGTGA 3’) and *IL2* as a control (FW: 5’ CTAGGCCACAGAATTGAAAGATCT 3’, RV: 5’ GTAGGTGGAAATTCTA GCATCATC 3’). Samples were then run on a thermal cycler with the following conditions: 94˚C for 5 mins followed by 30 cycles of: 94˚C for 1 min; 60˚C for 45 secs; 72˚C for 30 secs, and a final extension at 72˚C for 10 mins. Products were then run on a 2% agarose gel (1g agarose in 50mL TAE buffer) containing 1µL ethidium bromide with DNA Hyperladder IV (Bioline # BIO-33029) for 25 minutes at 60V. When visualised under UV light, non-transgenic mice present a single band at ~320 base pairs (bp) whereas transgenic mice present two bands, one at ~320bp and one at ~250bp.

2.2.3.3 Sub-culture of mouse SOD1^{G93A} astrocytes

All cell culture was performed under sterile conditions in a Labgard ES Class II Biological Safety Cabinet. Once the primary cell layer was 100% confluent, Parafilm® (Pechiney # PM996) was wrapped around the top of the flasks and they were placed onto a shaker overnight at 225 r. p. m. at 37˚C to remove overlying microglia. Overlying microglia could be harvested at this stage for use in experiments (Section 2.2.3.10). Cells were then washed with DMEM/Ham’s F12. This was then replaced with HBSS-/- containing 0.25% trypsin (without Versene Lonza # BE17-160E) and 1mM EDTA added

in a 1:2 ratio with DMEM/Ham's F12. Flasks were incubated at 37˚C for 45-60 minutes until the astrocytic monolayer detached as a sheet or as small pieces of a sheet. The flasks were then placed vertical, allowing astrocytic sheets to sink to the bottom where they were collected using a P1000 pipette. The astrocytic sheets were placed into 15mL falcon tubes with 6mL HBSS-/- containing 0.25% trypsin and incubated at 37˚C for 10 minutes, followed by trituration ~20 times to resuspend astrocytes as single cells. trypsin was neutralised with 6mL DMEM complete and falcons centrifuged for 4 minutes at 400g. Supernatant was removed and pellets resuspended in 12mL DMEM complete. This was then plated in T75 culture flasks. All subsequent passages were performed once flasks had reached 90% confluence. Cultures were trypsinised in HBSS-/- containing 0.25% trypsin and incubated at 37˚C for 15 minutes. Once cells were in suspension, DMEM complete was added in equal volume to HBSS-/- to neutralise trypsin, and the resulting solution was removed to a 15mL falcon tube. This was then spun at 400g for 4 minutes, the supernatant removed, and the pellet resuspended in DMEM complete. The resulting cell suspension was split between 2 or 3 x T75 culture flasks, and the volume of the flasks made up to 12mL using DMEM complete. Cells were kept at 37˚C with 5% CO_2.

2.2.3.4 Isolation and culture of primary embryonic motor neurons for separated co-culture

Motor neurons and astrocytes were cultured in a separated co-culture as in Ferraiuolo et al. (Ferraiuolo et al., 2007). In a tissue culture hood, paraffin wax was heated to ~100°C and three spots pipetted into the bottom of a well of a 24 well tissue culture plate for each replicate. Wax was allowed to set and wells were then washed twice with sterile distilled water. Poly-D-ornithine (1:1000) was pipetted in to cover the surface of the well and the plate was incubated overnight at 4°C. The following morning, poly-D-ornithine was removed and the plate washed twice with water, then allowed to dry completely. Once dry, laminin (1:200, Gibco #23017-015) was spotted in to the coverslips in 50µL volumes and plates were incubated at 37°C for a minimum of 2 hours.

Pregnant C57BL/6 mice were euthanised at gestational day 13 and the embryonic sac dissected out and placed into a petri dish on ice. In a tissue culture hood, embryos

were removed from the embryonic sac and placed into ice cold PBS in a petri dish. Using a dissecting microscope the head and lower limb buds were removed using sterile dissection instruments. The embryo was placed belly down and the skin cut along the back to reveal the spinal cord. The cord was removed from the body and meninges removed. It was then cut into 4 pieces and placed into a 15mL falcon tube containing 1 mL of ice cold PBS. This process was repeated until all embryos had been processed. Spinal cords were pooled in the last step into the 1mL of PBS. Cords were trypsinised by adding 10µL of 2.5% trypsin without versene followed by a 10 minute incubation at 37°C in which tissue was agitated at the halfway point. Trypsin was neutralised with 1mL containing 80% L15 media (Fisher # 10339113), 10% BSA (4%; Sigma # A3311-10G) and 10% DNAse (1mg/mL; Fisher # 11478533). The tube was agitated to disaggregate tissue fragments and then triturated twice with a P1000 pipette. The tissue fragments were allowed to settle and the supernatant was removed to a new tube. To the remaining fragments 1mL of a mix containing 88% L15, 10% BSA(4%) and 2% DNAse was added and the tissue triturated six times with a P1000 pipette. The fragments were allowed to settle and the supernatant removed. This step was repeated until the majority of tissue had been broken down. Using a sterile glass Pasteur pipette a 1.5mL cushion of BSA(4%) was added to the bottom of the tube, taking care to avoid mixing of the BSA and media, and preps were centrifuged for 5 minutes at 370g at room temperature. The supernatant was then removed and the pellet resuspended in 1mL of L15 by trituration six times with a P1000 pipette. Optiprep solution (3.7%) was prepared for density centrifugation of cells as follows: 0.8g D-glucose, 2mL Tricine (10mM), 1.23mL of Optiprep solution (Axis-Shield #1114542) and 16.77mL of sterile H2O, which was then filter-sterilised. Using a sterile glass Pasteur pipette 1.5mL of the 3.7% optiprep solution was layered underneath the cell suspension taking care not to mix the two. The cell suspension was then spun for 15 minutes at 755g at room temperature. After this step, motor neurons were located at the interface of the cell suspension and the 3.7% optiprep solution, whilst glial cells were contained in a glial pellet at the bottom of the tube. Neuronal cells were removed from the interface in a volume of 1mL and added to a new falcon tube containing 9mL L15 medium. A 1.5mL cushion of 4% BSA was added to the bottom of this tube as before and cells were spun for 5 minutes at 370g at room

temperature. Following this step the majority of supernatant was removed and the cell pellet resuspended in 200µL of complete motor neuron medium (Neurobasal medium (Fisher# 10770954) containing: 1X B27 (Fisher# 10620975), 2% horse serum (Life #16050-122), L-glutamine (0.5mM), 1% penicillin/streptomycin (Lonza #DE17-603E), L-glutamic acid (25µM), 5ng/mL CNTF (R&D systems #557-NT-010), 1ng/mL GDNF (R&D systems #512-GF-010), 1ng/mL BDNF (Fisher #10605414). L-glutamic acid was removed from medium after first 3-5 days. Excess laminin was removed from the 24 well plate and motor neurons added at a density of 5 x 10^4 cells per well. Medium was added to a final volume of 0.5mL. Motor neuron presence was confirmed by staining with antibodies against Islet 1 at 1:1000 (Abcam #ab109517), SMI32 at 1:1000 (Covance #Smi-32r) and Map2 at 1:2000 (Sigma #M4403).

2.2.3.5 Antibodies used for characterisation of murine cultures

Cell cultures were characterised using a combination of flow cytometry and immunocytochemistry (ICC) (Table 2.4).

2.2.3.6 Analysis of purity of cell cultures by flow cytometry of and ICC

Astrocytes were characterised using anti-mouse GLAST-APC conjugated antibody and isotype control. Microglia were characterised using anti-mouse CD11b-FITC and isotype control. Flow cytometry was performed on a FACSCalibur (BD) flow cytometer using PI (stock at 500µg/mL added as 2µL immediately prior to FACS analysis) to remove dead cells from the analysis. Due to dim staining of the CD11b antibody upon the microglial cultures, this antibody was tested in ICC to define culture purity, with a rabbit polyclonal anti-GFAP antibody used to identify contaminating astrocytes. Three separate preparations of microglia were performed (Section 2.2.3.3) and plated onto Poly-D-ornithine coated ø0.13mm coverslips. Coverslips were stained as in section 2.2.3.7. and fields of view were captured in a horizontal transect through the middle of the coverslip (12-13 images) as in section 2.2.3.9. The number of $CD11b^+$ cells in each field were counted by 3 independent scorers and the average of all three scorers calculated and expressed as percentage of all cells.

Table 2.4 Antibodies used in flow cytometry of astrocyte and microglial cultures.

Cellular target	Antigen	Conjugate	Isotype	Host species	Raised against	Dilution	Supplier and code
Primary antibodies							
Astrocyte	GLAST	APC	IgG2a	Mouse	Human, mouse, rat	1:11	Miltenyi Biotech # 130-098-803
Microglia	Cd11b	FITC	IgG2b	Rat	Mouse	1:100	Ebioscience # 11-0112-81
Isotype controls							
		APC	IgG2a	Mouse		1:11	Miltenyi Biotech # 130-098-850
		FITC	IgG2b	Rat		1:100	Ebioscience # 11-4031-81

2.2.3.7 Preparation of coverslips for staining of astrocytes and microglia

Under sterile conditions, 1.1mm coverslips (Scientific Laboratory Supplies # MIC3366) were sterilised in 70% ethanol and then submerged in 1:1000 (in water) poly-dL-ornithine for at least 30 minutes at room temperature. Coverslips were then placed into wells of a 24-well plate (Greiner bio one # 662160) and allowed to dry. Cultured cells were trypsinised and counted, and a minimum of 5000 cells aliquoted onto each coverslip in 50µL aliquots. The coverslips were incubated for 30 minutes to allow attachment of cells and then the media topped up to 1mL. Once cells had grown to at least 40% confluence, coverslips were fixed in 4% formaldehyde solution (4% w/v paraformaldehyde in PBS) for 20 minutes at room temperature. Coverslips were washed three times with PBS and used immediately for immunocytochemistry.

2.2.3.8 Procedure for staining of murine astrocytes and microglia

Cd11b staining of microglia was performed using the same antibody as used for flow cytometry (Table 2.4). Coverslips were washed 3 times with PBS and then blocked in 5% goat serum for 1 hour at room temperature. Primary antibodies were diluted as indicated in Table 2.4 in blocking solution. Coverslips were transferred to parafilm and 80µl of primary antibody added to each coverslip and incubated overnight at 4˚C. Following incubation, coverslips were transferred back to a 24 well-plate and washed

with PBS then mounted on glass microsope slides using Vectashield Hard-Set Mounting Medium with DAPI (Vector Laboratories #H-1500).

In order to identify astrocytic contamination in microglial cultures, GFAP staining of microglia was performed as above with the following additional steps. Following fixation and washing with PBS, cells were permeabilised in 0.1% TritonX-100 (VWR # 28817.295) for 3 minutes. Cells were then washed and received primary antibody and overnight incubation at 4˚C. Following incubation, coverslips were transferred back to a 24 well-plate and washed with PBS then transferred back to parafilm. 80µL of HRP-conjugated anti-rabbit secondary antibody diluted in blocking solution was added to coverslips and left for 1 hour at room temperature. Coverslips were then transferred back to the 24 well-plate and washed with PBS 3 times and mounted as with CD11b stained microglia.

Table 2.5 Antibodies used in Immunocytochemistry of astrocyte and microglial cultures.

Cellular target	Antigen	Conjugate	Isotype	Host species	Raised against	Dilution	Supplier and code
Primary antibodies							
Astrocyte	GFAP	N/A	IgG	Rabbit	Cow	1:1000	DAKO #Z0334
Microglia	Cd11b	FITC	IgG2b	Rat	Mouse	1:100	Ebioscience # 11-0112-81
Secondary antibodies							
	Rabbit FC region	HRP		Goat	Rabbit	1:1000	Dako #P0448

2.2.3.9 Imaging of murine astrocytes and microglia

For imaging of Cd11b stained microglial cells, microscopy was performed on a Zeiss Axioplan 2 microscope using the 20X objective. Images were captured using a Hamamatsu C4880-80 muti-format CCD Camera and the Openlab software version 5.0.2. (Improvision Ltd., Coventry, UK) using the settings in Table 2.6.

Table 2.6 Camera settings used for imaging of Alexa Fluor 488 and Hoescht 33342 fluorescence.

Stain	Exposure	Gain	Offset
GFAP (Alexa fluor 488)	200 ms	0	0
Hoescht 33342	30 ms	0	0

2.2.3.10 Treatment of microglia with astrocyte-conditioned medium

As in Wyss-Coray et al. (2003), serum free media (DMEM/F12 1:1) containing 1x N2 supplement (hereafter "serum-free medium") was used for inflammation studies involving astrocyte monocultures. This both reduced the inherent variability associated with the use of FBS, and also negated the potential inflammatory effects that FBS can induce. For co-culture experiments serum was removed from motor neuron medium and 1x N2 supplement added.

Serum free medium was added to T75 flasks of $SOD1^{G93A}$ and NTg astroctes at 90% confluence in a volume of 12mL and left for 3 days before being collected. Medium was spun at 400g for 4 minutes to remove cell debris and was then stored at -20°C.

For co-culture medium, astrocytes were plated onto poly-D-ornithine coated coverslips at a density of 5×10^5 and allowed to reach confluence in DMEM complete (see section 2.2.3.1). The day after primary motor neurons were plated, confluent astrocyte coverslips were inverted and placed face down on to the wax blobs in the motor neuron plates (see Section 2.2.3.4) such that the two cell types faced each other but were not touching. Co-cultures were left for 3 days before collection of media. Media was spun to remove debris and stored at -20°C.

Microglia were collected floating in the medium following the overnight shake of astrocyte cultures (Section 2.2.3.3) and were plated at a density of 7.5×10^5 per well in a 6 well plate that had been pre-coated with poly-D-ornithine. Cultures were maintained in 1:1 complete astrocyte medium:NTg-conditioned astrocyte medium (hereafter "microglial medium"). To assess whether microglial phenotype was altered by medium from $SOD1^{G93A}$ vs NTg astrocytes, microglial medium was replaced with a 1:1 mix of fresh serum-free medium with conditioned medium obtained from the above-mentioned monocultures and co-cultures of $SOD1^{G93A}$ and NTg astrocytes. Cultures were left for 3 days, at which point all medium was collected and stored at -20°C and cells collected in Trizol for subsequent analysis.

2.2.3.11 RNA extraction from cultured cells

RNA was extracted from cultured cells using Trizol reagent (Life # 15596-026). Trizol was added to cells in the tissue culture dish at a volume of 1mL per 10cm^2 culture area. Samples were collected in 1.5mL eppendorf tubes and stored at -20°C or taken forward for extraction. Samples were incubated for 5 minutes at room temperature, then 0.2mL chloroform was added per 1mL of Trizol used in initial collection. The samples were shaken vigorously for 15 seconds and then incubated for 3 minutes at room temperature. Samples were then centrifuged for 10 minutes at 12000g at 4°C. The aqueous phase was removed and transferred to a new 1.5mL eppendorf tube. Glyco-blue (Life # AM9516) was added to the aqueous phase at a quantity of 7.5µg to allow easier identification of the RNA pellet in subsequent steps. To this, 500µL of 100% isopropanol was added per 1mL of Trizol used in the initial collection. Samples were incubated for 10 minutes at room temperature before centrifugation for 10 minutes at 12000g at 4°C. The supernatant was then removed leaving the RNA pellet. The pellet was then washed with 75% ethanol by adding 1mL of ethanol per 1mL of initial Trizol reagent, vortexing the sample and centrifugation for 5 minutes at 7500g at 4°C. This step was repeated to achieve a thorough wash. Ethanol was then removed as much as possible and samples were left for 15 minutes at room temperature to air dry the pellet. RNA was resuspended in RNAse-free H_2O (Fisher # HYC-001-218C). RNA quantity was assessed on an Agilent Nanodrop spectrophotometer ND-1000 (Agilent Technologies, Santa Clara, CA).

2.2.3.12 Assay of β-hexosaminidase enzyme activity in murine spinal cord

Male SOD1^{G93A} and NTg mice were euthanised via intraperitoneal injection of pentobarbital at symptomatic and late-stage time-points (n=3 for each group at each time-point). As a further control, three male mice over-expressing human wild-type SOD1 and corresponding to a late-stage time-point were euthanised. Mice were perfused with sterile PBS and the spinal cord and brain were dissected and snap frozen in liquid nitrogen. Before freezing, spinal cords were cut just above the lumbar enlargement to give “upper cord” and “lower cord” portions. Sections of tissue (~5mg) were dissected on dry ice from the thoracic section of the upper cord and the lumbar section of the lower cord homogenised using a glass tissue homogeniser (Jencons,

England) in 95µL of distilled H2O. Protein concentration of homogenates was measured using BCA assay (Sigma #B9643) and samples diluted to 1mg/mL using distilled H2O. 5µL of diluted homogenate was added to 500µL McIlvaine citrate–phosphate pH 4.5 buffer and 100µL aliquots taken. All tubes and substrate solution (4-Methylumbelliferyl N-acetyl-β-D-glucosaminide, Sigma #M2133) were warmed for 2 minutes at 37°C, before substrate was added at timed intervals in 100µL volumes to all tubes. All tubes were then incubated at 37°C for 10 minutes and stopping solution (0.25M glycine buffer pH10.4) added at timed intervals. During this assay, the substrate is hydrolysed by β-hexosaminidase to 4-methylumbelliferone. Adding the alkaline stopping buffer causes the 4-methylumelliferone to fluoresce at a different wavelength to unhydrolysed substrate. Sample fluorescence was read using a FLUOstar Omega platereader (BMG Labtech) with excitation settings of 365nm and emission of 450nm.

2.2.3.13 Phagocytosis assay

Labelled cell debris was created using NSC34 cells and Vybrant Dil cell-labelling solution (Life #V-22885). Vybrant Dil (Vybrant) weakly fluoresces until bound to a cell membrane, where it becomes strongly fluorescent with the peak in the emission spectrum at 565nm. NSC34 cells were maintained in DMEM containing 10%FBS and 1% Penicillin/Streptomycin (complete medium) at 37°C and 5%CO_2. Vybrant was resuspended in complete medium to a final dilution of 1:200 and placed upon cells for 20 minutes at 37°C. Vybrant-containing complete medium was removed and fresh complete medium (free of Vybrant) was put on the cells for 10 minutes at 37°C. Control NSC34 flasks received the same treatment in the absence of Vybrant. Cells were incubated in serum free DMEM for 48 hours to induce cell death via oxidative stress. Medium was then collected containing the floating cells and cells were counted using a haemocytometer. Aliquots were then made and frozen at -80°C.

$SOD1^{G93A}$ and NTg astrocytes were plated into a 384-well optical plate (Greiner Bio One #781091) at a density of 3 x 10^3 cells per well. After 24 hours medium was changed to serum-free medium (DMEM/F12 1xN2). At 48 hours medium was replaced with serum-free medium containing Vybrant-labelled cellular debris at a density of 125 cells μL^{-1}. Cultures were then left for a further 48 hours to allow phagocytosis to take place.

Cultures were washed three times with PBS and fixed with 4% PFA for 15 minutes at room temperature and stained for GFAP as in section 2.2.3.5 and using the GFAP antibody in Table 2.7. Plates were analysed using the InCell analyser (GE Healthcare, Little Chalfont, UK) and InCell Developer Toolbox v. 1.9.

Table 2.7 Antibodies used in staining of phagocytosis assay.

Cellular target	Antigen	Conjugate	Isotype	Host species	Raised against	Dilution	Supplier and code
Primary antibodies							
Astrocyte	GFAP	N/A	IgG	Rabbit	Mouse Rat Cat Human	1:1000	AbCam #ab7260
Secondary antibodies							
	Rabbit FC region	Alexa fluor 488	IgG	Goat	Rabbit	1:200	Life #A11008

2.2.3.14 HMGCR and SREBP2 staining of murine spinal cord

Spinal cord sections (10µm) of late-stage murine SOD1^{G93A} and age-matched NTg spinal cord were stained for the presence of 3-hydroxy-3-methylglutaryl-CoA reductase (HMGCR), an important enzyme in the first steps of cholesterol synthesis, and sterol regulatory element binding protein 2 (SREBP2), a master regulator of cholesterol synthesis genes. Primary anti-body used was rabbit α-SREBP2 (AbCam #Ab28482) at 1:400 dilution and rabbit α-HMGCR (AbCam #Ab174830) at 1:100. Blocking solution, secondary antibody and ABC solution were all contained within the Vectastain rabbit IgG kit (Vector Labs # PK-6101). Tissue sections were fixed in acetone at 4°C for 10 minutes, followed by blocking for 30 minutes at room temperature (all subsequent steps at room temperature). Primary antibody was added to tissue sections for 1 hour followed by a 5 minute wash in TBS. Secondary antibody was added for 30 minutes and sections again washed for 5 minutes in TBS. ABC solution was then added for 30 minutes followed by a final 5 minute wash in TBS. Staining was visualised by adding diaminobenzidene for 3 minutes and then stopping the reaction in water. To visualise nuclei, slides were put in haemotoxylin for 20 seconds and placed in Scott's tap water for a few seconds. Slides were then dehydrated in a graded alcohol series of 70%, 90% and 100% ethanol followed by 10 minutes in xylene. Coverslips were mounted onto

slides using DPX mounting solution. SREBP2 staining was visualised on a Nikon Eclipse Ni microscope with a Nikon DS-Ri1 camera using brightfield settings of 9.5ms exposure for 20X magnified images and 44ms exposure for 40X magnified images.

2.2.4 Gene expression profiling of human astrocytes

2.2.4.1 Rapid staining procedure of human astrocytes

Sections (10µm) of human cervical spinal cord were placed on microscope slides and fixed in 4˚C acetone for 3 mins. Sections were then incubated in goat serum blocking solution for 3 mins at room temperature. Primary antibody anti-GFAP (DAKO # Z0334) at 1:150 in blocking solution was added to the slides and left for 3 mins at room temperature. Slides were washed 3 times in Tris-buffered saline (TBS) for 10 secs and incubated with secondary antibody (1:200 in TBS) for 3 mins. Slides were washed 3 times in TBS for 10 secs then incubated in ABC solution for 3 mins at room temperature. Goat serum, secondary antibody and ABC solution were from the Vectastain rabbit IgG kit (Vector Labs # PK-6101). Slides were washed 3 times in TBS for 3 mins and incubated in diaminobenzidene for 3 mins in the dark. The reaction was stopped in water for 15 secs and dehydrated in a graded alcohol series: 70%, 95% and 100% for 15 secs followed by xylene for 5-10 mins. Slides were then allowed to dry at room temperature for 30 mins.

2.2.4.2 Laser capture microdissection of human astrocytes

LCM was performed in the same manner as for the mouse study (Section 2.2.1.2). LCM of samples was performed with Dr Gabriela de Oliveira. The Veritas capture system was used to capture ~1500 astrocytes from the ventral horn of the cervical spinal cord per sample onto the Arcturus Capsure Macro LCM caps. RNA quantity and quality were then checked using the Nanodrop spectrophotometer ND-1000 and RNA 6000 PicoChip Kit respectively.

2.2.4.3 Microarray analysis

RNA was linearly amplified using the Two Rounds Amplification Kit (Affymetrix). At this stage cRNA was used to generate cDNA, which was then tested by PCR for presence of *GFAP*, *CD68*, and *OLIG2;* markers of astrocytes, microglia and oligodendrocytes respectively. Only the samples that were enriched for the astrocyte marker GFAP were

taken forward to be put on the arrays. RNA was linearly amplified using the Genechip two-cycle cDNA synthesis kit (Affymetrix #900432). cRNA was generated using the GeneChip Expression 3' Amplification Reagents for IVT labelling (Affymetrix). 15µg of cRNA for each of 3 x SOD1 patients and 4 x controls was fragmented and hybridised onto Human Genome U133 Plus 2.0 Genechips (Affymetrix # 900470).

2.2.4.4 Human astrocyte data analysis and enrichment analysis

As in the mouse study, Bioconductor and R (2014) were used for quality control of the human arrays using the simpleaffy, affyQCReport and affyPLM packages and the script in Appendix 1. Expression data was then filtered using the same script as in the mouse analysis and subsequent analysis of differential gene expression performed using the PUMA package (Pearson et al., 2009) (full script in Appendix 1). To exclude any genes differentially expressed due to gender differences between the SOD1 and control cases, a differential expression analysis was performed upon males versus females. Any genes shown as differentially expressed due to gender were removed from the final gene list. To exclude age as a confounding variable, genes of interest were subjected to correlation analysis of expression level with age and tested using the Pearson's correlation test for significance. Enrichment analyses were performed using the DAVID database.

2.2.4.5 qPCR validation of genes differentially expressed in human SOD1-ALS astrocytes.

Primers were designed for genes of interest using the same methods as for the mouse arrays (Section 2.2.2.2). Primers for the housekeeping gene *β-actin* were designed within the "X00351_3_at" probeset target sequence based upon it having a low standard deviation and high expression level across the arrays.

Primetime primers were ordered as pre-prepared assays for the assessment of tight junction gene expression in cultured HUVECs. A reaction volume of 10µL was used, consisting of: 5µL of Brilliant III Ultra-fast qPCR mix (Agilent #600880), 0.5µL of assay mix, 3.5µL of H_2O and 1µL of cDNA template (12.5ng/µL). qPCR was run using the programme described in section 2.2.2.2.

Table 2.8 Primers and primer concentrations used in qPCR validation of human microarray data. Asterisks represent primer pairs obtained from the primerbank database: http://pga.mgh.harvard.edu/primerbank (Wang and Seed, 2003, Spandidos et al., 2008, Spandidos et al., 2010).Primetime primers were used for qPCR of tight junction genes in cultured endothelia.

SYBR primers

Gene category	Gene name	Gene symbol	Primers (5' – 3')	Conc. Used (nM)
Inflammation	Chitinase 3 like 1	*CHI3L1*	FW: GGCAACCAGTGGGTAGGATA	300
			RV: CTTCAGGTACTGCACCTTGCT	300
Tight Junction	Claudin-5 *	*CLDN5*	FW: CTCTGCTGGTTCGCCAACAT	150
			RV: CAGCTCGTACTTCTGCGACA	150
	Junctional Adhesion Molecule 2	*JAM2*	FW: AAAGAAACCTCCTTCCAGAAGAGTA	150
			RV: GTAACAACGGTGGCTTTGGT	150
Gap junction	Gap junction protein, Gamma 1, 45kDa	*GJC1*	FW: TTGGGCGTCTCACCCTTTTC	150
			RV: GCACAAAGGGTGCAGTGTTC	150
Transcription factor	Endothelial PAS domain protein 1	*EPAS1*	FW: GGGACGACACCTCTGGTTTT	150
			RV: GTTGGCCCAATGTGCTTTGT	150
Signalling	Transforming growth factor beta 2	*TGFB2*	FW: GGAAGGGGTGAAGTGCTAGT	150
			RV: ACCATGCCAACGATCAAATTGT	150
	Transforming growth factor, beta receptor 1	*TGFBR1*	FW: ATGTTGCTCAGTTACTCAAATGGT	300
			RV: AGCCTAAAGAATCCTGCACAAA	300
Nucleocytoplasmic transport	Karyopherin alpha 6	*KPNA6*	FW: GAGGAACCCCTGAGCAGAT	300
			RV: AGCAAGTCACATAGGGGTTTG	300
House keeping	β-actin	*ACTB*	FW: TCCCCCAACTTGAGATGTATGA	300
			RV: AACTGGTCTCAAGTCAGTGTACAGG	300

Primetime primers

Gene category	Gene name	Gene symbol	IDT assay code
Transcription factor	Endothelial PAS domain protein 1	*EPAS1*	Hs.PT.58.39757158.g
Tight Junction	Junctional Adhesion Molecule 2	*JAM2*	Hs.PT.58.26304499

	Tight junction protein 2 (zona occludens 2)	*TJP2*	Hs.PT.58.2167474
	Occludin	*OCLN*	Hs.PT.58.15235048
House keeping	β-actin	*ACTB*	Hs.PT.56a.19461448.g

2.2.5 Functional studies of human astrocytes

2.2.5.1 Cell culture for human functional studies

iAstrocytes were produced from human fibroblasts of ALS patients and controls by Dr Kathrin Meyer as previously described (Meyer et al., 2013). iAstrocyte culture medium consisted of DMEM+GlutaMax (Gibco #10566-016) supplemented with 1% anti/anti (Gibco #15240-062), 1mL N2 (Gibco #17502-048) and 10% FBS. Human umbilical vein endothelial cells (HUVECs) were obtained as a gift from Professor Paul Evans at the University of Sheffield, U.K. and were also bought from a commercial supplier (Promo-cell #C-12250). HUVECs were cultured in Endothelial Culture medium (Sciencell #1001). GFP-expressing mouse motor neurons were obtained from cultures of embryoid bodies as in Wichterle et al. (2002) and Haidet-Phillips et al. (2011) by Dr Laura Ferraiuolo. Embryonic stem cells (ESC) were obtained from a mouse expressing enhanced green fluorescent protein (eGFP, hereafter "GFP") under the control of the motor neuronal HB9 promoter. These were grown on mouse embryonic fibroblasts (MEFs). Twice a week the mouse ESCs were lifted and dissociated using trypsin to form embryoid bodies (EBs), from which differentiation was induced by addition of 2μM retinoic acid (Sigma #R2625) and 2μM purmorphamine (Calbiochem #540220). After 5 days the EBs were dissociated and sorted by flow cytometry for GFP using a FACSVantage/DiVa flow cytometer (BD). Plates were prepared for motor neurons by coating with poly-D-ornithine (1:1000) for 24 hours at room temperature followed by laminin (1:200, Gibco #23017-015) coating for 24 hours at 37˚C. Motor neuron medium consisted of DMEM/F12 (Gibco #11320-074) supplemented with 5% horse serum, 1% N2 supplement, 1% B27 supplement (Fisher #10620975), 10ng/mL BDNF (Invitrogen #10908010), 10ng/mL GDNF (Invitrogen #PHC7041) and 10 ng/mL CNTF (Invitrogen #PHC7015). Co-cultures of astrocytes and endothelia were set up on Corning Transwell inserts (Corning #3470) in a 24 well plate. All inserts were coated on both sides with fibronectin (Millipore #FC010) diluted 1:200 in D-PBS by placing 100μL and 600μL in the top and bottom chambers respectively.

2.2.5.2 Co-culture of HUVECs, iAstrocytes and GFP-motor neurons

On day 1 astrocytes were seeded onto the underside of inverted inserts at a density of $2x10^4$ cells per insert in 70μL of iAstrocyte medium and placed into a $150cm^2$ petri dish

(Figure 2.1). Petri dishes were then placed into an incubator for 90 minutes to allow cells to adhere. After 90 minutes excess medium was removed and the transwells were placed in the correct orientation in a 24 well plate containing 600µL of fresh iAstrocyte medium per well. 100µL of iAstrocyte medium was then added to the top chamber and the cells were incubated overnight. Also on day 1, GFP-expressing motor neurons were sorted by flow cytometry and plated at a density of 3 x 10^4 intermediate-gate cells per well of a 24 well plate in motor neuron medium. After 24 hours incubation (day 2), media was removed from the transwells containing astrocytes and they were relocated into the same wells as the motor neurons. The upper and lower chambers of the new co-culture were given a full media change into 100µL and 600µL of motor neuron media respectively and placed at 37˚C for 48 hours (until day 4). On day 4 media was changed to both wells and 4 x 10^4 HUVECs seeded into the top chamber of the transwells. The resultant cultures will hereafter be termed BBB, for blood brain barrier. Co-cultures were then left for a further 3 days until day 7. On day 7, 100µL of motor neuron media was added to the top chamber and 400µL added to the bottom chamber such that total media for each chamber was 200µL (top) and 1000µL (bottom). This step was added as the higher volume allowed easier and more reproducible measurements using the transendothelial electrical resistance (TEER) equipment. Plates were then put at 37˚C for a further 2 hours to allow wells to equilibrate before measurements.

2.2.5.3 Preparation of selection plates used in cloning

LB-agar for selection plates was made using 32g LB-Agar powder in 1L of distilled water. After an autoclave cycle LB agar was allowed to cool and antibiotic added to a final concentration of 1X. Agar was then poured into 100mm^2 petri dishes and allowed to set. Terrific broth (TB) for growth of bacteria in suspension was made using 47g of TB (Invitrogen #22711-022) in 1L of distilled water with antibiotic added to a final concentration of 1X.

a)

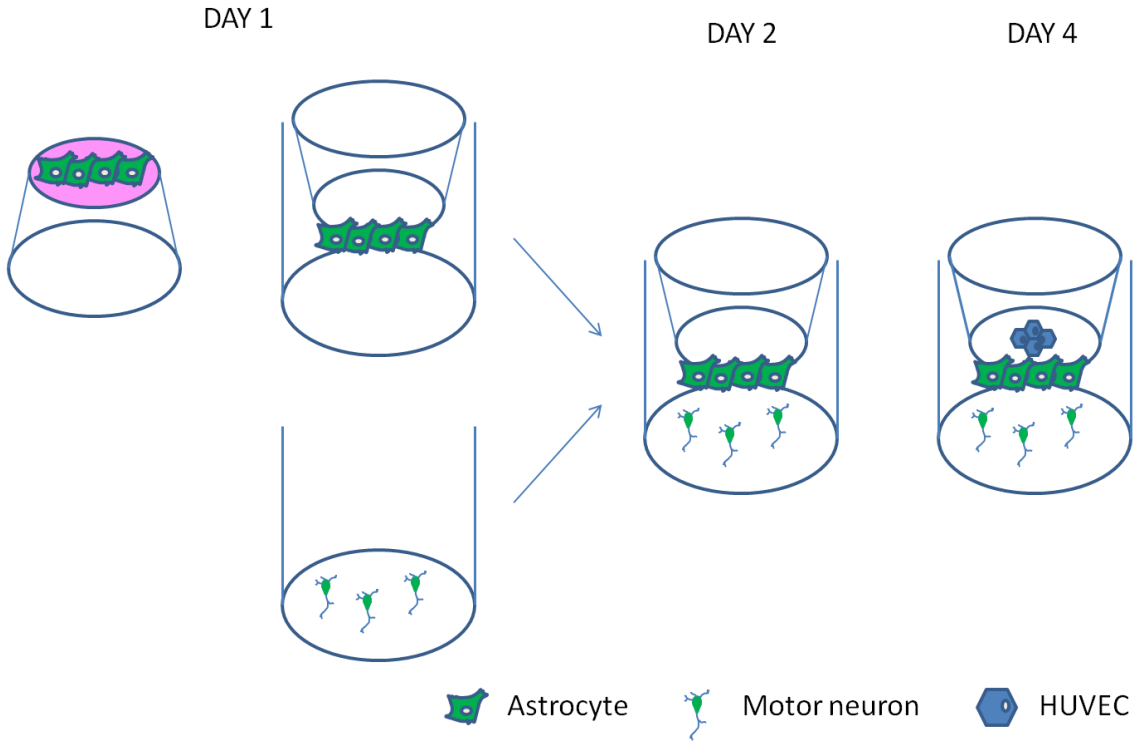

b)

	1	2	3	4	5	6
A						
B	Control BSCB	Control BSCB	Control BSCB	Control no HUVEC	Control no HUVEC	HUVEC only
C	ALS BSCB	ALS BSCB	ALS BSCB	ALS no HUVEC	ALS no HUVEC	HUVEC only
D						HUVEC only

Figure 2.1 a) Schematic of astrocyte-endothelia-motor neuron co-culture (BBB) setup. Astrocytes (2 x 10^4) were seeded onto inverted transwells for 90 minutes followed by culture for 24 hours in iAstrocyte medium. Also on day 1, GFP-motor neurons (3 x 10^4) were seeded into 24-well plates. Astrocytes and motor neurons were combined on day 2 and cultured in motor neuron medium for 2 days. On day 4, HUVECs (4 x 10^4) were added to the top chamber of transwells. Cultures were left for 3 days until day 7 before measurements of barrier integrity were performed. **b)** Diagram of plate setup for co-culture experiments. Three replicates were performed for all three cell types (BSCB) for both control and ALS, two replicates were performed for control cultures containing iAstrocytes and motor neurons but no HUVECs and three replicates were performed for control cultures containing HUVECs only.

2.2.5.4 *EPAS1* cloning

The anti-oxidant transcription factor endothelial PAS-domain containing protein 1 (*EPAS1*- also known as HIF2α) was purchased from Addgene (#18950). PCR was performed upon the plasmid isolated from the resultant cultures using the primers in Table 2.9.

Table 2.9 Primer sequences used in *EPAS1* cloning and sequencing. Recognition motifs for restriction enzymes are highlighted in red.

Primer	Restriction site	Sequence (5'-3')
Cloning		
FW (5'-3')	*Xba1*	AAAAAATCTAGAATGACAGCTGACAAGGAGAAG
RV (5'-3')	*Xba1*	AAAAAATCTAGATCAGGTGGCCTGGTCCAG
Sequencing		
LCNX Fw	N/A	AGCTCGTTTAGTGAACCGTCAGATC
EPAS1 Seq A Rv	N/A	CAATCTCACTCAGGACGTAGTTG
EPAS1 Seq B Fw	N/A	GAGGAGCTGCTTGGCCGCTCAG
EPAS1 Seq B Rv	N/A	ATGGTGGATCTGGGGGCCACTG
EPAS1 Seq C Fw	N/A	CACAGTCCCTTCCTCCTGGACAAG
pBOB Rv	N/A	GGCATTAAAGCAGCGTATCC

The PCR product was ligated into the pCR™-Blunt II-TOPO® (TOPO) vector using the Zero Blunt Topo PCR cloning kit (Invitrogen #450245). The plasmid was then transformed into One Shot TOP10 *E. coli* (Invitrogen #K2800-20) and plated onto kanamycin selection plates for 16 hours at 37˚C. Resistant colonies were picked and placed into 2mL kanamycin-TB and shaken at 225 rpm for 12 hours at 37˚C. Cultures containing the correctly orientated insert were chosen for scaling up by placing 50µL of culture into 50mL of fresh kanamycin-TB and placing on a shaker at 225 rpm for 12 hours at 37˚C. Cultures were harvested and plasmid DNA removed using the Genelute HP plasmid midi-prep kit (Sigma #NA0200-1KT). The *EPAS1* insert was removed using Xba1 and run on a 1% agarose gel containing 0.01% ethidium bromide. The band of correct size was cut from the gel and the DNA extracted using the Qiaquick Gel extraction kit (Qiagen #28706). Vector pCSC-SW-PW (pBOB) (Addgene #12335) DNA was also cut using Xba1 and dephosphorylation and ligation with insert performed using the Rapid DNA dephos and ligation kit (Roche #04898117001). The ligation was then transformed into One Shot Stbl3 *E. Coli* (Invitrogen #C7373-03) and grown for 16

hours at 37˚C on carbenicillin selection plates. Colonies were picked and expanded in carbenicillin-TB until a final culture of 1L was obtained and plasmid DNA extracted and purified using density gradient centrifugation in caesium trifluoroacetate with ethidium bromide followed by phenol-chloroform extraction. EPAS1 was sequenced externally using the primers in Table 2.9.

a)

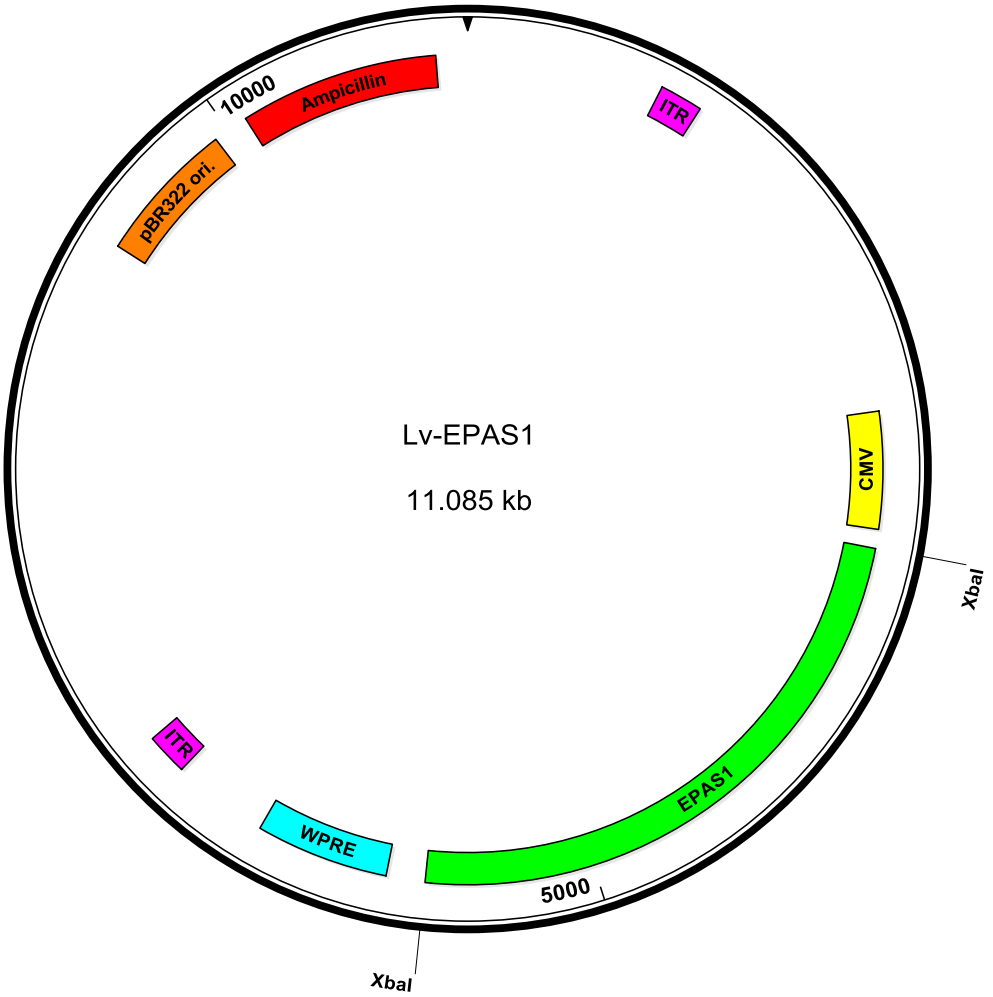

b)

Feature	Start	End
CMV promoter	2525	3029
EPAS1	3112	5724
WPRE	5893	6468
ITR	832/6886	1012/7066
pBR322 origin	9315	9934
Ampicillin resistance	10089	10949

Figure 2.2 A) Plasmid map of pBOB plasmid containing the *EPAS1* transgene and B) feature table containing locations of main features.

2.2.5.5 Lentivirus production

Lentivirus containing the plasmid with the gene of interest was produced in HEK293 cells which had been maintained in Iscove's Modified Dulbecco's Medium (IMDM; Gibco #12440053) medium (10%FBS, 1% L-glutamine, and 1% penicillin/streptomycin) in 2-chamber cellstack culture vessels (Corning #3269). On the day of transfection, media was changed 2 hours prior to addition of plasmids. Plasmids were added to 160mL of 2% IMDM at in the following amounts: MDL-helper containing gag and pol: 116.64µg; REV-helper containing rev: 45.28µg; CMV-VSV-G containing envelope gene: 60µg and plasmid containing transgene: 180µg. After 24 hours media was removed and 160mL of fresh low-serum (2% FBS) IMDM added. Media was then fully replaced at 48, 72 and 96 hours after transfection and old medium kept for virus collection. Collected medium was filtered using a 250mL vacuum filter bottle (Corning #430768) and placed into Beckman ultracentrifuge tubes (Beckman #326823) in 34mL aliquots and spun at 22500 rpm for 2 hours at 4˚C in a Sorval #630 rotor. Supernatant was decanted and virus eluted with 50µL of TNE buffer overnight at 4˚C.

2.2.5.6 Viral titration

Viral RNA was isolated using the Nucleospin RNA virus kit (Machery Nagel #PT4028-1) and subsequently titred using the Lenti-X qRT-PCR titration kit (Clontech #PT4006-2).

2.2.5.7 Transduction of iAstrocytes and HUVECs with EPAS1

Co-cultures were repeated with iAstrocytes, HUVECs, or both cell types transduced with *EPAS1* at $4.7x10^9$ copies per mL respectively corresponding to a multiplicity of infection (MOI) of 20. Virus was added in a 50µL aliquot to 7mL of medium 2 days before cells were due to be added to co-cultures. Media was changed 24 hours later. The plate setup for these experiments is shown in Figure 2.3.

Additionally, HUVECs were transduced with *EPAS1* (20MOI) in a 6 well culture dish and RNA collected after 48 hours using the Trizol method as in section 2.2.3.11. RNA was synthesised to cDNA using the Quantitect Reverse Transcription kit (Qiagen) for use in qPCR experiments.

A)

	1	2	3	4	5	6
A	Control BSCB -/+	Control BSCB +/-	Control BSCB +/+	ALS BSCB -/+	ALS BSCB +/-	ALS BSCB +/+
B	Control BSCB -/+	Control BSCB +/-	Control BSCB +/+	ALS BSCB -/+	ALS BSCB +/-	ALS BSCB +/+
C	Control BSCB -/+	Control BSCB +/-	Control BSCB +/+	ALS BSCB -/+	ALS BSCB +/-	ALS BSCB +/+
D						

B)

	1	2	3	4	5	6
A						
B		Control no HUVEC (+)	ALS no HUVEC (+)	HUVEC only (+)		
C		Control no HUVEC (+)	ALS no HUVEC (+)	HUVEC only (+)		
D				HUVEC only (+)		

Figure 2.3 Setup of plates for co-cultures where iAstrocytes, HUVECs, or both cell types had been transduced. (A) All variations of transduced BBB and B) transduced controls). -/- represents iAstrocytes/HUVECs.

2.2.5.8 Transendothelial Electrical Resistance (TEER) measurements

To measure the ease with which ions were able to pass through the BBB models, transendothelial electrical resistance (TEER) was performed using EVOM resistance measurement equipment with STX2 electrode (World Precision Instruments). An electrode is placed in each chamber of the transwell and the voltage required to reach 10µA of current measured. The EVOM uses Ohms law to produce a readout in Ohms. A fibronectin-coated transwell containing no cells was used as a blank control and values were subtracted from values for test transwells. The resultant value was divided by 0.33cm^2 (the area of the transwell) to give a final value of ohms per cm^2. An increased amount of tight junctional coupling leads to lower ion flux across the membrane and therefore higher resistance readings.

2.2.5.9 Dextran flux assay

Permeability of the BBB models to solutes was measured using FITC-conjugated 4 kDA Dextrans (Sigma Aldrich #46944). Following TEER measurement, media was removed from both chambers of test wells and replaced with 600µL of fresh media in the bottom chamber and 100µL of media containing 1mg/mL FITC-Dextran in the top chamber. Plates were incubated for 2 hours at 37˚C and 50µL aliquots of media removed from the bottom chamber into a 96 well ELISA plate. Fluorescence was read on an ELISA plate reader at 485nm excitation.

2.2.5.10 Immunocytochemistry of cells used in human functional studies

For staining of tight junction formation, HUVECs were seeded onto fibronectin coated coverslips (1:200) at a density of 40 000 cells per slip. Once confluent, medium was removed and cells were immediately fixed using a 1:1 ratio of fresh ECM: 4%PFA for 15 minutes at room temperature. Coverslips were washed three times with TBS and blocked for 1 hour at room temperature in TBS containing 10%FBS and 0.01% Triton X100. Primary antibody was put on at the dilutions indicated in Table 2.10 in blocking solution and coverslips stored at 4˚C overnight. Primary antibody was washed off three times with TBS followed by a 1 hour incubation at room temperature with secondary antibody. All secondary antibodies were used at a dilution of 1:200. Secondary antibody was removed and TBS containing DAPI (1:1000, Invitrogen) was put on the coverslips for five minutes at room temperature. TBS-DAPI was removed and coverslips were washed twice more with TBS and mounted using PVA –Dabco on glass non-coated slides. Microscopy was performed on an Olympus BX61 microscope using Slidebook software (v 5.5.4, Intelligent Imaging Innovations).

Table 2.10 Primary antibody dilutions used in immunocytochemistry of human iAstrocytes and HUVECs.

Cellular target	Antigen	Conjugate	Isotype	Host species	Raised against	Dilution	Supplier and code
Primary antibodies							
Astrocyte	α-CD44	N/A	IgG2b	Mouse	Human	1:1000	BD #550392
Astrocyte	α-S100β	N/A	IgG	Rabbit	Cow	1:500	Swant #37a
HUVEC	α-CD31	N/A	IgG1	Mouse	Human Mouse	1:500	AbCam #ab24590
HUVEC	α-Cldn5	N/A	IgG	Rabbit	Human	1:250	AbCam ab#131259
HUVEC	α-ZO1	N/A	IgG	Rabbit	Mouse Chicken Dog Human	1:100	Abcam #ab59720
HUVEC	α-Occludin	N/A	IgG	Rabbit	Dog Rat Human	1:100	Invitrogen #71-1500
Secondary antibodies							
	Rabbit FC region	Alexa fluor 488	IgG	Goat	Rabbit	1:200	Life #A11008
	Mouse FC region	Alexa fluor 488	IgG	Goat	Mouse	1:200	Life #A11001
	Mouse FC region	Cy3	IgG	Goat	Mouse	1:200	Life #A10521

CHAPTER 3

RESULTS

Gene expression profiling of SOD1^{G93A} astrocytes from symptomatic and late-stage disease

3 Results: Gene expression profiling of SOD1^{G93A} astrocytes from symptomatic and late-stage disease

3.1 Introduction

Microarray analysis was performed upon SOD1^{G93A} and NTg control astrocytes isolated by LCM from the ventral horn of the lumbar spinal cord in symptomatic (90 day old) and late-stage (120 day old) mice. Astrocytes from SOD1^{WT} overexpressing mice were not analysed due to the low number of differences seen between SOD1^{WT} and NTg controls from previous studies of LCM motor neurons (Ferraiuolo et al., 2007) and from the functional studies performed in the analysis of presymptomatic SOD1^{G93A} astrocytes (Ferraiuolo et al., 2011a). The hypothesis to be tested was that SOD1^{G93A} transgenic mice possess dysregulated gene expression that reveals the contribution of astrocytes to motor neuron death throughout the disease course. This was followed by enrichment analysis to identify targets for investigation by functional validation studies.

3.2 Quality control of astrocyte GeneChips

Quality control (QC) analysis of the astrocyte microarray data showed the GeneChip results from the symptomatic stage to be similar in percentage present call (mean = 50.42, range = 36.27-57.81) and scaling to the chips from the late-stage time-point (Figure 3.1). Affymetrix recommend that scale factors should be within 3-fold of each other for successful comparisons (Wilson et al.), and only one GeneChip (2835) fell outside these criteria when all GeneChips were analysed together (see blue strip in Figure 3.1). Within the symptomatic and late-stage groups, all GeneChips were within a 3-fold scaling factor of each other. *Actin* and *Gapdh* 3'-5' ratios were comparable for all GeneChips (*Actin* mean = 5.08, range = 3.89-5.89, *Gapdh* mean = 4.42 range = 3.51-5.16) and all six GeneChips within each time point showed similar mean RNA degradation patterns (Figure 3.2).

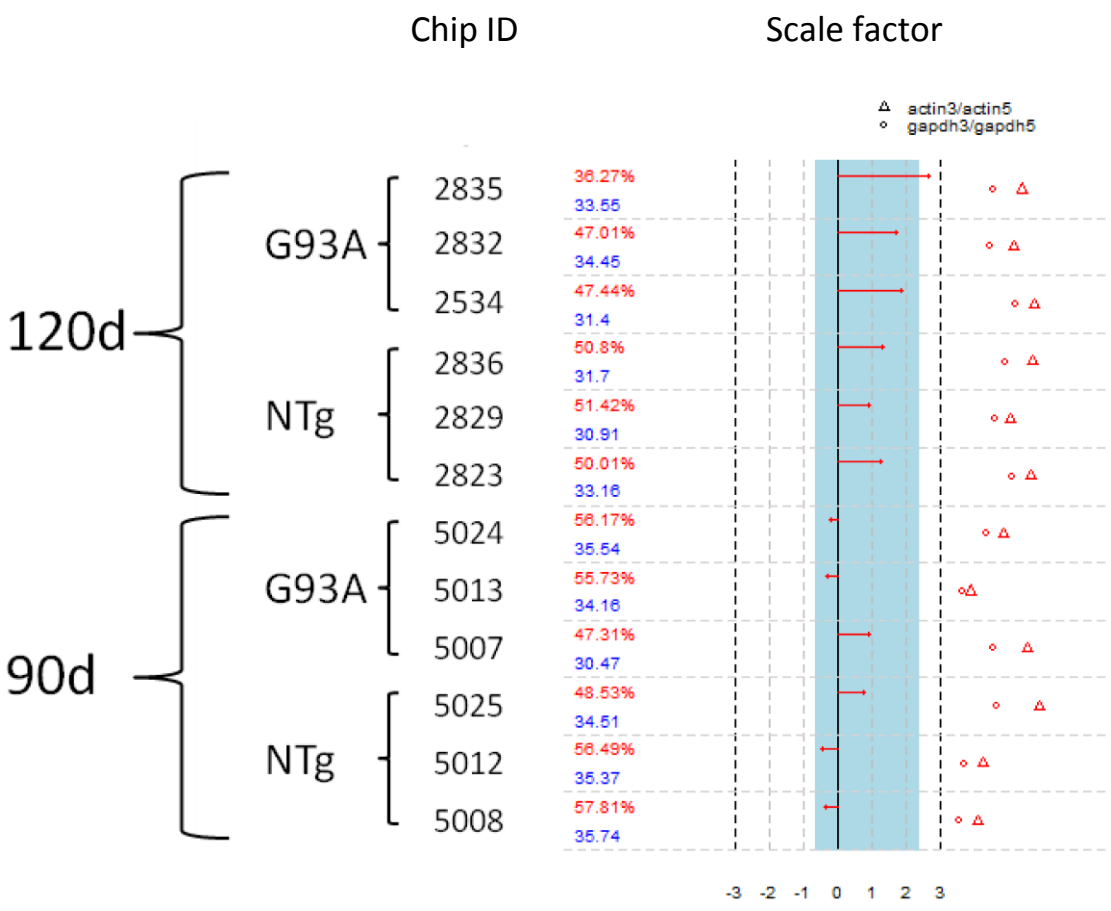

Figure 3.1 Quality control of symptomatic and late-stage microarray chips for SOD1^{G93A} and NTg control astrocytes. Pre-normalisation performed in Bioconductor using the simpleaffy package. Chips are listed on the left, percentage present call is in red, average background is in blue to the right of chip ID. The scale factor graph to the right of each chip represents the signal intensity for each chip. The blue strip represents the range where the individual average chip intensities are within three-fold of the overall chip intensity. The symptomatic and late-stage time-points are similar both in terms of percentage present call and also in scale factor. On the far right of the figure are triangles and circles indicating the ratio of 5' actin to 3' actin and 5'gapdh to 3'gapdh respectively. This is a measure of RNA degradation; when the symbol is coloured red it indicates a greater than 3-fold ratio between the 3' and 5' ends of the transcript.

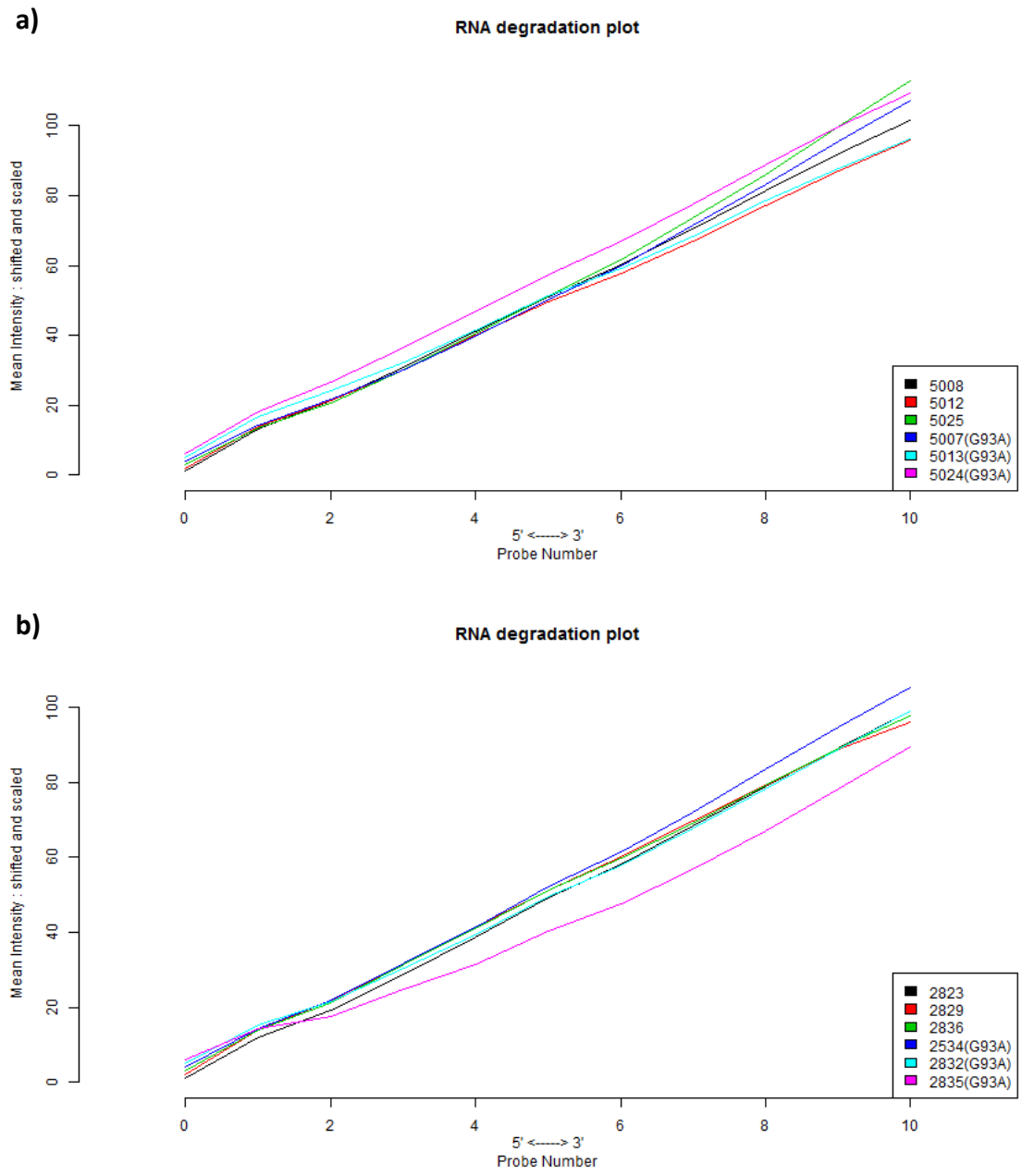

Figure 3.2 RNA degradation plot showing the mean intensity of probes, from the 5' to the 3' ends of their respective target sequence, for each of the **a)** symptomatic GeneChips and **b)** late-stage GeneChips. All arrays are similar to each other in RNA degradation profile.

3.3 Symptomatic GeneChip quality control analysis

Normalised unscaled standard error (NUSE) and relative log expression (RLE) plots are both measures of assessing array quality included within the *simpleaffy* package (Miller) in Bioconductor. NUSE plots allow comparisons of the standard error for probesets on each array (Figure 3.3). Each probeset on the array is normalised by

setting its median standard error across the GeneChips as 1 (Eijssen et al., 2013, Hruz et al., 2008, Genevestigator.com). Consequently a poor quality GeneChip will have a larger standard error than 1 for the majority of its probesets and will show as higher on the graph. A NUSE score of 1.1 is considered a sign of a poor quality array. The GeneChips used for analysis of symptomatic SOD1^{G93A} and NTg astrocytes are all below the 1.1 level. The higher position and larger spread of values for 5025 (SOD1^{G93A}) and 5007 (NTg) are indicative of slightly lower quality data for these arrays (Figure 3.3). However, these two GeneChips are split between the two conditions and all other GeneChips are of good quality, therefore all GeneChips were carried forward to downstream analysis.

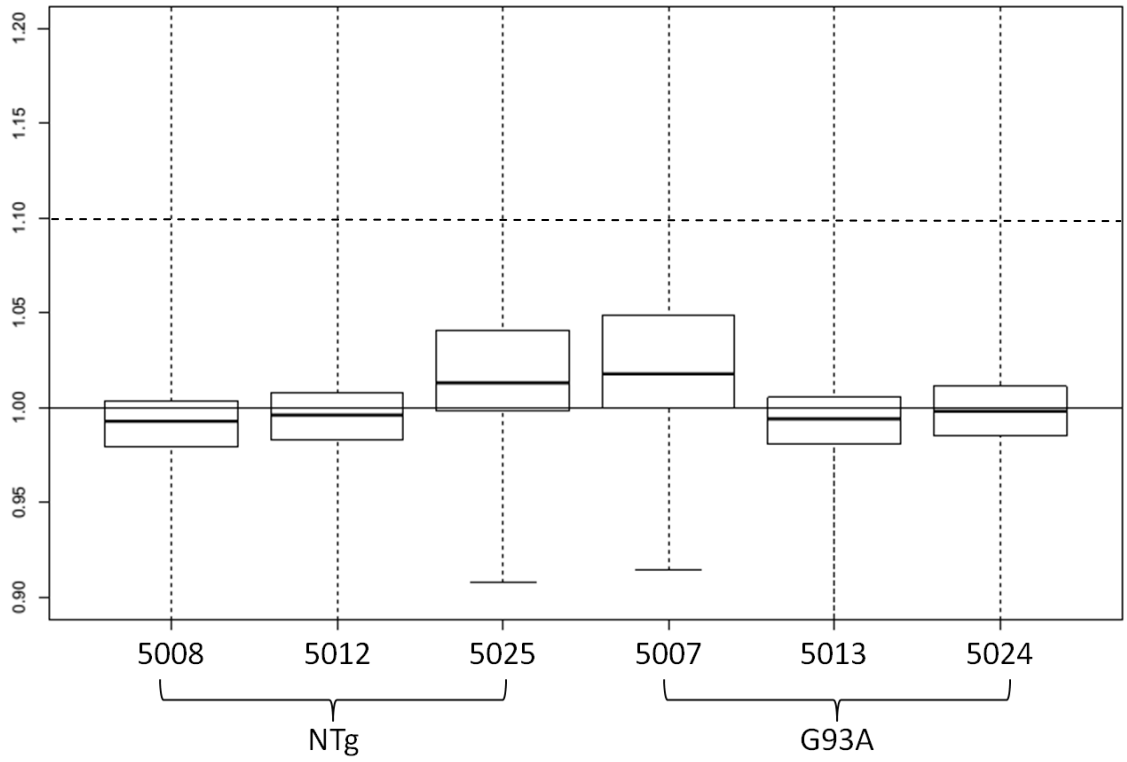

Figure 3.3 Normalised unscaled standard error (NUSE) plot for GeneChips from symptomatic SOD1^{G93A} astrocytes and NTg controls. Probesets have been normalised across arrays such that for each probeset the median expression across arrays is equal to one. Therefore lower quality GeneChips have a standard error greater than one and show as higher on the plot. An average level of 1.1 (dotted line) indicates a low quality array. Although 5025 and 5007 are of a lower quality than the other arrays in the experiment, they are below the 1.1 level and are split between the conditions.

The relative log expression (RLE) plot is another method of visualising array quality. RLE values are derived by dividing the probeset expression level by the median expression level for that probeset across the arrays in the experiment. Thus, RLE shows how much a particular GeneChip deviates from the group of GeneChips as a whole. Poorer quality GeneChips will show a larger spread of values. As with the NUSE plot, 5025 ($SOD1^{G93A}$) and 5007 (NTg) are a poorer quality than the rest of the GeneChips used in the experiment but are still centred close to 0 and are only slightly larger in terms of data-spread (Figure 3.4).

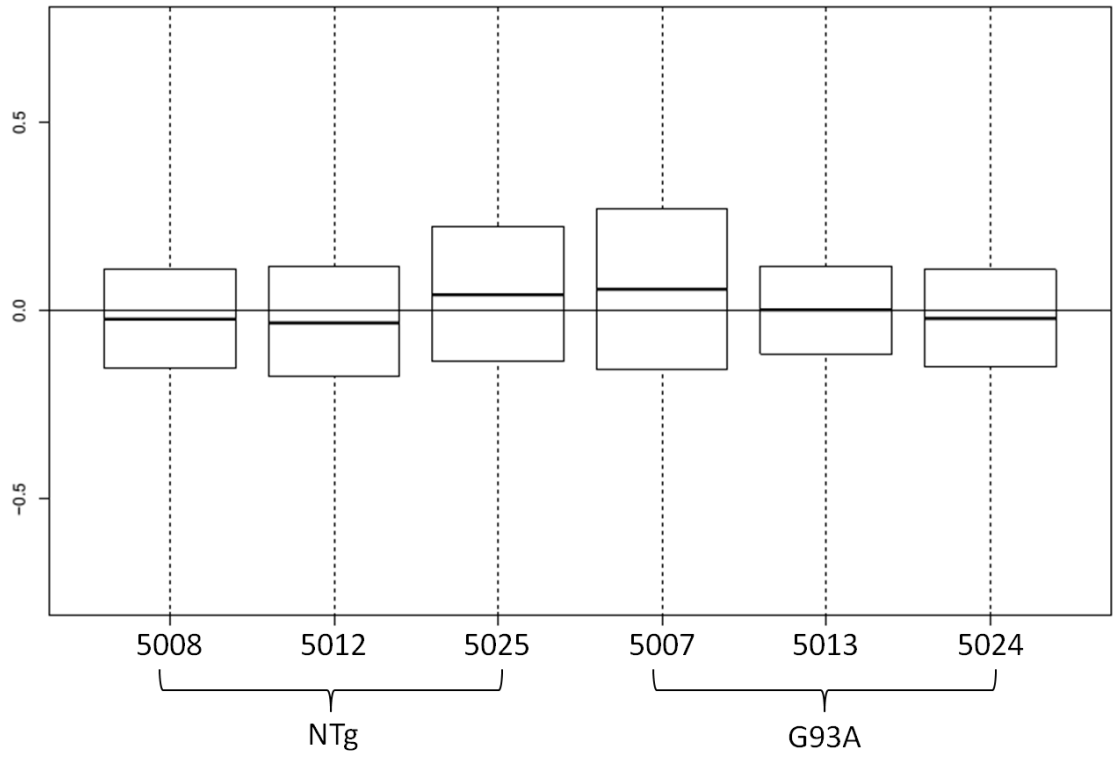

Figure 3.4 Relative log expression (RLE) for the GeneChips used in analysis of symptomatic $SOD1^{G93A}$ astrocytes. The RLE is derived by dividing probeset expression level by the median expression level for that probeset on all GeneChips. The more variable a GeneChip is from the median, the larger its spread of values on the RLE plot. There is a bigger spread of values for the 5025 and 5007 GeneChips, implying that these arrays are of a lower quality than those in the rest of the experiment.

Following the results of the NUSE and RLE plots, the signal intensities across the arrays were analysed. This step can help to identify outlying arrays which have average intensity different to the group as a whole. As can be seen in Figure 3.5a, 5025 and 5007 have a greater amount of probesets with a lower signal intensity in comparison to the other four GeneChips. This indicates that the quality control issues are due to inefficient hybridisation of target cRNA to probes. GeneChips were normalised using the PLIER algorithm, in keeping with a previous analysis of pre-symptomatic astrocytes performed by Ferraiuolo et al. (2011a). The PLIER algorithm uses data from the mismatch probe (MM) to calculate background signal and subtracts this from the perfect match (PM) probe giving a signal intensity value. This value is then normalised across arrays using quantile normalisation. Following normalisation GeneChips 5025 and 5007 showed similar profiles to the rest of the GeneChips in the experiment (Figure 3.5b).

a)

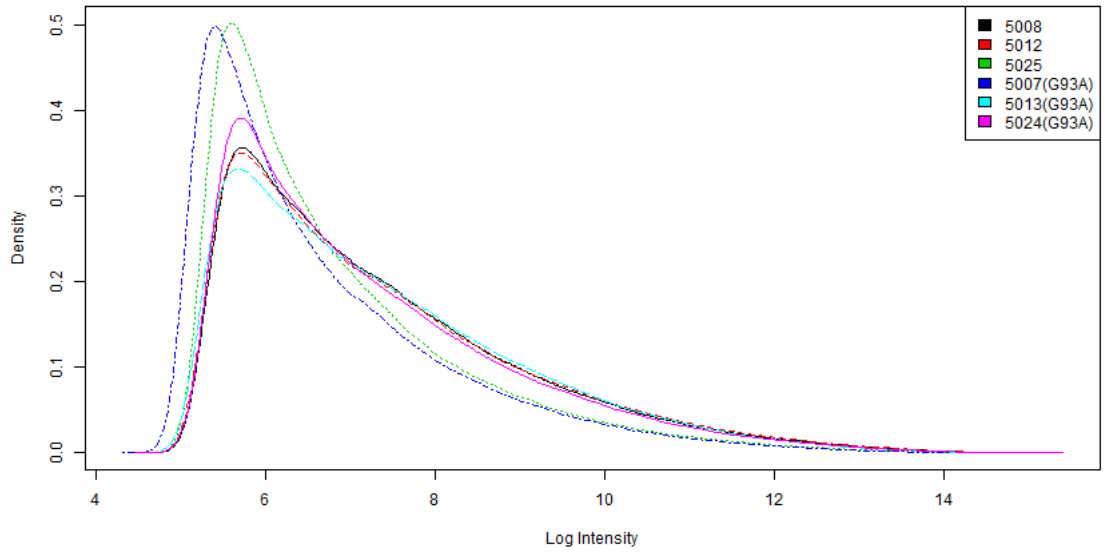

b)

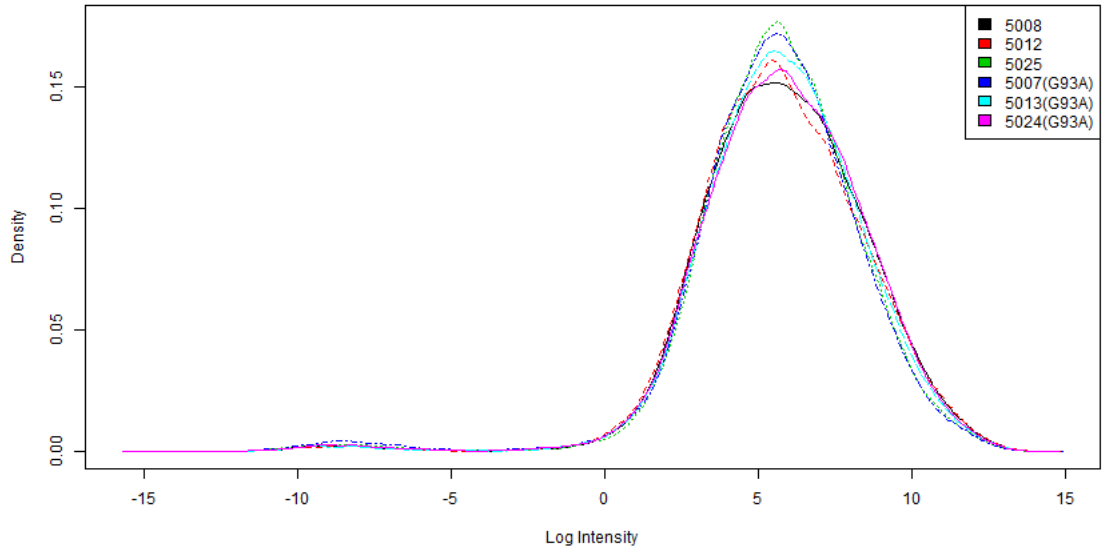

Figure 3.5 Density plot of log intensity values for symptomatic SOD1^{G93A} astrocytes and NTg controls prior to (a) and following (b) normalisation. **a)** Even before the normalisation step all six arrays show a similar distribution in intensity values indicating a similar level of hybridisation. **b)** After the normalisation step all six arrays are very similar in their distribution of intensity values indicating that normalisation was effective.

3.4 Late-stage GeneChip analysis

GeneChips for late-stage SOD1^{G93A} and NTg astrocytes were analysed using the same quality control measures as for the symptomatic GeneChips. As shown in Figure 3.1, Figure 3.2b and Figure 3.6. to Figure 3.8 the late stage analysis suggests an outlying GeneChip: 2835 (SOD1^{G93A}). This GeneChip has a lower percentage present call versus the average of all GeneChips (Figure 3.1Figure 3.1) and shows a lower quality when looking at the NUSE (Figure 3.6) and RLE (Figure 3.7) plots where it contains a larger spread of values. However 2835 is within the three-fold scale factor required by Affymetrix to analyse GeneChips as a group, *Actin* and *Gapdh* 3'-5' ratios are similar for all GeneChips (Figure 3.1), the entire group of arrays show a similar RNA degradation profile (Figure 3.2), and the NUSE plot is centred below 1.1 (Figure 3.6). Pre normalisation there is a slightly higher density of intensities at the lower end of the scale compared to the other late-stage GeneChips (Figure 3.9). However, following normalisation the similarity between intensities of the late-stage GeneChips is improved. Therefore it was decided to keep 2835 within the experiment and proceed with further analysis.

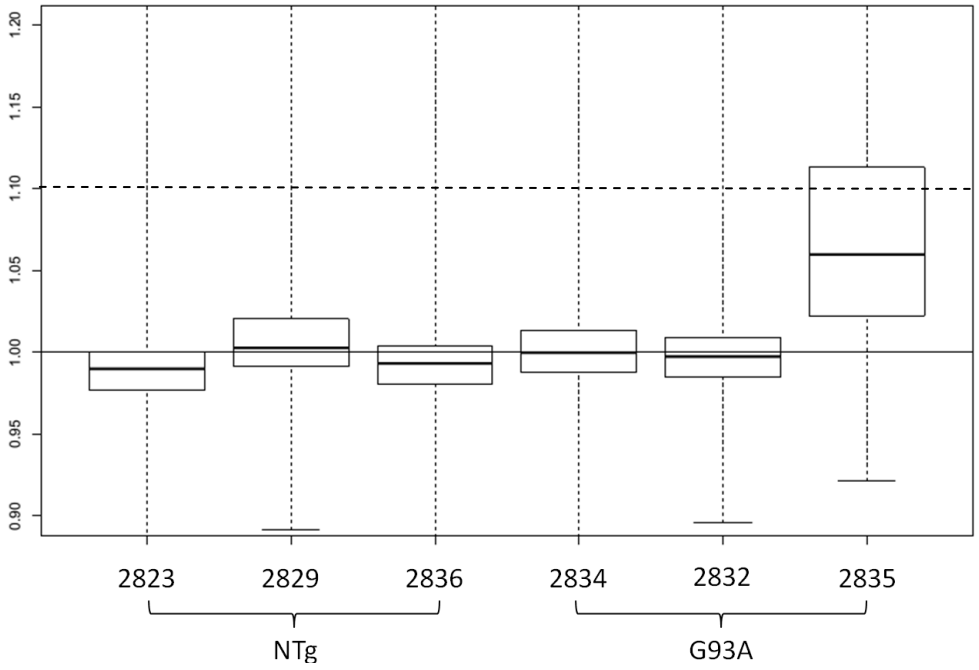

Figure 3.6 NUSE plot for late stage SOD1^{G93A} and NTg astrocytes. As described in (Figure 3.3), probesets have been normalised across arrays such that for each probeset the median expression across arrays is equal to one. Lower quality GeneChips have a standard error greater than one and show as higher on the plot. An average level of 1.1 (dotted line) indicates a low quality array. Array 2835 is clearly an outlier in this analysis and of a lower quality than the other late-stage GeneChips.

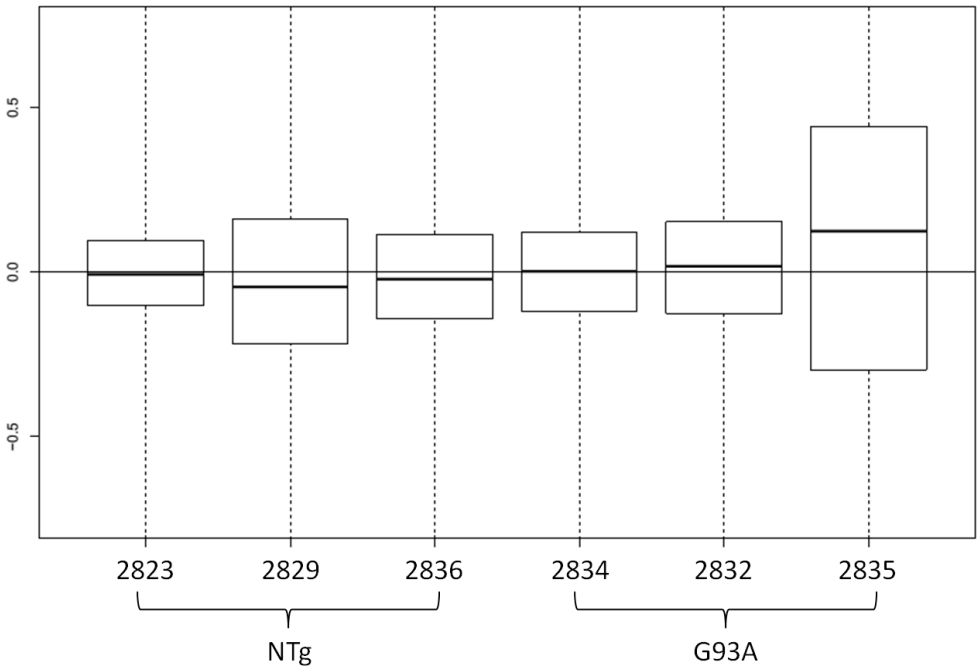

Figure 3.7 RLE plot for late stage SOD1^{G93A} and NTg astrocytes. Array 2835 is lower quality than the rest of the arrays as many more of its probesets deviate from the median values obtained from the whole group.

a)

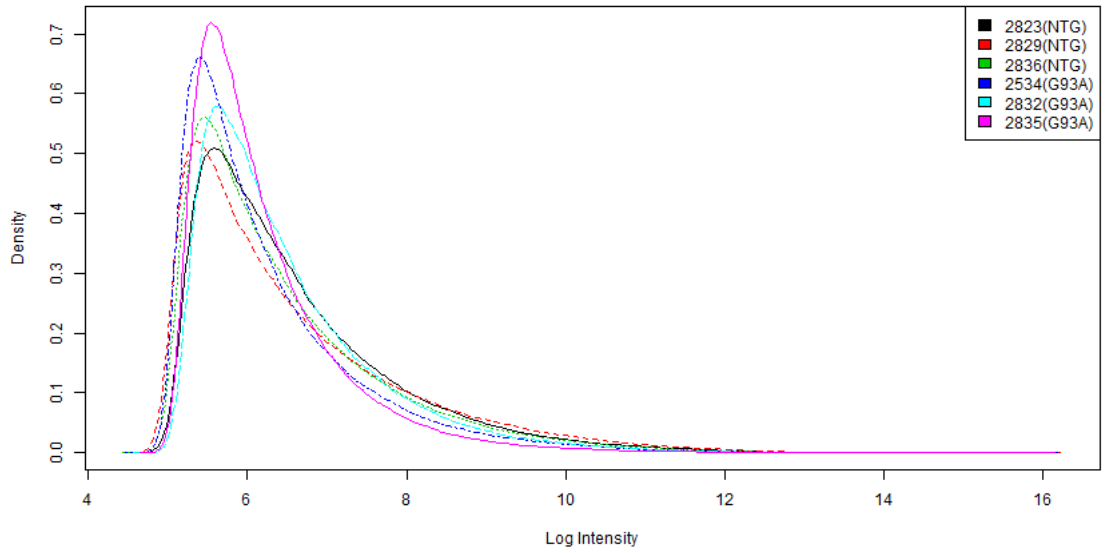

b)

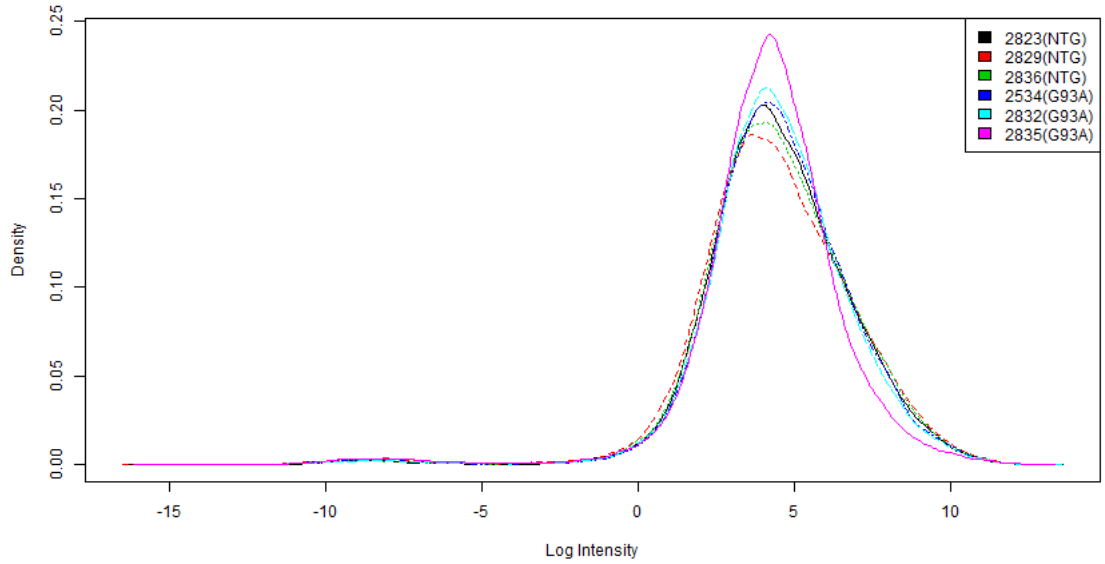

Figure 3.8 Density plot of log intensity for late-stage SOD1^{G93A} and NTg astrocytes **a)** before and **b)** after normalisation. **a)** All GeneChips show a similar shaped curve with no outliers in terms of log intensity. Even the outlier 2835, identified through the NUSE and RLE plots, was in line with other GeneChips. **b)** The similarity between GeneChips was further improved following normalisation.

3.5 Enrichment of glial cellular markers

Markers of different cell types present within isolated astrocytes from the murine spinal cord were looked at in terms of PLIER-normalised expression value to determine the degree of enrichment for astrocytes on the arrays (Figure 3.9). Astrocyte markers *Gfap*, *S100b*, and *Aqp4* were enriched within both datasets, particularly in comparison to markers of microglia, endothelia and pericytes. *Gfap,* a marker of astrocyte activation, was increased in expression in SOD1^{G93A} versus NTg, as was *Aqp4*. In contrast S100b appeared decreased in SOD1^{G93A} versus NTg. The oligodendrocyte markers *Mbp* and *Mobp* were also enriched within the dataset for both the symptomatic and late-stage GeneChips. A table of individual expression values for all transcripts is provided in Appendix 2.

To assess whether cellular markers of other cell types (such as *Mbp*) might be expressed by astrocytes, and therefore represent astrocyte signal on the arrays, GeneChips from cultured SOD1^{G93A} and NTg astrocytes previously analysed at The University of Sheffield were processed using PLIER and the expression levels of different cellular markers assessed (Figure 3.10). These cultures represent a ≥95% pure population of astrocytes, and astrocytic markers such as *Aqp4*, *Gfap* and *Aldh1l1* are enriched within the dataset in comparison to markers of other cell types. In contrast to LCM-captured material, transcripts representing oligodendrocytes are low upon these arrays. In summary, the LCM-captured material represents an enriched population of astrocytes and oligodendrocytes. For simplicity, material will hereafter be referred to as astrocytic in origin and functional experiments will be used to confirm astrocytic contribution.

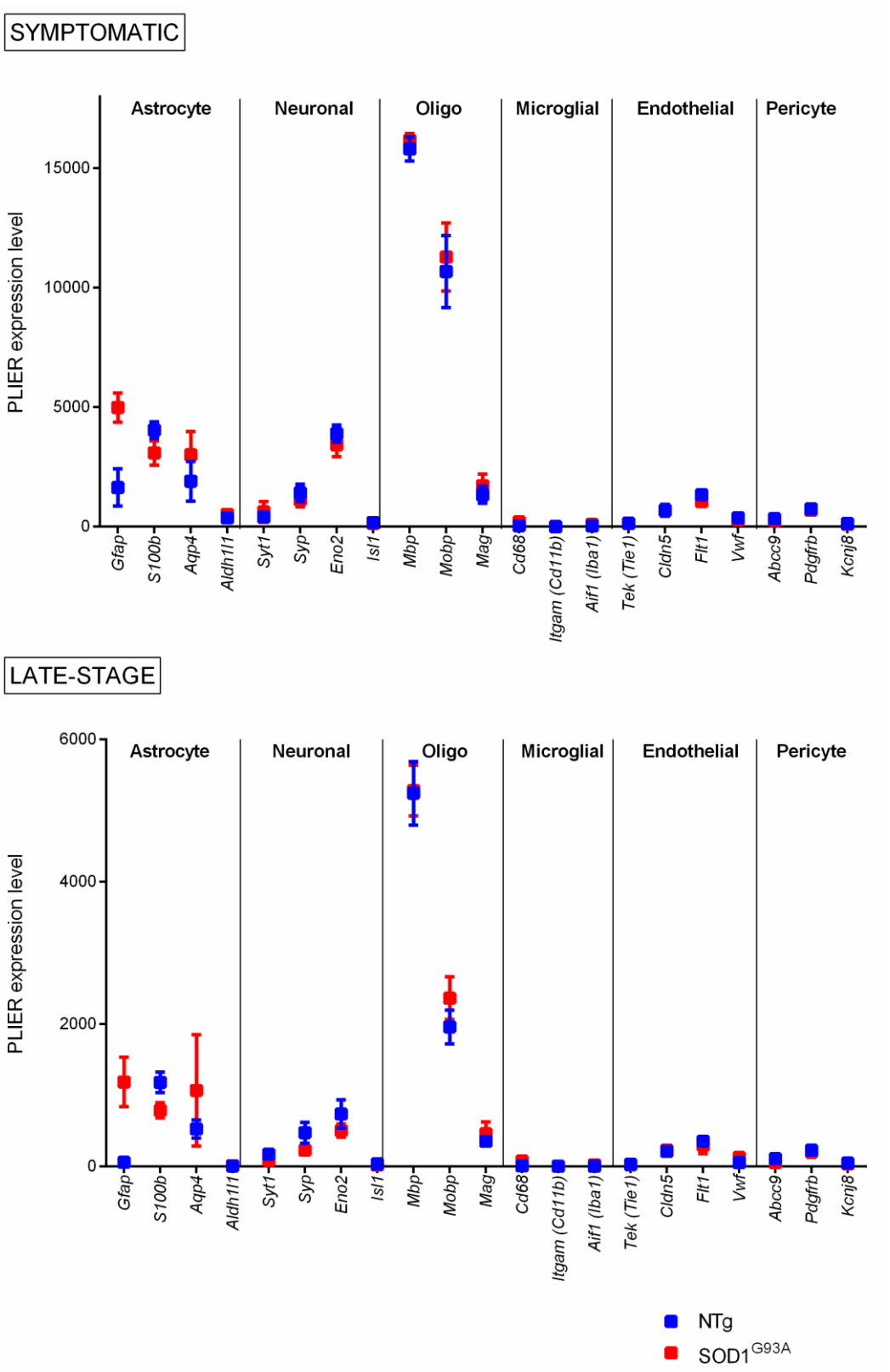

Figure 3.9 PLIER expression values for different cellular markers upon the symptomatic and late-stage GeneChips. In circumstances where multiple probesets are present for a marker, the highest expression levels have been used. On both arrays there is enrichment of astrocyte markers and also of oligodendrocyte markers, whilst markers of neurons, microglia, endothelia and pericytes are comparatively low. Error bars = standard deviation.

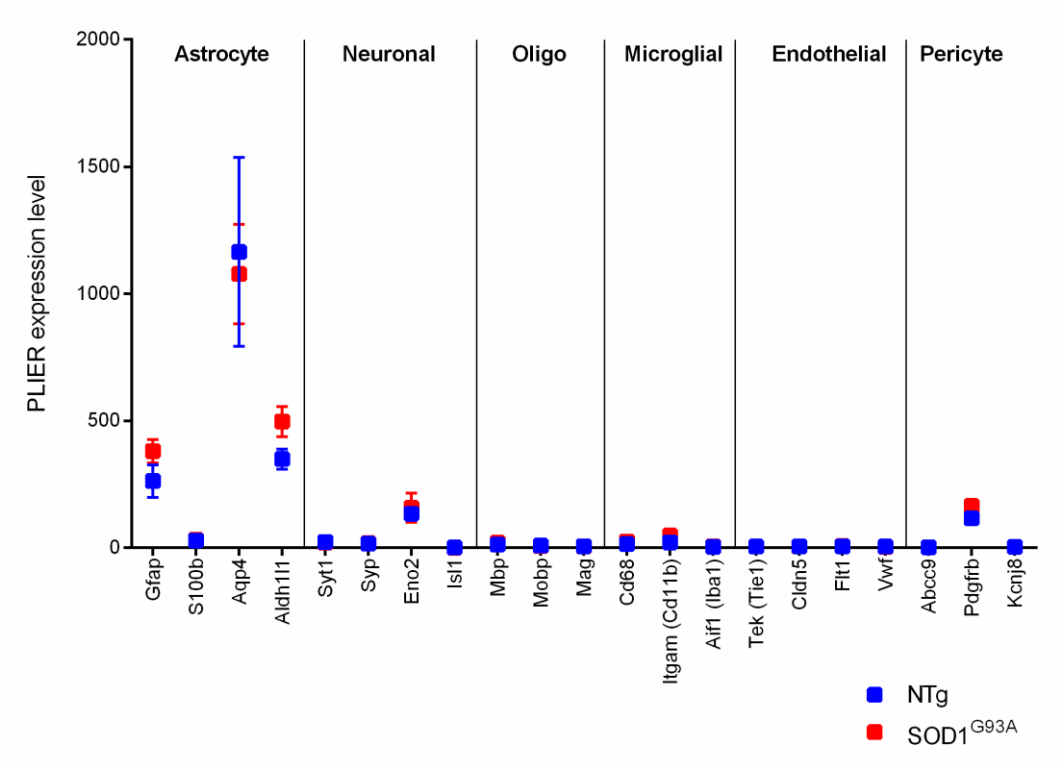

Figure 3.10 PLIER expression values for different cellular markers upon the GeneChips generated from cultured SOD1^{G93A} astrocytes and NTg controls. GeneChips show a high expression level for astrocyte markers such as *Gfap*, *Aqp4* and *Aldh1l1* whereas markers of other cell types are comparatively low. Error bars = standard deviation.

3.6 Differential expression analysis results

A list of genes with FC≥2 and p<0.05 for both symptomatic and late-stage categorised by gene function is shown in Appendix 3. The fold change cutoff of 2 or greater and p-value threshold of 0.05 were chosen for consistency with the presymptomatic dataset from Ferraiuolo et al. (2011a) and to give a smaller gene list that was easier to analyse. At the symptomatic time point 321 probesets were differentially expressed with fold change ≥ 2 and p<0.05 in SOD1^{G93A} astrocytes compared to NTg controls, with 139 probesets showing decreased expression and 182 probesets increased expression. Due to the presence of multiple probesets for certain transcripts, this corresponded to 117 transcripts decreased in expression and 159 transcripts increased in expression. At late-stage 2066 probesets were differentially expressed with fold change ≥2 and p≤0.05, with 1595 probesets showing decreased expression and 471 probesets with

increased expression. This corresponded to 1330 transcripts decreased and 355 transcripts increased in expression.

3.7 Analysis of differentially expressed genes in symptomatic and late-stage SOD1^{G93A} astrocytes

The gene lists obtained for the symptomatic and late-stage astrocytes were submitted to the Database for Annotation, Visualisation and Integrated Discovery (DAVID) online analysis software to identify enriched gene categories within the dataset. The functional annotation clustering tool allows annotations from multiple databases to be aggregated and combined for each probeset. The degree of enrichment of an annotation term in the gene list compared to what would be expected at random can be calculated.

3.7.1 Enrichment analysis of differentially expressed genes from symptomatic SOD1^{G93A} astrocytes

Differentially expressed transcripts from SOD1^{G93A} astrocytes extracted at the symptomatic disease stage were subjected to functional annotation clustering using DAVID. The most enriched categories within the dataset were those involved in channel activity and ion homeostasis (ranked 1 and 10), those involved in possible immune function (ranked 2, 3, 4, 6, 7, 8 and 9) and the lysosome (ranked 5) (Table 3.1).

Functional annotation clustering of the full gene list does not show which categories are increased or decreased in expression in SOD1^{G93A} vs. NTg astrocytes. Therefore, to assess enrichment within up-regulated and down-regulated transcripts separately, the gene list was split based upon direction of regulation and reanalysed in DAVID (Table 3.2 and Table 3.3). The most enriched categories within the up-regulated genes were those involved in phagocytosis (ranked 1, 3 and 5), the lysosome (ranked 2) and other categories involving the immune response (ranked 4, 6, 7 and 8). In terms of down-regulated transcripts, most of the gene categories were involved in ion homeostasis (ranked 1-5, 7 and 9). The top five clusters for the up-regulated transcripts contained annotation terms that passed a false discovery rate (FDR) of ≤ 0.05, whereas for the down-regulated transcripts the top 4 clusters contained annotation terms that passed below an FDR cut-off of 0.05 (for full details of clustering analysis see Appendices 4-6).

Table 3.1 All differentially expressed transcripts in symptomatic SOD1^{G93A} astrocytes with p≤0.05 and FC≥2 were put through the DAVID functional annotation clustering tool on highest stringency settings using the databases for Gene Ontology (GO) Biological Process, Cellular Component and Molecular Function. The top 10 enriched categories ranked by DAVID enrichment score are summarised. Count = number of genes in list belonging to category, % = percentage of gene list made up by these genes, PValue is derived by comparison to the amount of enrichment that would be expected in a gene list based on the whole genome. The DAVID enrichment score is calculated based upon the significance of individual annotation enrichments within each cluster, the higher the significance of cluster terms the higher the enrichment score.

	Summarised Cluster Term	# genes	% of gene list	Most significant cluster term	p (most sig term)	DAVID Enrichment score
1	Ion homeostasis	16	5.84	GO:0006873~cellular ion homeostasis	6.38E-05	3.70
2	Immune response/antigen presentation	4	1.46	GO:0019864~IgG binding	4.71E-05	2.97
3	Regulation of immune effector process	7	2.55	GO:0002706~regulation of lymphocyte mediated immunity	6.10E-04	2.92
4	Complement pathway	5	1.82	GO:0006958~complement activation, classical pathway	8.98E-04	2.83
5	Lysosome	11	4.01	GO:0005764~lysosome	0.001754	2.62
6	Regulation of response to external stimulus	4	1.46	GO:0002863~positive regulation of inflammatory response to antigenic stimulus	3.24E-04	2.51
7	Positive regulation of immune effector process	5	1.82	GO:0002708~positive regulation of lymphocyte mediated immunity	0.003036	2.44
8	Positive regulation of acute inflammatory response	3	1.09	GO:0001803~regulation of type III hypersensitivity	0.001	2.42
9	Leukocyte proliferation	5	1.82	GO:0042098~T cell proliferation	0.001	2.38
10	Channel activity	14	5.11	GO:0022838~substrate specific channel activity	0.005	2.28

Table 3.2 Up-regulated transcripts (FC≥2, p≤0.05) in symptomatic SOD1^{G93A} astrocytes were analysed by functional annotation clustering in DAVID and clusters are summarised as in Table 3.1. Categories relating to immune function are enriched within the dataset, including phagocytosis and the lysosome.

	Summarised Cluster Term	# genes	% of gene list	Most significant cluster term	p (most sig term)	DAVID Enrichment score
1	Regulation of endocytosis/phagocytosis	7	4.46	GO:0050766~positive regulation of phagocytosis	4.77E-08	5.94
2	Lysosome	11	7.00	GO:0005764~lysosome	3.95E-06	5.22
3	Phagocytosis/endocytosis	8	5.10	GO:0006909~phagocytosis	2.94E-07	4.01
4	Regulation of immune effector process	6	3.82	GO:0002712~regulation of B cell mediated immunity	7.21E-06	4
5	Immune response/antigen presentation	4	2.55	GO:0019864~IgG binding	5.60E-06	3.32
6	Cell proliferation	5	3.18	GO:0042098~T cell proliferation	1.18E-04	2.85
7	Positive regulation of immune effector process	4	2.55	GO:0002714~positive regulation of B cell mediated immunity	2.57E-04	2.74
8	Positive regulation of response to external stimulus	3	1.91	GO:0001803~regulation of type III hypersensitivity	2.50E-04	2.55
9	Regulation of cytoskeleton organisation	5	3.18	GO:0032956~regulation of actin cytoskeleton organization	0.002	2.39
10	Positive regulation of cell death	8	5.10	GO:0043065~positive regulation of apoptosis	0.008	2.08

Table 3.3 Down-regulated transcripts (FC≥2, p≤0.05) in symptomatic SOD1^{G93A} astrocytes were analysed by functional annotation clustering in DAVID and clusters are summarised as in Table 3.1. Most enriched categories relate to ion transport and channel activity.

	Summarised Cluster Term	# genes	% of gene list	Most significant cluster term	p (most sig term)	DAVID Enrichment score
1	Voltage-gated channel activity	8	6.84	GO:0022843~voltage-gated cation channel activity	1.63E-06	5.08
2	Gated channel activity	9	7.69	GO:0005261~cation channel activity	1.47E-05	4.74
3	Channel activity	10	8.55	GO:0005216~ion channel activity	2.78E-05	4.44
4	Potassium ion transport	7	5.98	GO:0030955~potassium ion binding	2.06E-05	3.67
5	Ion homeostasis	7	5.98	GO:0006873~cellular ion homeostasis	0.004	1.95
6	Regulation of neurogenesis	4	3.42	GO:0045664~regulation of neuron differentiation	0.02	1.43
7	Cation homeostasis	4	3.42	GO:0006875~cellular metal ion homeostasis	0.02	1.40
8	Positive regulation of immune response	4	3.42	GO:0050778~positive regulation of immune response	0.04	1.18
9	Ion binding	23	19.66	GO:0046872~metal ion binding	0.11	0.92
10	Muscle development	3	2.56	GO:0007519~skeletal muscle tissue development	0.07	0.87

3.7.2 Enrichment analysis of differentially expressed genes from late-stage SOD1^{G93A} astrocytes

Enrichment analyses for late-stage SOD1^{G93A} astrocytes were performed as per the symptomatic gene list (section 3.6.1). As with the symptomatic analysis (Table 3.1), a similar pattern was observed where the highest ranked categories for all genes involved channel activity (Table 3.4). However there was a lower enrichment of transcripts involved in the immune response and a greater enrichment of transcripts involved in ATP biosynthesis (ranked 2, 4, 5, 6 and 7).

When the gene list was divided into up and down-regulated genes a similar pattern to the symptomatic time-point was observed in the up-regulated transcripts, where lysosomal genes (Lysosome, rank 1) were the most enriched in the up-regulated gene list (Table 3.5) and phagocytosis transcripts were also enriched (rank 3). In the down-regulated gene list, transcripts involved in ion homeostasis were the most enriched with ATP metabolism featuring in many of the other top-ranked categories (Table 3.6). Only the “lysosome” cluster contained annotations that passed a false discovery rate (FDR) of 0.05 for the up-regulated transcripts whereas the clusters “channel activity”, “nucleoside binding” and “cellular protein catabolic process” contained annotation terms that passed FDR ≤ 0.05 for the down-regulated transcripts (for full details of clustering analysis see Appendix 7-9).

Table 3.4 All differentially expressed transcripts in late-stage SOD1^{G93A} astrocytes with p≤0.05 and FC≥2 were put through the DAVID functional annotation clustering tool on highest stringency settings. The top 10 enriched categories are summarised as in Table 3.1.

	Summarised Cluster Term	# genes	% of gene list	Most significant cluster term	p (most sig term)	DAVID Enrichment score
1	Channel activity	62	3.71	GO:0022838~substrate specific channel activity	6.56E-06	5.05
2	Nucleotide biosynthesis	31	1.85	GO:0009165~nucleotide biosynthetic process	0.002901	2.41
3	Cellular protein catabolic process	71	4.25	GO:0019941~modification-dependent protein catabolic process	0.003951	2.14
4	ATPase activity coupled to transmembrane movement of substances	18	1.08	GO:0043492~ATPase activity, coupled to movement of substances	0.013	1.88
5	ATP metabolic process	18	1.08	GO:0046034~ATP metabolic process	0.008	1.70
6	Nucleoside triphosphate biosynthetic process	17	1.02	GO:0006754~ATP biosynthetic process	0.008	1.66
7	Nucleoside binding	173	10.35	GO:0030554~adenyl nucleotide binding	0.04	1.35
8	Cyclic nucleotide biosynthetic process	6	0.36	GO:0016849~phosphorus-oxygen lyase activity	0.06	1.18
9	Ion transmembrane transport	8	0.48	GO:0015985~energy coupled proton transport, down electrochemical gradient	0.07	1.08
10	Negative regulation of lipid/steroid biosynthesis	3	0.18	GO:0010894~negative regulation of steroid biosynthetic process	0.06	0.98

Table 3.5 Up-regulated transcripts (FC≥2, p≤0.05) in late-stage SOD1^{G93A} astrocytes were analysed by functional annotation clustering in DAVID and clusters are summarised as in Table 3.1. As in the symptomatic analysis, the lysosomal and phagocytic pathways are enriched along with several other immune-related pathways.

	Summarised Cluster Term	# genes	% of gene list	Most significant cluster term	p (most sig term)	DAVID Enrichment score
1	Lysosome	16	4.64	GO:0005764~lysosome	1.71E-05	4.55
2	Complement pathway	6	1.74	GO:0006958~complement activation, classical pathway	2.52E-04	3.33
3	Positive regulation of endocytosis/phagocytosis	6	1.74	GO:0050766~positive regulation of phagocytosis	7.64E-05	2.99
4	Positive regulation of locomotion	6	1.74	GO:0030335~positive regulation of cell migration	0.001759	2.57
5	Regulation of immunoglobulin mediated immune response	4	1.16	GO:0002891~positive regulation of immunoglobulin mediated immune response	0.001	2.30
6	Negative regulation of kinase activity	6	1.74	GO:0006469~negative regulation of protein kinase activity	0.008129	2.07
7	Protein maturation	7	2.03	GO:0051605~protein maturation by peptide bond cleavage	0.003	2.02
8	Positive regulation of acute inflammatory response	3	0.87	GO:0002894~positive regulation of type II hypersensitivity	0.006	2.01
9	Regulation of phosphate metabolic process	15	4.35	GO:0042325~regulation of phosphorylation	0.01	1.91
10	Regulation of adaptive immune response	5	1.45	GO:0002821~positive regulation of adaptive immune response	0.005	1.90

Table 3.6 Down-regulated transcripts (FC≥2, p≤0.05) in late-stage SOD1^{G93A} astrocytes were analysed by functional annotation clustering in DAVID and clusters are summarised as in Table 3.1. As in the symptomatic analysis, several terms relating to channel activity are enriched within the gene list.

	Summarised Cluster Term	# genes	% of gene list	Most significant cluster term	p (most sig term)	DAVID Enrichment score
1	Channel activity	58	4.36	GO:0005216~ion channel activity	2.23E-10	9.14
2	Nucleoside binding	160	12.02	GO:0030554~adenyl nucleotide binding	4.68E-09	8.09
3	Cellular protein catabolic process	66	4.96	GO:0043632~modification-dependent macromolecule catabolic process	6.27E-07	5.81
4	Nucleobase, nucleoside, nucleotide and nucleic acid biosynthetic process	28	2.10	GO:0009165~nucleotide biosynthetic process	5.03E-05	4.15
5	ATPase activity, coupled to transmembrane movement of substances	17	1.28	GO:0016820~hydrolase activity, acting on acid anhydrides, catalyzing transmembrane movement of substances	6.49E-04	3.19
6	Purine nucleoside triphosphate metabolic process	16	1.20	GO:0046034~ATP metabolic process	0.001	2.56
7	Nucleoside triphosphate biosynthetic process	15	1.13	GO:0006754~ATP biosynthetic process	0.001	2.46
8	Anion binding	11	0.83	GO:0005254~chloride channel activity	0.009	1.88
9	Intermediate filament-based process	5	0.38	GO:0060053~neurofilament cytoskeleton	0.001	1.71
10	Cyclic nucleotide biosynthetic process	6	0.45	GO:0009975~cyclase activity	0.02	1.66

3.7.3 Lysosomal gene up-regulation in symptomatic and late-stage astrocytes

The lysosome is an organelle located within the cytoplasm responsible for the breakdown of waste products. Many enzymes are located within the lysosome for breakdown of carbohydrates, fats, protein and nucleic acids. There is a clear increase in expression of lysosomal genes in SOD1^{G93A} astrocytes at both symptomatic & late-stage time points (Table 3.7). The genes involved include several lysosomal digestive proteases: cathepsin D (*Ctsd*), cathepsin H (*Ctsh*), cathepsin S (*Ctss*), cathepsin Z (*CtsZ*); two glycosidases: hexosamindase A (*Hexa*) and hexosaminidase B (*Hexb*); and two minor lysosomal membrane proteins: solute carrier family 11 member 1 (*Slc11a1*) and lysosomal associated transmembrane protein 5 (*Laptm5*).

Table 3.7 Lysosomal genes are enriched in differentially expressed genes of SOD1^{G93A} astrocytes at the symptomatic and late-stage time-points. Where multiple probesets were differentially expressed the fold-change of the most significant probeset is given. Blank spaces indicate where genes are not significantly differently expressed ($p \leq 0.05$).

Gene	Full name	Symptomatic FC	Late-stage FC
Cd68	cd68	+4.16	+3.74
Ctsb	cathepsin B		+2.34
Ctsd	cathepsin D	+2.32	+3.28
Ctsh	cathepsin H	+2.4	+2.77
Ctss	cathepsin S	+2.53	+4.07
Ctsz	cathepsin Z	+3.22	+4.67
Hexa	hexosaminidase A	+2.26	+2.38
Hexb	hexosaminidase B	+2.54	+2.96
Laptm5	lysosomal-associated transmembrane protein 5	+2.81	+6.45
Slc11a1	solute carrier family 11 (proton-coupled divalent metal ion transporters), member 1	+2.87	+3.2

3.7.4 Immune response and complement cascade up-regulation in astrocytes from the symptomatic and late disease stages

Gene categories relating to the immune response are increased in expression at both the symptomatic and late-stage time-points in SOD1^{G93A} astrocytes. In particular the complement pathway, an innate immune mechanism for the destruction of invading pathogens, is up-regulated at both stages (Table 3.8). The complement pathway consists of a cascade of protein activation, centred around C1q, the three components of which (C1qA, B & C) are up-regulated at symptomatic and further at late-stages in the microarray of astrocytes (Table 3.8). C1q binds to antigen-antibody and stimulates

the formation of the C3 convertase complex, which cleaves C3 to the pro-inflammatory anaphylatoxin C3a. C3a is a potent inducer of chemotaxis in phagocytes and acts upon complement component 3a receptor 1, which is up-regulated in symptomatic astrocytes (90d: +2.37). C3b, the other product of C3 hydrolysis, forms part of the C5 convertase complex producing C5a, which also has chemotactic activity and triggers formation of the membrane attack complex (MAC) which permeabilises the pathogen cell wall (van Beek et al., 2003). Dysregulated complement components are present in both symptomatic and late stage SOD1^{G93A} astrocyte gene lists, with C4b and C1q showing the highest significance ($p \leq 0.0001$) of all dysregulated genes at late stage disease.

Table 3.8 Genes involved in the complement cascade are enriched in differentially expressed genes of SOD1^{G93A} astrocytes at the symptomatic and late-stage time-points. Where multiple probesets were differentially expressed the fold-change of the most significant probeset is given. Blank spaces indicate where genes are not significantly differently expressed ($p \leq 0.05$).

Gene	Full name	Symptomatic FC	Late-stage FC
Itgb2	integrin beta 2	+2.85	
A2m	alpha-2-macroglobulin	+3.28	+11.38
C1qa	complement component 1	+3.97	+7.98
C1qb	complement component 1	+3.4	+8.89
C1qc	complement component 1	+3.91	+5.75
C3	complement component 3		+9.44
C3ar1	complement component 3a receptor 1	+2.37	
C4b	complement component 4b	+6.27	+28.67
Cd55	cd55	-2.48	

In addition to the up-regulation of the complement system there is also up-regulation of chemotactic genes (Figure 3.9). Seven genes in the KEGG chemokine signalling pathway are differentially expressed in symptomatic SOD1^{G93A} astrocytes. Only two of these genes, *Ccl6* and *Cxcl10* are differentially expressed at late-stage. *Ccl3* has the second highest positive fold change (90d: +9.01) of all genes at the symptomatic time-point.

Table 3.9 Genes in chemokine signalling pathways that are differentially regulated with FC≥2 in SOD1^{G93A} astrocytes at the symptomatic and late-stage time-points. All chemokines show an up-regulation and only *ccl6* and *cxcl10* are differentially expressed at both time-points (p≤0.05). Where multiple probesets were differentially expressed the fold-change of the most significant probeset is given. Blank spaces indicate where genes are not significantly differently expressed (p≤0.05).

Gene	Full name	Symptomatic FC	Late-stage FC
Adcy7	adenylate cylase 7	+3.02	
Ccl3	chemokine (C-C motif) ligand 3	+9.01	
Ccl4	chemokine (C-C motif) ligand 4	+2.12	
Ccl6	chemokine (C-C motif) ligand 6	+4.42	+2.85
Ccl9	chemokine (C-C motif) ligand 9	+2.05	
Cxcl10	chemokine (C-X-C motif) ligand 10	+3.54	+10.37
Dock2	dedicator of cyto-kinesis 2	+2.54	

The gene with the highest p-value between SOD1^{G93A} and NTg astrocytes at the symptomatic time-point was activating transcription factor 3 (*Atf3*) (90d: +6.82; 120d: -2.51). This transcription factor is part of a regulatory circuit involving the inflammatory transcription factor C/EBPδ (90 day: +2.97) and NFκB that is involved in innate immune response and modulation (Litvak et al., 2009).

3.7.5 Disrupted ion transport in symptomatic and late-stage astrocytes

There is a down-regulation of genes involved in ion homeostasis at both the symptomatic and late-stage time-points (Table 3.3Table 3.3 and Table 3.6). In particular genes involved in potassium transport are enriched within the two datasets (Table 3.13), indicating that there may be a loss of normal astrocyte buffering capacity. Astrocytes are important in the process of potassium buffering and loss of this function would impact upon processes such as action potential generation and voltage-gated channel activity (Kofuji and Newman, 2004). One of the main mechanisms of potassium uptake is via Na+/K+ ATPase pumps, of which three different forms (*Atp1a1, Atp1a3* and *Atp1b1*) are down-regulated by late-stage disease. A down-regulation of several inwardly rectifying potassium channels, which allow greater ion influx than efflux, is also seen (*Kcnj3, Kcnj14*).

Table 3.10 Transcripts involved in potassium transport that are differentially expressed in SOD1^{G93A} astrocytes at the symptomatic and late-stage of disease. All genes show a down-regulation. Where multiple probesets were differentially expressed the fold-change of the most significant probeset is given. Blank spaces indicate where genes are not significantly different in expression ($p \leq 0.05$).

Gene	Full name	Symptomatic FC	Late-stage FC
Atp1a1	ATPase, Na+/K+ transporting, alpha 1 polypeptide	-3.19	-2.33
Atp1a3	ATPase, Na+/K+ transporting, alpha 3 polypeptide		-2.61
Atp1b1	ATPase, Na+/K+ transporting, beta 1 polypeptide		-2.69
Kcna1	potassium voltage-gated channel, shaker-related subfamily, member 1		-2.17
Kcna6	potassium voltage-gated channel, shaker-related, subfamily, member 6	-2.28	
Kcnab1	potassium voltage-gated channel, shaker-related subfamily, beta member 1	-2.12	-3.75
Kcnb1	potassium voltage gated channel, Shab-related subfamily, member 1	-2.08	
Kcng4	potassium voltage-gated channel, subfamily G, member 4	-2.37	-2.53
Kcnj14	potassium inwardly-rectifying channel, subfamily J, member 14	-3.66	-3.96
Kcnj3	potassium inwardly-rectifying channel, subfamily J, member 3	-2.09	-4.06
Kcnk1	potassium channel, subfamily K, member 1		-2.58
Kcnq5	potassium voltage-gated channel, subfamily Q, member 5	-2.04	
Kcnq5	potassium voltage-gated channel, subfamily Q, member 5	-2.25	-2.48

3.7.6 Altered cholesterol metabolism transcripts in late-stage SOD1^{G93A} astrocytes

In addition to DAVID enrichment analyses, during compilation of symptomatic and late-stage gene lists (Appendix 3) it was noticed that the late-stage gene list had many transcripts involved in cholesterol processing. Thirty-eight transcripts involved in the processing and transport of cholesterol were differentially expressed in the late-stage gene list, the majority of which (35 transcripts) were decreased in expression (Table 3.11). Interrogation of the symptomatic gene list found four of these transcripts to be differentially expressed at the earlier stage, suggesting altered cholesterol metabolism to be a feature of late-stage disease. When these transcripts were mapped onto the pathway of cholesterol synthesis, decreased transcripts were seen to occur at the top and bottom of the pathway as well as in key transport steps (Figure 3.11).

Table 3.11 Transcripts involved in cholesterol processing and metabolism that are differentially expressed in symptomatic and late-stage SOD1^{G93A} astrocytes. Where multiple probesets were differentially expressed the fold-change of the most significant probeset is given. Blank spaces indicate where genes are not significantly different in expression ($p \leq 0.05$).

Gene	Full name	Symptomatic FC	Late-stage FC
Abca5	ATP-binding cassette, sub-family A (ABC1), member 5		-3.21
Abcb7	ATP-binding cassette, sub-family B (MDR/TAP), member 7		-2.44
Abcc8	ATP-binding cassette, sub-family C (CFTR/MRP), member 8		-2.06
Abcd2	ATP-binding cassette, sub-family D (ALD), member 2		-2.58
Acat2	Acetyl-Coenzyme A acetyltransferase 2		-2.33
Acsl4	acyl-CoA synthetase long-chain family member 4		-2.35
Acsl6	acyl-CoA synthetase long-chain family member 6		-2.59
Acss2	acyl-CoA synthetase short-chain family member 2		-2.23
ApoE	Apolipoprotein E	+2.18	+5.23
Capn7	calpain 7		-2.00
Ch25h	cholesterol 25-hydroxylase		-2.63
Cyp51	cytochrome P450, family 51		-2.62
Dbi	diazepam binding inhibitor		+2.04
Dhcr24	24-dehydrocholesterol reductase		-2.97

Gene	Full name	Symptomatic FC	Late-stage FC
Extl2	exostoses (multiple)-like 2		-3.38
Fads6	fatty acid desaturase domain family, member 6		-2.14
Far1	fatty acyl CoA reductase 1		-2.41
Hmgcs1	3-hydroxy-3-methylglutaryl-Coenzyme A synthase 1		-3.11
Hsd11b1	hydroxysteroid 11-beta dehydrogenase 1,	-2.32	-5.05
Hsd17b7	hydroxysteroid (17-beta) dehydrogenase 7	-2.05	-2.88
Insig1	insulin induced gene 1		-2.14
Insig2	insulin induced gene 2		-2.58
Ldlr	low density lipoprotein receptor		-3.39
lpl	lipoprotein lipase	+5.99	-11.21
Lrp11	Low density lipoprotein receptor-related protein 11		-3.96
Lrp12	Low density lipoprotein-related protein 12		-2.28
Lypd6b	LY6/PLAUR domain containing 6B		-2.84
Nsdhl	NAD(P) dependent steroid dehydrogenase-like		-2.96
Nus1	nuclear undecaprenyl pyrophosphate synthase 1 homolog (S. cerevisiae)		-2.01
Osbpl1a	oxysterol binding protein-like 1A		-2.69
Osbpl6	oxysterol binding protein-like 6		-3.19
Osbpl8	oxysterol binding protein-like 8		-2.17
Sc4mol	sterol-C4-methyl oxidase-like		-2.97
Sc5d	sterol-C5-desaturase (fungal ERG3, delta-5-desaturase) homolog (S. cerevisae)		-3.33
Scd1	stearoyl-Coenzyme A desaturase 1		-2.43
Sqle	squalene epoxidase		-3.09
Stard4	StAR-related lipid transfer (START) domain containing 4		-2.93
Tspo	translocator protein		+2.04

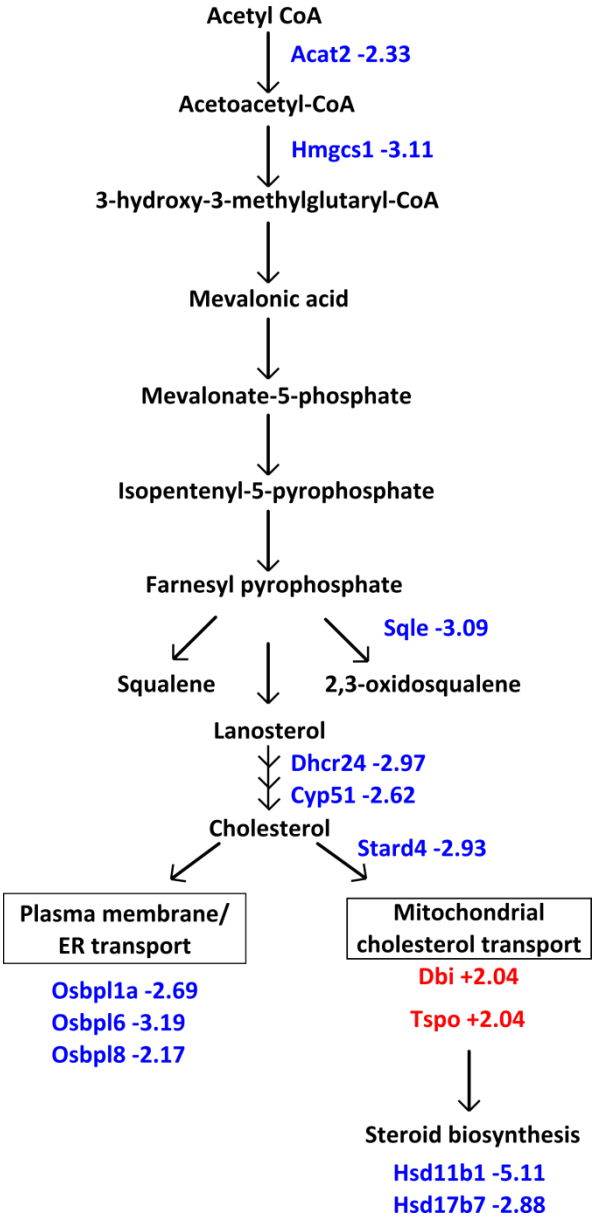

Figure 3.11 Transcripts differentially expressed in late-stage SOD1^{G93A} astrocytes mapped onto some of the key steps in the synthesis of cholesterol. Downstream transport to plasma membrane/ER and mitochondria are also depicted.

3.8 Comparison of pre-symptomatic, symptomatic and late-stage gene expression profiling of SOD1^{G93A} astrocytes

SOD1^{G93A} astrocytes from the pre-symptomatic stage have already undergone gene expression profiling by Ferraiuolo et al. (2011a) which enables a comparison of the gene lists generated at three time-points of the disease. The number of transcripts with differential expression passing $p \leq 0.05$ and $FC \geq 2$ in common between all three time-points was investigated using a Venn diagram (Figure 3.12). There is high variability in the number of transcripts differentially expressed at $FC \geq 2$ between the three time-points, with the symptomatic stage showing a lower number of transcripts (294) compared to the pre-symptomatic (904) and late-stage (1986) GeneChips. The highest proportion of genes shared is between the symptomatic and late-stage time-points. When these 180 genes are analysed for enrichment of gene categories, the immune response, lysosome and ion homeostasis are the most enriched categories (Table 3.12).

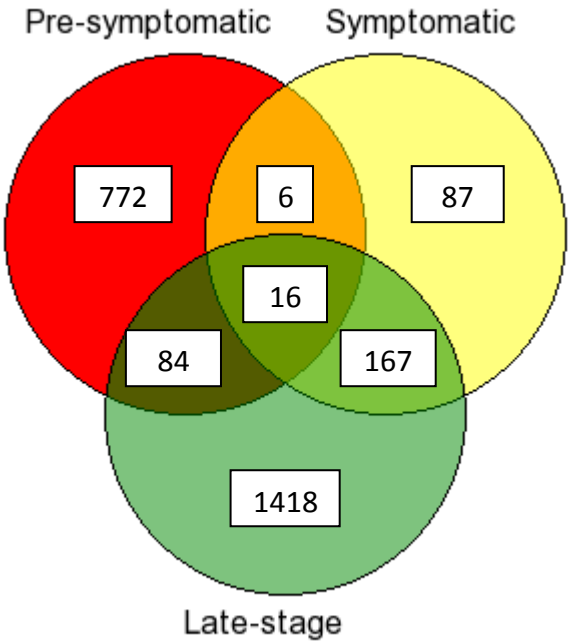

Stages	% genes shared
Pre-symptomatic + symptomatic	1.94%
Pre-symptomatic + late-stage	4.01%
Symptomatic + late-stage	10.29%
All stages	0.63%

Figure 3.12 Venn diagram of the differentially expressed genes passing statistical significance ($p \leq 0.05$) and an $FC \geq 2$ for all three time-points. The percentage overlap in differentially expressed transcripts is shown in the table below the Venn diagram. The symptomatic and late-stage GeneChips show the largest overlap in differentially expressed transcripts, with the pre-symptomatic and symptomatic gene-lists showing the lowest amount of overlap.

Table 3.12 Enriched gene categories within genes shared between the symptomatic and late-stage gene lists.

Rank	Term	Count	%	Enrichment score
1	Positive regulation of immune response	12	6.70	5.71
2	Lysosome	11	6.15	4.47
3	Ion homeostasis	13	7.26	4.29
4	Regulation of endocytosis	6	3.35	3.68
5	Regulation of adaptive immune response	5	2.79	2.97
6	Region of interest: Linker 2/Coil 2A/Coil 2B	3	1.68	2.57
7	Alpha-2-macroglobulin	3	1.68	2.51
8	Regulation of phosphorylation	10	5.59	2.40
9	Complement pathway	4	2.23	2.39
10	Positive regulation of cell death	9	5.03	2.32

When the gene lists are separated into up-regulated and down-regulated genes and compared there is a clear difference in the degree of overlap between the three stages (Figure 3.13). There are many more up-regulated genes shared between the symptomatic and late-stages than any other combination of time-points (for full lists of shared genes see Appendix 10). The separation also shows that there is a large amount of transcriptional down-regulation at late-stage disease compared to the other time-points which are more evenly split. The overlap between the pre-symptomatic + late-stage and symptomatic + late-stage time-points is more evenly matched for down-regulated transcripts, whereas the overlap between the pre-symptomatic and symptomatic time-points is again very small. Enrichment analysis was performed for the up and down-regulated transcripts shared between the symptomatic and late-stage time-points (Table 3.13). Similar to the total gene list for each time-point (Table 3.2 and Table 3.5), the lysosome was the most enriched category within the up-regulated transcripts. Ion homeostasis was also enriched within the down-regulated transcripts, however the level of enrichment was much lower than the top three up-regulated categories as seen by DAVID enrichment score. Finally, the up-regulated transcripts shared between all three time-points all belong to the immune and inflammatory response, whilst the eleven down-regulated transcripts contain a variety of annotation groups.

a) **b)**

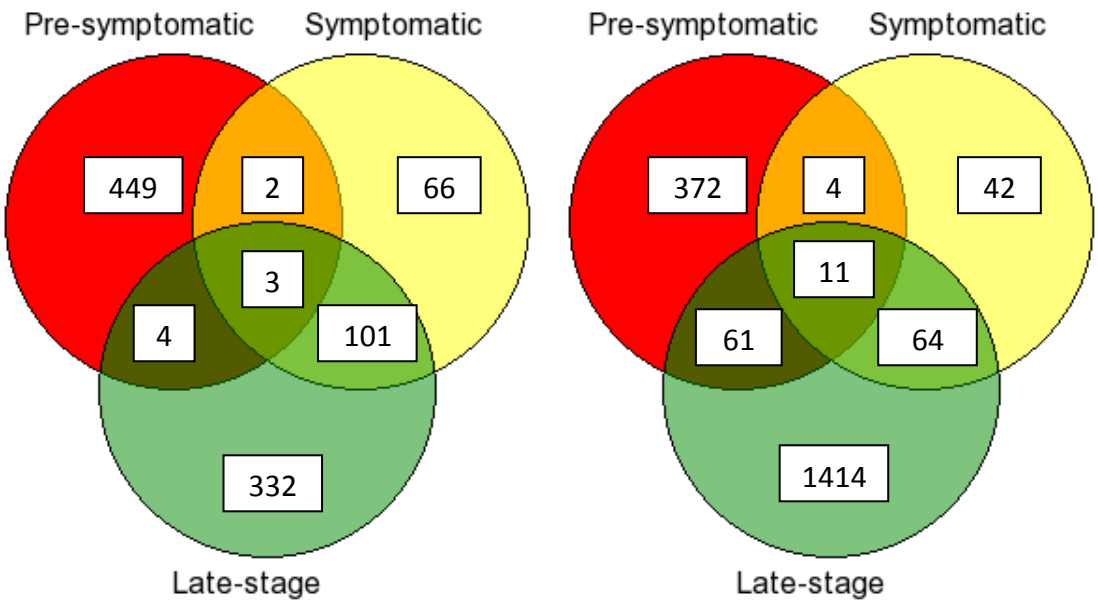

Stages	% up-regulated genes shared	% down-regulated genes shared
Pre-symptomatic + symptomatic	0.8	2.6
Pre-symptomatic + late-stage	0.8	3.6
Symptomatic + late-stage	17	4.5
All stages	0.31	0.56

Figure 3.13 Venn diagram of the **a)** up-regulated and **b)** down-regulated genes that are differentially expressed in $SOD1^{G93A}$ astrocytes at pre-symptomatic, symptomatic and late-stage disease. Numbers do not sum to those in Figure 3.12 as some transcripts change direction of differential expression through the disease course.

Table 3.13 Enriched gene categories within the transcripts shared between the symptomatic and late-stage gene lists. The top categories by enrichment score are the lysosome, immune response and phagocytosis categories. Potassium transport is also enriched within the down-regulated transcripts. Count= number of genes, % = proportion of gene list.

	Term	Count	%	Enrichment score
Up-regulated transcripts				
1	Lysosome	11	10.58	6.81
2	Positive regulation of immune response	9	8.65	4.84
3	Positive regulation of phagocytosis	5	4.81	4.01
4	Phagocytosis	6	5.77	3.04
5	Alpha-2-macroglobulin	3	2.88	2.95
6	Mononuclear cell proliferation	4	3.85	2.73
7	Regulation of organelle organisation	5	4.81	2.66
8	Ion homeostasis	8	7.69	2.60
9	Positive regulation of adaptive immune reponse	4	3.85	2.57
10	Cation homeostasis	6	5.77	2.53
Down-regulated transcripts				
1	Potassium transport	6	8.00	3.45
2	Channel activity	5	6.67	2.03
3	Synaptic transmission	5	6.67	1.91
4	Muscle organ development	4	5.33	1.70
5	Cholesterol/steroid biosynthesis	3	4.00	1.59
6	Regulation of phosphorylation	5	6.67	1.52
7	Regulation of protein modification	4	5.33	1.49
8	Ion homeostasis	5	6.67	1.36
9	Sex differentiation	3	4.00	1.14
10	Cation homeostasis/cell adhesion	3	4.00	1.07

Table 3.14 Transcripts differentially expressed at pre-symptomatic, symptomatic and late-stage disease in SOD1^{G93A} astrocytes. Very few transcripts are differentially expressed at all stages of the disease.

Gene symbol	Gene name	Functional category	Pre-symptomatic FC	Symptomatic FC	Late-stage FC
Up-regulated transcripts					
Cxcl10	chemokine (C-X-C motif) ligand 10	Chemokine	+2.94	+3.54	+10.37
Csf2rb	colony stimulating factor 2 receptor, beta, low-affinity (granulocyte-macrophage)	Immune response	+2.62	+2.54	+3.23
Ncf4	neutrophil cytosolic factor 4	Inflammation	+2.00	+2.04	+2.20
Down-regulated transcripts					
Sv2b	synaptic vesicle glycoprotein 2 b	Neurotransmission	-2.03	-2.31	-3.94
Nefh	neurofilament, heavy peptide	Cytoskeleton	-2.06	-2.01	-3.84
Susd2	sushi domain containing 2	Immune response	-2.19	-2.55	-3.31
Hsd17b7	hydroxysteroid (17-beta) dehydrogenase 7	Cholesterol/steroid metabolism	-2.41	-2.05	-2.88
Dffa	DNA fragmentation factor, alpha subunit	Apoptosis	-2.49	-2.49	-2.94
Atp1a1	ATPase, Na+/K+ transporting, alpha 1 polypeptide	Ion transport	-2.61	-3.19	-2.88
Polr3g	polymerase (RNA) III (DNA directed) polypeptide G	Immune response	-2.63	-2.21	-2.14
Rspo2	r-spondin 2 homolog (Xenopus laevis)	Signalling	-2.74	-9.64	-4.75
Myh10	myosin, heavy polypeptide 10, non-muscle	Axonogenesis	-3.42	-2.01	-2.94
Cd24a	CD24a antigen	Immune response	-4.85	-3.84	-3.28
Chodl	chondrolectin	Carbohydrate transport	-6.97	-12.45	-7.46

3.9 qPCR validation of transcripts of interest

To verify that genes called statistically significant after microarray analysis were regulated in the correct direction and to test for false positives, qPCR validation was performed upon RNA from the symptomatic time-point. Transcripts were chosen for qPCR validation from the up-regulated categories involving the lysosome, complement and immune pathways, for which astrocytes could feasibly be involved. Differentially expressed transcripts involved in the modification of the extracellular matrix (ECM) were also investigated due to their possible role in the immune response via infiltration of immune cells (Figure 3.14). Genes from the immune response category included: chemokine (C-C motif) ligand 6 (*Ccl6;* 90d: +4.42, 120d: +2.85), chemokine (C-X-C motif) ligand 10 (*Cxcl10*; 90d: +3.54, 120d: +10.36), the first part of the complement cascade complement component 1 Q subcomponent B chain (*C1qb*; 90d: +3.4, 120d: +8.9) the stress response gene activating transcription factor 3 (*Atf3;* 90d: +6.82, 120d: +4.23) and the serpin peptidase inhibitor Serpina3n (90d: +3.9, 120d: +8.0). Lysosomal genes tested for validation were hexosaminidase A (*Hexa;* 90d: +2.26, 120d: +2.38), cathepsin D (*Ctsd;* 90d: +2.32 120d: +3.28), cathepsin S (*Ctss;* 90d: +2.53, 120d: +4.07) and lysosomal protein transmembrane 5 (*Laptm5;* 90d: +2.81, 120d: +6.45). In order for immune cells to infiltrate the CNS alterations need to be made to the structure of the ECM. The matrix metalloproteinase Mmp9 and its inhibitor Timp1 were differentially expressed at both the symptomatic (*Mmp9*: -4.9; *Timp1*: +7.7) and late-stage (*Mmp9*: -4.2; *Timp1*: +6.35) time-points and were included for validation. Other genes tested for validation included chondrolectin (*Chodl*) which had the highest negative fold change on the symptomatic arrays, lipoprotein lipase (*Lpl*) and *Igfbp5.* Of the fourteen genes tested for qPCR validation, ten were confirmed significantly differentially expressed whilst the remaining four were regulated in the same direction but did not reach significance (Figure 3.14).

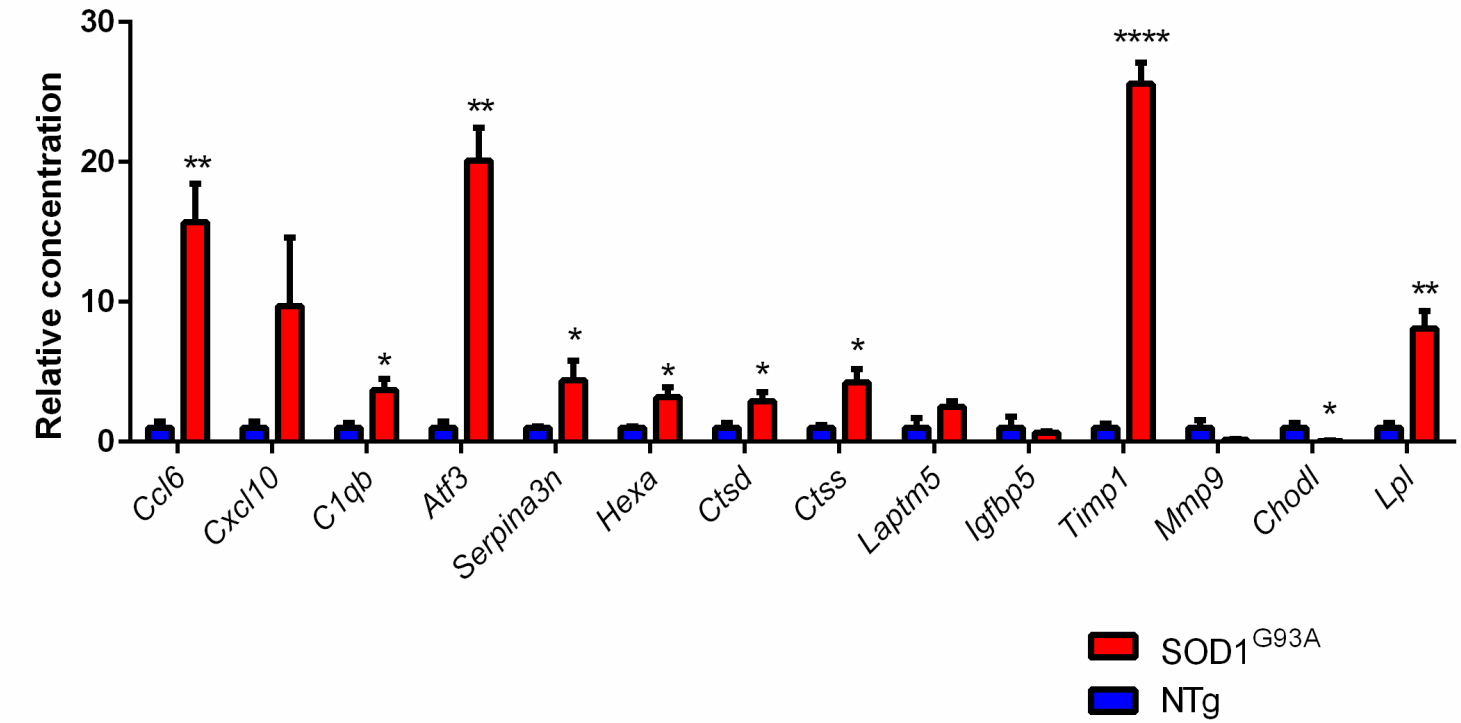

Figure 3.14 A summary of genes chosen for qPCR validation of symptomatic SOD1^{G93A} and NTg astrocytes. Genes involved in the immune response: the chemokines *Ccl6* and *Cxcl10*, the complement component *C1qb*, the stress response genes *Atf3* and *Serpina3n*. Genes involved in the lysosome: *Hexa*, *Ctsd*, *Ctss*, *Laptm5*. Genes involved in extracellular processes: *Igfbp5*, *Timp1*, *Mmp9*, *Chodl*, *Lpl*. Ten of the fourteen genes tested (71%) showed a significant difference by one-tailed t-test, whilst all genes showed a trend in the direction indicated on the microarrays. Values for SOD1^{G93A} are normalised to their respective NTg control. n=3 for each group. Error bars = SEM.

3.10 Discussion

Microarray analysis has been successfully performed upon symptomatic and late-stage astrocytes laser captured from the SOD1^{G93A} mouse model for the first time. This novel study has allowed enriched pathways of differentially expressed genes to be identified and compared to earlier studies of pre-symptomatic astrocytes (Ferraiuolo et al., 2011a). The resulting datasets provide information on the changing behaviour of astrocytes throughout motor neuron degeneration which is currently impossible to obtain from study of the human disease.

3.10.1 Genes chosen for validation by qPCR

As described in section 3.9, validation of the microarray analysis was carried out by performing qPCR of a select number of genes to replicate the microarray results. Targets were chosen that were present at both time-points to further avoid the chance of false positive results and also to enable future therapeutic strategies to target behaviour that is relevant throughout the disease course. The categories with the highest enrichment scores in Table 3.13, i.e. the lysosome, immune response and phagocytosis, were chosen for further investigation as they all might be involved in an immuno-active astrocyte phenotype. The decision was made to focus upon this aspect of the astrocyte phenotype rather than the defect in potassium transport and cholesterol processing due to the higher enrichment scores for the up-regulated categories in the DAVID analysis of shared genes (Table 3.13).

Ten of the fourteen transcripts tested by qPCR replicated the significant difference seen between SOD1^{G93A} and NTg in the microarray analysis. These transcripts included three of the four lysosomal targets tested, the complement component *C1qb*, the chemokine *Ccl6* and the stress response factors *Atf3* and *Serpina3n*, reinforcing the finding of a reactive astrocyte phenotype seen in the symptomatic and late-stage time-points. Further targets of interest were: *Chodl* which is potentially involved in binding of sugar residues on pathogen cell membranes; *Lpl* which is involved in lipid metabolism but has also been seen to influence phenotype of the J774 macrophage cell line *in vitro* (Li and Renier, 2007) and is decreased in expression in NSC34 cells harbouring the SOD1^{G93A} mutation (Kirby et al., 2005); and *Igfbp5* which has previously been seen as up-regulated in ALS patient spinal cord and SOD1^{G93A} mice and may

disrupt IGF signalling (Wilczak et al., 2003, Corti et al., 2007). Wilczak et al. suggest that Igfbp5 sequesters IGF from MN which kills them. It was interesting to see if astrocytes were down-regulating *Igfbp5* in response to this, however the differential expression of *Igfbp5* was not confirmed by qPCR. For the four genes (*Cxcl10, Laptm5, Igfbp5* and *Mmp9)* which were not found to be significantly differentially expressed between $SOD1^{G93A}$ and NTg astrocytes by qPCR, these transcripts still show a trend in the same direction as shown by the microarray data analysis.

3.10.2 Overlapping gene expression between time-points

The Venn diagrams of all three time-points show the symptomatic and late-stage gene lists to be more similar to each other than either time-point is with the pre-symptomatic gene list (Figure 3.12 and Figure 3.13), particularly in terms of up-regulated genes. In comparison to the pre-symptomatic time-point, only 2 of the 14 transcripts tested for qPCR validation are in common: *Cxcl10* and *Chodl*. *Cxcl10* is considered anti-inflammatory and has been shown to correlate with a slower disease progression (Tateishi et al., 2010) showing that astrocytes at early stage may still be non-reactive. The other shared transcript is chondrolectin, which encodes a protein required for endocytosis of glycoproteins and pathogens with carbohydrate-bearing surfaces and is down-regulated at all three time-points (Table 3.14). *Chodl* is also highly expressed in neurons and isoform-1 has been seen to be reduced in spinal muscular atrophy, another motor neuron disease (Sleigh et al., 2014).

The pre-symptomatic time-point is highly associated with a loss of supportive function in $SOD1^{G93A}$ astrocytes, such as the provision of lactate to motor neurons (Ferraiuolo et al., 2011a). Other supportive functions are also lost in astrocytes as the disease progresses, such as the possible loss of potassium buffering capacity from down-regulation of several potassium transporters (Table 3.10) through to the loss of cholesterol processing transcripts at late-stage (Table 3.11). However there is also a robust up-regulation of immune response behaviour at the symptomatic stage which also continues to late-stage disease (Table 3.7-Table 3.9). This suggests that a transition occurs between the pre-symptomatic and symptomatic time-points leading to a reactive astrocyte phenotype characterised by increased chemokine secretion, lysosomal up-regulation and up-regulation of stress response factors. This is reinforced

by a recent microarray study of SOD1^{G93A} spinal cord at the pre-symptomatic ages of 40 days and 80 days which showed an increased expression of antigen presentation transcripts at the later time point (de Oliveira et al., 2013). The smaller gene list seen at the symptomatic time-point may represent a midway point between the pre-symptomatic astrocyte characterised by loss of supportive function through to the late-stage astrocyte where the disease burden has led to dysregulation of many genes. Culture of astrocytes from neonatal SOD1^{G93A} mice showed that they are less able to respond to activating factors such as glutamate and LPS and consequently release lower amounts of trophic factors (Benkler et al., 2013), reinforcing the notion that younger astrocytes show a phenotype characterised by loss of normal supportive function. Additionally, reduction of mutant SOD1 in astrocytes does not disrupt disease initiation but does slow disease progression in the SOD1^{G37R} mouse model (Yamanaka et al., 2008b). Perhaps in this study, reduction of SOD1^{G37R} in astrocytes delayed the process by which astrocytes become reactive in disease, and may suggest that a reduction in this reactivity will ameliorate disease progression. These data are also in keeping with work that Appel and colleagues have performed with microglia in the SOD1^{G93A} mouse, where microglia transition from a neuro-supportive to a neuro-toxic phenotype from early to late-stage disease (Liao et al., 2012).

3.10.3 Comparison of astrocyte data with previous motor neuron analyses

Having data for these three time-points of disease in the mouse model also allows comparison to an earlier microarray study conducted by Ferraiuolo et al. (2007) into motor neurons of the SOD1^{G93A} mouse at pre-symptomatic, symptomatic and late-stage disease. Similar to this analysis, differential expression was weighted towards up-regulated transcripts at the pre-symptomatic and symptomatic time-points, whereas a large degree of transcriptional repression was seen at the late stage. Also in common, the symptomatic stage of disease contained the lowest number of differentially expressed genes suggesting that a transition occurs not only in astrocytes as the disease process takes hold. At pre-symptomatic stage in motor neurons there is an increase in transcripts involved in transcriptional and translational processes as well as lipid and carbohydrate metabolism and the electron transport chain. At symptomatic stage only 51 transcripts were differentially expressed, which also featured an

increased expression of genes involved in transcriptional regulation. However at late-stage disease transcriptional repression was observed as well as a decrease in antioxidant pathways. Protein degradation pathways were increased, perhaps because of aggregated misfolded SOD1, and several cell cycle components were up-regulated suggestive that motor neurons are unsuccessfully trying to re-enter the cell cycle. Of note, components of the complement pathway are up-regulated, in common with late-stage astrocytes, which may be linked to the astrocyte activation seen in the present microarray study.

3.10.4 Enrichment of immune response genes at symptomatic and late-stage disease

The enrichment of pathways involved in the immune response is in keeping with current literature. There is much evidence suggesting complement activation in ALS; complement component C3 is upregulated in $SOD1^{G93A}$ mouse spinal cord at 126 days and C1q and C3 are expressed in the neuromuscular junction at both 47 days and 126 days (Heurich et al., 2011). In human ALS patients, increased levels of complement component C4d are seen in CSF (Tsuboi and Yamada, 1994) and increased complement component C3 is seen in serum (Goldknopf et al., 2006). In human sALS spinal cord there is increased staining for C1q and C3d in astrocytes and C1q, C3d and the membrane attack complex C5b-9 (MAC) in microglia (Sta et al., 2011). Sta et al. (2011) also showed an increased expression of C4 by qPCR, although their qPCR results found no significant difference between C1q expression in ALS vs. control, showing that expression at the RNA level and protein level do not always correlate. The use of whole spinal cord rather than specific cell types in qPCR may be the reason for these conflicting findings and shows an advantage of the LCM technique used in the current study. Previous microarray analysis of $SOD1^{G93A}$ murine motor neurons identified components of the complement cascade as up-regulated (Ferraiuolo et al., 2007), however this was only at the late-stage time point, with a trend for increased expression at the symptomatic time point. Thus, the current data point to an earlier astrocytic role in the recruitment of immune cells during the disease. Previous work has shown C5ar up-regulation in astrocytes in ALS and that inhibition of this receptor resulted in a prolonged life span in the mouse model (Woodruff et al., 2008). Our results add to evidence that complement dysregulation in astrocytes is important in

ALS, especially within the very early components of the pathway (C1qA, B and C are all up-regulated) which may mean that a therapeutic effect requires blocking the complement system in astrocytes at this stage of the cascade. Indeed, Stevens et al. (2007) found that C1q was important for pruning of synapses by astrocytes during development of the retina and that it became aberrantly re-expressed in retinal synapses in a mouse model of the neurodegenerative eye condition glaucoma. C1q was initially considered a tempting target for therapeutic intervention given that its up-regulation in astrocytes during disease could lead to unwanted synaptic elimination. However, knockout of *C1qa* by Lobsiger et al. (2013) did not lead to a significant delay in disease onset or progression in the $SOD1^{G37R}$ mouse model. Additionally, Lobsiger et al. (2013) showed C3 deletion did not alter the disease course in the $SOD1^{G93A}$ model, providing further evidence that complement induction may not be a major contributor in the SOD1-ALS disease process. This may mean that the inflammatory response is not a key target for therapeutic intervention in astrocytes in ALS. For example it has recently been shown that selective knockdown of NFκB in astrocytes of the $SOD1^{G93A}$ mouse does not alter toxicity towards co-cultured motor neurons (Frakes et al., 2014). Alternatively, it may be that the numerous pathological mechanisms operating in the aggressive mouse model of disease mean that there is a redundancy in the pathophysiological processes.

In addition to the up-regulated complement system, an up-regulation of chemokines is also seen at the two later time-points in disease, which could promote immune cell infiltration of the spinal cord, a matter of conflicting evidence. Using the marker Ly6C to distinguish monocytes derived from the spleen Butovsky et al. (2012) demonstrated monocyte recruitment to the spinal cord during disease progression in the $SOD1^{G93A}$ mouse. However parabiosis experiments using a mouse expressing GFP in all haematopoietic cells coupled to a $SOD1^{G93A}$ mouse showed minimal infiltration of GFP-expressing cells to the CNS (Ajami et al., 2007) and a more recent experiment using FACS analysis of $SOD1^{G93A}$ mouse spinal cord failed to replicate the observation of increased Ly6C-expressing cells (Chiu et al., 2013) although there was a small increase in infiltrating lymphocytes. Given that such controversy exists, and that $SOD1^{G93A}$ astrocytes show differential expression of transcripts for a host of immuno-modulatory

factors, the simplest explanation would be that astrocytes are having a direct effect upon the recruitment and activation of microglia, the resident CNS immune cell. Microglia are seen to transition from a neuro-protective, or M1, phenotype to a neuro-toxic (M2) phenotype during disease progression in the $SOD1^{G93A}$ mouse model (Liao et al., 2012). In addition, LPS-mediated M1 polarisation of microglia leads to increased production of nitrite and nitrate with a resulting significant negative correlation with motor neuron viability when in co-culture, an effect which is reversed by exogenous application of the M2-promoting cytokine IL4 (Zhao et al., 2006). Treatment of microglial cells with mutant SOD1 (mSOD1) led to M1 polarisation, through interaction with TLR 2 and 4 and CD14, and subsequent toxicity towards motor neurons when placed in co-culture (Zhao et al., 2010). It is important to appreciate that microglia in ALS are not polarised to either extreme and have a distinct disease phenotype (Chiu et al., 2013), however it still seems possible to measure which end of the spectrum these cells are leaning towards.

3.10.5 Lysosomal up-regulation indicative of increased phagocytosis?

At the symptomatic and late-stage time-points, transcripts for several lysosomal digestive enzymes are differentially expressed, including proteases, glycosidases and major and minor lysosomal membrane proteins.

CtsD has previously been shown to be up-regulated in ALS spinal cord but reduced in motor neurons (Wootz et al., 2006). *CTSD* is down-regulated in human SOD1-related ALS motor neurons (Kirby et al., 2011) and in *CHMP2B*-related ALS motor neurons along with cathepsin B (*CTSB*) (Cox et al., 2010). By contrast, astrocytes show up-regulation of *CtsB* in late-stage $SOD1^{G93A}$ mice (+2.23), and *CtsH* is up-regulated in astrocytes and microglia of the ventral horn in the mutant SOD1 mouse model as shown by immunohistochemistry (Fukada et al., 2007). This suggests that up-regulation of the lysosomal system in ALS is astrocyte-specific.

In contrast to a large increase in CtsD expression, an endogenous inhibitor of cathepsins, Cystatin C, is only slightly increased in $SOD1^{G93A}$ mouse spinal cord (Wootz et al., 2006) and mass spectrometry has been used to confirm a decreased level of Cystatin C in CSF of ALS patients compared to controls (Ranganathan et al., 2005,

Pasinetti et al., 2006). Hexosaminidase A (HexA) has previously been investigated as a cause of ALS or ALS-like disorders but a link was found to be unlikely (Drory et al., 2003). However this study investigated HexA deficiency due to mutation rather than investigating up or down regulation e.g. through over-expression or knockdown.

Increases in lysosomal-associated protein transmembrane 5 (*LAPTM5*) are seen in regressing neuroblastoma cells and overexpression of LAPTM5 leads to lysosomal-membrane permeabilisation and non-caspase dependent cell death (Inoue et al., 2009). Increased Laptm5 expression also leads to a significant increase in CTSD leakage in to the cytosol. Inoue et al (2009) found the increased accumulation of Laptm5 to be associated with decreased protein degradation efficiency, and perhaps the up-regulation of *Laptm5* seen in this study could bring about the same effects.

Up-regulation of lysosomal proteins could be as a result of increased amounts of autophagy, perhaps to deal with $SOD1^{G93A}$ protein. Wild-type and mutant SOD1 are degraded by autophagy in vitro (Kabuta et al., 2006). SOD1 and CTSD co-localisation in motor neurons of sALS patients has also been shown (Forsberg et al., 2010). However, in the symptomatic and late-stage data there is no up-regulation ($p \leq 0.05$, FC ≥ 2) for the classic autophagy related genes such as *Beclin 1*, *Lc3-II*, *Vps34* or the *Atg* group of genes (Virgin and Levine, 2009). This means that if autophagy is increased, it is due to altered autophagic flux rather than induction. Alternatively, lysosomal up-regulation could be a result of increased phagocytosis of neuronal debris. Phagocytosis is enriched in astrocytes at symptomatic and late-stage in this study (Table 3.12) Astrocytes are enriched in genetic pathways that put them forward as professional phagocytes (Cahoy et al., 2008). Furthermore, astrocyte phagocytosis of cellular debris has been demonstrated *in vitro* (Chang et al., 2000) and appears to be protective to co-cultured neurons (Loov et al., 2012).

3.10.6 Quality of material used for microarray

The data shown here portray astrocytes as undergoing a phenotypic change throughout the disease course. In order to perform an analysis using GeneChips from all three time-points and therefore have an overarching view of gene expression changes throughout the disease, it was necessary that array quality at each time-point

was similar. The LCM technique is vital for obtaining RNA from an enriched population of cells. However, a drawback of the technique is the degradation of RNA that occurs during the time taken to stain and laser-capture cells (Goldsworthy et al., 1999, Mikulowska-Mennis et al., 2002), hence the need for a rapid staining protocol that minimises the risk of RNA degradation (Mojsilovic-Petrovic et al., 2004). Even so, this leads to a lower quality of RNA on the arrays than could be achieved using cells obtained from *in vitro* cultures etc. Given this, it is important that samples put onto arrays are comparable in terms of RNA degradation such that valid comparisons can be made. All samples used for the arrays are outside the 3-fold boundary set by Affymetrix in terms of *Gapdh* and *Actin* 3'-5' ratios (Figure 3.1). However, RNA degradation is expected to be higher in samples obtained through LCM and the RNA degradation plots in Figure 3.2 and Figure 3.7 show that all samples within each time-point have a similar RNA degradation profile. To try to use the best quality RNA for microarray analysis, the RNA integrity number (RIN) of samples can be measured using the RNA 6000 PicoChip Kit. However, RIN values may not be an accurate predictor of RNA quality, as cDNA lengths do not seem to vary with differing RIN (Trabzuni et al., 2011). The plot in Figure 3.1 shows that the samples from all the symptomatic and late-stage time-points are comparable in terms of quality metrics. The pre-symptomatic Gene Chips previously analysed by Ferraiuolo et al. (2011a), whilst comparable within this time-point, were more than a scale-factor of three outside the GeneChips from the symptomatic and late-stage time-points meaning that an analysis where all GeneChips are analysed together could not be performed. However, the consistency of GeneChips within groups means that each time-point could be analysed separately and comparisons made subsequently.

3.10.7 Astrocyte enrichment upon GeneChips

The data in Figure 3.9 showing the abundance of different cellular markers on the arrays shows an enrichment for markers of astrocytes and oligodendrocytes. The levels of oligodendrocyte transcripts are higher than those found in expression data from cultured astrocytes (Figure 3.10). This is not unusual, markers of non-target cell types have previously been observed in material captured by LCM (Simpson et al., 2011). In addition previous analyses of laser captured motor neurons have shown differential

expression of myelin-related transcripts such as *Mbp (Ferraiuolo et al., 2007)*. It is important to note however, that the relationship between transcript number and cell number is variable, therefore this is not the most robust measure of purity of LCM samples. For example the oligodendrocyte transcript *Mbp* is very highly expressed in oligodendrocytes due to their main role in production of the myelin sheath, meaning that a higher number of *Mbp* transcripts per cell will be seen versus a transcript such as *Gfap*. In support of this, recent RNA sequencing of purified mouse CNS-cell populations shows *Mbp* to be 55416-fold more highly expressed in oligodendrocytes than astrocytes, whereas *Gfap* does not feature in the top 500 transcripts which discriminate these two cell types (Zhang et al., 2014). Furthermore, the markers of each cell type must be looked at in the context of where the cells have been LCM captured; *Gfap* is not highly expressed in grey matter astrocytes (Cahoy et al., 2008) and so will not show as highly expressed on the arrays as would be expected in an astrocyte-enriched population from white matter. Lastly, the differing location of probesets within transcripts for different genes can mean that certain transcripts are more easily detected than others. If a probeset for *Mbp* is more 3' than a probeset for *Gfap* it may lead to a higher level of detection in an RNA sample derived from degraded material. It is important to bear these caveats in mind when assessing enrichment based upon expression values from arrays. Nevertheless the data do show that astrocytes have been enriched within the samples and by focusing on genetic pathways that are more likely to occur in astrocytes than oligodendrocytes one can remove some of the bias that contaminating oligodendrocyte material might produce.

3.10.8 Conclusions

Based upon the enriched pathways described here, the major questions for functional studies of astrocytes are: 1) Are astrocytes involved in the immune modulation of microglia?; 2) Is there a difference between levels of phagocytosis in NTg vs $SOD1^{G93A}$ astrocytes? Functional studies should focus on providing data to answer these questions.

CHAPTER 4

RESULTS

Functional studies of $SOD1^{G93A}$ astrocytes

4 Results: Functional studies of SOD1^{G93A} astrocytes

4.1 Introduction

To validate the results of gene expression profiling in symptomatic and late-stage SOD1^{G93A} astrocytes *in* vitro experiments were designed. This involved the culture of murine neonatal astrocytes, microglia and embryonic motor neurons to investigate the previously identified categories of the lysosome, immune response and phagocytosis and immunohistochemistry to investigate altered cholesterol processing at late-stage disease.

4.2 Purity of cultures used for mouse functional experiments

Before conducting *in vitro* experiments, cultures were first tested for purity to ensure correct attribution of results to cell-type. Using flow cytometry, astrocyte cultures were found to be >95% (mean = 95.55% SD = 3.24 n=4) positive for the astrocyte marker GLAST (Figure 4.1a) and 0.51% positive for the microglial marker CD11b (SD = 0.47 n = 4) with a 71.76 fold increase in GLAST-APC fluorescence over isotype control compared to a 1.14-fold increase in CD11b-FITC fluorescence over isotype control (Figure 4.1b). The shift in GLAST-APC fluorescence is clear when viewed against a histogram of the unstained control cells (Figure 4.1c).

Microglial cultures were also established so as to investigate the astrocyte effect upon these cells. For microglial cultures, 52.53% (SD = 14.65 n = 4) of cells stained positively for Cd11b compared to 4.12% (SD = 1.01 n= 4) of cells which stained positively for GLAST (Figure 4.2). This corresponded to a 5.09-fold increase in CD11b fluorescence over isotype control compared to a 1.3-fold increase in median fluorescence for GLAST-APC over isotype control. Upon examination of median fluorescence histograms it was clear that there was a shift in fluorescence of the entire population of cells but that the level of fluorescence was insufficient to distinguish all cells from unstained controls. Therefore, microglial cultures were stained for CD11b (Figure 4.2d) and manually counted by three independent scorers. Microglial cultures comprised 93.81% CD11b^{+} cells (SD = 2.50 n = 3).

In order to establish a more realistic astrocyte phenotype, astrocytes were co-cultured with neuronal cultures enriched in motor neurons. This approach has previously revealed defects in lactate metabolism not seen when astrocytes were cultured as a mono-culture (Ferraiuolo et al., 2011a). Neuronal cultures used for astrocyte stimulation stained positively for the neuronal marker MAP2 and also contained cells expressing the motor neuronal marker Islet1 (Figure 4.3a). Islet1 is expressed only transiently in developing motor neurons (Kobayashi et al., 2011) therefore staining was also performed for the motor neuronal marker SMI32 which showed an increased amount of positive staining in comparison to Islet1 (Figure 4.3).

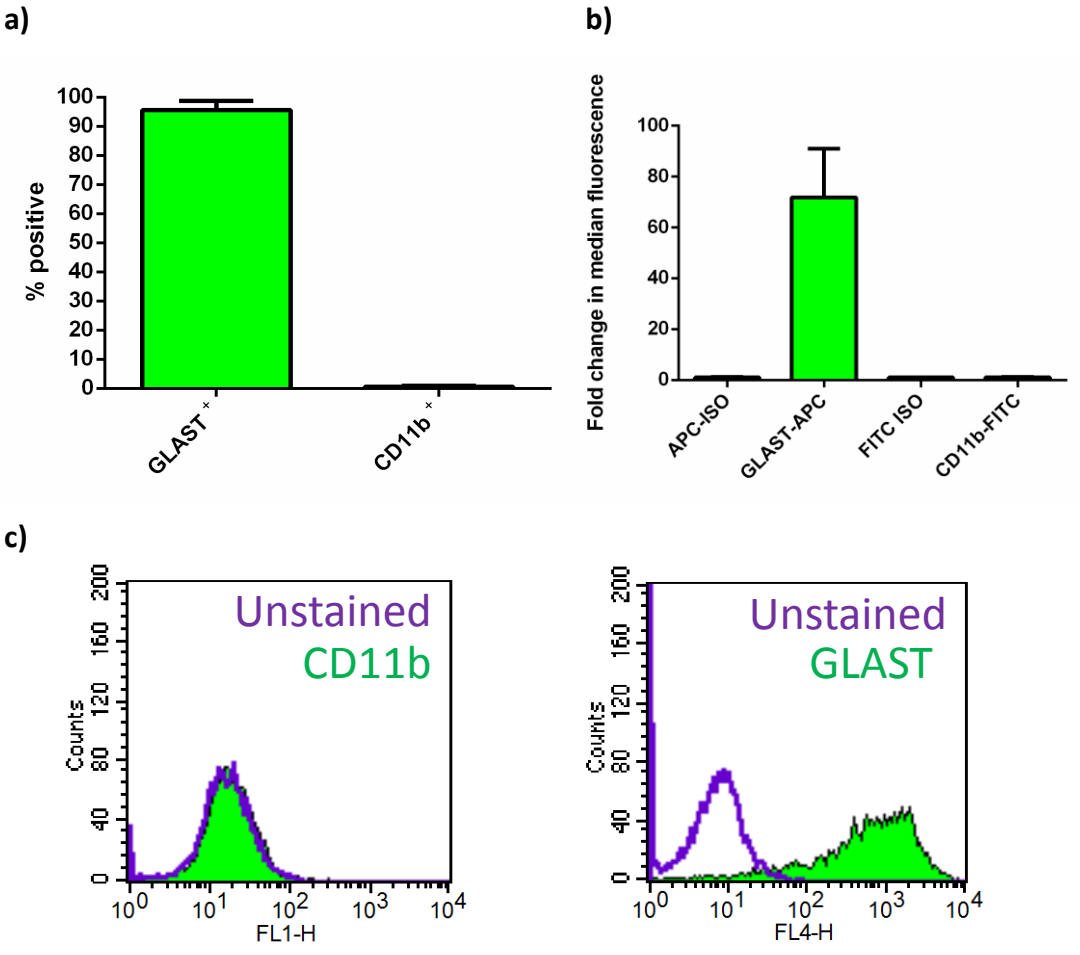

Figure 4.1 Purity of astrocyte cultures as measured by flow cytometry. Astrocytes purified by mild trypsinisation were stained for the astrocytes marker GLAST and the microglial marker CD11b. **a)** Purity of astrocytes cultures is estimated to be 95.55% with 0.51% Cd11b positive cells. (n=4).**b)** GLAST-APC median fluorescence was 71.76-fold higher than respective isotype control whilst CD11b-FITC fluorescence was 1.14-fold higher than respective isotype control. **c)** Histograms of fluorescence for CD11b-FITC (left) and GLAST-APC (right) show a shift in fluorescence in the APC channel that is not observed in the FITC channel. Error bars = S.E.M.

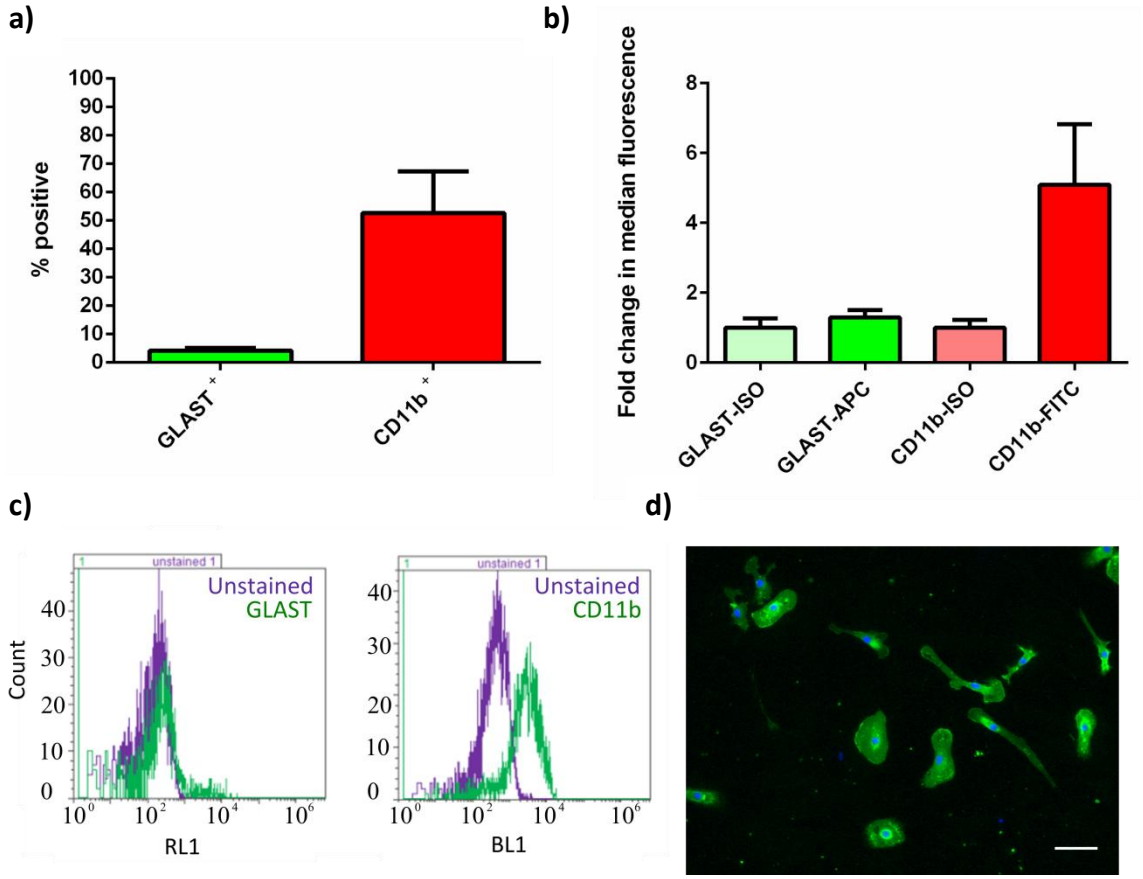

Figure 4.2 Purity of microglial cultures measured by flow cytometry. **a)** Microglia purified by shaking were stained for the microglial marker CD11b with 52.53% detected as $CD11b^+$ compared to 4.12% $GLAST^+$ cells. **b)** Median fluorescence for CD11b-FITC was 5.09 fold higher than isotype control whilst GLAST-APC median fluorescence was increased by 1.3-fold. **c)** Median fluorescence histogram showing the shift in GLAST-APC (left) and CD11b-FITC (right) fluorescence versus unstained cells. **d)** CD11b immunocytochemistry showing $CD11b^+$ microglia. Scoring by three independent scorers showed a microglial cultures to be comprised of 93.81% $CD11b^+$ cells. n=4 for all flow cytometry, image taken at x20 magnification Scale bar = 50µm. Error bars = S.E.M.

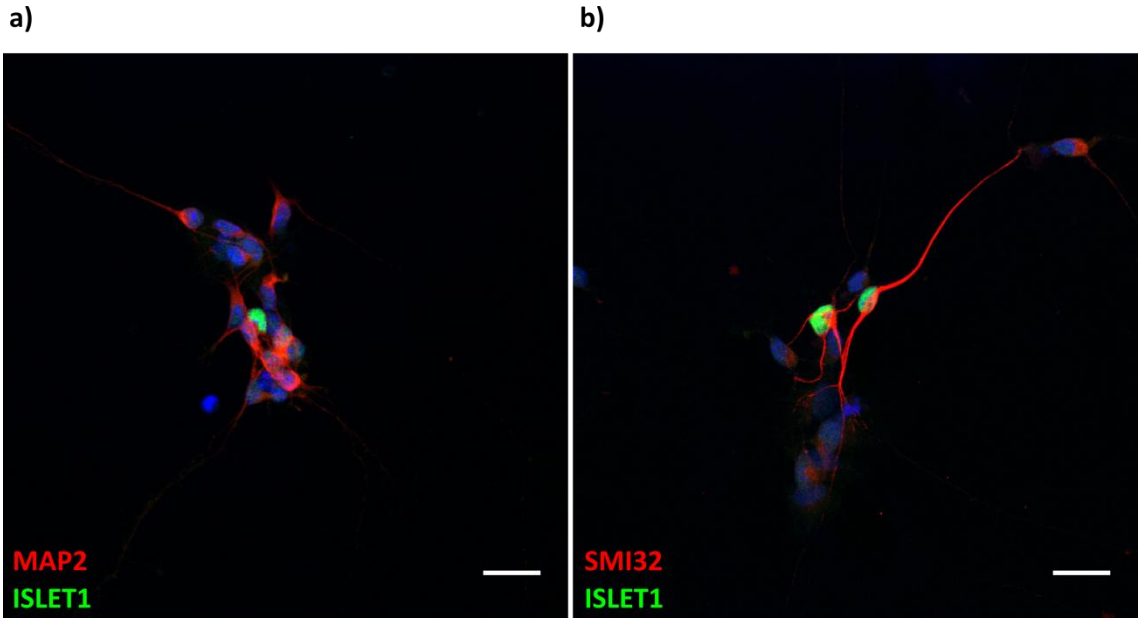

Figure 4.3 Staining of neuronal cultures. **a)** Neuronal cultures contained cells that stained positively for the pan-neuronal marker MAP2 (red) and the motor neuronal marker Islet1 (green). **b)** More cells stained positively for the motor neuronal marker SMI32 (red) compared to Islet 1 (green) indicating that these cells may be in different stages of development. Images taken at x63 magnification. Nuclei stained blue with Hoescht stain. Scale bar = 25µm.

4.3 qPCR for array genes on cultured astrocytes

To test whether transcripts of interest from the microarray studies of symptomatic and late-stage SOD1^{G93A} were differentially expressed in neonatal astrocytes in culture, RNA was extracted from NTg and SOD1^{G93A} astrocytes and qPCR performed (Figure 4.4). qPCR was performed on RNA from astrocytes that had been maintained in isolation (mono-culture) and those that had been co-cultured with motor neurons (co-culture). Transcripts were chosen from the significant transcripts in microarray validation involved in the immune response (*Ccl6* and *C1qb*), lysosome (*Ctss* and *Hexa*), lipid processing (*Lpl*), stress response (*Atf3*) and extracellular matrix (*Timp1*) (Section 3.8).

None of the tested transcripts was significantly differently expressed in SOD1^{G93A} astrocytes versus NTg controls in either mono-cultured or co-cultured conditions. For mono-cultured astrocytes, *C1qb* and *Ctss* showed a trend towards the direction of regulation on the microarrays of symptomatic and late-stage SOD1^{G93A} astrocytes,

whilst for co-cultured astrocytes *C1qb* and *Timp1* showed a trend in the same direction as the arrays.

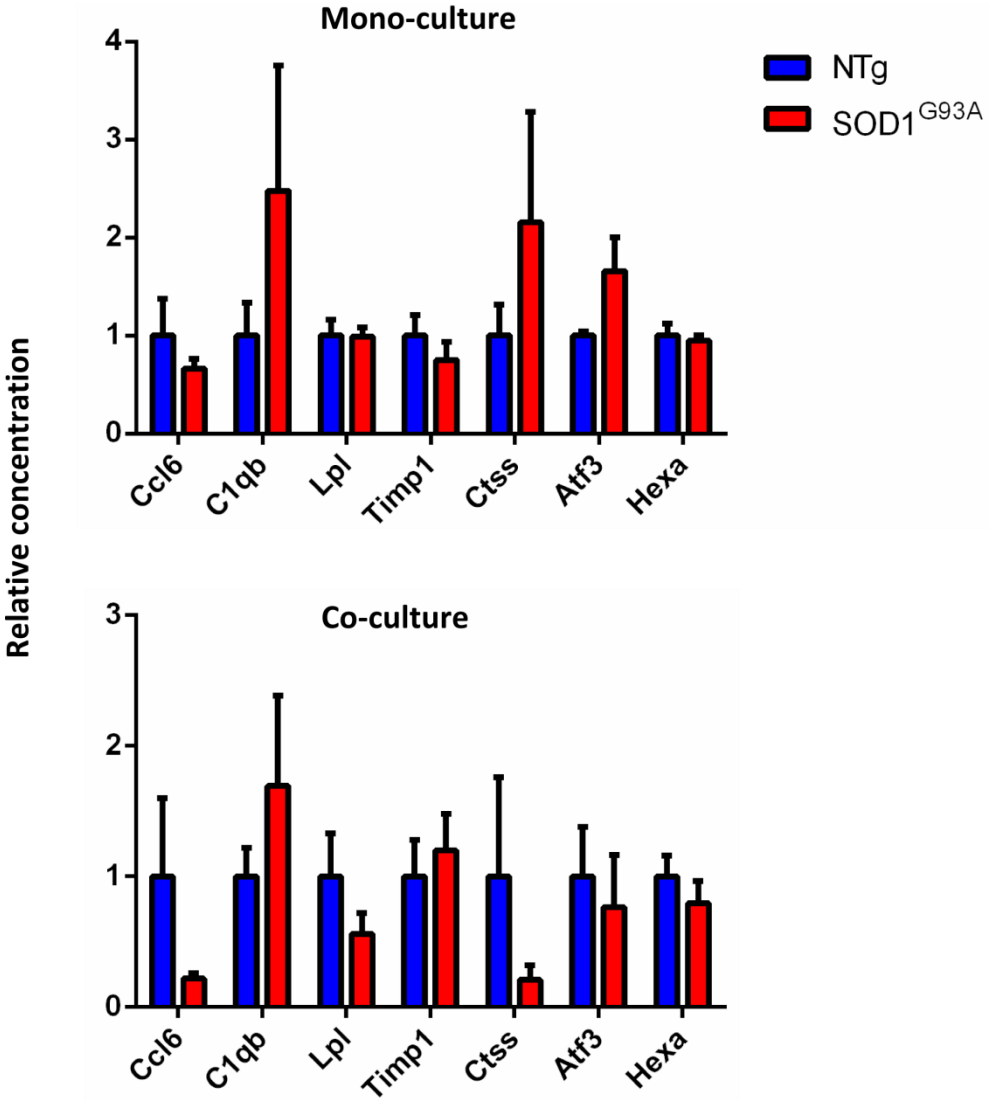

Figure 4.4 qPCR of transcripts called significant in microarray validation. **a)** qPCR of selected transcripts from microarray validation in mono-cultured astrocytes. n = 5 NTg and n=4 $SOD1^{G93A}$. **b)** qPCR of selected transcripts from microarray validation in astrocytes co-cultured with motor neurons. No transcripts were differentially expressed in either mono- or co-cultured astrocytes. For co-cultures n = 4 NTg and n = 3 $SOD1^{G93A}$. Error bars = SEM. $SOD1^{G93A}$ have been normalised to respective NTg controls.

4.4 Treatment of microglia with astrocyte conditioned medium – expression of M1 and M2 markers

Due to the increased expression of genes involved in the immune response in the microarray data from symptomatic and late-stage SOD1^{G93A} astrocytes (Section 3.6.4), the effect of SOD1^{G93A} astrocytes upon microglial phenotype was investigated. Microglia transition from an M2 "non-inflammatory" phenotype to an M1 "classically activated" phenotype during disease progression in the SOD1^{G93A} mouse (Liao et al., 2012) and given the differential expression of multiple chemokines in the symptomatic and late-stage SOD1^{G93A} gene lists the hypothesis was generated that: SOD1^{G93A} astrocytes are able to modulate microglial phenotype. This was tested by taking astrocyte-conditioned medium (ACM) from SOD1^{G93A} and NTg astrocytes for treatment of NTg microglia, which were then assayed for markers of M1 and M2 microglia by qPCR. As in section 4.2, this experiment was run with mono-cultured and co-cultured astrocytes to see if astrocytes required activation by motor neurons to elicit an effect. No significant difference was seen between NTg and SOD1^{G93A} for the expression of the M1 markers nitric oxide synthase 2 (*Nos2*) and cyclo-oxygenase 2 (*Cox2*) or for the M2 marker arginase 1 *(Arg1*) in either mono- or co-cultured astrocytes (Figure 4.6). In addition the M2 marker *Ym1* was assayed by qPCR but was not expressed at a high enough level to provide robust results via qPCR. To confirm these results, the medium of both astrocytes, and microglia that had been treated with ACM, were assayed for the presence of M1- or M2-polarising cytokines using flow cytometry. Cytokines tested were the pro-inflammatory cytokine IL1β, the "anti-inflammatory" cytokine IL10 and two chemoattractant cytokines: monocyte chemoattractant protein 1 (MCP1 a.k.a. CCL2) and keratinocyte chemoattractant (KC). In astrocyte media, none of the tested cytokines was significantly different in concentration between NTg and SOD1^{G93A} astrocytes, for either mono-cultured or co-cultured cells (Figure 4.6). This situation was the same for media from microglia that had been treated with ACM (Figure 4.7). When the cytokine profiles from both sets of cells were compared (Figure 4.9), it was observed that microglia secrete higher amounts of IL1β and IL10 into the media, which reached significance for Il1β in microglia treated with NTg-cc astrocyte media and for IL10 in microglia treated with NTg-mono astrocyte media. MCP1 and KC were

expressed at much higher levels than IL1β and IL10 in both astrocytes and microglia and showed similar levels of expression between the two cell types.

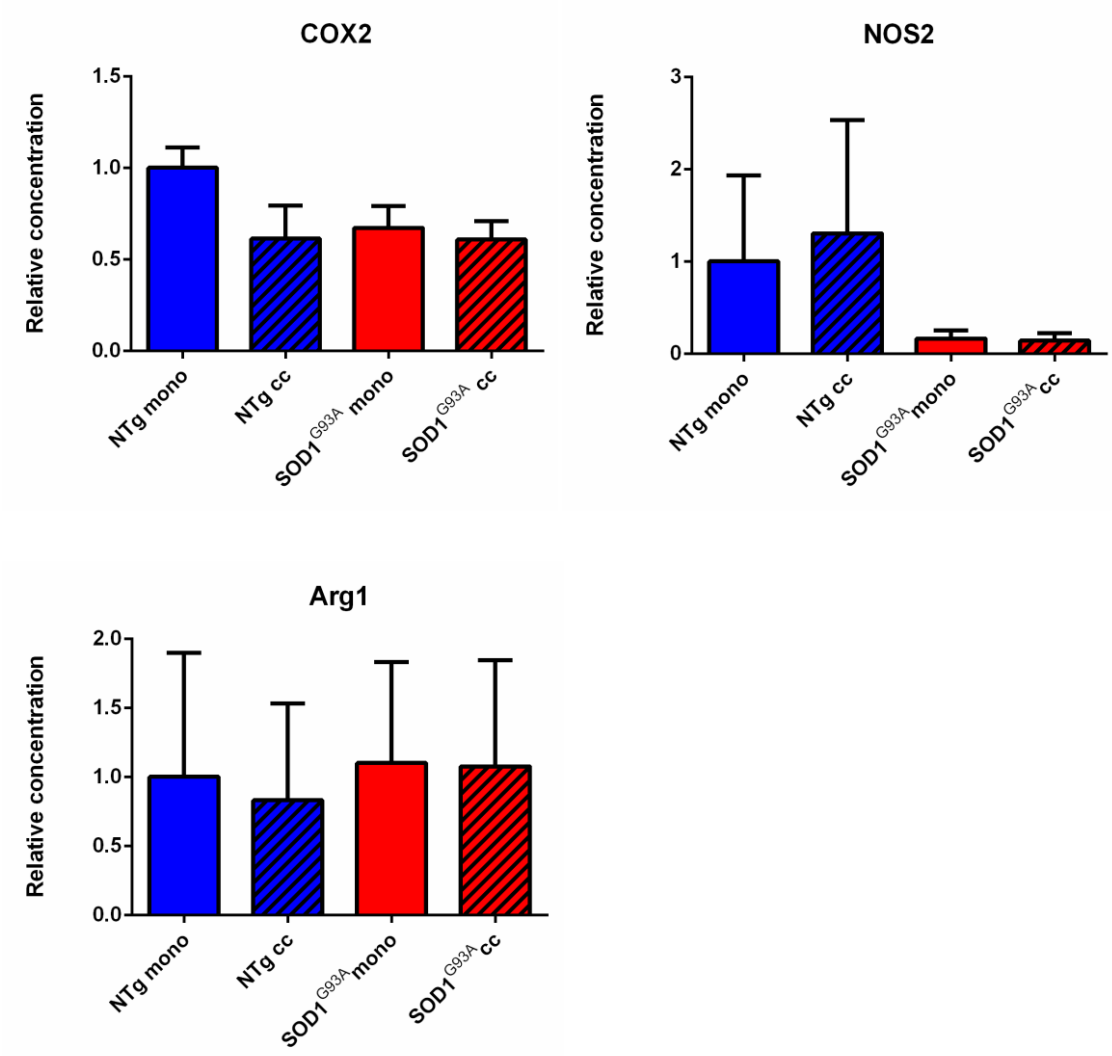

Figure 4.5 qPCR for the M1 markers *Cox2* and *Nos2* and the M2 marker *Arg1* in microglia treated with media from NTg and SOD1^{G93A} astrocytes in monoculture (mono) and astrocytes co-cultured with motor neurons (cc). None of the tested genes were significantly different between disease and control astrocytes. One-way ANOVA with Tukey post-hoc test.. Error bars = S.E.M. NTg mono and NTg cc: n=3. SOD1^{G93A} mono and SOD1^{G93A} cc: n=4.

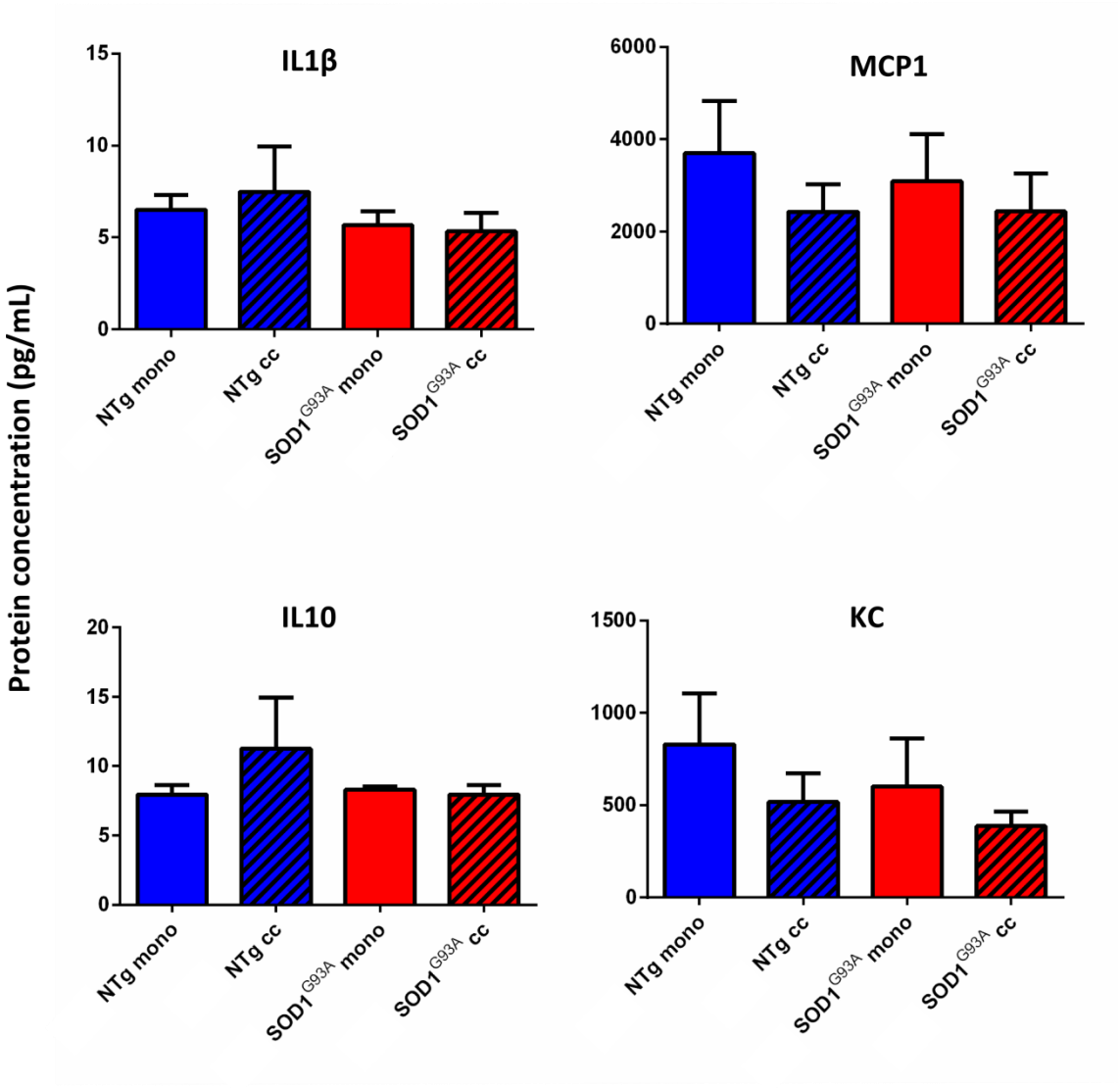

Figure 4.6 Presence of different cytokines in media from NTg and SOD1^{G93A} astrocytes in monoculture (mono) or co-cultured (cc) with motor neurons. None of the cytokines tested was significantly different between disease and control astrocytes. One-way ANOVA with Tukey post-hoc test. n=4 NTg mono and NTg cc, n=3 SOD1^{G93A} mono and SOD1^{G93A} cc. Error bars = S.E.M.

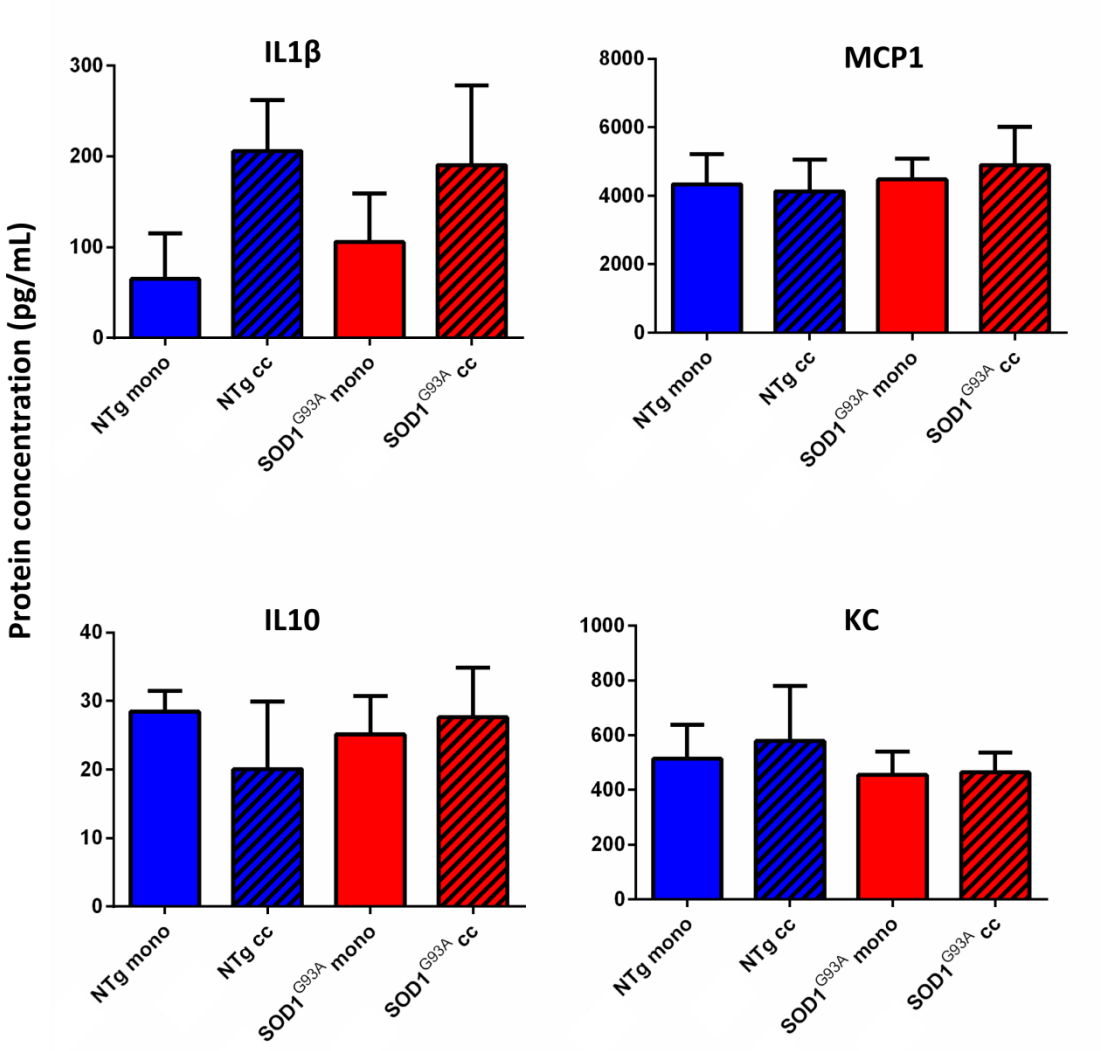

Figure 4.7 Presence of different cytokines in media from NTg microglia treated with NTg and SOD1^{G93A} astrocytes in monoculture (mono) or co-cultured (cc) with motor neurons. None of the cytokines tested was significantly different between disease and control astrocytes. One-way ANOVA with Tukey post hoc test. n=3 NTg mono and NTg cc, n=4 SOD1^{G93A} mono and SOD1^{G93A} cc. Error bars = S.E.M.

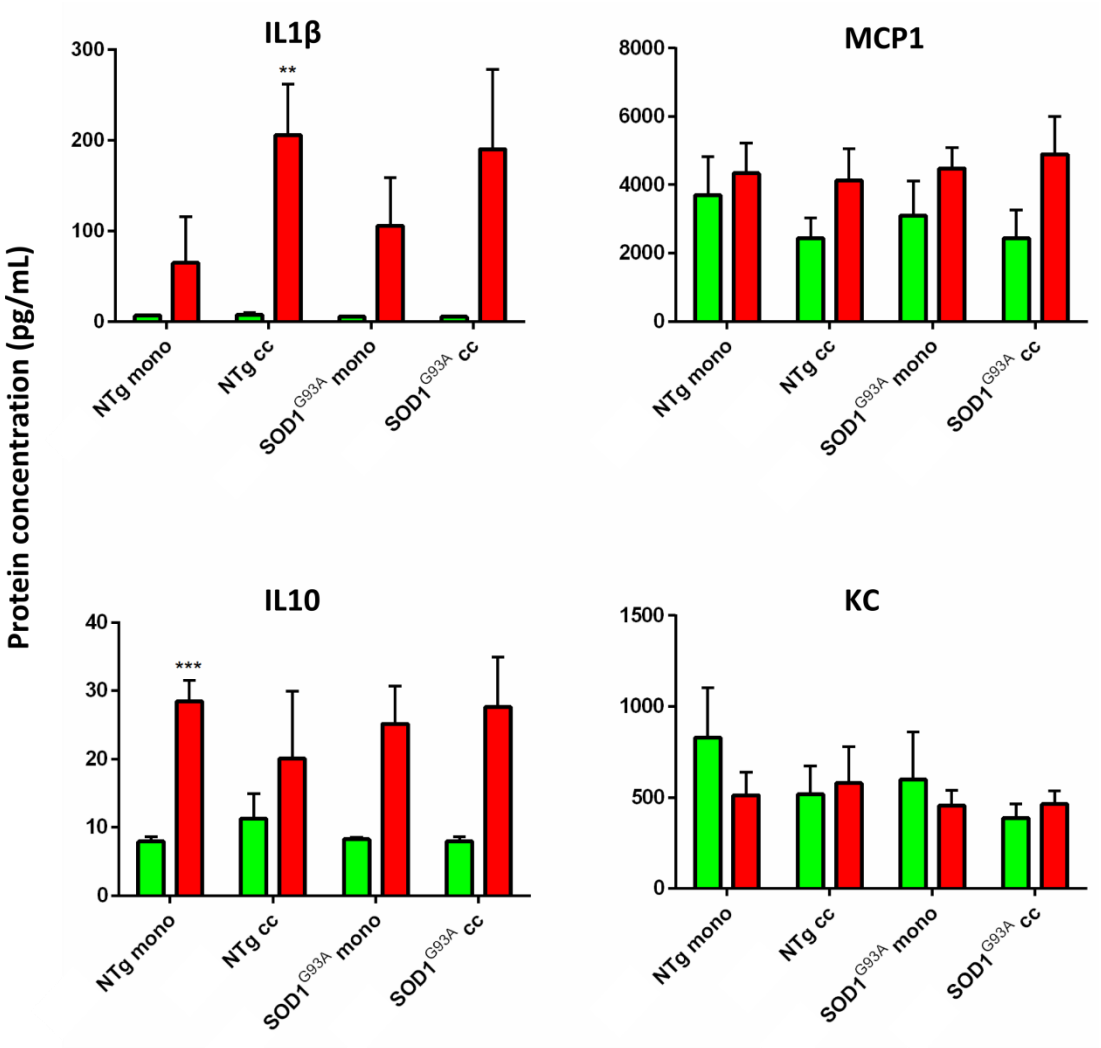

Figure 4.8 Comparison of cytokine expression between mono-cultured and co-cultured NTg and SOD1^{G93A} astrocytes (green bars) and NTg microglia (red bars) that have been treated with ACM from said astrocytes. Microglia show a trend for higher secretion of IL1β and IL10 compared to astrocytes for all conditions which reaches significance for IL1β (NTg-cc) and IL10 (NTg-mono), whereas levels of MCP1 and KC are comparable. Independent samples t-test. Error bars = S.E.M. ** = p≤0.01, *** = p≤0.001.

4.5 Up-regulation of lysosomal function in symptomatic and late-stage astrocytes

To confirm that the increased expression of lysosomal transcripts seen by qPCR validation (Section 3.8) was carried through to a functional up-regulation, an enzymatic activity assay was carried out for β-hexosaminidase (β-hex). The α- and β-subunits of β-hex are increased in expression at both symptomatic and late-stage disease in the microarray study (α-subunit (*Hexa*): 90d: +2.26, 120d: +2.38; β-subunit (*Hexb*): 90d: +2.54, 120d: +2.97). *Hexa* and *Hexb* showed a significantly increased expression and a trend for increased expression respectively when analysed by qPCR (Section 3.8 and Figure 3.12). To assess β-hex activity in different locations of the nervous system, sections of tissue were cut from the lower cord (~lumbar), upper cord (~thoracic) and motor cortex. As a control, tissue was collected from ≥120 day old mice over-expressing the wild-type human form of SOD1 ($SOD1^{WT}$). As an additional control β-galactosidase (β-gal) activity, which was not differentially expressed at either symptomatic or late-stage, was assayed in lumbar cord.

β-hex activity was found to be significantly increased in $SOD1^{G93A}$ compared to $SOD1^{WT}$ (855.3 ± S.D. 82.67) and NTg (90d: 819.8 ± S.D. 85.41 , 120d: 984.6 ± S.D. 223.1) in upper spinal cord sections at late-stage disease whilst showing a trend towards increased activity at the symptomatic time-point (90d: 1232 ± S.D. 139.2, 120d: 2442 ± S.D. 419.4) (Figure 4.5a). Similarly, in lower cord, β-hex activity was significantly increased in $SOD1^{G93A}$ compared to $SOD1^{WT}$ (1045 ± S.D. 162.6) and NTg (90d: 921.7 ± S.D. 329.1, 120d: 677.3 ± S.D. 403.4) at late-stage in lumbar cord whilst showing a trend towards increased activity at the symptomatic time-point (90d: 1167 ± S.D. 247, 120d: 2303 ± S.D. 620.1) (Figure 4.5b). In the motor cortex, there was no significant difference between any of the groups (Figure 4.5c). There was also no significant difference in the lower spinal cord between any of the groups for β-gal activity, which was also much lower than that seen for β-hex, reinforcing the findings of the microarray analysis.

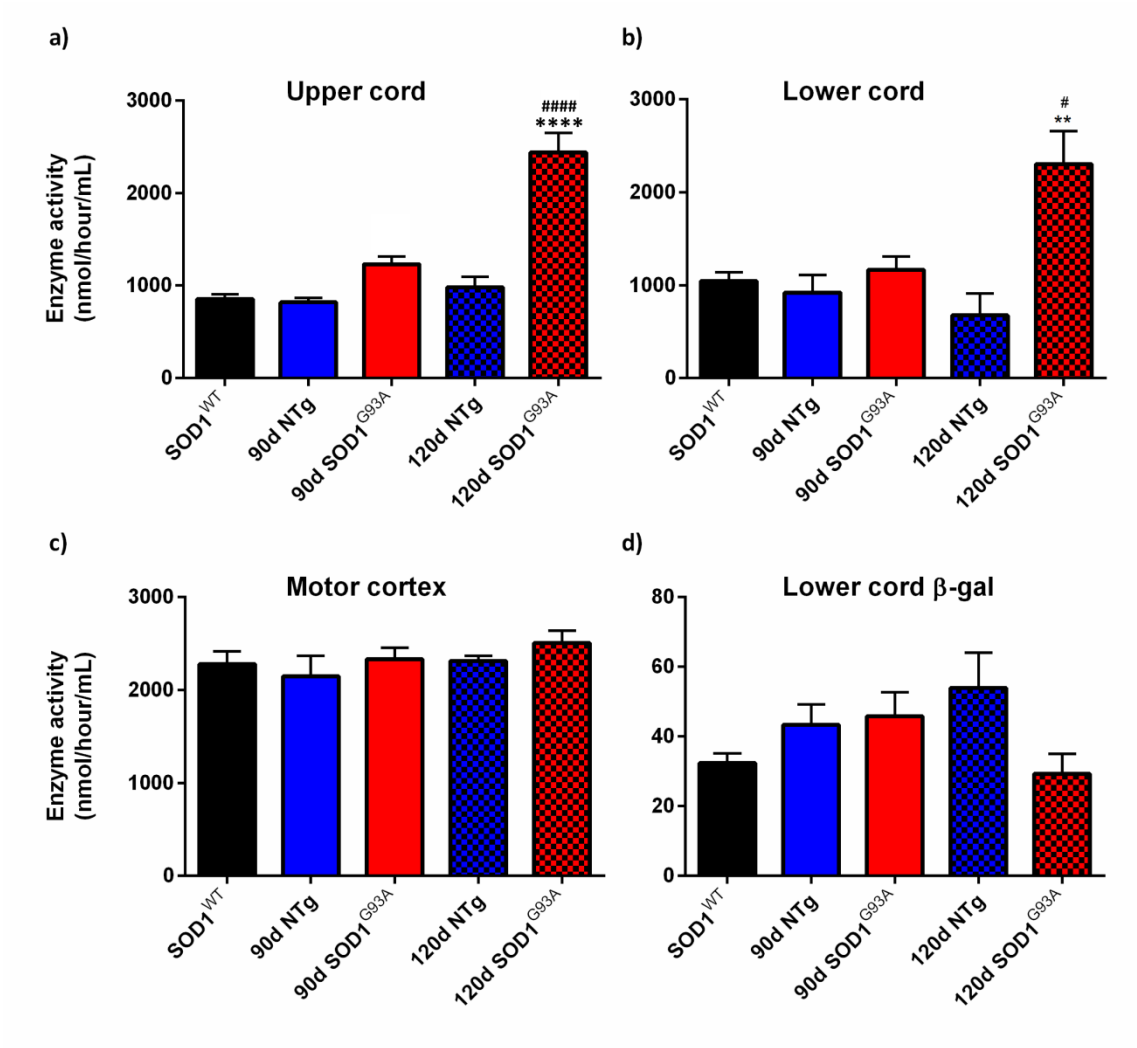

Figure 4.9 Assay of β-hexosaminidase (β-hex) activity in homogenates of upper cord, lower cord and motor cortex. **a)** In upper cord, there was a trend towards higher β-hex activity at symptomatic stage and β-hex activity was significantly higher in SOD1^{G93A} than either NTg or SOD1^{WT} in late-stage SOD1^{G93A} mice (SOD1^{WT}, 90d NTg and 90d SOD1^{G93A}: n=3, 120d NTg and 120d SOD1^{G93A}: n=4). **b)** In lower cord there was a trend towards higher β-hex activity in symptomatic SOD1^{G93A} spinal cord and a significantly higher activity in late-stage SOD1^{G93A} mice compared to NTg and SOD1^{WT} mice (n=3 for all groups). **c)** In the motor cortex no difference was seen for β-hex activity between any group. (n=3 for all groups except NTg 120d n=4). **d)** No difference was observed between any group for the control enzyme β-galactosidase (n=3 all groups). 90d = symptomatic, 120d = late-stage. ** = p≤0.01, **** = p≤0.0001 vs NTg control, ## = p≤0.01, #### = p≤0.0001 vs SOD1^{WT} (one-way ANOVA with Tukey post-hoc t-test). Error bars = S.E.M.

4.6 Increased phagocytosis in SOD1^{G93A} astrocytes

Transcripts for phagocytosis were enriched in the microarray data of both symptomatic and late-stage SOD1^{G93A} astrocytes (Section 3.6). To investigate this further, an assay was adapted from the method used by Sargsyan et al. (2011) to investigate SOD1^{G93A} microglial phagocytosis, which measured the amount of Cy3-labelled NSC34 cell debris taken up by astrocytes over a period of 48 hours. Astrocytes were observed with large accumulations of NSC34 cell debris within them (Figure 4.10a). To confirm that NSC34 debris had been phagocytosed, the assay was performed upon coverslips and visualised using confocal microscopy (Figure 4.10b). This confirmed the presence of red debris in the same plane as GFAP staining, as observed in the y/z and x/z planes. Taken together this increased the confidence in astrocyte phagocytosis occurring under these experimental conditions. The assay was analysed using the InCell 2000 analyser and the average amount of debris per cell quantified from 9 fields of 5 wells per cell line (number of cell lines NTg =3 SOD1^{G93A} = 3). The values for SOD1^{G93A} astrocytes in each experiment were normalised to their respective NTg controls. The results of three experiments show a significantly larger amount of NSC34 debris is phagocytosed per cell in SOD1^{G93A} astrocytes versus NTg controls (204.83% ± S.D. 36.6 vs. 100% ± S.D. 17.84) (Figure 4.10c).

Riluzole is currently the only drug used in the treatment of ALS and prolongs life by 2-3 months (Miller et al., 2007). Apart from its effects in reducing excitotoxicity in disease, other effects are unknown. Therefore riluzole was added to the phagocytosis assay at a concentration of 25µM to assess whether it has an effect upon phagocytic activity of astrocytes. The results show that whilst riluzole had no significant effect upon NTg controls, there was a trend towards a decrease in amount of debris phagocytosed per cell in SOD1^{G93A} astrocytes treated with riluzole. However, this result was not significantly different to non-treated SOD1^{G93A} astrocytes and SOD1^{G93A} astrocytes treated with DMSO only.

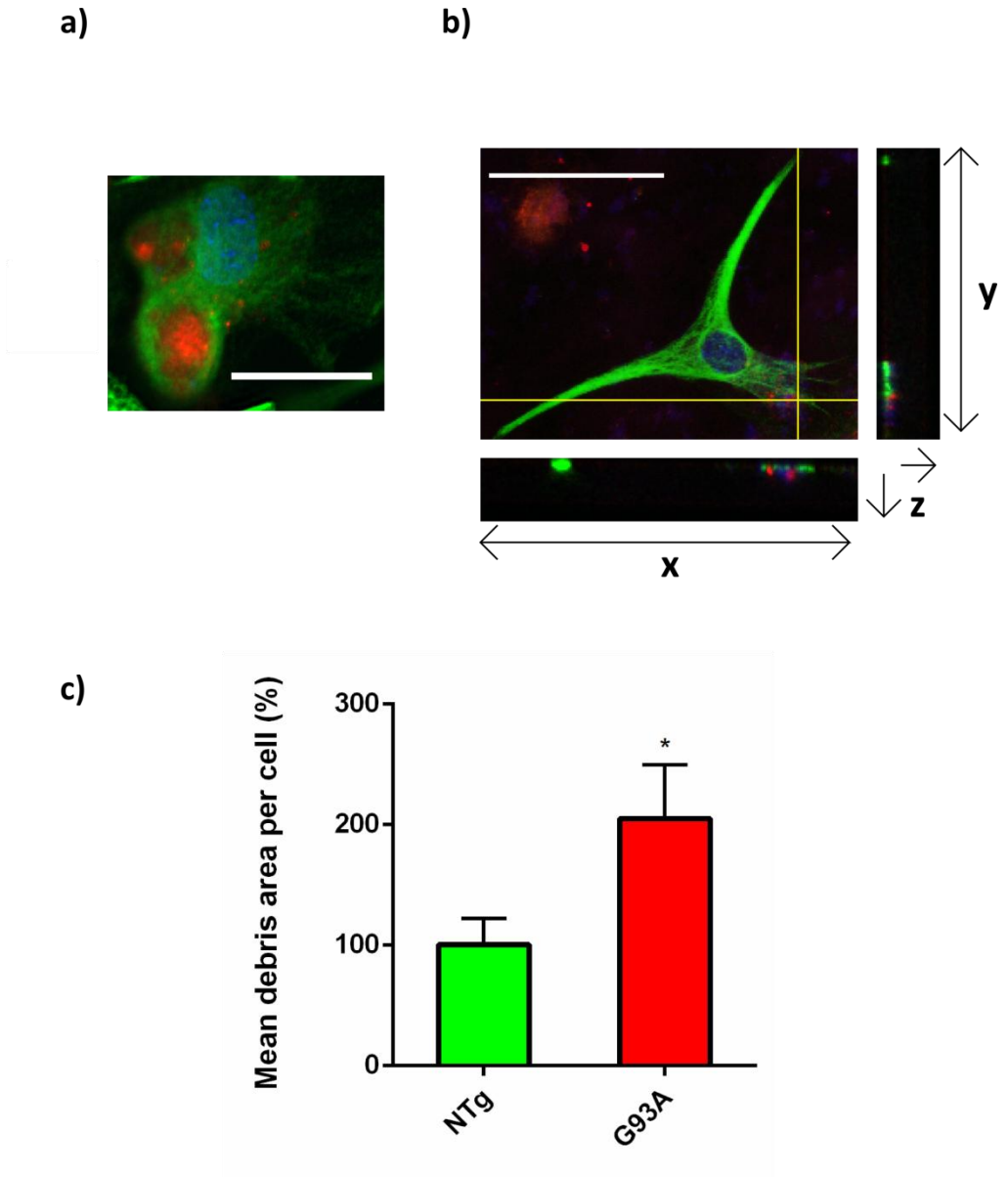

Figure 4.10 Phagocytosis of Cy3-labelled NSC34-cell debris by NTg and SOD1^{G93A} astrocytes. **a)** Astrocytes were labelled with GFAP (green) and imaged using the InCell at x63 magnification. Some cells contained large accumulations of NSC34 cell debris (red). **b)** Confocal microscopy confirmed that NSC34 debris were located in the same plane as GFAP staining suggesting that it is inside the cell rather than on the surface. Crosshairs indicate location of y/z and x/z planes. Within these planes the green and red staining are seen in close localisation. **c)** Mean debris area per cell in SOD1^{G93A} astrocytes was normalised to NTg controls. A significant increase (> 2-fold) in debris area per cell was observed in SOD1^{G93A} astrocytes versus control. * = p≤0.05, independent samples t-test. n=3. Error bars = S.E.M. Scale bars = 25µm.

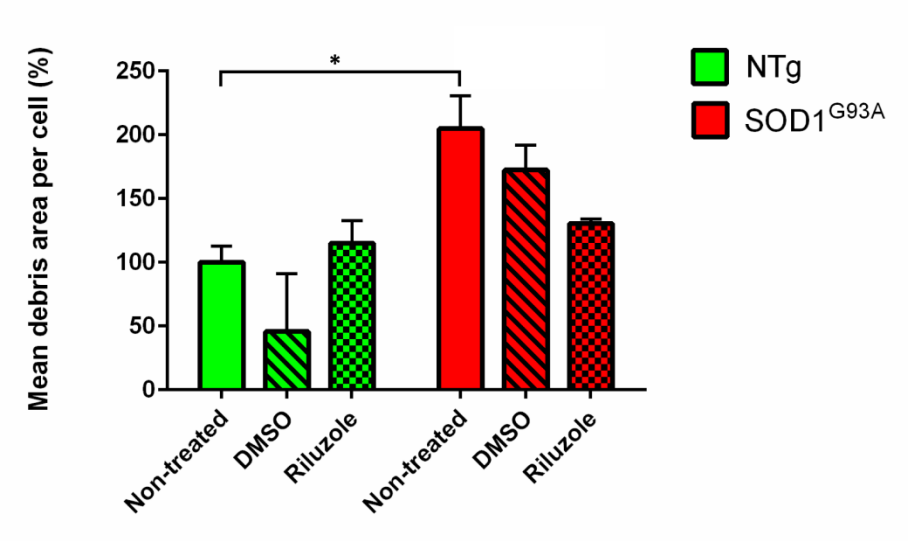

Figure 4.11 Mean debris area per cell in NTg and SOD1^{G93A} astrocytes treated with Cy3-labelled NSC34 cell debris alone or in combination with DMSO or riluzole (25µM). Apart from difference in phagocytosis of Cy3-labelled NSC34 cell debris previously seen, no significant difference was observed between groups in NTg or SOD1^{G93A} astrocytes upon treatement with Riluzole or DMSO. * = p≤0.05, one way ANOVA with Tukey's post-hoc test. Error bars = S.E.M. n = 3 per group.

4.7 Altered distribution of markers of cholesterol metabolism in late-stage SOD1^{G93A} astrocytes

At late-stage disease, several transcripts involved in cholesterol synthesis were dysregulated in SOD1^{G93A} astrocytes versus NTg controls (Section 3.6.6). To investigate whether cholesterol synthesis genes were affected at the protein level, immunohistochemistry (IHC) was performed for 3-hydroxy-3-methylglutaryl-CoA reductase (HMGCR), an important enzyme in the first steps of cholesterol synthesis, and Sterol regulatory element binding protein 2 (SREBP2) which is the master regulator of cholesterol synthesis and is involved in activating transcription of genes such as HMGCR. SREBP2 is normally located at the endoplasmic reticulum (ER) where it is sequestered until low cholesterol concentrations occur. This triggers the SREBP-cleavage activating protein (SCAP) to transport SREBP2 to the Golgi where it is processed to its active form and can proceed to the nucleus to activate genes involved in cholesterol synthesis (Brown and Goldstein, 1997).

Staining for HMGCR in the lumbar spinal cord of late-stage mice showed no difference in HMGCR expression or distribution between NTg and SOD1^{G93A}. For SREBP2, a change in the staining intensity of this protein was seen between the NTg and SOD1^{G93A} spinal cords (Figure 4.12). In NTg spinal cord cells with the morphology of motor neurons (dashed areas in Figure 4.13) stained negatively for SREBP2, whilst in SOD1^{G93A} cells with motor neuronal morphology were positive for SREBP2. In addition the SOD1^{G93A} spinal cord also contained cells with the morphology of astrocytes throughout the grey matter with SREBP2 outlining the processes of these cells (arrowhead in Figure 4.13).

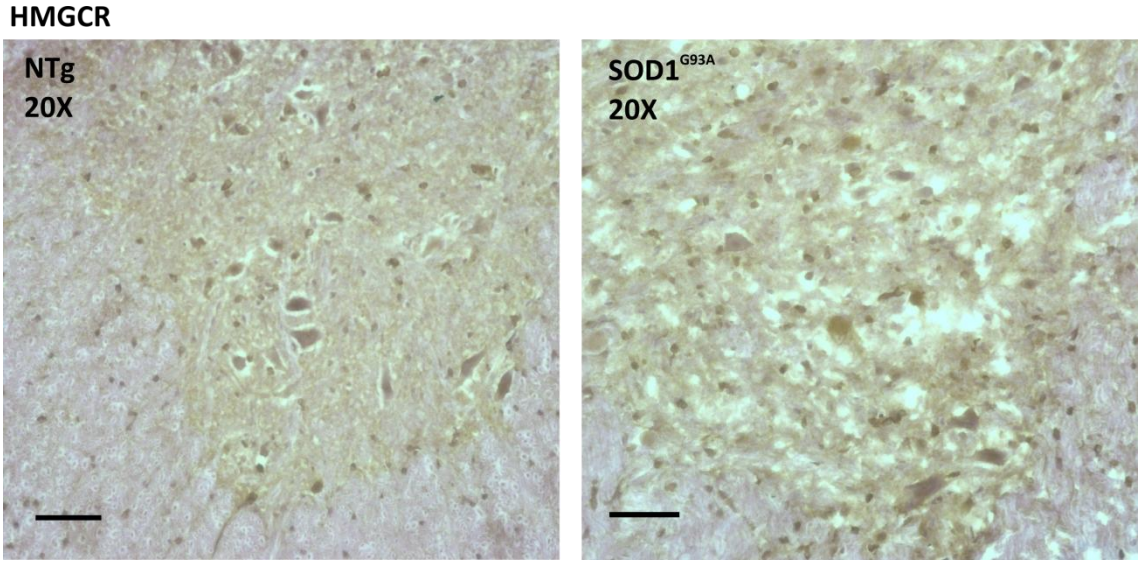

Figure 4.12 Staining for HMGCR in late stage NTg and SOD1^{G93A} spinal cord. HMGCR showed no difference between the NTg and SOD1^{G93A} condition, apart from the clear motor neuronal staining in the NTg cord that was absent in the SOD1^{G93A} cord due to neuronal loss. Scale bar = 100µm. Images representative of 3 animals per genotype.

SREBP2

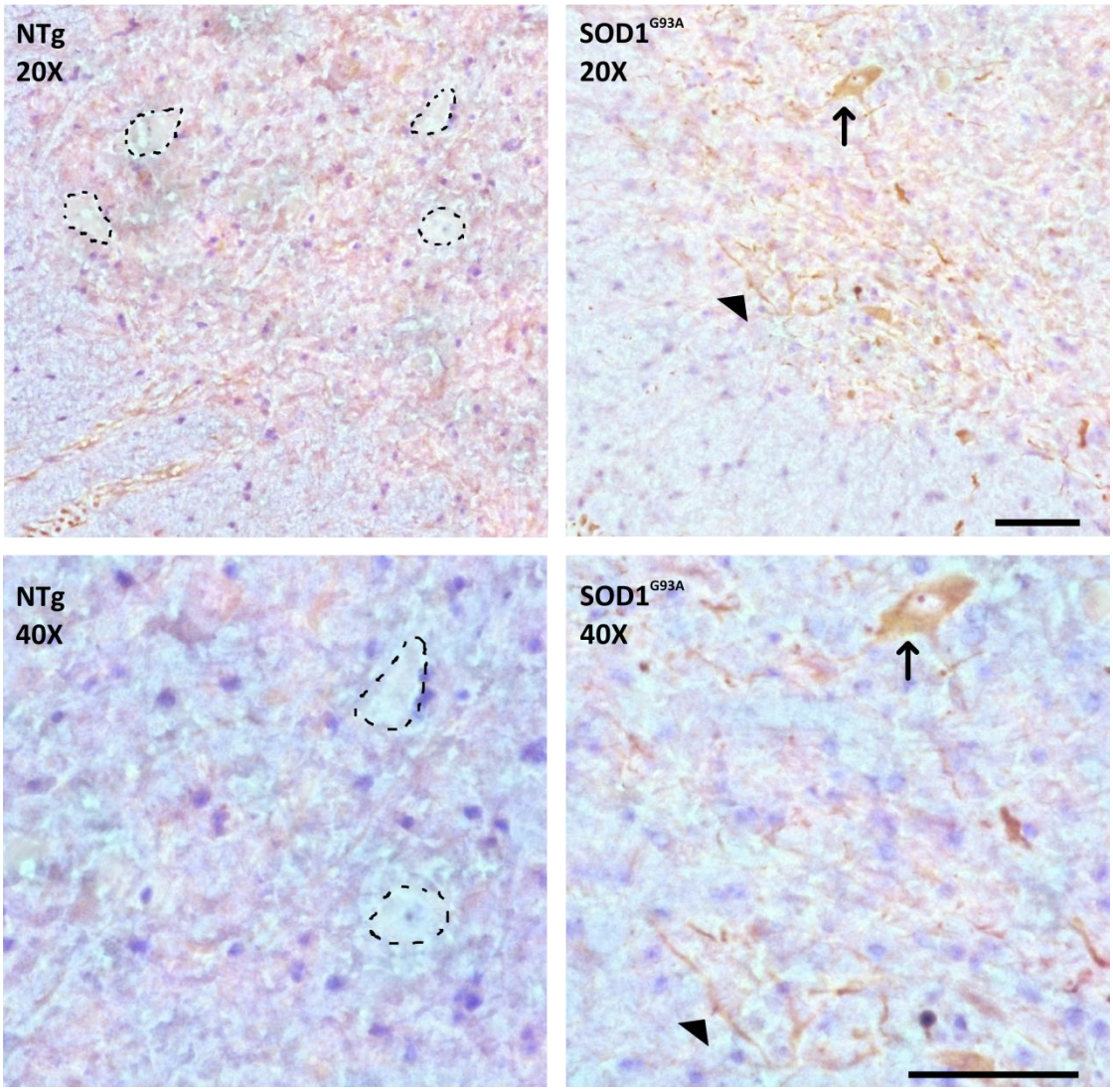

Figure 4.13 Staining for SREBP2 in late stage NTg and SOD1^{G93A} spinal cord. SREBP2 staining is altered in staining intensity between the NTg and SOD1^{G93A} condition. In NTg cord, negative staining is seen in areas with the morphology of motor neurons (dashed areas) whereas in the SOD1^{G93A} cord positive staining is seen in neurons (arrow) and in structures resembling astrocyte processes (arrowhead). Scale bar = 100µm. Images representative of 3 animals per genotype.

4.8 Discussion

4.8.1 The use of neonatal SOD1^{G93A} astrocyte cultures for modelling symptomatic and late-stage disease processes

The first objective for *in vitro* studies of SOD1^{G93A} astrocytes was to assess if these cells replicated some of the features of symptomatic and late-stage astrocytes seen in the array studies. Genes already validated as significantly differentially expressed upon the arrays were tested by qPCR in mono-cultured astrocytes and astrocytes co-cultured with motor neurons (Figure 4.4). None of the genes tested reached significance in either the mono- or co-cultured conditions, and only two genes per condition were differentially expressed in the direction indicated on the arrays. These results might seem surprising. However, in this model system astrocytes may not be stimulated by the factors secreted from other cell types *in vivo* leading to differences in gene expression between the cultured cells and those used in the arrays. In addition, co-cultures were performed for three days before collection of medium and RNA. This may not have been sufficient time for motor neuronal stress, and consequent gene expression changes in co-cultured astrocytes, to occur. Finally, neonatal cells may not have been exposed to mutant SOD1 long enough to replicate all of the features of adult SOD1^{G93A} astrocytes.

4.8.2 Astrocyte-conditioned medium did not activate microglia *in vitro*

Given the microarray findings of increased immune response transcripts in SOD1^{G93A} astrocytes, it was decided to investigate whether astrocytes could modulate microglial phenotype *in vitro*. Microglia are seen to progress from an M2 (or non-activated) phenotype characterised by secretion of “anti-inflammatory” cytokines at the start of disease to an M1 (classically activated) phenotype characterised by increased secretion of pro-inflammatory cytokines and reactive oxygen species towards the end-stage of disease in the SOD1^{G93A} mouse (Liao et al., 2012). Cultures of astrocytes obtained from neonatal SOD1^{G93A} mice have previously been shown to reproduce many of the gene expression changes seen in spinal cord of adult SOD1^{G93A} mice during the progressive phase of disease (Phatnani et al., 2013). It is therefore surprising that cultured astrocytes, with or without the presence of motor neurons, did not alter the expression of the M1 markers *Cox2* or *Nos2* or the M2 marker *Arg1* (Figure 4.6). This is

in agreement with the qPCR data from mono and co-cultured astrocytes which did not replicate the significant differences in gene expression seen in the microarrays of *in vivo* astrocytes (Figure 4.4). When assayed for the presence of modulatory cytokines there was no significant difference in the levels of IL1β, IL10, MCP or KC in astrocyte medium or in the medium of microglia treated with astrocyte medium (Figure 4.7 and Figure 4.8). Concordant with their increased immune role, microglia showed a trend for increased production of the cytokines IL1β and IL10 over astrocytes, which passed significance after treatment with NTG-cc medium (IL1β) and NTG-mono medium (IL10) (Figure 4.9).

Astrocyte-conditioned medium was obtained after three days of mono- or co-culture, which may not have been enough time for a sufficient level of modulatory factors to build up, and therefore future studies should focus upon extending the amount of time before which medium is collected. Ferraiuolo et al. (2011a), in their previous study of pre-symptomatic $SOD1^{G93A}$ astrocytes, co-cultured motor neurons and astrocytes for 14 days before which revealed the perturbation in lactate release suggested from their microarrays. Therefore the duration and type of stimulus must be optimised further to investigate astrocyte effects upon microglia.

In contrast to the previously mentioned study by Phatnani et al. (2013) showing that neonatal astrocytes reproduce the gene expression characteristics of adult $SOD1^{G93A}$ spinal cord, Benkler et al. (2013) showed that neonatal $SOD1^{G93A}$ astrocytes are characterised by a lack of supportive function and are unable to respond to activating factors. If neonatal astrocytes are unable to respond to activating factors this may be the reason for them not modulating microglial phenotype in the current experiments. Data from Chiu et al. (2013) suggest it may be too simplistic to use a few markers to define the phenotype of microglia. Their data show that microglia in ALS do not occupy either the M1 or the M2 ends of the spectrum but have a distinct phenotype unique to the disease process occurring around them in which they express both neuroprotective and neurotoxic factors simultaneously. Adult murine microglial cultures are now optimised (Frakes et al., 2014) and further efforts should be made to optimise the culture of adult astrocytes for future co-culture investigations. The use of these cell types and a secretome-mapping approach may prove more useful in

answering the question of whether astrocytes are involved in microglial phenotype modulation.

4.8.3 Lysosomal up-regulation is present in symptomatic and late-stage SOD1^{G93A} mice

Several lysosomal transcripts were increased in expression in both the symptomatic and late-stage astrocyte gene expression profiles. The activity of total β-hexosaminidase (β-hex) was therefore assayed, as the *Hexa* (encoding the α-subunit) and *Hexb* (encoding the β subunit) transcripts were up-regulated in SOD1^{G93A} astrocytes at both time-points on the arrays with *HexA* significantly increased and *HexB* showing a trend for increased expression by qPCR. Two β-hex isoenzymes exist, HexA and HexB, which hydrolyse GM_2 gangliosides. HexA is a heterodimer of an α and β subunit whilst Hex B is a homodimer of two β subunits (Mahuran, 1995). The increase in total β-hex activity seen in symptomatic and late-stage SOD1^{G93A} spinal cord validates the up-regulation seen in the microarray analyses at these time-points. A caveat of the experiments performed here is the use of whole spinal cord homogenate in the assay. This means that the increased activity of β-hex cannot be ascribed to a particular cell type. Chiu et al. (2013) found that lysosomal transcripts were increased in expression in SOD1^{G93A} microglia using deep sequencing, and localised Ctsb and Ctss expression to microglia using immuno-staining. However, the levels of microglial marker transcript expression on the arrays is low in comparison to those of astrocytes (Section 3.4). A previous study by Fukada et al. (2007) has found Cathepsin H expression to be increased in the spinal cord of the Leu126delTT mouse model of ALS. This increased expression was localised to both astrocytes and microglia. In addition Cathepsin B expression has been localised to GFAP^{+} astrocytes in symptomatic SOD1^{G93A} mouse spinal cord (Wootz et al., 2006). This suggests that both types of glial cell are activated in the same way during disease progression.

4.8.4 Phagocytosis is increased in SOD1^{G93A} astrocytes

Several transcripts were increased in expression in SOD1^{G93A} astrocytes that suggested an increased phagocytic activity (Table 3.12). Sargsyan et al. (2011) have previously shown that SOD1^{G93A} microglia phagocytose significantly less Cy3-labelled NSC34 cell debris compared to NTg controls. Using the same assay as Sargsyan et al. (2011),

SOD1^{G93A} astrocytes phagocytose significantly more NSC34 debris than NTg controls, reinforcing the up-regulation seen in the microarray analysis. This assay also provides evidence for the purity of the arrays and the assigning of these immune transcripts to astrocytes, as astrocyte cultures were ≥95% pure (Figure 4.1) and only cells that were GFAP^{+} were measured.

Astrocyte phagocytosis of apoptotic cell debris is protective to co-cultured neurons (Loov et al., 2012), therefore the increased phagocytic ability of SOD1^{G93A} astrocytes might be a protective mechanism if it exists *in vivo*. In contrast to Sargsyan et al. (2011), Frakes et al. (2014) showed SOD1^{G93A} microglia were more toxic to co-cultured neurons and that they attacked and phagocytosed neuronal debris. Given the differing findings of Sargsyan et al. (2011) and Frakes et al. (2014) this may mean that either astrocytes are able to compensate for reduced microglial phagocytosis in the diseased spinal cord or that both cell types work in concert in phagocytosing increased amounts of debris. To answer this question, future experiments could use SOD1^{G93A} mice with GFP-tagged motor neurons, with subsequent immunohistochemical analysis of GFP-labelled debris within astrocytes and microglial cells.

Riluzole is currently the only therapy approved for the treatment of ALS. Its known mechanisms of action include reduction of excitotoxic damage to neurons via inhibition of neurotransmitter release and modulation of Na^{+} and K^{+} currents (Bellingham, 2011). Little is known about the effect of riluzole upon astrocytic behaviour, therefore we sought to see if there was an effect of riluzole upon phagocytic ability of SOD1^{G93A} and NTg astrocytes (Figure 4.11). Riluzole had no effect upon the phagocytosis of NSC34 debris in NTg astrocytes. In contrast phagocytosis of NSC34 debris by SOD1^{G93A} astrocytes was significantly decreased in the presence of riluzole. This decrease was not significantly different to the decrease observed when SOD1^{G93A} astrocytes were treated with DMSO alone, therefore further replicates will need to be added to assess whether this observation is robust. If phagocytosis of cellular debris is protective as previously suggested by Loov et al. (2012), these data may suggest that Riluzole has a detrimental effect by reducing astrocyte phagocytosis, which may be a contributing factor to the relatively short extension of lifespan observed with riluzole treatment. Future therapies would therefore need to look at

combinatorial approaches that might preserve protective behaviours that are negatively affected by riluzole treatment.

Astrocytes in culture have been found to engulf cells via a classic non-professional phagocyte mechanism involving the proteins Megf10 and Crk (Loov et al., 2012). Other proteins thought to be involved in non-professional phagocytosis are Dock180, Elmo, Gulp1, and abca1 (Kinchen et al., 2005). Only Crk (120d: -2.07) and Elmo2 (120d: -2.48) are differentially expressed in the microarray data of SOD1^{G93A} astrocytes and in the opposite direction than expected given the increased phagocytic ability of SOD1^{G93A} astrocytes seen *in vitro*. However, transcripts for recognition of IgG are increased in expression, such as *Fcgr1*, *Fcgr2b* and *Fcgr3* (Appendix 3). IgG removed from serum of ALS patients and injected into healthy mice is seen to localise to motor neurons (Engelhardt et al., 2005), and thereby might promote phagocytosis by astrocytes. The effect of IgG upon astrocyte phagocytosis needs to be investigated further, however this might signify a difference in the behaviour of *in vivo* and *in vitro* astrocytes, whereby the array data shows phagocytosis to operate by recognition of opsonin-bound debris *in vivo* and the data of Loov et al. (2012) shows it to operate by recognition of markers of apoptotic cells *in vitro*. Regardless, these data demonstrate and add to the growing evidence of astrocyte phagocytosis and its importance in the CNS.

4.8.5 Cholesterol synthesis is dysregulated in late-stage SOD1^{G93A} astrocytes

In addition to functional studies that investigated the reactive phenotype of astrocytes, immunohistochemistry was performed to investigate the down-regulation of many transcripts involved in cholesterol processing in the late-stage SOD1^{G93A} data (Section 3.6.6). Genes involved in cholesterol processing are key in other neurodegenerative diseases such as Alzheimer's disease (AD) which features polymorphisms in *APOE* (up-regulated in late-stage SOD1^{G93A} astrocytes by 5.23-fold) and also *ACAT1* (*Acat2* is -2.23 at late-stage) as risk factors (Liu et al., 2010). Niemann-Pick Disease, which is a lysosomal storage disorder characterised by neurodegeneration, features a defect in the ability of the lysosome to process sphingosine and a subsequent accumulation of cholesterol (Vanier, 2014). In ALS, cholesterol esters and the sphingolipid sphingomyelin are increased in the spinal cord

of sALS patients versus controls (Cutler et al., 2002). A side effect of increased intracellular lipid concentrations may operate in SOD1-ALS with regard to misfolding of SOD1; the A4V mutation, which is the most common variant in American SOD1-ALS cases (Cudkowicz et al., 1997), confers an increased propensity for SOD1-misfolding when in increasing concentrations of fatty acids (Kim et al., 2005).

Given the increased phagocytic and lysosomal activity demonstrated here, it is tempting to suggest that increased cholesterol accumulates in the cell through phagocytosis of cell debris. Much cholesterol is contained within the cell membranes of this debris, along with sphingolipids such as gangliosides, which are broken down by the concomitant increase in activity of β-hexosamindase. Poirier et al. (1993) showed that after damage to the rat entorhinal cortex, the cholesterol synthesis of the nearby hippocampal tissue was significantly decreased by 8-days post-lesion and that the hippocampal APOE content was significantly increased by this timepoint. This is consistent with the pattern seen within the late-stage $SOD1^{G93A}$ microarray data in which cholesterol synthesis genes are decreased in expression whereas *ApoE* expression is increased. Increased APOE activity might function to redistribute excess astrocytic cholesterol to neurons, and future study should focus upon confirming the increased expression of APOE at the protein level. The increased motor neuronal and astrocytic staining of SREBP2 seen in late-stage $SOD1^{G93A}$ lumbar spinal cord (Figure 4.12b) may be due to these increased cholesterol levels inhibiting the processing and movement of SREBP2 to the nucleus. Indeed the staining for SREBP2 appears to be located throughout the cytoplasm of motor neurons and the processes of astrocytes rather than the nucleus. To investigate this further, cholesterol measurements of the spinal cord need to be performed in order to confirm an increased cholesterol content in $SOD1^{G93A}$ vs NTg controls. In addition, *in vitro* studies should be performed to investigate whether increased extracellular cholesterol leads to cytoplasmic SREBP2 localisation in astrocytes and if the $SOD1^{G93A}$ mutation affects this.

CHAPTER 5

RESULTS

Gene expression profiling of astrocytes from SOD1-ALS patients

5 Gene expression profiling of astrocytes from SOD1-ALS patients

5.1 Introduction

Microarray analysis was performed upon ~1500 astrocytes laser captured from the ventral horn of the lumbar spinal cord of 3 SOD1-ALS cases and 6 non-ALS controls. The ALS cases consisted of: 34/92 (age 40, female), 37/04 (age 60, female) and 49/94 (age 66, female) with a mean age of 55.33 ± S.D. 13.61. The control group consisted of 2JK3 (age 71, male), 2JK4 (age 80, female), 2JK7 (age 54, female), 135.34 (age 89, female), 2JK10 (age 82, male), 20/07 (age 77, male) with a mean age of 75.5 ± S.D. 12.08.

5.2 RNA amplification and fragmentation

RNA quality was assessed immediately after laser capture, following amplification and following fragmentation steps of the microarray preparation procedure (Figure 5.1). Amplification effectively increased the amount of RNA for use in array analysis (Table 5.1) and fragmentation effectively produced shorter species of RNA with a smaller spread in sequence length, thereby increasing the likelihood of binding to the complementary 25mer probe sequences on the GeneChips.

Table 5.1 RNA yields of samples used in microarray analysis of human SOD1-ALS and control astrocytes following 1-round and 2-round amplification.

Sample	Disease status	RNA yield 1st round amplification	RNA yield 2nd round amplification
135.34	Control	57.64	1032.05
2JK4	Control	83.92	714.15
2JK7	Control	78.07	856.95
20/07	Control	80.47	1389.3
2JK10	Control	82.12	1721.89
2JK3	Control	65.15	958.91
49/94	SOD1-ALS	68.19	882.34
37/04	SOD1-ALS	69.2	501.32
34/92	SOD1-ALS	73.53	1813.72

5.3 Quality control of human astrocyte GeneChips

As in the mouse analysis (Chapter 3) GeneChips were first subjected to quality control analysis in Bioconductor (Figure 5.2). Three SOD1-ALS cases and six controls were run on the arrays. It is apparent in Figure 5.2 that the three SOD1-ALS cases possess higher percentage present calls as a group than the 6 controls (SOD1 mean: 46.94 range: 46.41-47.57; Control mean: 33.99 range: 14.92-46.33). Meanwhile, average background values were consistent across all chips (SOD1 mean: 28.95 range = 28.07-30.39; Control mean: 28.03 range: 26.77-31.65).

When the percentage present calls of each of the GeneChips was individually assessed, two GeneChips, 2JK3 and 2JK7, possessed lower percentage present values than the rest of the group. 2JK3 is more than a factor of three-fold outside the experiment average chip intensity (blue band in Figure 5.2) and has a percentage present call much lower than the other GeneChips (14.92%). Likewise 2JK7 is only just within the scale factor viewed as acceptable by Affymetrix and also has a low percentage present call (24.89%). The lower percentage present calls of 2JK3 and 2JK7 indicate errors in the hybridisation process for these samples. In addition to lower percentage present calls, RNA degradation analysis showed 2JK3 and 2JK7 to have lower mean intensity values than the rest of the GeneChips for probesets at the 3' end of target transcripts. This is also indicative of less efficient hybridisation for these two samples. NUSE analysis of 2JK3 and 2JK7 showed both samples to have a larger spread of values compared to the rest of the samples and the mean of 2JK3 to be close to 1.1, indicative of low quality (Figure 5.4). Finally, RLE analysis confirmed 2JK3 and 2JK7 as lower quality samples due to the larger spread of values and the mean for these samples not being centred around zero (Figure 5.5).

Due to the results of the quality control analysis indicating a lower level of hybridisation for 2JK3 and 2JK7, the decision was made to remove these GeneChips from all subsequent analyses. Removal of 2JK3 and 2JK7 resulted in a more similar mean and range of percentage present calls to the SOD1-ALS GeneChips (control mean: 41.03 range: 34.04-46.33). NUSE and RLE plots also revealed that removal of

2JK3 and 2JK7 resulted in a more uniform set of GeneChips for further analysis (Figure 5.6).

The resulting 3 SOD1-ALS and 4 control GeneChips were processed using the PUMA package. All GeneChips showed similar distributions of intensity values prior to and following normalisation using the MMGMOS algorithm (Figure 5.7) and consequently differential expression analysis was performed.

a) POST-LCM

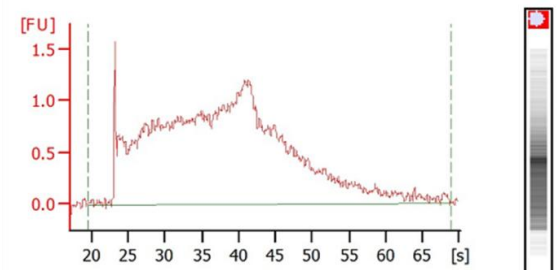

Overall Results for sample 4 : 20/07 RNACon

RNA Area:	63.8
RNA Concentration:	6,254 pg/µl
rRNA Ratio [28s / 18s]:	0.0
RNA Integrity Number (RIN):	2.3 (B.02.08)
Result Flagging Color:	
Result Flagging Label:	RIN: 2.30

b) POST-AMPLIFICATION

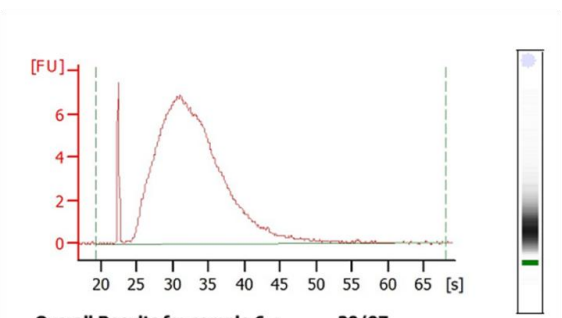

Overall Results for sample 6 : 20/07

RNA Area:	217.8
RNA Concentration:	148 ng/µl
rRNA Ratio [28s / 18s]:	0.0
RNA Integrity Number (RIN):	2 (B.02.08)
Result Flagging Color:	
Result Flagging Label:	RIN:2

c) POST-FRAGMENTATION

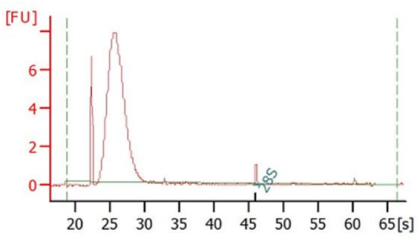

Overall Results for sample 6 : 20/07

RNA Area:	85.8
RNA Concentration:	72 ng/µl
rRNA Ratio [28s / 18s]:	0.0
RNA Integrity Number (RIN):	2.6 (B.02.08)
Result Flagging Color:	
Result Flagging Label:	RIN: 2.60

Fragment table for sample 6 : 20/07

Name	Start Time [s]	End Time [s]	Area	% of total Area
28S	45.92	46.55	0.6	0.7

Figure 5.1 Representative picochip (**a**) and nanochip (**b** and **c**) results for LCM-RNA post-LCM (**a**), post-amplification (**b**) and post fragmentation (**c**). Fragmentation of cDNA was successful in creating a smaller and tighter distribution of RNA species which were detected before 30 seconds (**c**). Graphs are representative of all 7 samples.

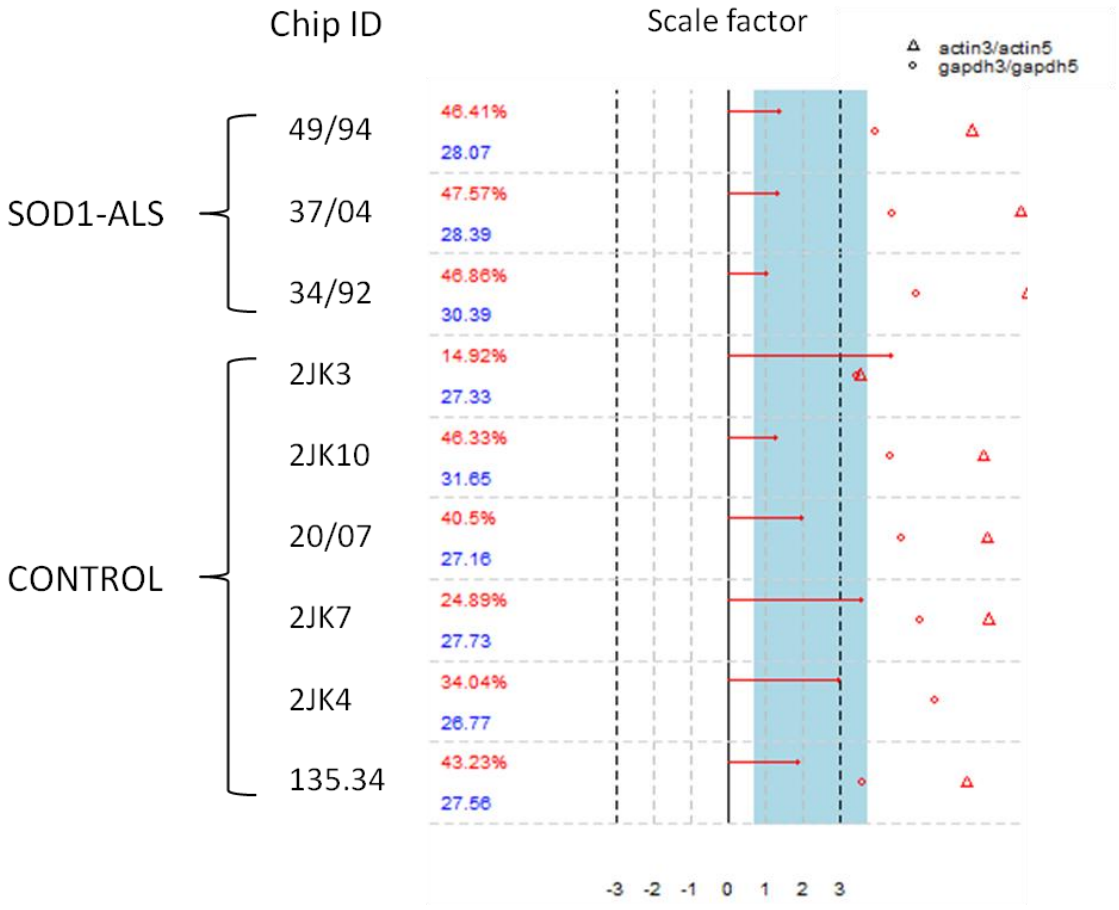

Figure 5.2 Quality control of microarray chips for SOD1-ALS and control astrocytes pre-normalisation performed in Bioconductor using the *simpleaffy* package. Chips are listed on the left, percentage present call is in red, average background is in blue to the right of chip ID. The scale factor graph to the right of each chip represents the signal intensity for each chip. The blue strip represents the range where the individual average chip intensities are within three-fold of the overall chip intensity. The GeneChips "2JK3" and "2JK7" are inconsistent with the rest of the analysed GeneChips both in terms of percentage present call and also in scale factor. On the far right of the figure are triangles and circles indicating the ratio of 5' *ACTIN* to 3' *ACTIN* and 5'*GAPDH* to 3'*GAPDH* respectively as a measure of RNA degradation; where red indicates a value above the recommended ratio. 34/92 (SOD1) and 2JK4 (Control) both contain an *ACTIN* 3'-5' ratio that is beyond the bounds of the graph and therefore a triangle is not shown for these samples.

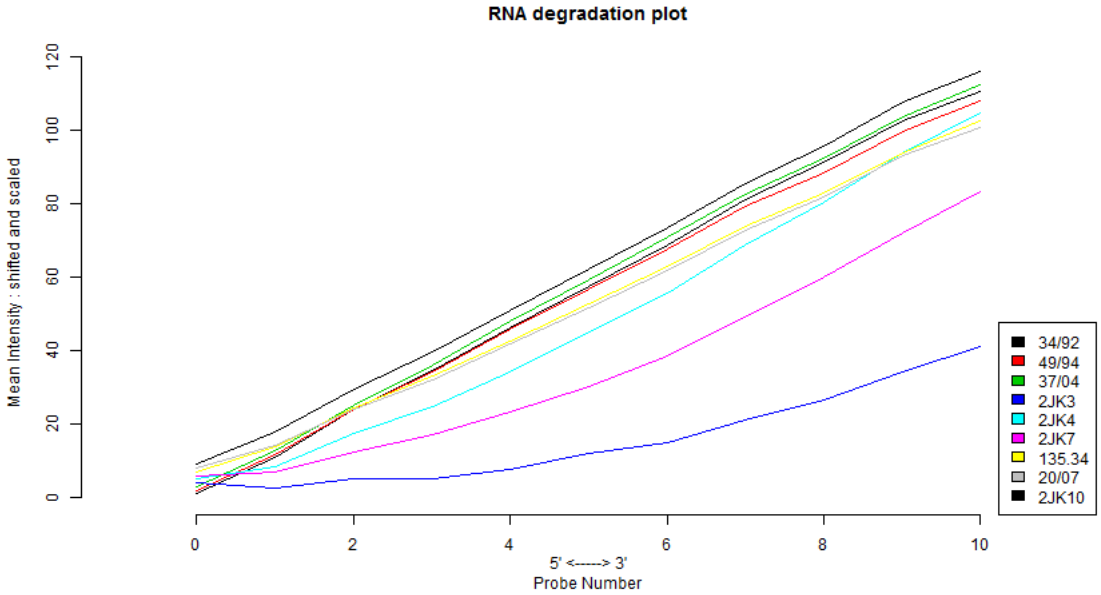

Figure 5.3 RNA degradation plot for all GeneChips initially run in the analysis of human SOD1 astrocytes versus controls. The mean intensity of each probe within a probeset from the most 5' to the most 3' is given. GeneChips 2JK3 and 2JK7 are again of lower quality showing lower mean intensity values at the 3' end than GeneChips from the other samples. This indicates a lower amount of RNA hybridisation has taken place for these GeneChips.

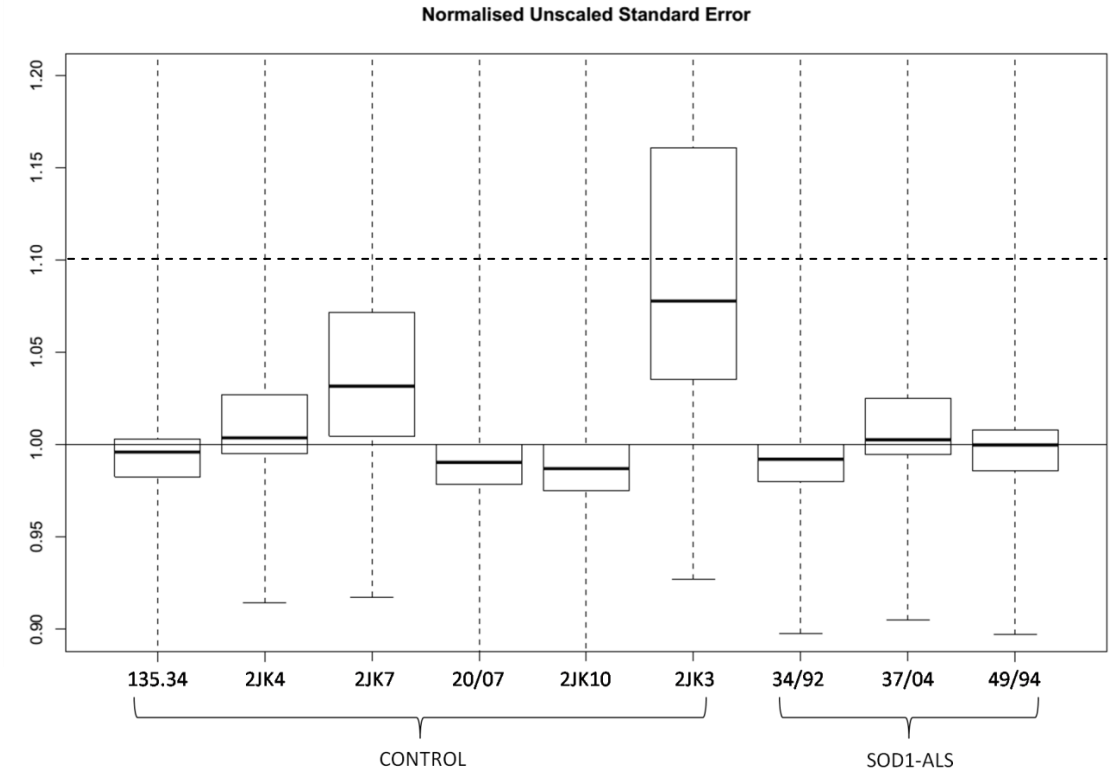

Figure 5.4 Normalised Unscaled Standard Error (NUSE) plot for human SOD1-ALS and control astrocytes. Lower quality GeneChips have a standard error greater than one and show as higher on the plot. An average level of 1.1 (dotted line) indicates a low quality array. The NUSE plot shows 2JK7 and 2JK3 to be lower quality arrays than the rest of the analysed GeneChips.

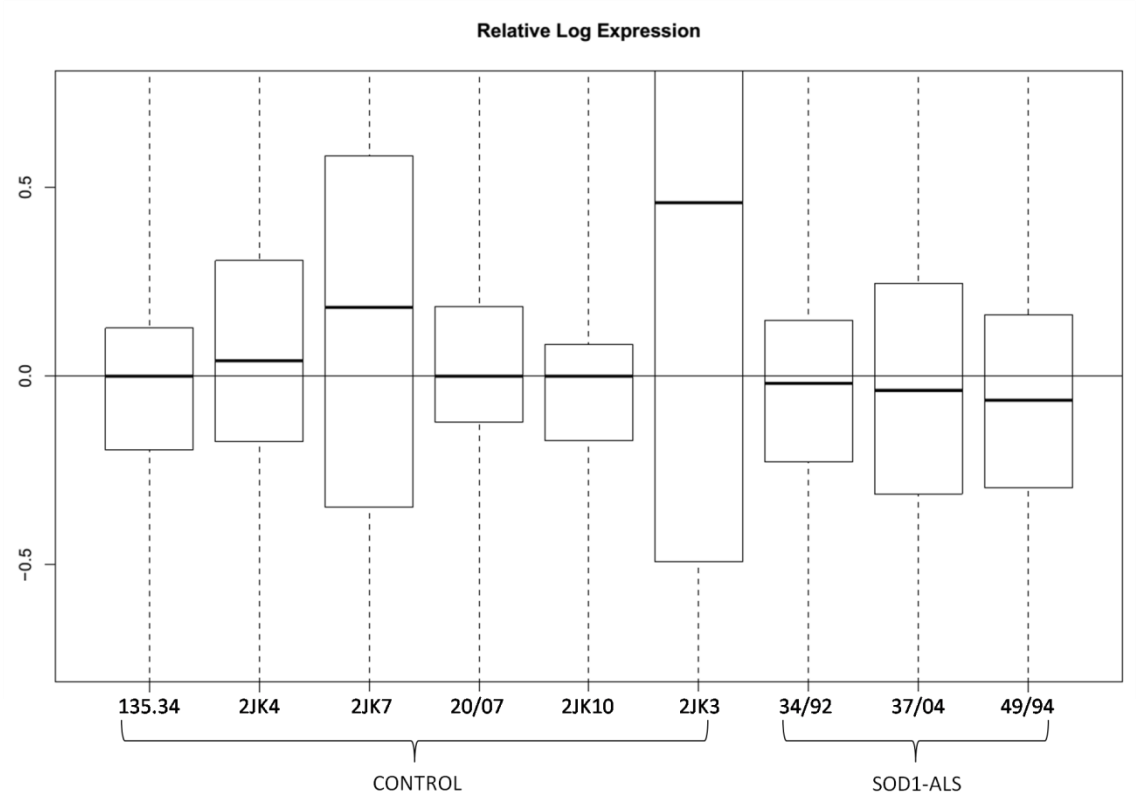

Figure 5.5 Relative Log Expression (RLE) plot of human SOD1-ALS and control astrocytes. The more variable a GeneChip is from the median, the larger its spread of values on the RLE plot. GeneChips should be centred around zero and possess a similar spread. The RLE plot reinforces the findings from previous analyses in that 2JK7 and 2JK3 are identified as outliers in terms of quality.

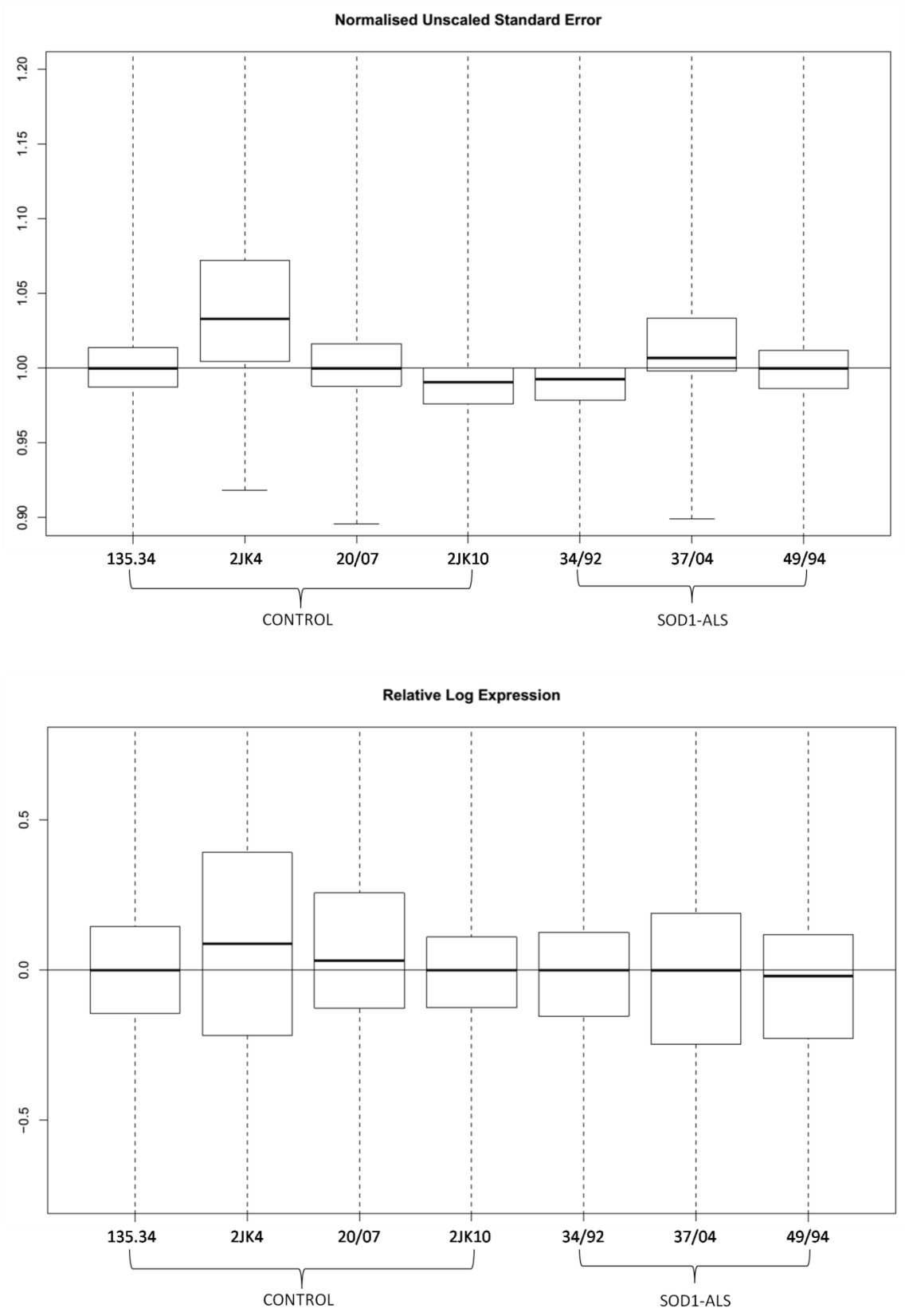

Figure 5.6 NUSE and RLE plots for astrocytes from SOD1-ALS patients and controls following removal of 2JK3 and 2JK7. All GeneChips now fall below 1.1 on the NUSE plot and show a similar spread of values on the RLE indicating that they are of a similar quality.

a)

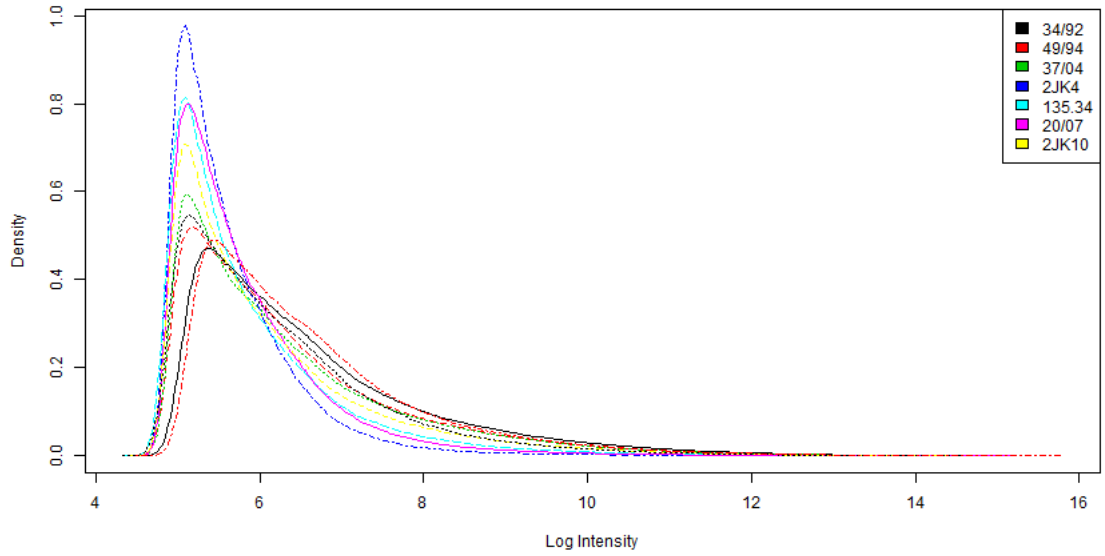

b)

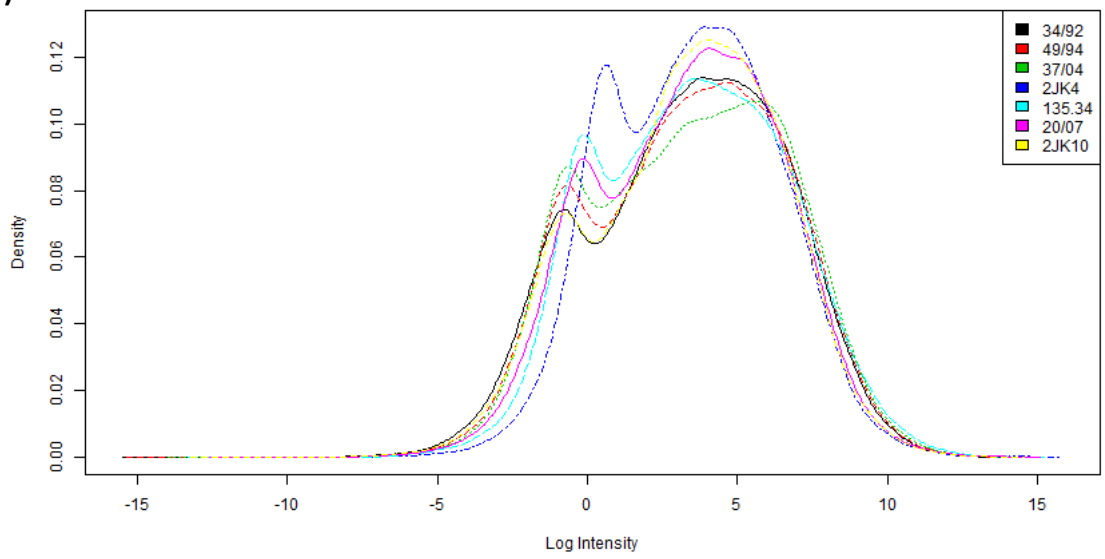

Figure 5.7 Density plot of log intensity values for astrocytes from SOD1-ALS patients and controls prior to (**a**) and following (**b**) normalisation. **a)** Before normalisation step the seven arrays showed a similar distribution in intensity values indicating a similar level of hybridisation. **b)** After the normalisation step all seven arrays are still very similar in their distribution of intensity values indicating that normalisation has not created differences between chips.

5.4 Enrichment of cellular markers on human arrays

As in the analysis of mouse arrays markers of different cell types were assessed for expression level to give an estimate of cellular enrichment in the initial LCM samples (Figure 5.8). Again, an enrichment of markers for astrocytes and oligodendrocytes is seen, with the two highest expression levels belonging to *GFAP* (astrocyte) and *MBP* (oligodendrocyte). In comparison, markers of neurons, microglia, endothelia and pericytes are much lower than astrocytic and oligodendrocyte markers.

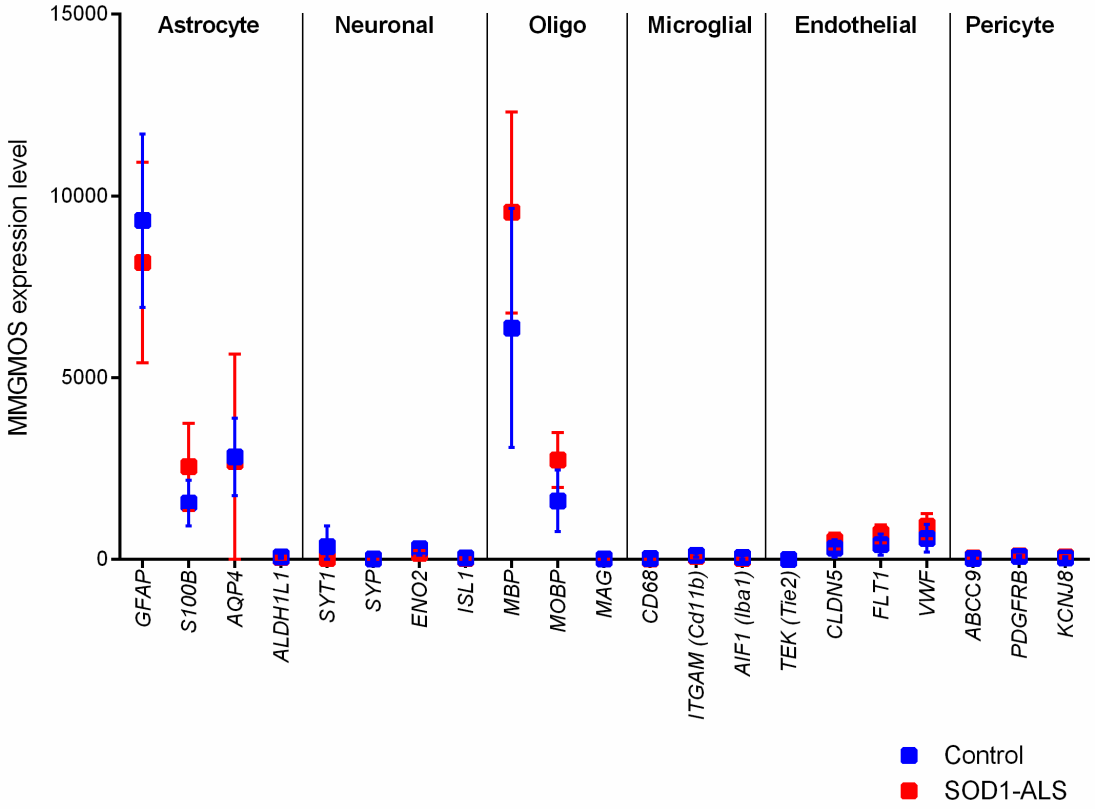

Figure 5.8 Markers of different cell types were analysed by MMGMOS expression level across the arrays used in analysis of human SOD1 and control astrocytes. The GeneChips are enriched for markers of astrocytes and oligodendrocytes.

5.5 Differential gene expression analysis results

As described in Methods 2.2.4.4 transcripts identified as differentially expressed due to gender were excluded from the SOD1-ALS versus control analysis. From the initial list of 1455 differentially expressed probesets, this left a total of 1231 differentially expressed probesets in human SOD1-ALS astrocytes compared to controls, with 769 of those up-regulated and 462 down-regulated. On Affymetrix GeneChips, certain transcripts have multiple probesets for detection. Thus, of these 1231 probesets 1132 corresponded to unique differentially expressed transcripts, of which 719 were up-regulated and 413 were down-regulated.

5.6 Gene enrichment analysis of differentially expressed transcripts in human SOD1-ALS astrocytes

The Database for Annotation, Visualisation and Integrated Discovery (DAVID) was used to assess enrichment of differentially expressed transcripts for particular gene annotations (Table 5.2). When all transcripts were analysed together, the top-ranked category housed genes that encode proteins involved in nuclear import, such as four members of the Importin family (karyopherin alpha 1, karyopherin alpha 2, karyopherin alpha 6, importin 11). Also enriched in the list containing all transcripts were genes involved in purine biosynthesis (ranked 2, 4 and 5) and gene silencing (ranked 3 and 6), though the latter two categories contained fewer genes than other enriched clusters.

The gene list was divided into up- and down-regulated transcripts and each list interrogated separately. Within the up-regulated transcripts, a large group of 52 genes involved in protein transport was the most significantly enriched category, which also included within it the majority of genes from the nuclear import category. The nuclear import genes were second-ranked in the up-regulated transcripts. In common with the all genes analysis (Table 5.2a), transcripts involved in purine biosynthesis (ranked 3, 5 and 7) and gene silencing (ranked 4 and 6) are also enriched within the up-regulated data set (Table 5.2b). Transcripts common between the purine biosynthesis categories include ATP synthases present within the mitochondrial F1 complex (*ATP5B* +1.22 and *ATP5A1* +1.42) and there is also increased expression of ATPases (*ATP8B4 +4.72,*

ATP13A3 +1.79*, ATP2A2* +1.45*, ATP8A1* -4.23) including those present within the lysosome (*ATP6V1C1* +1.64*)* and plasma membrane *(ATP2B4* +1.25*).* Although the fold-changes for some of these transcripts are very low, this may suggest an increased energy requirement in SOD1-ALS astrocytes. The miRNA category includes transcripts encoding two eukaryotic translation initiation factors (*EIF2C4* +1.51 and *EIF2C3 +2.30*), two probesets for trinucleotide repeat containing 6 (*TNRC6A* +1.57 and +1.44), RNA binding motif protein 3 (*RBM3* +2.02) and a zinc finger domain containing protein (*ZCCHC11* +1.28). *EIF2C4 and EIF2C3* encode argonaute proteins which bind miRNAs and play a role in gene silencing, whilst *TNRC6A* encodes a protein (GW182) that associates with argonaute proteins and mRNA during gene silencing and is important in preserving miRNA stability (Yao et al., 2012). Differential expression of factors involved in miRNA stability suggests miRNA differential expression in addition to the mRNA differential expression currently under investigation.

For down-regulated transcripts (Table 5.2c) the top ranked categories were ovulation cycle process and sex differentiation, despite gender correction having been performed. These categories contained genes such as vascular endothelial growth factor a (*VEGFA* -2.00), leptin receptor (*LEPR* -1.78) and progesterone receptor (*PGR* -3.66). Such genes have a variety of roles additional to those in female sexual differentiation, therefore these categories were not investigated further. Down-regulated transcripts were also enriched for haemoglobin transcripts and transcripts involved in focal adhesion (ranked 4 and 5), as well as 3 categories related to programmed cell death (ranked 6, 7 and 9) which included transcripts involved in both the positive and negative regulation of this process.

Table 5.2 Functional annotation clustering of transcripts differentially expressed (p≤0.05) in SOD1-ALS astrocytes compared to control. Transcripts were analysed using the DAVID functional annotation clustering tool with highest stringency settings. The top 10 enriched categories ranked by DAVID enrichment score within **a)** all genes, **b)** up- and **c)** down-regulated categories are summarised below. Each cluster consisted of multiple similar annotations and has been given a summarised cluster term. The number of genes is listed along with the proportion of those genes within the full gene list of differentially expressed transcripts. The most significant cluster term within the cluster is listed along with its p-value. Finally the DAVID enrichment score is given, which is calculated by summarising the significance of enriched annotations within each cluster, the higher the enrichment score the more significant the enrichment of that cluster within the dataset. Full details of all clusters is contained within Appendices 12-14.

a) All transcripts

	Summarised Cluster Term	# genes	% of gene list	Most significant cluster term	p (most sig term)	DAVID Enrichment score
1	Nuclear import	14	1.24	GO:0006606~protein import into nucleus	0.002	2.49
2	Purine ribonucleoside triphosphate metabolic process	14	1.24	GO:0009206~purine ribonucleoside triphosphate biosynthetic process	0.007	1.90
3	Gene silencing by RNA	6	0.53	GO:0016441~posttranscriptional gene silencing	0.008	1.83
4	Purine ribonucleotide metabolic process	15	1.33	GO:0009152~purine ribonucleotide biosynthetic process	0.013	1.63
5	Nitrogen compound catabolic process	9	0.80	GO:0009166~nucleotide catabolic process	0.012	1.59
6	Regulation of translation, ncRNA-mediated	3	0.27	GO:0035278~gene silencing by miRNA, negative regulation of translation	0.033	1.47
7	Primary active transmembrane transporter activity	13	1.15	GO:0042626~ATPase activity, coupled to transmembrane movement of substances	0.036	1.31
8	Isoprenoid biosynthetic process	3	0.27	GO:0035238~vitamin A biosynthetic process	0.021	1.29
9	Cyclic nucleotide catabolic process	4	0.35	GO:0009214~cyclic nucleotide catabolic process	0.004	1.28
10	Positive regulation of cell death	36	3.18	GO:0043065~positive regulation of apoptosis	0.059	1.20

b) Up-regulated transcripts

	Summarised Cluster Term	# genes	% of gene list	Most significant cluster term	p (most sig term)	DAVID Enrichment score
1	Protein localisation	52	7.14	GO:0015031~protein transport	2.10E-04	3.18
2	Protein localisation in nucleus	12	1.65	GO:0006606~protein import into nucleus	6.20E-04	3.07
3	Nitrogen compound catabolic process	8	1.10	GO:0009166~nucleotide catabolic process	0.004	2.08
4	Gene silencing	5	0.69	GO:0035195~gene silencing by miRNA	0.004	1.72
5	Ribonucleoside triphosphate metabolic process	10	1.37	GO:0006754~ATP biosynthetic process	0.009	1.66
6	Cytoplasmic mRNA processing body	3	0.41	GO:0035278~gene silencing by miRNA, negative regulation of translation	0.015	1.54
7	Ribonucleotide biosynthetic process	11	1.51	GO:0009152~purine ribonucleotide biosynthetic process	0.019	1.53
8	Regulation of interleukin-1 production	4	0.55	GO:0032731~positive regulation of interleukin-1 beta production	0.017	1.47
9	Chromosome segregation	6	0.82	GO:0000070~mitotic sister chromatid segregation	0.014	1.44
10	Amino acid activation	6	0.82	GO:0043039~tRNA aminoacylation	0.036	1.42

c) Down-regulated transcripts

	Summarised Cluster Term	# genes	% of gene list	Most significant cluster term	p (most sig term)	DAVID Enrichment score
1	Ovulation cycle process	9	2.18	GO:0022602~ovulation cycle process	6.83E-05	4.05
2	Sex differentiation	11	2.66	GO:0048608~reproductive structure development	5.34E-04	3.06
3	Negative regulation of biosynthetic process	25	6.05	GO:0010558~negative regulation of macromolecule biosynthetic process	0.001	2.43
4	Oxygen carrier	4	0.97	GO:0005833~hemoglobin complex	0.002	2.27
5	Cell-substrate junction	8	1.94	GO:0005925~focal adhesion	0.007	2.07
6	Regulation of cell death	29	7.02	GO:0042981~regulation of apoptosis	0.014	1.83
7	Negative regulation of cell death	16	3.87	GO:0043066~negative regulation of apoptosis	0.014	1.82
8	Negative regulation of transcription	20	4.84	GO:0016481~negative regulation of transcription	0.014	1.80
9	Positive regulation of cell death	18	4.36	GO:0043065~positive regulation of apoptosis	0.018	1.75
10	Haemopoiesis	12	2.9	GO:0030097~hemopoiesis	0.018	1.52

5.7 Disruption of nucleocytoplasmic transport in SOD1-ALS astrocytes

The most enriched category in the all transcripts analysis and in the analysis of up-regulated transcripts is involved in the localisation and import of proteins into the nucleus (Table 5.3). This category is also more enriched than any of the down-regulated categories after the exclusion of the sexual differentiation clusters. The 14 significant probe set IDs within the nuclear import category corresponded to 12 transcripts due to multiple significant probesets for *BCL6* and *RERE*. The majority of transcripts (9 of 12) are increased in expression. Several members of the karyopherin family are present: *KPNA1, KPNA2, KPNA6* and *IPO11*. The products of these genes are involved in the localisation of proteins which contain nuclear localisation signals, such as transcription factors, to the nuclear envelope (Cautain et al., 2014). Other transcripts directly involved in nucleocytoplasmic transport include nucleoporin 205kDa (*NUP205*) which encodes a protein that is a structural component of the nuclear pore (Cautain et al., 2014) and *RPAIN* which also encodes a protein that localises other proteins to the nuclear pore (Jullien et al., 1999).

The SOD1-ALS group and the control group have different mean ages (Section 5.1). This could provide a confounding variable which may lead to differential expression of genes. Therefore, to test that these transcripts of interest were not differentially regulated due to the confounding variable of age, a Pearson's R statistic was calculated. Of the 12 transcripts, 3 transcripts (*BCL6*, *RERE*, and *RPAIN*) were found to significantly correlate with age.

Table 5.3 Transcripts linked to nucleocytoplasmic transport that are differentially expressed in SOD1-ALS astrocytes compared to controls. R^2 values of MMGMOS expression value versus age are given with P value Pearson's R statistic, notice that most transcripts show a non-significant correlation with age.

Gene	Full Name	FC	R^2	P
BCL6	B-cell CLL/lymphoma 6	+1.88*	0.75	0.012
FYB	FYN binding protein (FYB-120/130)	+1.97	0.20	0.32
IPO11	importin 11	-9.78	0.38	0.14
JAK2	Janus kinase 2	+2.06	0.33	0.18
KPNA1	karyopherin alpha 1 (importin alpha 5)	+2.29	0.26	0.24
KPNA2	karyopherin alpha 2 (RAG cohort 1, importin alpha 1); karyopherin alpha-2 subunit like	+1.62	0.41	0.12
KPNA6	karyopherin alpha 6 (importin alpha 7)	+1.74	0.39	0.14
MCM3AP	minichromosome maintenance complex component 3 associated protein	+1.43	0.39	0.14
NUP205	nucleoporin 205kDa	+1.47	0.52	0.067
RERE	arginine-glutamic acid dipeptide (RE) repeats	-1.97*	0.63	0.033
RPAIN	RPA interacting protein	+1.33	0.61	0.038
SPTBN1	spectrin, beta, non-erythrocytic 1	-1.43	0.32	0.19
TGFB2	transforming growth factor, beta 2	+1.47	0.48	0.083
TMCO6	transmembrane and coiled-coil domains 6	+3.65	0.28	0.22

5.8 Pathway enrichment analysis reveals decreased expression of tight junction transcripts in SOD1-ALS astrocytes

To investigate if pathways of genes were enriched within the dataset, an enrichment analysis was performed to identify the presence of differentially expressed genes within pathways stored in the Kyoto Encyclopaedia of Genes and Genomes (KEGG) (Table 5.4). This showed enrichment of pathways such as adherens junction and the complement cascade in the up-regulated transcripts. However, by far the most significant enrichment by p-value was that for transcripts involved in tight junctions in the down-regulated gene list. Other enriched categories within the down-regulated transcripts include transendothelial migration and VEGF signalling, which in conjunction with a down-regulation of tight junction components might indicate a dysregulation of the blood brain barrier (BBB).

Table 5.4 Enrichment of transcripts within pathways stored on the Kyoto Encyclopaedia of Genes and Genomes (KEGG). DAVID was used to analyse differentially expressed transcripts in SOD1-ALS astrocytes for their presence in canonical pathways. Transcripts were split into up- and down-regulated lists prior to analysis. The most significant enrichment within a pathway was seen for transcripts involved in the tight junction.

Term	Count	%	p-value	Fold Enrichment
Up-regulated transcripts				
Adherens junction	6	1.33	0.032	3.34
One carbon pool by folate	3	0.66	0.054	7.84
Glycerophospholipid metabolism	5	1.11	0.074	3.12
Epithelial cell signaling in Helicobacter pylori infection	5	1.11	0.077	3.07
Complement and coagulation cascades	5	1.11	0.077	3.07
Glycosaminoglycan degradation	3	0.66	0.080	6.27
Down–regulated transcripts				
Tight junction	11	3.45	2.61E-04	4.13
Focal adhesion	10	3.13	0.017	2.50
Leukocyte transendothelial migration	7	2.19	0.026	3.02
Pathways in cancer	13	4.08	0.029	1.96
Renal cell carcinoma	5	1.57	0.051	3.51
VEGF signaling pathway	5	1.57	0.061	3.32
Adherens junction	5	1.57	0.063	3.28

Tight junctions are inter-cellular junctions that restrict the flow of ions and water between cells. These junctions are particularly important in the endothelium of the blood brain barrier (BBB) where they act to restrict the entry of unwanted pathogens or substances. Some of the principle components of tight junctions are the occludin, claudin, junctional adhesion molecule (JAM) and zona occludens proteins (Gonzalez-Mariscal et al., 2008) of which transcripts for all four are down-regulated in SOD1-ALS astrocytes (Table 5.5 and Figure 5.9). Other down-regulated transcripts encoding proteins with important roles in tight junction and BBB integrity include the cortactin and the epsilon isoform of protein-kinase C. Of the 11 transcripts in Table 5.4 only *TJP2* and *CDC42* were seen to significantly correlate with age of sample.

Table 5.5 Transcripts belonging to the KEGG pathway "Tight junction" within SOD1-ALS astrocytes. Members of the principle tight junction components Claudin, Occludin, JAM and Zona occludens are all represented within the genelist. R^2 values of MMGMOS expression value versus age are given with P value Pearson's R statistic. Of the 11 transcripts, only CDC42 and TJP2 are significantly correlated with age.

Gene	Full name	Fold change	R^2 age	P
CDC42	cell division cycle 42 (GTP binding protein, 25kDa); cell division cycle 42 pseudogene 2	-1.56	0.83	0.0042
CLDN5	claudin 5	-2.40	0.28	0.22
CTTN	cortactin	-1.77	0.29	0.21
EPB41	erythrocyte membrane protein band 4.1 (elliptocytosis 1, RH-linked)	-2.02	0.16	0.38
F11R	F11 receptor (junctional adhesion molecule 1)	-6.11	0.156	0.38
JAM2	junctional adhesion molecule 2	-2.07	0.50	0.074
OCLN	occludin pseudogene; occludin	-2.22	0.47	0.087
PARD3	par-3 partitioning defective 3 homolog (C. elegans)	-1.74	0.27	0.23
PRKCH	protein kinase C, eta	-1.72	0.56	0.052
PTEN	phosphatase and tensin homolog; phosphatase and tensin homolog pseudogene 1	-1.30	0.41	0.12
TJP2	tight junction protein 2 (zona occludens 2)	-2.39	0.70	0.018

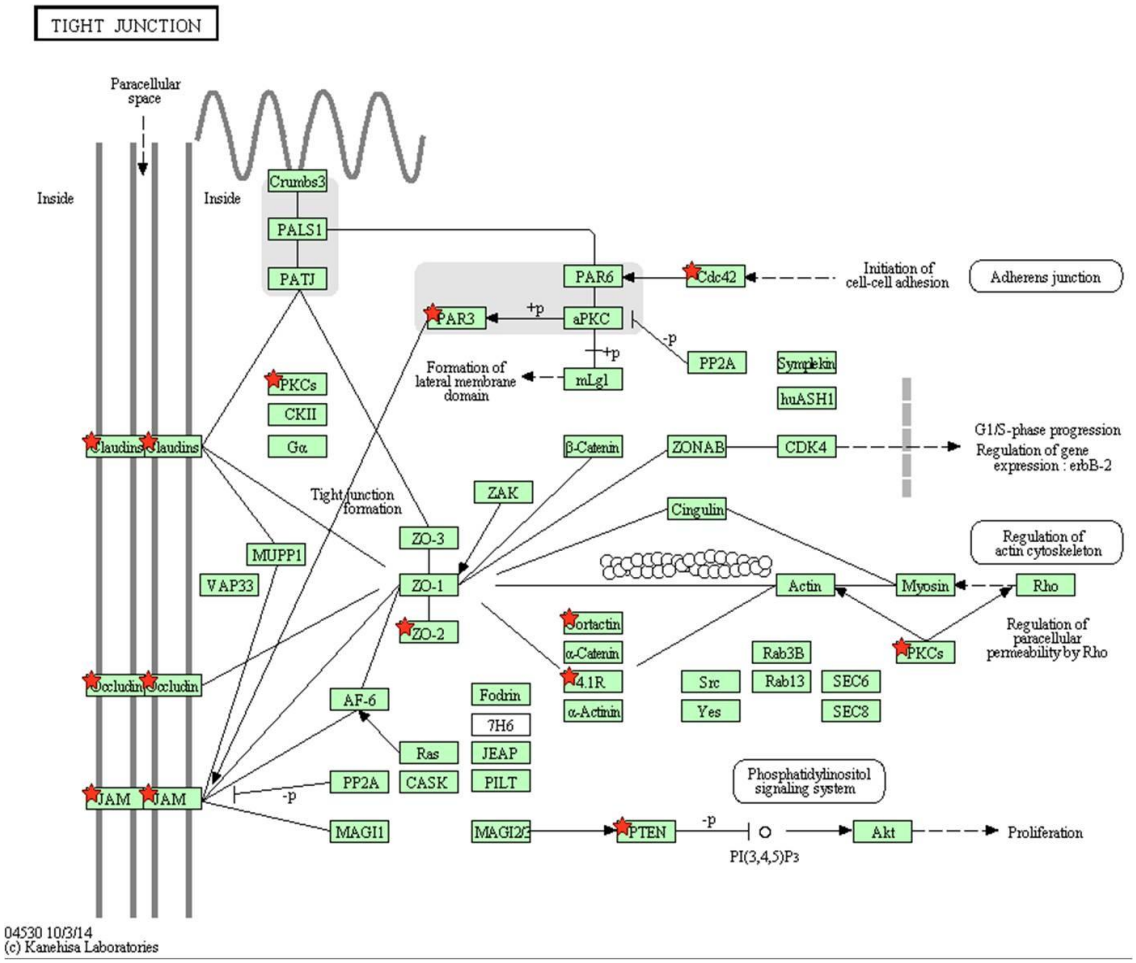

Figure 5.9 Components of the tight junction dysregulated in SOD1-ALS astrocytes. DAVID was used to identify enrichment of transcripts within pathways stored in the Kyoto Encyclopaedia of Genes and Genomes (KEGG). Red stars indicate where corresponding transcripts have been identified as down-regulated in the microarray of SOD1-ALS astrocytes. Image obtained from KEGG (**www.genome.jp/kegg**).

5.9 qPCR validation

As with the mouse microarray analysis (Section 3.8) qPCR was used to validate the findings of the arrays in terms of the direction of differential regulation and the genes of interest identified in the arrays. To validate the nucleocytoplasmic transport category karyopherin alpha 6 (*KPNA6*) was tested for differential expression. The majority of genes chosen were involved in BBB and tight junction integrity and included: the tight junction genes *CLDN5* and *JAM2*; transforming growth factor β (*TGFB)* and transforming growth factor β receptor 1 (*TGFBR1)* which are involved in astrocyte-endothelial crosstalk at the BBB (Abbott et al., 2006); and endothelial PAS-domain containing protein 1 (*EPAS1*) which is a transcription factor important in vascular development and protection of endothelial cells against stress (Duan et al., 2014). Also included for validation were: gap junction channel 1 (*GJC1*), due to the importance of gap junctions in astrocyte-astrocyte interactions; and chitinase 3-like 1 (*CHI3L1*) which had the highest positive fold-change on the arrays. Of the genes tested for validation, only *CHI3L1* showed a significant correlation with age of sample (R^2 = 0.93 p = 0.0005). As shown in Figure 5.10, all genes tested showed differential expression in the direction indicated on the microarrays with five of the eight genes tested showing a significant difference in expression level ($p \leq 0.05$).

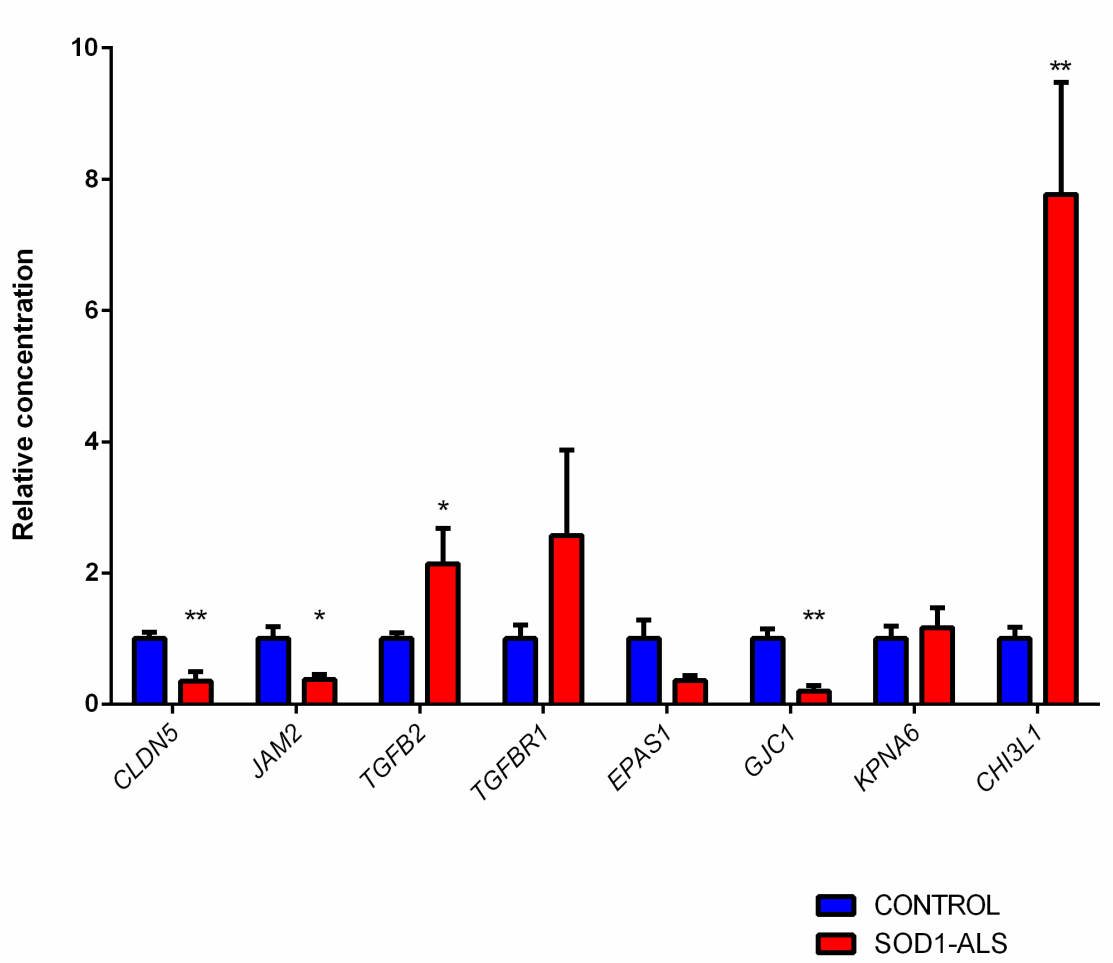

Figure 5.10 qPCR validation of transcripts identified as differentially regulated by microarray analysis of astrocytes from SOD1-ALS and controls. * = p≤0.05, ** = p≤0.01 vs. control, Independent samples t-test, error bars = S.E.M.

5.10 Comparison to SOD1^{G93A} mouse astrocyte microarray analyses

The gene list from human SOD1-ALS-related astrocytes was compared to the gene-lists from the three stages of disease in the SOD1^{G93A} mouse model to look for common patterns of dysregulation (Table 5.6). A small number of genes overlapped with the pre-symptomatic (11) and symptomatic (2) stages which increased to 37 common transcripts with the late-stage gene-list.

Of the shared genes at all time points, only one gene is present at multiple time-points: nel-like 1 (*NELL1)*, which is up-regulated in human SOD1-ALS astrocytes but down-regulated in symptomatic and late-stage disease in the SOD1^{G93A} mouse model. *NELL1* encodes a secreted protein with growth factor properties that is seen to be important in both neural and skeletal development (Zhang et al., 2010). Of the shared genes between the human gene list and all mouse time-points combined: 38 are up-regulated and 13 down-regulated in human astrocytes whereas 14 are up-regulated and 37 are down-regulated in mouse astrocytes. Fourteen genes are in agreement in terms of direction of differential expression between the two analyses. These include genes that encode proteins involved in GTP binding (*GNAS, CDC42, SEPT7*), ribonucleotide binding (*EPHA5, GNAS, CDC42, RUNX1, SEPT7*) and proteins containing transmembrane regions (*ELOVL5, EPHA5, GPR160, CNNM4, MS4A7*).

Table 5.6 Genes in common between the human SOD1-ALS astrocytes and pre-symptomatic, symptomatic and late-stage SOD1^{G93A} astrocytes. + = up-regulated, - = down-regulated. Up- and down-regulated genes have been coloured red and blue respectively.

Gene	Full name	Human FC	Mouse FC
Pre-symptomatic time-point			
BUB3	budding uninhibited by benzimidazoles 3 homolog (yeast)	-1.18	+4.01
CNNM4	cyclin M4	+1.78	+3.3
FAM184B	family with sequence similarity 184, member B	+1.50	-2.73
GNAS	GNAS complex locus	-2.14	-2.79
GPR160	G protein-coupled receptor 160	+2.27	+3.23
JAK2	Janus kinase 2	+2.06	-2.57
KIF3A	kinesin family member 3A	+1.46	-2.16
LEF1	lymphoid enhancer-binding factor 1	-1.88	+3.67
RUNX1	runt-related transcription factor 1	-1.95	-2.31

Gene	Full name	Human FC	Mouse FC
SOCS4	suppressor of cytokine signaling 4	+1.21	+2.71
TYMS	thymidylate synthetase	+9.45	+2.05
UBE3A	ubiquitin protein ligase E3A	+1.27	-2.18
Symptomatic time-point			
MS4A7	membrane-spanning 4-domains, subfamily A, member 7	+2.73	+2.20
NELL1	NEL-like 1 (chicken)	+3.52	-2.18
Late-stage time-point			
ACSL6	acyl-CoA synthetase long-chain family member 6	+3.55	-2.59
ANG	angiogenin, ribonuclease, RNase A family, 5	-1.68	+2.76
ARIH2	ariadne homolog 2 (Drosophila)	+1.60	+2.33
ARL4C	ADP-ribosylation factor-like 4C	+2.19	-2.17
ATPAF1	ATP synthase mitochondrial F1 complex assembly factor 1	+2.02	-3.37
B4GALT5	UDP-Gal:betaGlcNAc beta 1,4-galactosyltransferase, polypeptide 5	+1.70	-2.11
C3	similar to Complement C3 precursor; complement component 3; hypothetical protein LOC100133511	+2.51	+9.44
CDC42	cell division cycle 42 (GTP binding protein, 25kDa); cell division cycle 42 pseudogene 2	-1.56	-2.24
CPSF6	cleavage and polyadenylation specific factor 6, 68kDa	+1.37	-2.13
ELOVL5	ELOVL family member 5, elongation of long chain fatty acids (yeast)	-2.50	-2.13
EPHA5	EPH receptor A5	-1.89	-2.06
EXOC8	exocyst complex component 8	+1.37	-2.55
GRIA3	glutamate receptor, ionotropic, AMPA3 (alpha 3)	+1.56	-2.05
GRM5	glutamate receptor, metabotropic 5	+3.07	-2.00
KANK4	KN motif and ankyrin repeat domains 4	-1.50	-2.32
KIF3A	kinesin family member 3A	+1.46	-2.53
MAPK9	mitogen-activated protein kinase 9	+1.63	-2.68
MEIS2	Meis homeobox 2	+1.34	-2.06
NECAP1	NECAP endocytosis associated 1	+1.51	-2.86
NELL1	NEL-like 1 (chicken)	+3.52	-2.87
NRIP3	nuclear receptor interacting protein 3	+2.95	-2.41

Gene	Full name	Human FC	Mouse FC
OGT	O-linked N-acetylglucosamine (GlcNAc) transferase (UDP-N-acetylglucosamine:polypeptide-N-acetylglucosaminyl transferase)	+1.44	-2.28
OPA1	optic atrophy 1 (autosomal dominant)	+1.40	-2.86
PAK1	p21 protein (Cdc42/Rac)-activated kinase 1	+2.48	-2.70
PCYT1A	phosphate cytidylyltransferase 1, choline, alpha	+1.53	+2.33
PDXP	pyridoxal (pyridoxine, vitamin B6) phosphatase	+2.36	-2.18
RPL27	ribosomal protein L27	-1.36	+2.04
RPL34	ribosomal protein L34	-1.28	+2.72
RRM2B	ribonucleotide reductase M2 B (TP53 inducible)	+1.37	-2.43
SEPT7	Septin 7	-1.65	-2.31
SGIP1	SH3-domain GRB2-like (endophilin) interacting protein 1	+2.50	-2.66
SCL9A6	solute carrier family 9 (sodium/hydrogen exchanger), member 6	+1.81	-2.23
SNX13	sorting nexin 13	+1.38	-2.41
TAX1BP1	Tax1 (human T-cell leukemia virus type I) binding protein 1	+1.66	-2.02
TCS22D1	TSC22 domain family, member 1	-1.59	2.34
UHMK1	U2AF homology motif (UHM) kinase 1	+1.42	-3.16
YTHDC2	YTH domain containing 2	+1.56	-2.84

5.11 Comparison to SOD1-ALS motor neuron analysis

The list of transcripts differentially expressed in SOD1-ALS astrocytes was compared to a previous analysis of SOD1-ALS motor neurons performed by Kirby et al. (2011). From a total gene list size of 1231 and 1170 transcripts for astrocytes and motor neurons respectively, 22 differentially expressed transcripts were shared between the two cell types (Table 5.7). Of these transcripts, 14 were differentially expressed in the same direction and 8 were differentially expressed in opposite directions. The shared gene groups represent common themes seen throughout the analysis of $SOD1^{G93A}$ astrocytes (Chapter 3) and human SOD1-ALS astrocytes; three transcripts are involved in ion channel activity (*CLIC5, KCNN3* and *SCN2A*), three are involved in regulation of transcription (*NAA16*, *RBM15*, and *TAF11*) and three are involved in ATP binding (*ATP8B4, FPGT* and*PDXK*).

Table 5.7 Transcripts differentially expressed in both SOD1-ALS astrocytes and motor neurons. + = up-regulated, - = down-regulated. Up- and down-regulated genes have been coloured red and blue respectively.

Gene Symbol	Gene.Name	Astro FC	MN FC
APOC1	apolipoprotein C-I	+2.32	+6.09
ATP8B4	ATPase, class I, type 8B, member 4	+4.72	-2.97
CHI3L1	chitinase 3-like 1 (cartilage glycoprotein-39)	+17.22	+4.70
CLIC5	chloride intracellular channel 5	-1.46	+2.89
FPGT	TNNI3 interacting kinase; fucose-1-phosphate guanylyltransferase	+4.02	+2.45
INA	internexin neuronal intermediate filament protein, alpha	+5.63	+4.49
KCNN3	potassium intermediate/small conductance calcium-activated channel, subfamily N, member 3	+2.03	+2.73
LOC729799	SEC14-like 1 (S. cerevisiae); SEC14-like 1 pseudogene	-1.39	-2.99
NAA16	NMDA receptor regulated 1-like	-2.04	-2.79
NPHP4	nephronophthisis 4	+4.61	-2.08
PDXK	pyridoxal (pyridoxine, vitamin B6) kinase	-1.43	-3.90
PKP4	plakophilin 4	-3.39	-4.10
PTEN	phosphatase and tensin homolog; phosphatase and tensin homolog pseudogene 1	-2.10	+7.92
PTPRB	protein tyrosine phosphatase, receptor type, B	-1.97	+2.84
RBM15	RNA binding motif protein 15	+1.30	-3.41
RHAG	Rh-associated glycoprotein	-2.22	+3.74
SCN2A	sodium channel, voltage-gated, type II, alpha subunit	+4.76	+2.94
SLCO4C1	solute carrier organic anion transporter family, member 4C1	-2.09	+4.47
SNRPN	small nuclear ribonucleoprotein polypeptide N; SNRPN upstream reading frame	+3.27	+5.26
SRRM1	serine/arginine repetitive matrix 1	+1.41	+2.03
TAF11	TAF11 RNA polymerase II, TATA box binding protein (TBP)-associated factor, 28kDa	+1.63	+3.70
ZMYM3	zinc finger, MYM-type 3	+1.43	+4.09

5.12 Discussion

The data here represent the first microarray analysis of astrocytes from human SOD1-ALS spinal cord. The analysis of RNA from human astrocytes and subsequent gene expression profiling is more challenging than that performed previously for murine astrocytes (Chapter 3). The increased *post mortem* interval for human tissue versus mouse before LCM can lead to greater RNA degradation. In addition, there is increased variability due to factors such as: differing ages of human samples, gender of human samples and increased genetic heterogeneity of humans versus mice. Sample quality appears to have been compromised for two of the control samples (2JK3 and 2JK7) used in the analysis of SOD1-ALS astrocytes. This is evidenced by inefficient hybridisation upon the GeneChips, thereby causing these samples to be outliers in terms of array quality (Figures 5.2-5.5). Removal of these GeneChips gave a more consistent set of samples for subsequent analysis (Figure 5.6). The SOD1-ALS and control groups also differed in terms of mean age, therefore a Pearson's R statistic was calculated for each gene of interest to identify those affected by this confound. Lastly, to counteract any gender bias from the different gender composition of each group, an analysis of male versus female GeneChips was performed and the resultant differentially expressed genes excluded from the SOD1-ALS versus control gene list. The result is a list of 1231 probesets with which to proceed to further analysis (Appendix 11).

As with the microarray analysis of LCM-captured $SOD1^{G93A}$ astrocytes, an enrichment was seen for transcripts highly expressed by astrocytes and oligodendrocytes (Figure 5.8). Transcripts of other cell types were not enriched within the dataset, which is reinforced by the low level of overlap between the SOD1-ALS astrocyte gene list and the gene-list of LCM-captured SOD1-ALS motor neurons from Kirby et al. (2011) (Table 5.7). In conclusion, LCM has successfully been used to capture astrocyte material from human spinal cord and functional experiments using astrocytes will be used to confirm attribution of array data to astrocytes.

Results of enrichment analyses show enrichment of genes involved in nucleocytoplasmic transport, purine biosynthesis and gene silencing (Table 5.2). In

addition pathway analysis shows an enrichment of down-regulated transcripts involved in the tight junction which together with transcripts involved in VEGF signalling and leukocyte transendothelial migration indicate a potential perturbation of the blood brain barrier (Table 5.4, Table 5.5 and Figure 5.9).

5.12.1 Nucleocytoplasmic transport disruption in SOD1-ALS astrocytes

Microarray analysis of human SOD1-ALS astrocytes has shown a dysregulation of genes involved in protein transport, particularly transport of proteins into the nucleus (Table 5.2). The gene group particularly affected is the Karyopherin (a.k.a. Importin alpha) gene group, with *KPNA1, KPNA2, KPNA6* and *IPO11* all significantly up-regulated in disease. This group of genes codes for proteins that localise other proteins such as transcription factors to the nuclear pore complex, allowing entry to the nucleus (Cautain et al., 2014). A transcription factor identified as being protective against oxidative stress and currently of high interest in ALS is nuclear factor erythroid 2-related factor 2 (Nrf2). Nrf2 is expressed more highly in astrocytes than neurons (Kraft et al., 2004), where antioxidant response element (ARE) genes are down-regulated in ALS (Kirby et al., 2005), and when over-expressed in astrocytes Nrf2 was seen to significantly delay disease onset and extend survival time in an ALS-mouse model (Vargas et al., 2008a). Under normal conditions, Nrf2 is stopped from entering the nucleus and turning on antioxidant response (ARE) genes by being bound to its inhibitor Keap1. Importin alpha 7 (KPNA6) is seen to interact with Keap1, allowing the nuclear import of Keap1 and removal of Nrf2 from the nucleus, and when over expressed in the NIH 3T3 fibroblast cell line KPNA6 was seen to reduce Nrf2 activity (Sun et al., 2011). KPNA6 is increased in human SOD1 astrocytes in our microarray analysis, which may be a reason for the observed reduction in Nrf2 activity. *KPNA6* was tested for validation by qPCR, however it was not confirmed as differentially expressed. Therefore, nucleocytoplasmic transport was not investigated further using functional studies.

5.12.2 Blood-brain-barrier (BBB) and blood-spinal-cord-barrier (BSCB) disruption in ALS

BBB dysfunction in ALS is seen in both animal models and human patients. Increased leakage of Evans blue, a dye which binds to albumin, was observed in both cervical and

lumbar spinal cord of the SOD1^{G93A} mouse at early and late-stage disease (Garbuzova-Davis et al., 2007b). Ultra-structure analysis using electron microscopy upon these animals showed high levels of oedema in the neuropil of the spinal cord and swelling of the mitochondria within endothelial cells whilst the tight junctions appeared to remain intact (Garbuzova-Davis et al., 2007a). In contrast, in the SOD1^{G37R} and SOD1^{G85R} models of ALS there is a significant loss of the tight junction transcripts Claudin-5, Occludin and ZO1 in vessels of the anterior horn coupled to a decreased rate of blood flow and an increased leakage of IgG, all of which preceded motor neuron loss (Zhong et al., 2008, Miyazaki et al., 2011). This work is reinforced by Nicaise et al (2009a), who found decreased levels of Occludin and ZO1 mRNA in the SOD1^{G93A} rat spinal cord only once disease symptoms had begun. Leakage of Evans blue was significantly higher in the brainstem and spinal cord of symptomatic rats over wild-type and pre-symptomatic and there was also evidence of IgG, IgM and Hemosiderin deposition. Magnetic resonance imaging (MRI) has shown living SOD1^{G93A} rats have higher leakage of Gd-DTPA, a marker of BBB permeability, in the brain (Andjus et al., 2009). Astrocytes in the SOD1^{G93A} rat exhibit swollen end feet when observed using electron microscopy, providing evidence of damage to the entire neurovascular unit (Nicaise et al., 2009a). Aquaporin-4, a water channel protein expressed on astrocyte endfeet, was significantly up-regulated at both the mRNA and protein level in the grey matter of the SOD1^{G93A} rat model at end stage (Nicaise et al., 2009b) and exhibits increased immuno-staining in the trigeminal nuclei, motor cortex and glia limitans of the same model (Bataveljic et al., 2012).

Leonardi et al (1984) were the first to notice heightened levels of IgG and albumin within the CSF of ALS patients. In the cervical spinal cord of both sALS and fALS patients there is a significant leakage of haemoglobin and significantly increased erythrocyte extravasation from the capillaries (Winkler et al., 2013). This increased permeability could be due to decreased endothelial tight junction expression; Henkel et al (2009) found significantly decreased levels of the tight junction transcripts Occludin and ZO1 within ALS patients with earlier (under 57 years) onset of disease. As in the SOD1 animal models an astrocytic defect is seen in ALS patients, with detachment of endfeet from endothelial cells (Miyazaki et al., 2011) consistent with an

increase in collagen deposition around capillaries seen by electron microscopy (Garbuzova-Davis et al., 2012).

Despite the aforementioned evidence for BBB and BSCB disruption in ALS, this area remains controversial. Although MRI scans of the $SOD1^{G93A}$ rat show leakage of Gd-DTPA, MRI of ALS patients has not revealed significant micro-haemorrhages (Verstraete et al., 2010). IgG from ALS patients localises to motor neurons when injected intraperitoneally (Engelhardt et al., 2005), suggesting that IgG leakage may be due to its inherent ability to cross the BBB rather than an increase in barrier leakiness. Further, excision of $SOD1^{G37R}$ solely in endothelia of the $SOD1^{G37R}$ mouse by Cre-lox mediated excision led to a significant decrease in IgG leakage compared to diseased animals, however the disease onset and duration was not affected (Zhong et al., 2009). Lastly, the immunostaining performed in the study by Miyazaki et al. (2011) is not conclusive of endfoot detachment, although the electron microscopy studies performed by Garbuzova-Davis et al. (2007a, 2012) do support astrocyte end-foot disruption.

In this analysis of SOD1-ALS astrocytes, all of the main components of tight junctions, such as claudins, occludin, junctional adhesion molecules and zona occludens, have been identified as down-regulated (Table 5.4), reinforcing previous findings of decreased tight junction gene expression (Zhong et al., 2008, Henkel et al., 2009, Miyazaki et al., 2011). *CLDN5* and *JAM2* were confirmed as differentially expressed by qPCR (Figure 5.10). The tight junction genes, with the exception of *TJP2* are not affected by the confounding variable of age (Table 5.5). Even if age were a confounding variable in this analysis, evidence points to an increased permeability of the BBB with age and a mislocalisation of tight junction proteins (Bake et al., 2009), suggesting that if age were affecting tight junction expression in this analysis, then it should be lower in the controls than in the SOD1-ALS group. Tight junction genes are classically associated with endothelial cells, however the levels of endothelial transcripts upon the arrays is low suggesting low endothelial cell contamination (Table 5.3), and the tight junction proteins Occludin and Zona occludin 1 have been detected in astrocytes (Simpson et al., 2010). The finding that genes involved in focal adhesions are also enriched within the down-regulated gene list (Table 5.3) also adds weight to a

disruption of BBB integrity due to the finding that blockade of interactions with the ECM result in a decrease in Claudin-5 expression of endothelial cells (Osada et al., 2011). In addition, other transcripts that could affect tight junction formation are dysregulated, such as Protein kinase C ε-isoform (*PRKCH*) which is reported to increase tight junction formation (Yoo et al., 2003). There is differential expression of transcripts involved in signalling to endothelia, such as *VEGFA* which increases BBB permeability (Gavard and Gutkind, 2006) and *TGFB2* and its receptor *TGFBR2*. The TGFβ signalling pathway is specifically enriched within astrocytes in comparison to oligodendrocytes and neurons (Cahoy et al., 2008) thereby increasing confidence in a disrupted astrocyte-endothelial interaction in SOD1-ALS.

Further experiments are necessary to address the abovementioned controversy existing in ALS as to the involvement of BBB/BSCB disruption in disease pathogenesis. To date there have been no studies of astrocyte-endothelial co-cultures using cells derived from ALS patients, despite this interaction being a vital part of the neurovascular unit.

5.12.3 Discrepancies between mouse and human arrays

The microarrays performed for the symptomatic and late-stage $SOD1^{G93A}$ astrocytes and those performed for human SOD1-ALS astrocytes do not overlap greatly. The common themes identified in the mouse analysis of lysosome and immune up-regulation and down-regulated ion homeostasis are not present within the human gene-list, whilst the tight junction category is not present within the mouse data. When the pre-symptomatic data from Ferraiuolo et al. (2011a) is included it can be seen that the late-stage $SOD1^{G93A}$ astrocytes share the most dysregulated genes with the human SOD1-ALS astrocytes (Table 5.5). This is likely due to the fact that the late-stage mouse astrocyte and end-stage human astrocyte are closer to each other in terms of disease stage. However, though 37 genes are shared between late-stage $SOD1^{G93A}$ astrocytes and human SOD1-ALS astrocytes, only 9 transcripts show differential expression in the same direction. If all mouse lists are combined, only 14 transcripts show differential expression in the same direction.

The low amount of overlap between the two datasets demonstrates that key differences exist between the mouse model and human forms of SOD1-related ALS. In addition to the aforementioned differences between the mouse and human studies with regard to *post mortem* interval, age, gender and genetic heterogeneity, there may also be differences due to the type of SOD1 mutation present. For example, the mouse model contains the human SOD1 gene with a mutation at position G93A (p.G94A), whereas the cases used in the human microarray study consisted of two patients with mutations at I113T (p.I114T) and one case with a mutation at E100G (p.E101G). Different mutations in SOD1 are known to confer different disease courses (Turner and Talbot, 2008). In the $SOD1^{G93A}$ mouse model mutant-SOD1 is expressed at 11-fold higher than endogenous levels with a disease onset of 3-4 months and a duration of 1-2 months. However another commonly used model, containing a mutation at G85R (p.G86R) features an endogenous-level of mutant-SOD1 expression and a disease onset at 8-14 months and duration of just half a month (Turner and Talbot, 2008). In human SOD1-ALS the A4V mutation leads to short survival compared to the G37R, G41D and G93C mutations (Cudkowicz et al., 1997) and the D90A mutation which leads to a slow disease progression (Andersen et al., 1995). Such heterogeneity in disease course caused by mutations in the same gene could explain the lack of similarity between the human and mouse gene-lists shown here.

Another reason for the lack of similarity seen between the two sets of astrocyte data is the use of GFAP as a marker of astrocytes in the human analysis and ALDH1L1 in the mouse analysis. GFAP is associated with a reactive astrocyte phenotype, and was not used in the mouse analysis as ALDH1L1 had been identified as a pan-astrocyte marker (Cahoy et al., 2008) that would lead to a gene-list not biased by reactive astrocytes. Conversely, in human tissue ALDH1L1 was not a robust marker of astrocytes as seen by Waller et al. (2012), and GFAP lead to more easily identifiable cells for capture. Consequently the human LCM material has a higher enrichment of GFAP compared to the mouse (Figure 5.8 and Figure 3.9) and thus the use of different populations of astrocytes may contribute to the differences in gene expression seen here.

CHAPTER 6

RESULTS

Functional studies of human SOD1-ALS astrocytes

6 Functional studies of human SOD1-ALS astrocytes

6.1 Introduction

Astrocytes from human SOD1-ALS patients showed differential expression of transcripts involved in the tight junction complex and factors that might affect the vasculature (Section 5.5, Chapter 5). Given this, it was hypothesised that astrocytes in SOD1-ALS are involved in the BBB and BSCB (hereafter referred to simply as "BBB") breakdown observed in animal models and patients (Zhong et al., 2008, Henkel et al., 2009). To investigate this, astrocytes derived from human fibroblasts of controls and patients with ALS were co-cultured with human umbilical vein endothelial cells (HUVECs) to measure the effect of co-culture upon barrier properties. In addition, motor neurons were added to cultures to recreate a more accurate astrocyte phenotype.

6.2 Cultures used for human functional studies

It has recently been shown that mouse embryonic fibroblasts can be directly converted, i.e. rather than reprogrammed back to an iPS state, to a neural precursor cell (NPC) that can be differentiated into neurons, astrocytes and oligodendrocytes using either the four classical iPS factors *Oct4, Sox2, Klf4* and *c-Myc* with subsequent NPC-stimulating growth factors (Kim et al., 2011) or with the three factors *Foxg1*, *Sox2* and *Brn2* (Lujan et al., 2012). This work was built upon by Meyer et al. (2013) who used the method of Kim et al. (2011) to reprogramme adult human fibroblasts from control and ALS patients to NPCs with subsequent differentiation to neurons, astrocytes and oligodendrocytes. The astrocytes, hereafter referred to as i-astrocytes, recapitulate the toxic phenotype towards motor neurons observed in animal models of ALS. Using this technique, i-astrocytes were produced by Dr Kathrin Meyer (Nationwide Children's Hospital, Columbus OH, U.S.A.) for use in astrocyte-endothelial co-cultures. After possession of i-astrocytes had been taken, the cells were stained for the astrocyte markers CD44 and S100b, with nearly all cells showing as CD44 and S100b positive.

To study the effect of i-astrocytes upon endothelia, primary human umbilical vein endothelial cells (HUVECs) were cultured for use in the culture cell model of the BBB.

HUVECs were stained for the endothelial markers Claudin-5 and CD31 which again showed nearly 100% of cells to be stained positively for these markers (Figure 6.2). Claudin-5 staining showed a high degree of localisation to the periphery of the cells indicating tight junction formation and confirming these cells as a model for tight junction integrity in further experiments.

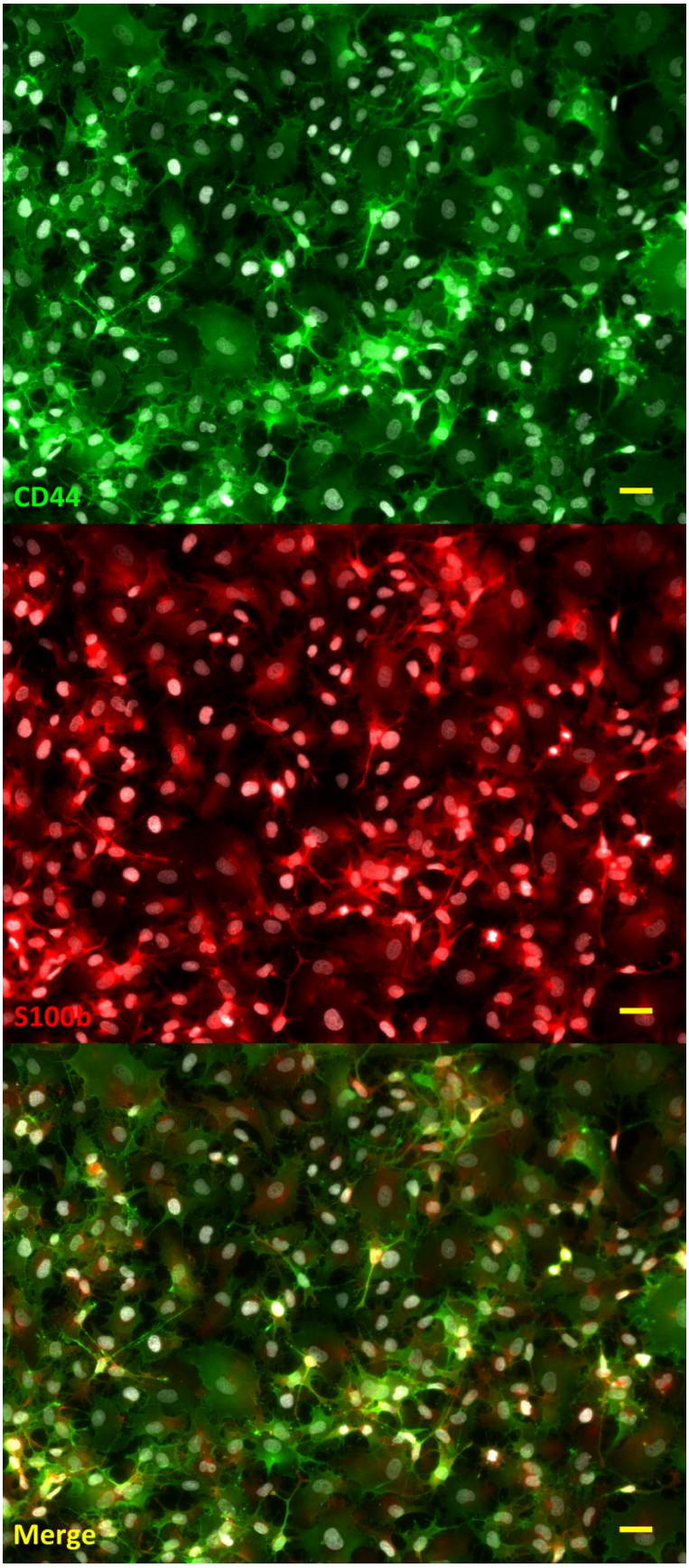

Figure 6.1 Human i-Astrocytes stained with anti-CD44 (green) and anti-S100b (red) with nuclei stained with Hoescht (white). Magnification = 20X. Scale bar = 50µm.

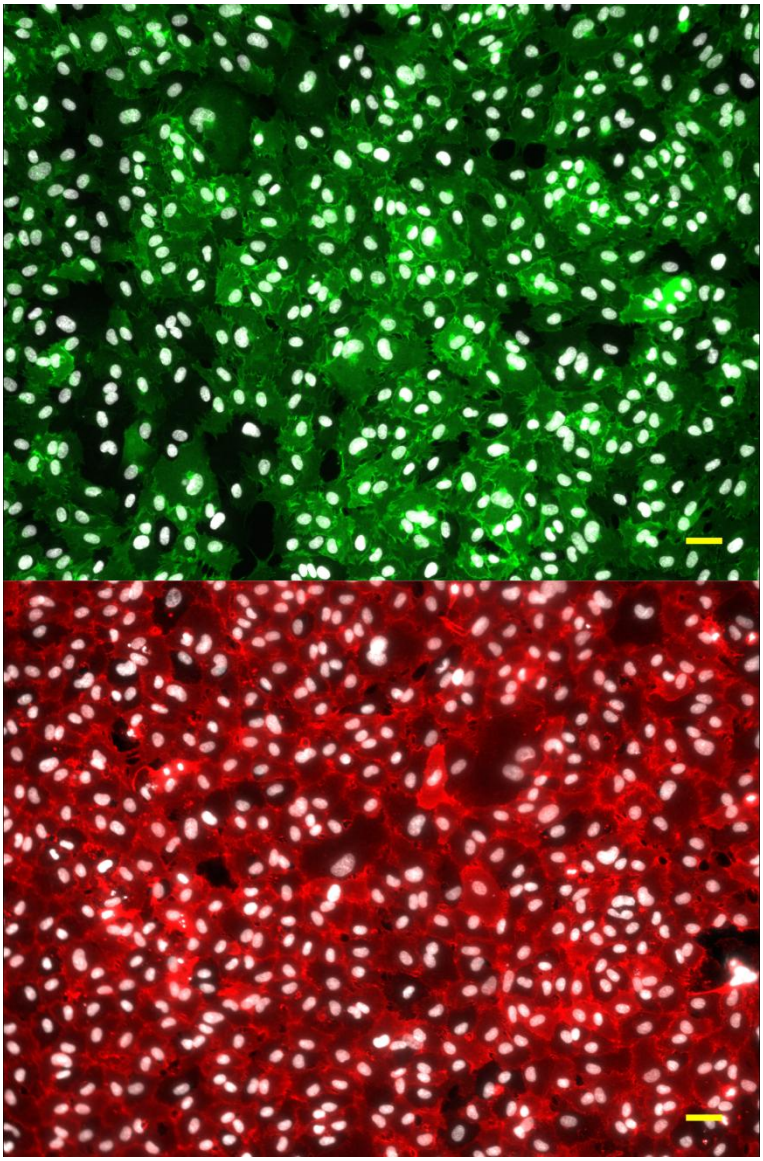

Figure 6.2 Human umbilical vein endothelial cells stained for the endothelial markers Claudin-5 (green) and CD31 (red). Nuclei stained for Hoescht (white), magnification = 20X, scale bar = 50µm.

6.3 Co-culture of HUVECs and i-astrocytes and BBB permeability measurements

HUVECs were co-cultured with i-astrocytes on either side of a transwell membrane. To ensure a more accurate astrocyte phenotype, transwells were placed into a 24-well plate which contained mouse wild-type motor neurons on the bottom of each well. At day 3 of triple co-culture, transendothelial electrical resistance (TEER) measurements were made across the membrane to assess ion permeability and thus tight junction integrity (Figure 6.3a). TEER measurement involves the placement of an electrode on each side of the barrier, and measurement of the voltage required to reach 10 µA of current, thus TEER is a way of assessing the ionic flow across the membrane. High tight junctional coupling would lead to low ionic permeability and therefore a high resistance measurement whereas low tight junctional coupling would allow more ions to flow between cells and thus a lower resistance measurement. In addition to tight-junctional coupling, confluence of cell monolayers also influences TEER readings. Therefore, in addition to measurement of the BBBs, measurements were also taken for wells containing astrocytes-only in the absence of HUVECs such that any variation in astrocyte confluence which might affect barrier measurements could be subtracted, and the resultant measurements are hereby termed delta (Δ) measurements. Following TEER measurement, another test of barrier permeability was performed using 4kDa dextrans conjugated to FITC. Dextrans were placed into the top chamber and left for two hours, at which point aliquots were made from the bottom chamber and the fluorescence of these aliquots measured on a plate-reader. A highly permeable barrier would show greater fluorescence in the bottom chamber than a barrier with low permeability. This measurement is different to TEER in that it is testing barrier permeability to macromolecules, thus differences in dextran transport should either be due to large scale cell death and holes within the monolayer, or increased endocytosis and trans-cellular transport of the dextrans. As in the TEER measurements, the BBB values were corrected for the values from astrocyte-only controls wells.

Three separate experiments were performed, using two SOD1 i-astrocyte lines and one sALS i-astrocyte line. The reason for inclusion of the sALS line was to test whether results obtained were applicable to the wider sporadic ALS population. For each experiment, one control and one ALS i-astrocyte line were co-cultured with HUVECs

simultaneously. Experiments 1 (SOD1-ALS) and 2 (sALS) were conducted in the Kaspar Laboratory at Nationwide Children's Hospital, Ohio, U.S.A. using FACS-sorted murine GFP-expressing motor neurons for stimulation of i-astrocytes. Experiment 3 was performed at The University of Sheffield, U.K. using murine motor neurons prepared from E13.5 embryos using density-gradient centrifugation. Due to limitations in the amount of motor neurons obtained from a primary motor neuron preparation versus FACS sorted motor neurons, the experimental conditions in experiment 3 were repeated in duplicate rather than in triplicate as in experiments 1 and 2.

The results of the three experiments were combined to give an average of ALS BBB versus control BBB TEER readings (Figure 6.3). Values were normalised to mono-cultured HUVECs in each experiment before data were combined. TEER readings were found to be significantly different between monocultured HUVECs and HUVECs co-cultured with control or ALS i-astrocytes ($p=0.0061$). HUVECs cultured in BBBs containing ALS i-astrocytes had significantly lower relative TEER readings (123.51 ± S.D. 33.2) than either control i-astrocytes (205.02 ± S.D. 26.95) or monocultured HUVECs (100 ± S.D. 14). In contrast, although significant differences were seen between groups for dextran permeability ($p=0.0166$), this difference lay between monocultured HUVECs and co-cultured HUVECs, and a significant difference was not seen between control (63.45 ± S.D. 10.89) and ALS BBBs (67.85 ± S.D. 8.99) (Figure 6.4b).

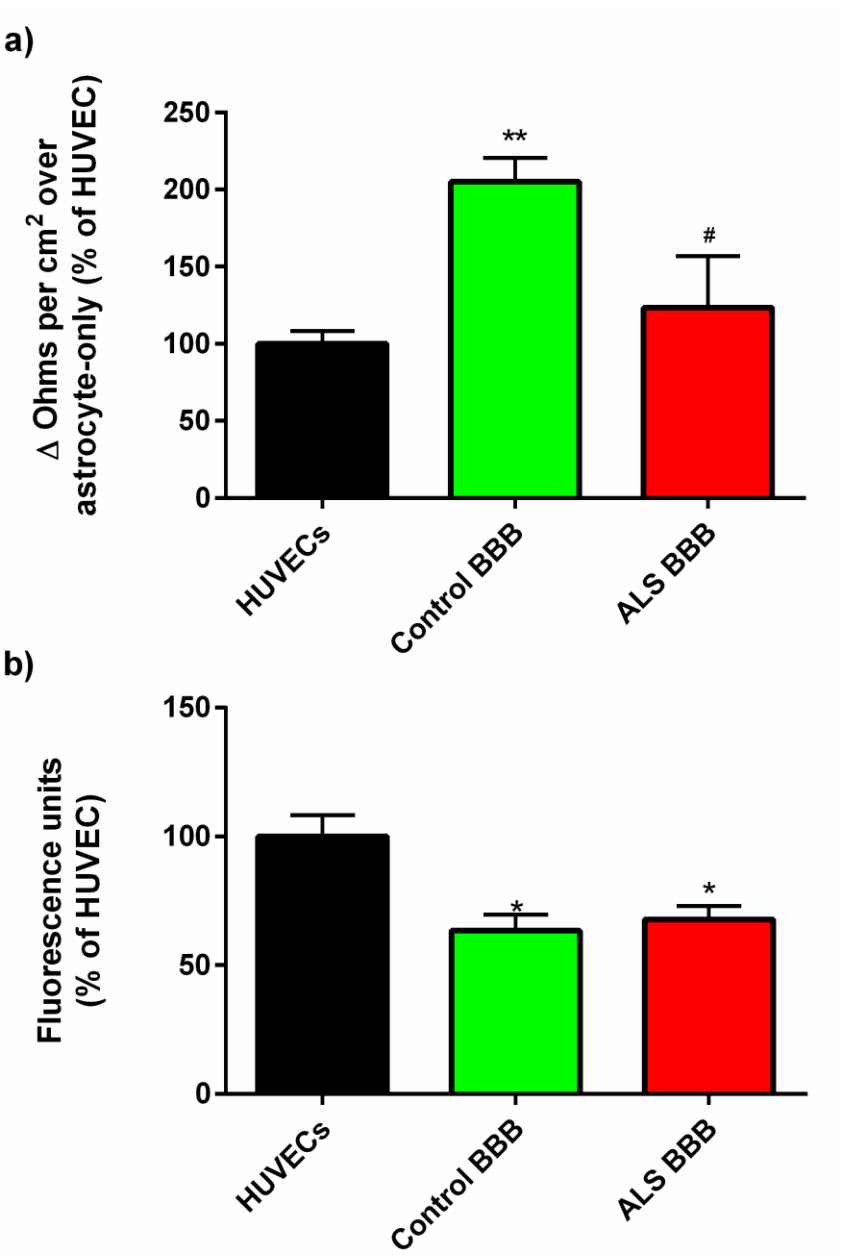

Figure 6.3 Average TEER readings and dextran permeability measurements for HUVECs cultured in monoculture or with control i-astrocytes or ALS i-astrocytes in BBBs. The ALS BBBs consist of two SOD1-ALS lines and one sALS line of i-astrocytes. **a)** TEER readings for HUVECs cultured in ALS BBBs were significantly lower than monocultured HUVECs or HUVECs cultured in control BBBs. HUVECs cultured in ALS BBBs showed a trend for increased TEER measurements over monocultured HUVECs which did not reach significance. **b)** Dextran permeability was significantly lower than monocultured HUVECs for HUVECs cultured in either control or ALS BBBs. Values from 3 independent experiments normalised to respective HUVEC controls. BBB values represent measurements corrected for astrocyte-only recordings. * = $p \leq 0.05$, ** = $p \leq 0.01$ vs. monocultured HUVECs. # = $p \leq 0.05$ vs control BBB (one-way ANOVA with Tukey post-hoc test). Error bars = S. E. M.

6.4 Identification of EPAS1 for transduction of HUVECs and i-astrocytes

Due to the decreased TEER readings seen for HUVECs co-cultured in ALS BBBs compared to controls (Figure 6.3) transcripts on the microarrays were investigated for their applicability to rescue this deficit via a gene-therapy approach. Transcription factors were investigated rather than individual tight junction genes due to the potential to act upon an entire pathway of genes which might influence barrier integrity.

Endothelial PAS domain protein 1 (*EPAS1*), which encodes the protein known as Hypoxia-inducible factor 2α (HIF2α), is a transcription factor decreased in expression by 1.61-fold in SOD1-ALS astrocytes and present within annotation cluster 10 (haemopoiesis) in the enrichment analysis of down-regulated transcripts (Table 5.1c, Chapter 5). This cluster was first investigated due to its relationship to the vasculature and thus the BBB. Gruber et al. (2010) found that postnatal ablation of *Epas1* led to a disrupted blood-testis-barrier in mice and a trend for decreased expression of tight junction transcripts. Additionally, HIF2α expression in astrocytes drives the expression of erythropoietin (*EPO*) (Chavez et al., 2006), which is able to protect against VEGF-mediated endothelial permeability (Martínez-Estrada et al., 2003).

EPAS1 was highly expressed in comparison to other differentially expressed transcription factors (Figure 6.4) and possessed the third largest range between the highest expression level in control and the lowest expression level in disease. Only two other transcription factors had larger ranges, Staphylococcal nuclease and tudor domain containing 1 *(Snd1)* and TSC22 domain family, member 1 (*Tsc22d1)*. *SND1* is a part of the RNA-induced silencing complex (RISC) involved in microRNA processing and is shown to be increased in expression in cancer (Tsuchiya et al., 2007) and was therefore disregarded for use in an overexpression study. *TSC22D1* encodes the protein TGFβ-stimulated clone 22 (TSC22) which acts as a tumour suppressor (Yoon et al., 2012). Another transcription factor, homeodomain interacting protein kinase 2 (*HIPK2*), had five probe sets differentially expressed between SOD1-ALS and control astrocytes. *HIPK2*, like *TSC22D1*, encodes a protein with tumour suppressor function that interacts with p53 and also has a repressive effect upon the anti-oxidant

transcription factor HIF1α (Nardinocchi et al., 2009). The transcription factor ZNF595 is not reported to have any effects upon BBB function, *MECOM* encodes a protein involved in leukaemia (Jolkowska and Witt, 2000), *LEF1* knockout has been shown to not affect tight junction expression or TEER readings in keratinocytes (Fehrenschild et al., 2012) and *LHX6* which is involved in interneuron development (Liodis et al., 2007). In conclusion, none of the other down-regulated transcription factors present upon the arrays at a robust concentration was as well supported in the literature as *EPAS1* for manipulation of BBB properties.

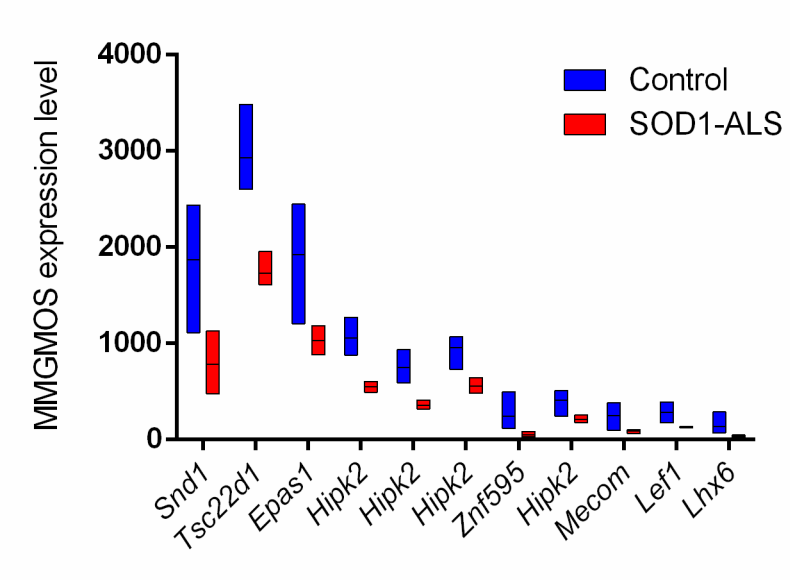

Figure 6.4 The top 10 down-regulated transcription factors by expression level in the microarray analysis of SOD1-ALS astrocytes vs. controls. Transcripts have been ranked by range between highest expression level and lowest expression level. Multiple probesets were differentially expressed for the transcription factor *Hipk2*. *Epas1* was highly expressed and had a large range between control and disease samples.

6.5 Effect of Lv*EPAS1* transduction upon tight junction gene expression

To assess the affect of *EPAS1* over-expression upon tight junction formation, *EPAS1* was cloned and put into a lentiviral vector. *EPAS1* sequencing showed one nucleotide substitution in the *EPAS1* sequence: a G→A substitution at position 129 encoding a silent mutation. Lentivirus was used to transduce HUVECs with the *EPAS1* gene (hereby designated (Lv*EPAS1*) at at multiplicity of infection (MOI) of 20. To control for the transduction process, lentiviral transduction of HUVECs with green fluorescent protein (Lv*GFP*) was also performed at 20 MOI. Both types of transduced cell were compared by qPCR to non-transduced (non-trans) controls for the expression of *EPAS1* and tight junction genes *CLDN5, ZO2, OCLN,* and *JAM2* as well as transforming growth factor beta 2 (*TGFB2)* (Figure 6.5). Transduction with Lv*EPAS1* led to significantly increased *EPAS1* expression in HUVECs relative to non-trans and Lv*GFP* transduced controls (p=<0.0001). In terms of tight junction transcripts: *CLDN5* expression was significantly increased over non-trans and Lv*GFP* transduced cells (p=0.02); as was *ZO2* (p=0.0038); *OCLN* expression was significantly decreased in Lv*GFP* HUVECs versus non-trans HUVECs suggesting that lentiviral transduction has a negative effect upon this transcript (p=0.02 between groups), and *JAM2* expression was significantly increased in Lv*EPAS1* HUVECs versus non-trans controls but was not significantly different to Lv*GFP* control cells (p=0.02 between groups). In addition *TGFB2*, the protein of which modulates astrocyte-endothelial interactions at the BBB (Abbott et al., 2006), was investigated and found to be significantly increased in Lv*EPAS1* HUVECs compared to non-trans and Lv*GFP* controls (p=0.0009).

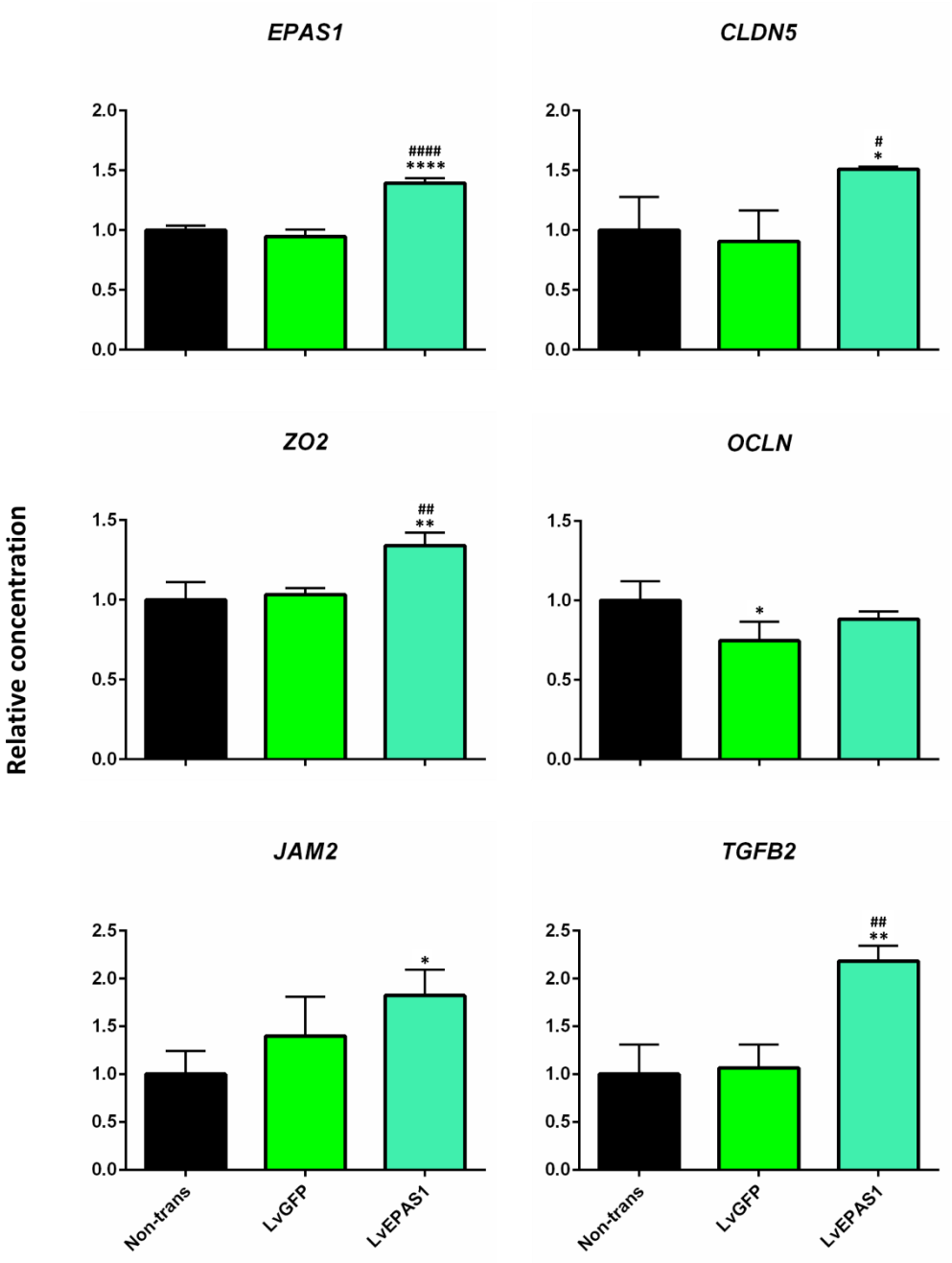

Figure 6.5 HUVECs transduced with Lv-*EPAS1* were assayed by qPCR for expression of tight junction transcripts and modulators of BBB permeability. * = p ≤ 0.05, ** = p ≥ 0.01, *** = p ≥0.001 vs non-transduced control. # = p ≥ 0.05, ## = p ≥ 0.01, ### = p ≥0.001 vs Lv-*GFP* control (one-way ANOVA with Tukey post-hoc test). Data represent three technical replicates. Error bars = S.E.M.

6.6 Transduction of i-astrocytes with Lv*EPAS1* and treatment of HUVECs with astrocyte conditioned medium

In light of the promising results for *CLDN5* and *ZO2* expression in Lv*EPAS1*-transduced HUVECs, i-astrocytes were transduced with Lv*EPAS1* and medium collected (iACM) to see if *EPAS1* over-expression in i-astrocytes led to factors being secreted that modified HUVEC gene expression. Comparisons were made to media taken from the same cell-lines without *EPAS1* transduction. As a control, HUVECs were treated with just medium, and gene expression values for each cell-line were normalised to this control. HUVECs were treated with iACM for 24 hours and then assayed by qPCR for the expression of the four tight junction transcripts *CLDN5, ZO2, OCLN* and *JAM2* (Figure 6.6). Media from four i-astrocyte cell lines was used: the two control lines AG and 209, and two SOD1-ALS lines p91 and 295. The sALS line 009 was not included in this experiment due to limited sample material.

Media from the control i-astrocyte line AG led to a trend for decreased expression of *CLDN5* in HUVECs compared to media only controls, with a trend for decreased *CLDN5* expression in AG-*EPAS1* iACM treated HUVECs. Conditioned media from the second control i-astrocyte cell-line 209, whether transduced or not, also led to trend for decreased *CLDN5* expression in HUVECs. For HUVECs treated with iACM from the SOD1-ALS i-astrocyte line p91 there was again a trend for decreased expression of *CLDN5* which reached significance for p91-*EPAS1* iACM, whilst the second SOD1-ALS i-astrocyte line 295 also showed a trend for decreased expression of *CLDN5*. 295-*EPAS1* iACM-treated HUVECs had significantly lower *CLDN5* expression compared to those treated with just media or 295 iACM. In contrast to *CLDN5* expression, the expression of *ZO2* was not affected by treatment of HUVECs with any of the conditioned media.

For *OCLN*, AG induced a trend for decreased expression in both non-transduced and *EPAS1*-transduced conditions. Similarly, expression of *OCLN* in HUVECs treated with iACM from 209 was not significantly different from media alone, however treatment with iACM from 209-*EPAS1* led to a significant decrease in *OCLN* expression versus media alone and 209 iACM. *OCLN* showed a small non-significant decrease in expression in p91 and p91-*EPAS1* treated HUVECs. In HUVECs treated with medium from 295 there was a significant decrease in *OCLN* expression versus media. In contrast

to all other tested lines, *OCLN* expression was actually significantly higher in HUVECs treated with 295-*EPAS1* iACM compared to 295 iACM.

The expression of *JAM2* in HUVECs was significantly increased upon treatment with media from AG over media alone but not upon treatment with AG-*EPAS1* media, whilst *JAM2* expression was not significantly altered from media alone in either 209 or 209-*EPAS1* treated HUVECs. In contrast to iACM taken from *EPAS1*-transduced control i-astrocyte lines, *JAM2* expression was significantly increased over both media and non transduced p91 iACM when HUVECs were treated with iACM from p91-*EPAS1*. As with p91, HUVECs treated with iACM from 295-*EPAS1* showed significantly higher expression of *JAM2* over media and 295-iACM. The increased expression of *JAM2* in HUVECs treated with *EPAS1* SOD1-ALS i-astrocytes is in direct contrast to the effect of *EPAS1* overexpression in control i-astrocytes, media from which led to a decreased expression of *JAM2* in HUVECs compared to media from non-transduced control i-astrocytes.

In summary, *CLDN5* expression appears reduced in HUVECs treated with iACM regardless of transduction by Lv*EPAS1*, whilst Lv*EPAS1* transduction appears to have a different effect upon *JAM2* expression between control and disease cell lines. The expression of *ZO2* and *OCLN* appears variable dependent upon the cell-line used and shows no consistent effect of media from Lv*EPAS1*-astrocytes upon the expression of these genes.

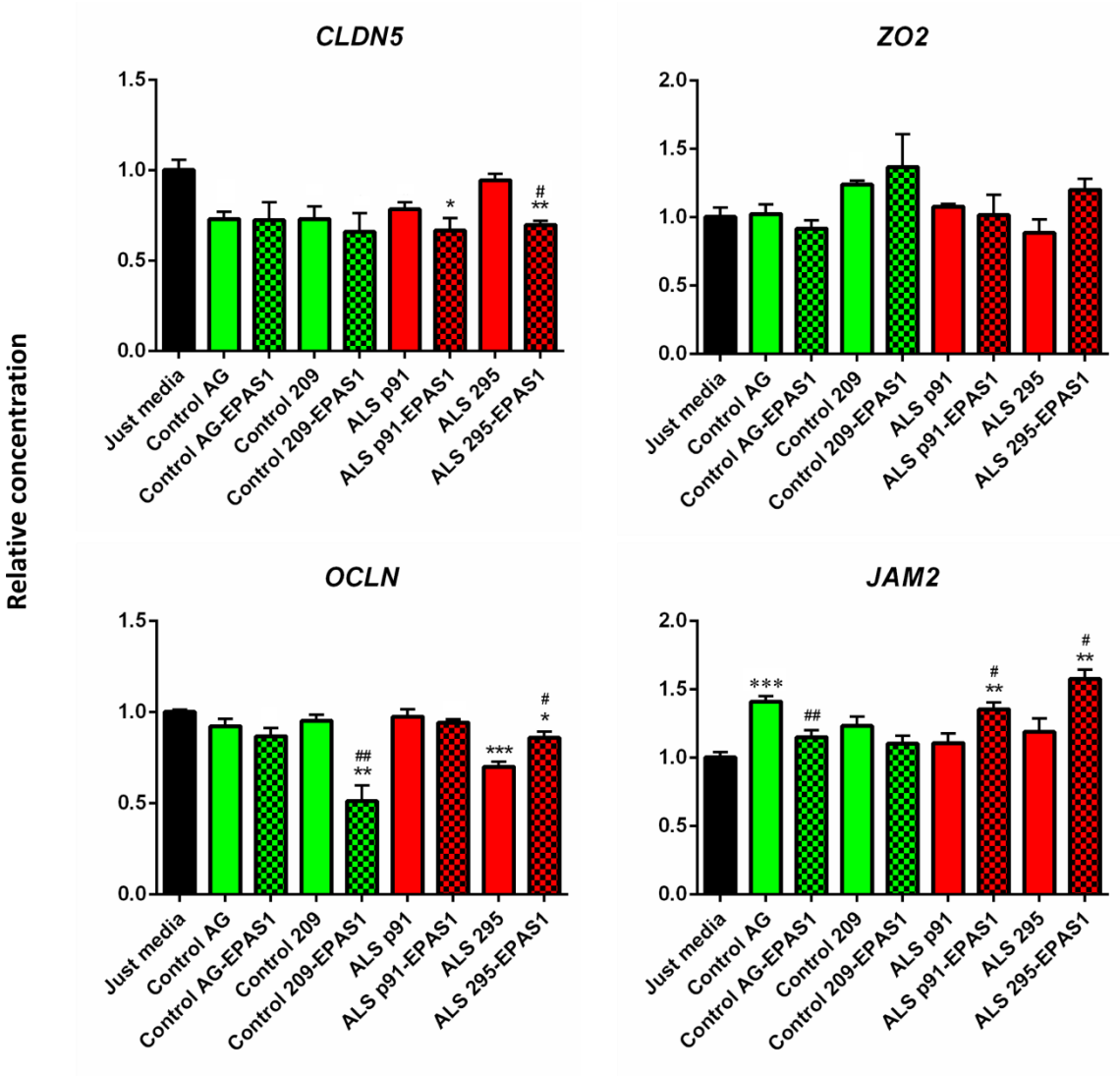

Figure 6.6 Tight junction transcript expression in HUVECs treated with conditioned medium from control or SOD1-ALS i-astrocytes which were either non-transduced or transduced with Lv*EPAS1*. Three technical repeats per cell line. * = p ≤ 0.05, ** = p ≤ 0.01, *** = p ≤ 0.001 vs. HUVECs cultured in media alone. # = p ≤ 0.05, ## = p ≤ 0.01, ### = p ≤ 0.001 vs. HUVECs treated with respective non-transduced i-astrocyte conditioned medium (one-way ANOVA with Tukey post-hoc test). Error bars = S. E. M.

6.7 Co-culture of i-astrocytes and HUVECs and effect of transduction with Lv*EPAS1*

HUVECs and i-astrocytes were transduced by Lv*EPAS1* and placed together in transwells to assess whether there was an effect upon HUVEC tight junction integrity using TEER and dextran permeability measurements. All different combinations of transduction were tested, resulting in transwells containing transduced i-astrocytes with non-transduced HUVECs, non-transduced i-astrocytes with transduced HUVECs or both cell types transduced. As previously (Section 6.3), three separate experiments were performed, with experiments 1 (SOD1-ALS) and 2 (sALS) being performed at the Kaspar Laboratory at Nationwide Children's Hospital, Ohio, U.S.A. and experiment 3 (SOD1-ALS) being performed at The University of Sheffield, U.K.

The transduction of monocultured HUVECs with Lv*EPAS1* ($HUVEC^{EPAS1}$) showed a trend for increased TEER and also showed a significant decrease in dextran-permeability (Figure 6.7). Similarly, the transduction of HUVECs with Lv*EPAS1* and co-culture with non-transduced control i-astrocytes ($Astro/Endo^{EPAS1}$) led to a significant increase in TEER over transwells containing non-transduced control i-astrocytes and HUVECs. The significant difference between control Astro/Endo and disease Astro/Endo transwells was still seen in the $Astro/Endo^{EPAS1}$ culture condition. $Astro^{EPAS1}/Endo$ and $Astro^{EPAS1}/Endo^{EPAS1}$ conditions were only repeated twice but show minimal differences between control and disease transwells for both TEER and dextran readings. No significant differences were observed for any of the transduction combinations in terms of dextran readings.

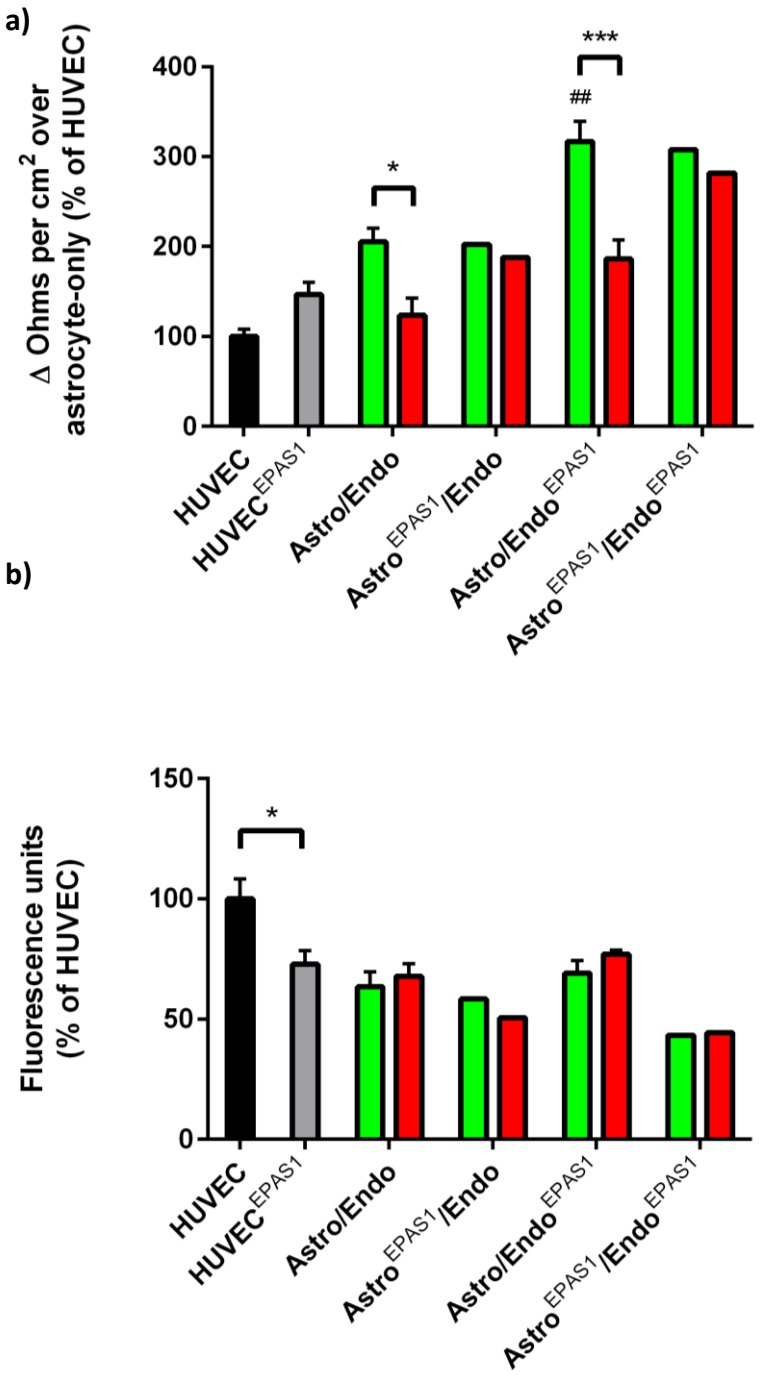

Figure 6.7 TEER reading and Dextran permeability of HUVECs co-cultured with control and ALS i-astrocytes under different Lv*EPAS1* transduction conditions. **a)** TEER readings of HUVEC-only controls and transwells containing either HUVECs-only, i-astrocytes-only or both cell types transduced with Lv-*EPAS1* (as denoted by superscript text). *EPAS1* overexpression increased TEER readings in control Astro/Endo^{EPAS1} transwells relative to non-transduced Astro/Endo transwells. **b)** Dextran permeability measurements of the cultures used in a). *EPAS1* overexpression decreased the permeability of HUVECs cultured alone but did not significantly decrease the permeability of any of the transwell cultures relative to non-transduced Astro/Endo co-cultures. All experiments had n=3 apart from Astro^{EPAS1}/Endo and Astro^{EPAS1}/Endo^{EPAS1} which had n=2. Values are normalised to non-transduced HUVECs after subtraction of astrocyte only-control values. * = $p \leq 0.05$, *** = $p \leq 0.001$. ## = $p \leq 0.01$ vs Astro/Endo. One-way ANOVA with Sidak's multiple comparisons test. Error bars = S. E. M.

6.8 Discussion

This study shows the first evidence of endothelial function being disrupted by i-astrocytes obtained from patients with SOD1 and sporadic ALS. When HUVECs were co-cultured with control and ALS i-astrocytes, the delta value, corresponding to the transwell resistance once astrocyte-only values had been subtracted, was significantly higher in control transwells versus ALS transwells (Figure 6.3). Delta values were used instead of total resistance values due to the heterogeneous nature of the i-astrocytes; monolayer tightness and density was variable between cell lines. TEER readings are affected by confluence of monolayers, thus it was therefore necessary to subtract values obtained from astrocyte-only control wells.

The lower TEER readings observed for transwells containing ALS i-astrocytes could be through a lack of supportive factors, an increase in toxic factors, or an alteration of signalling to the endothelia. The i-astrocytes produced by this method have previously been shown to decrease viability of co-cultured motor neurons compared to those co-cultured with control i-astrocytes (Meyer et al., 2013). Toxic factors such as lead acetate and malathion are capable of inducing decreased transwell TEER readings and expression of tight junction proteins (Balbuena et al., 2010a, Balbuena et al., 2010b). Therefore it may be possible that as yet unidentified factors are being secreted by i-astrocytes that are toxic to endothelial cells.

It is more likely however that there is an altered signalling between ALS i-astrocytes and endothelia. This is due to the observation that dextran permeability is similar between control and ALS transwells (Figure 6.3). If toxicity were occurring, one would expect disruption to endothelia to occur on a large enough scale to allow greater solute permeability. The fact that a disruption is seen only in the TEER readings, which represent the ionic permeability of the barrier, suggests that a more subtle effect is operating at the level of the tight junction. Astrocytes are able to signal to endothelia through a variety of signalling factors such as prostaglandins and cytokines such as IL1β and TGFβ (Abbott et al., 2006). Perhaps the increased expression of transcripts for factors such as TGFB2, validated previously by qPCR (Figure 5.10, Chapter 5), can explain the increased permeability of ALS transwells versus controls.

Upon the finding that i-astrocytes from ALS patients are less supportive/disrupted in signalling to HUVECs compared to those from controls, a gene therapy approach was investigated to see whether this defect could be rescued. Transcription factors decreased in expression in the human microarrays were investigated for their applicability in modulating the properties of the BBB (Figure 6.4). *EPAS1* was identified as a highly expressed transcription factor that has the potential to regulate tight junction transcripts (Martínez-Estrada et al., 2003, Chavez et al., 2006, Gruber et al., 2010). This study has identified *EPAS1* as a transcription factor which when over-expressed at the transcript level leads to an increased expression of tight junction transcripts such as *CLDN5* and *ZO2* and the BBB modulator *TGFB2* in HUVECs. Claudin-5 and ZO2 are intimately linked in the cell; ZO1 and ZO2 are scaffolding proteins which localise to the intra-cellular side of the plasma membrane and are vital for correct localisation of tight junction proteins and, in particular, the polymerisation of Claudin proteins (Umeda et al., 2006). The linkage of *EPAS1* with tight junction gene expression also reinforces previous work which found a trend for decreased tight junction expression in response to *EPAS1* deletion (Gruber et al., 2010). In contrast to *CLDN5* and *ZO2*, the expression of *OCLN* and *JAM2* was not significantly different to non-transduced or Lv*GFP*-transduced controls, meaning that other factors may have to be investigated for the manipulation of these genes. Functionally, *EPAS1* over-expression led to increased TEER readings and significantly decreased permeability to dextrans in HUVEC monolayers (Figure 6.7).

The choice of *EPAS1* for over-expression studies was also based upon the previous observation that HIF2α, the protein encoded by *EPAS1*, drives EPO expression in astrocytes during hypoxic conditions and that EPO is a factor important in maintaining barrier integrity (Martínez-Estrada et al., 2003, Chavez et al., 2006). In contrast to these studies, over-expression of *EPAS1* in astrocytes appeared to decrease tight junction transcript expression in HUVECs treated with iACM (Figure 6.6). The one robust effect of Lv*EPAS1* transduction upon iACM-mediated tight junction expression was for *JAM2* which was increased in expression when treated with media from Lv*EPAS1* transduced i-astrocytes. Thus it appears that factors secreted by Lv*EPAS1*-astrocytes can up-regulate *JAM2* whilst Lv*EPAS1*-HUVECs feature up-regulation of

CLDN5 and *ZO2*. Further study should focus upon increasing the number of cell lines used to see if the effects observed are consistent. However, the experiments described here highlight the differing behaviour of the two cell types upon transduction.

In the transwell co-culture experiments (Figure 6.7), transduction of HUVECs alone and co-culture with i-astrocytes in Astro/Endo^{EPAS1} transwells increased TEER readings relative to the levels seen in Astro/Endo conditions, which reached significance for the control transwells. This also appears to be the case for Astro^{EPAS1}/Endo^{EPAS1} transwells, although more replicates will be needed to confirm this finding. This suggests that expression of *EPAS1* in the two cell types may lead to different or synergistic effects upon BBB integrity. If future therapeutic strategies were to use viral delivery of transgenes or RNAi to the BBB then the differing reactions of all BBB cell types should be thoroughly investigated.

Future studies could also look at whether *EPAS1* over-expression in i-astrocytes leads to an increased expression of *TGFB2* as it does in HUVECs here (Figure 6.5). TGFB2 increases HUVEC permeability when applied exogenously (Ishihara et al., 2008), and may be a contributing factor to the increased permeability of Astro^{EPAS1}/Endo transwells relative to Astro^{EPAS1}/Endo^{EPAS1} transwells. Alternatively, HIF2α has also been shown to affect the transcription of VEGF in the absence of HIF1α (Shinojima et al., 2007). VEGF is also able to increase endothelial permeability (Gavard and Gutkind, 2006, Argaw et al., 2012), and thus over-expression of *EPAS1* could lead to increased VEGF production by astrocytes. In support of this, HIF1α has recently been shown to be unstable in sALS fibroblasts during hypoxia, leading to significantly lower levels of HIF1α protein compared to control fibroblasts (Raman et al., 2014). If this is also the case in the SOD1 and sALS astrocytes used here, the subsequent over-expression of HIF2α could therefore drive the transcription of VEGF. In summary, the applicability of *EPAS1* for gene therapy of the observed TEER deficit in ALS transwells has not yet been proven, and requires further investigation to clarify these interesting pilot data. As an alternative to the gene therapy approach, future strategies could investigate the use of factors such as glycerophosphoinositol (GPI) or dexamethasone, which have been found to increase TEER in a similar *in vitro* BBB model (Cucullo et al., 2004).

6.8.1 The contribution of endothelia in the transwell co-culture requires further investigation

The contribution of the endothelial cells in the transwells should not be overlooked as they are also capable of modulating astrocyte properties. Endothelia treated with ammonia had increased translocation of NFκB to the nucleus and conditioned medium taken from these cells induced swelling of astrocytes (Jayakumar et al., 2012). Perhaps endothelia secrete factors to ALS i-astrocytes that exacerbate the situation, or perhaps the use of wild-type endothelia here dampened the effect of ALS i-astrocytes. Li et al (2013) have recently shown that fibroblasts can be converted to endothelia through a similar direct conversion method as used for the i-astrocytes in this study. Therefore a valuable future study would be to use ALS endothelia in co-culture with i-astrocytes to see if the effects are exaggerated when both cell types are diseased.

6.8.2 Attribution of tight junction transcript expression to astrocytes

Future studies should be designed to confirm whether the tight junction transcripts identified as down-regulated in the microarrays of SOD1-ALS versus control astrocytes are truly dysregulated in astrocytes in ALS or are due to expression by contaminating endothelial cells from LCM-capture. OCLN and ZO2 expression has previously been seen in astrocytes (Simpson et al., 2010), however CLDN5 has not. Although the level of contaminating transcripts for endothelial cells is very small relative to those of astrocyte transcripts, three of the transcripts used to identify endothelia (*vWF, FLT1* and *CLDN5*) are differentially expressed between the controls and SOD1-ALS cases (Figure 5.8, Chapter 5).

The majority of signal upon the microarrays is from astrocytes, due to GFAP being used as a marker during LCM and the high expression levels of astrocyte transcripts. However the intricate inter-twining of non-neuronal cells in the spinal cord, especially astrocytes which contact the vasculature and neurons with their processes, means that a small amount of contaminating signal from other cell types is inevitable. Rather than disregard the enrichment of tight junction transcripts as contamination, one could hypothesise that the decrease in tight junction transcripts in SOD1-ALS cases is due to either a) astrocyte toxicity towards endothelia and subsequent loss of contaminating endothelial cells in ALS-LCM samples or b) astrocyte-mediated down-regulation of

tight junction transcripts in ALS and a consistent level of endothelial contamination in LCM samples from ALS and controls. The results presented here support the latter hypothesis; astrocyte-conditioned medium is able to influence tight junction transcript expression, whilst HUVECs co-cultured with i-astrocytes derived from ALS fibroblasts show a significantly lower level of TEER than those cultured with i-astrocytes from control fibroblasts. Finally, the lack of a difference between control and ALS transwells with regards to dextran permeability indicates that endothelial cell death death resulting from i-astrocyte toxicity is not occurring. Signalling between the different components of the blood brain barrier in ALS and its effect upon disease progression therefore merits further investigation.

CHAPTER 7

Discussion

7 Discussion

This project used microarray technology to address the hypothesis that gene expression profiling of murine SOD1^{G93A} astrocytes will identify dysregulated gene expression that reveals the contribution of astrocytes to motor neuron death throughout the disease process. Though this hypothesis was fairly broad, microarray technology is itself a hypothesis generation tool. Thus, the microarray analysis of SOD1^{G93A} astrocytes generated the subsequent hypotheses that the immune response, lysosome and cholesterol pathways are dysregulated in symptomatic and/or late-stage SOD1^{G93A} astrocytes. Similarly, microarray technology was used to address the hypothesis that astrocytes in SOD1-ALS human subjects possess dysregulated gene expression that reveals the contribution of astrocytes to motor neuron death. Through identification of the differential expression of tight junction transcripts on the arrays, it was hypothesised that SOD1-ALS astrocytes contribute to the BBB breakdown that is seen in ALS mouse models and patients. These hypotheses, generated at the transcript level, could then be tested at the functional level using tissue and *in vitro* studies. In this way, the initial hypotheses have been answered: microarray profiling of murine SOD1^{G93A} and human SOD1-ALS astrocytes did reveal dysregulated gene expression and led to functional experiments that revealed phenomena that may affect survival of motor neurons.

7.1 Similarities of these findings to other neurodegenerative conditions

Non-cell autonomy is now recognised as a key feature in neurodegenerative disease. The data here show that a multitude of processes within astrocytes are being dysregulated during ALS progression in the SOD1^{G93A} mouse and within human SOD1-ALS astrocytes (Figure 7.1). Some of the astrocyte behaviours seen in this study and in ALS are common to other neurodegenerative diseases. For example, reactive astrogliosis is also a key feature of Alzheimer's disease (AD) and Parkinson's disease (PD) (Beach and McGeer, 1988, Sacino et al., 2014). Reactive astrocytes are even seen in the spinal cord of these patients (Samantaray et al., 2013), which is not the main region of pathology for these diseases.

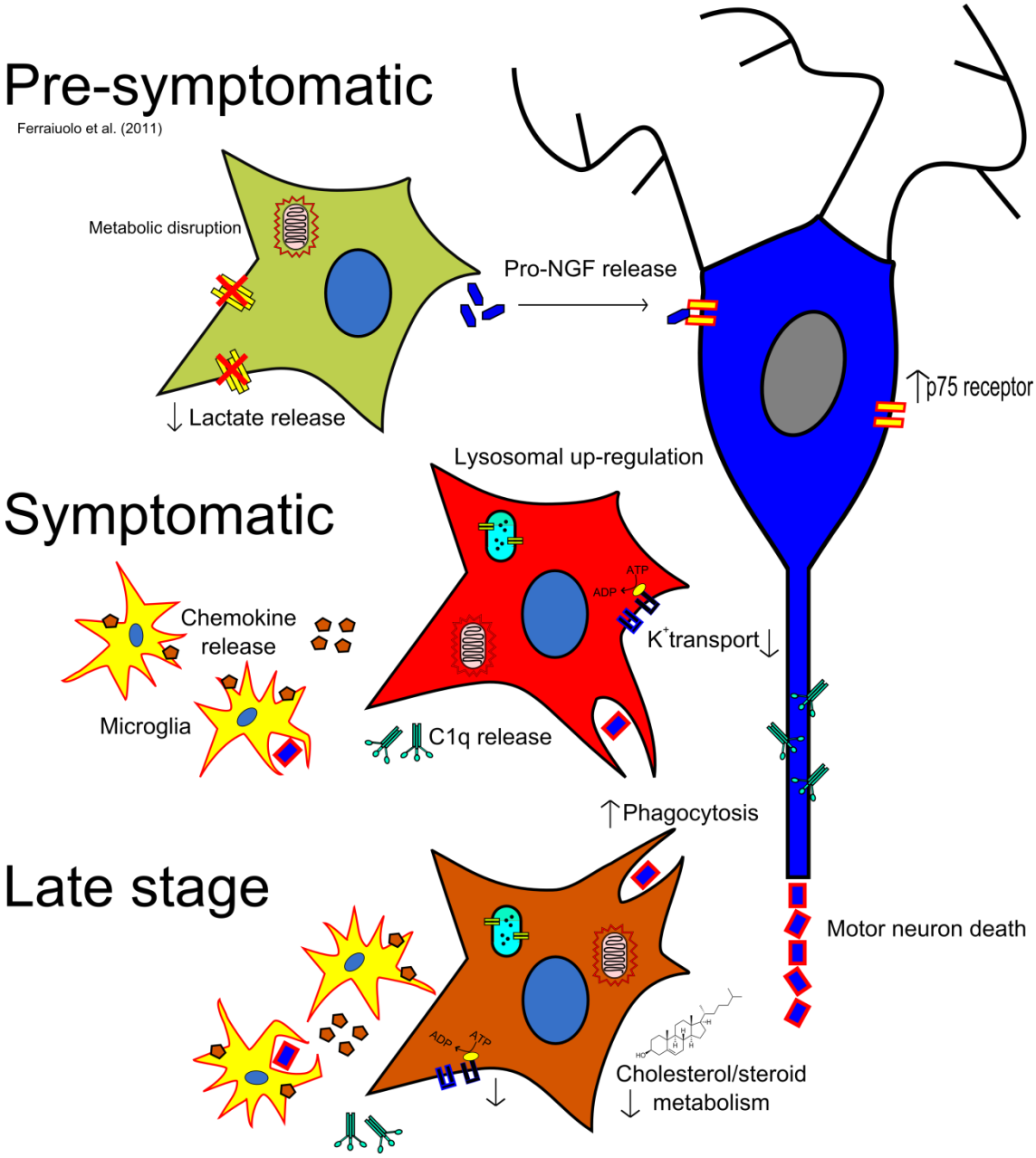

Figure 7.1 The changing phenotype of astrocytes during disease progression in the SOD1^{G93A} mouse. Key dysregulated gene categories are shown from the pre-symtptomatic, symptomatic and late-stages of disease.

The data in the current study of murine astrocytes suggest that this reactive phenotype contains protective elements, at least in the symptomatic phase of disease before the pathology becomes overwhelming. It is now generally accepted that astrocytes become reactive as a defence response for the protection of neurons (Rodriguez-Arellano et al., 2015). This would make sense in ALS, where an increased number of astrocytes could clear excess glutamate and ROS. In contrast to ALS, AD and

PD, mouse models of the neurodegenerative disorder Huntington's disease (HD) feature no increase in astrogliosis at symptom onset (Tong et al., 2014), and it would be interesting to see if stimulation of astrocyte proliferation in HD models is neuroprotective.

If gliosis and neuro-inflammation are largely protective strategies in ALS, this may be the reason why anti-inflammatory therapies have had limited effect on disease progression. For example, many anti-inflammatory treatments have shown promise in the $SOD1^{G93A}$ mouse which have not translated to humans. The inhibition of cyclo-oxygenase 2 (COX2), which is involved in the synthesis of pro-inflammatory cytokines, with the drug celecoxib significantly enhanced survival time by 25% in the $SOD1^{G93A}$ mouse (Drachman et al., 2002). However, the use of this drug in human ALS showed no effect upon disease progression (Cudkowicz et al., 2006). Minocycline is a drug which inhibits microglial activation and inflammation which has also been trialled in ALS. Presymptomatic administration of minocycline to mSOD1 mice delayed the onset of neurodegeneration and extended survival time by 5 weeks when administered in high doses in food (Kriz et al., 2002) and around 16% when given in lower doses via intra-peritoneal injection (Van Den Bosch et al., 2002). However minocycline actually seemed to worsen disease outcomes in humans, as demonstrated by a faster decline in the ALSFRS-R (Gordon et al., 2007). Therefore, inflammation may be a feature of the mouse model which is either not important in human disease, or plays a positive role in disease pathophysiology.

Increased activity of lysosomal enzymes was also a key feature of the symptomatic and late-stage $SOD1^{G93A}$ astrocytes. One contributing factor for this in ALS may be that one of the two identified proteins contained within bunina bodies is the lysosomal cysteine protease inhibitor Cystatin C (Okamoto et al., 2008), thereby removing a source of lysosomal inhibition. Lysosomal dysfunction is also seen in other neurodegenerative diseases. Similar to the findings here of increased lysosomal activity, lysosomal content of vulnerable neurons in human AD cases is increased around two to eight-fold over age-matched controls (Cataldo et al., 1996) and increased lysosomal staining of astrocytes is seen in human AD brain compared to controls (Kobayashi et al., 2002). In contrast, the treatment of dopaminergic neurons with 1-methyl-4-phenyl-1,2,3,6-

tetrahydropyridine (MPTP), which models PD, features a depletion of lysosomes within dopaminergic neurons (Dehay et al., 2010). Restoration of lysosomes through treatment with rapamycin proved protective against MPTP exposure, providing evidence that increased lysosomal function may be neuroprotective.

Lysosomal dysfunction in neurodegenerative disease is of particular interest due to the lysosome being the end-point for the process of autophagy, which is the cellular process for degradation of macromolecules, organelles and protein aggregates. Protein aggregation is particularly pertinent in repeat expansion disorders such as Huntington's disease, in which large increases in lysosomes are seen, possibly in response to decreased lysosomal enzyme activity (Cortes and La Spada, 2014). Coupled with defective loading of autophagosomes, this leads to decreased turnover of misfolded mutant huntingtin protein. Thus, in ALS, which features aggregated proteins in all genetic subtypes, and also features C9ORF72-ALS with a repeat-expansion component, lysosomal function is likely to be of importance.

In terms of the reduced expression of cholesterol transcripts in late-stage SOD1^{G93A} astrocytes (Chapter 4), it is interesting that HD also features dysfunctional metabolism of cholesterol with lower activation of SREBP2 and reduction in cholesterol synthesis genes (Leoni and Caccia, 2015). In AD, it has been known for some time that the *APOE4* allele confers an increased susceptibility to AD development (Strittmatter et al., 1993). *APOE4* encodes an isoform of apoliprotein E, which is important in the transport of cholesterol from astrocytes to neurons, and confers a different domain structure and stability than the *APOE2* and *APOE3* alleles (Zhong and Weisgraber, 2009). Meanwhile in PD, there is less clear-cut evidence for cholesterol playing a role in neuronal death (Martin et al., 2014). The data from the current study add to the limited evidence of dysregulation of cholesterol pathways currently present in the ALS field. However, the occurrence of this process in other neurodegenerative diseases warrants its further investigation in ALS.

For human SOD1-ALS astrocytes, the microarray study led to the hypothesis that astrocytes are involved in the BBB breakdown seen in ALS. This is also suggested in other neurodegenerative conditions. For example in PD, increased reactive gliosis is

seen with subsequent release of pro-inflammatory cytokines which can disrupt the BBB (Cabezas et al., 2014). In AD, Aβ damages endothelium via stimulation of superoxide production (Thomas et al., 1996). This is particularly interesting given the increased amount of ROS produced by astrocytes and microglia in SOD1-ALS and also given the fact that provision of SOD1 rescued the endothelial damage caused by Aβ (Thomas et al., 1996).

7.2 Comparative analyses of mouse and human data

As already discussed in section 5.12.3, it was interesting that there was little overlap of the mouse and human gene expression data. However, large differences in gene expression are seen between cells of the same type in different locations in the CNS (Doyle et al., 2008). Perhaps the different locations of picked astrocytes, lumbar spinal cord in the mouse study versus cervical spinal cord in the human cases, could be one reason for the different outcomes of the two studies, or perhaps there is a more fundamental difference in astrocyte behaviour between mouse and man.

Human astrocytes are known to be more complex than murine astrocytes e.g. by possession of more processes and a faster rate of calcium-wave conduction (Oberheim et al., 2009). This is thought to be linked to the enhanced cognitive abilities of humans compared to mice, and murine memory and learning is improved when glial restricted precursors are implanted into the mouse brain (Han et al., 2013). In addition, multiple different subtypes of astrocyte are observed in human brain that are not present in rodent brain (Oberheim et al., 2009). This difference in astrocyte complexity means that the lack of overlap between the human and mouse datasets is not surprising. In addition variation between the human and mouse arrays will be influenced by the factors mentioned in Chapter 5 section 5.12.3 such as post mortem interval, age, gender, genetic heterogeneity of humans versus mice, type of SOD1 mutation, over-expression of mSOD1 in the mouse model and the use of different markers of astrocytes for LCM.

7.3 Discrepancies between mouse models and human disease

The $SOD1^{G93A}$ mouse model has allowed many of the pathological mechanisms of ALS to be elucidated and has proved invaluable in this study where it has allowed study of

pre-symptomatic and symptomatic disease, something that is not possible in human SOD1-ALS. However, although the mSOD1 models of ALS recapitulate human disease pathology and progression, no therapies have successfully transitioned from the mSOD1 mouse to the clinic. It may be that the low percentage of SOD1-ALS cases, only 20% of fALS and therefore only 2% of cases overall, will mean that most trials using large numbers of patients are likely to fail, as any effects identified in the mouse model could be SOD1-specific. It is therefore important for the ALS community to generate models using the other known ALS-causative mutations, the most important of these being C9ORF72 and TDP-43 related ALS.

C9ORF72-related ALS accounts for around 40% of fALS and up to 7% of sALS, meaning that if a good model could be made, there may be more successful translation from model to clinic. Progress is occurring on this front, as recently a tetracycline-inducible mouse model which produces C9ORF72 RNA containing 80 GGGGCC repeats has been created (Hukema et al., 2014). Three hypotheses exist for the pathogenicity of C9ORF72 containing repeat expansions: 1) expanded C9ORF72 mRNA sequesters RNA binding proteins and leads to abnormal splicing events, 2) expanded C9ORF72 upon one allele leads to haploinsufficiency, and 3) the dipeptide repeat proteins (DPR) encoded by the expansion cause toxicity through formation of protein aggregates (Walsh et al., 2014). The inducible mouse model of Hukema et al. (2014) contains ubiquinated inclusions in the nucleus of striatal neurons and in the neuropil but does not show expression of DPR proteins commonly associated with C9ORF72-ALS, meaning that it is a good model to study the mechanisms of RNA toxicity in isolation. No cell loss is observed in this model after 12 weeks of C9ORF72 induction, suggesting that it may be the DPRs that mediate the toxic effect. In support of this, generation of drosophila lines carrying stop codons in the C9ORF72 expansion, thereby removing DPR production, did not suffer ocular degeneration, whereas ocular degeneration did occur when expanded C9ORF72 did not contain stop codons (Mizielinska et al., 2014).

The use of TDP-43 models has proven problematic due to the fact that over-expression of wild-type human TDP-43 in mice is toxic (Stallings et al., 2010). Thus comparisons between mutant TDP-43 models and a wild-type TDP-43 control model are difficult to make. Knockout of TDP-43 is embryonic lethal in mice (Wu et al., 2010), however

partial knockout mouse models in which TDP-43 is knocked out of motor neurons have demonstrated ALS-like pathology (Wu et al., 2012b). These data show that wild-type TDP-43 has both the propensity to misfold and that its normal function is vital for the survival of the cell.

As shown in the current study, even when studying the same disease-causing gene, there is a marked difference between the mouse and human gene expression signatures. As previously mentioned in Chapter 1, different mutations in SOD1 can cause very different disease progressions. As more causative genes are being found, it is becoming increasingly apparent that ALS is a spectrum of disorders leading to a common endpoint, so it may be that astrocytes play different roles in each ALS sub-type, and corresponding therapies will need to take this into account.

7.4 Toxicity or loss of support

As mentioned in Chapter 1, one of the main questions regarding astrocyte biology in ALS is that of whether astrocytes are toxic to motor neurons or whether their supportive function is compromised. Certainly there is evidence for both of these phenomena occurring *in vitro*. The evidence presented in the two microarray studies conducted here upon astrocytes that were as close to *in vivo* as possible, seems to show that a loss of supportive function makes up a larger component of astrocyte behaviour than toxicity. It is postulated that the immune function and lysosomal up-regulation detected in symptomatic SOD1^{G93A} astrocytes may actually be a protective function, allowing the phagocytosis and recycling of neuronal debris. Similarly, the putative disruption of the BBB by astrocytes seen in the human study is not a direct toxic effect of these cells upon neurons. Furthermore, the disruption in ion homeostasis observed in symptomatic and late-stage astrocytes indicates that one of the main supportive roles, that of homeostatic regulation of the external environment, has been severely impaired in disease. The data accumulated from the microarray analyses of the pre-symptomatic, symptomatic and late-stage disease in the SOD1^{G93A} mouse appear to show, amongst many dysregulated processes, a progressive loss of support for neurons, beginning with decreased lactate secretion and continuing with problems in ion homeostasis and cholesterol biosynthesis (Figure 7.1).

This is not to say that there is no toxicity of astrocytes toward motor neurons in ALS or other neurodegenerative disorders. In AD, delivery of the peptide inhibitor VIVIT to astrocytes using adeno-associated virus interfered with the pro-inflammatory "nuclear factor of activated T-cells" pathway leading to decreased astrogliosis, improved cognition, synaptic function and lower Aβ levels (Furman et al., 2012). Thus, astrocytes do have the capacity to be damaging to neuronal function. Similar to the M2 to M1 microglial switch in ALS, perhaps astrocytes could be said to transition from an A2 (supportive) to an A1 (reactive) phenotype during disease progression, where an increase in reactivity occurs in parallel to a decrease in supportive function.

7.5 Future work

To provide more evidence for the observed phenomena in the mouse and human array studies, more functional studies need to be performed, particularly in the area of cholesterol processing in $SOD1^{G93A}$ mice. For example, it is widely known that motor neurons co-cultured with $SOD1^{G93A}$ astrocytes show lower viability than those co-cultured with wild-type cells. It would be interesting to use GFP-motor neurons co-cultured with $SOD1^{G93A}$ astrocytes to see if phagocytosis of neuronal debris occurs *in vitro* and whether this phagocytosis leads to cytoplasmic localisation of SREBP2, as proposed in Chapter 6. At the moment it is unanswered as to whether phagocytosis is the reason for decreased cholesterol processing transcripts in astrocytes, or whether there is a more fundamental problem with cholesterol homeostasis.

Microarray experiments are great hypothesis generation tools. However the sheer number of hypotheses that can be generated given the list of differentially expressed genes can sometimes mean that interesting phenomena are left uninvestigated. A key feature of the murine astrocyte arrays that has not been functionally investigated is that to do with K^+ homeostasis. Astrocytes are key in K^+ buffering of the interstitial fluid (Kofuji and Newman, 2004) and a simple validation of whether astrocytes carrying the $SOD1^{G93A}$ mutation are defective in K^+ buffering capacity could be performed by measuring K^+ in the medium of astrocytes *in vitro*. With relevance to the differential expression of ion homeostasis genes seen in the mouse study, the potassium channel Kir4.1 is lost from astrocytes in mouse models of Huntington's disease, leading to elevated extracellular K^+ levels and neuronal death. This was rescued by viral delivery

of Kir4.1 (Tong et al., 2014). Thus K^+ buffering of ALS astrocytes is an important mechanism for investigation.

Another feature of the array analyses which warrants further investigation is the differential expression of mitochondrial or ATP-biosynthesis transcripts. Mitochondrial transcripts are dysregulated in murine presymptomatic $SOD1^{G93A}$ astrocytes and a dysregulation of ATP-biosynthetic transcripts is observed in human SOD1-ALS astrocytes here. This is a common theme amongst neurodegenerative disorders, with both AD (Liang et al., 2008) and PD (Duke et al., 2007) featuring differential expression of mitochondrial transcripts. Interestingly, the AD study using laser-captured neurons showed a decreased expression of mitochondrial transcripts, whereas the PD study using whole tissue and the present study of human SOD1-ALS astrocytes saw an increased expression of mitochondrial transcripts. In SOD1-ALS motor neurons, there is an equal split between increased and decreased transcripts involved in the electron transport chain (Kirby et al., 2011). It would therefore be interesting in future to investigate cell-specific mitochondrial dysfunction beyond the transcript level during disease progression.

In the human microarray study, the use of a new method to produce i-astrocytes through direct conversion of fibroblasts allowed the hypothesis that SOD1-ALS astrocytes are involved in BBB disruption to be tested using *in vitro* BBB models. This study has shown for the first time that ALS i-astrocytes induce higher permeability in endothelial monolayers in comparison to control i-astrocytes. The use of i-astrocytes will be beneficial for future research, as it means that the problems associated with transitioning between mouse disease to human disease will be removed. There is also the opportunity to create new lines of i-astrocytes from AD and PD fibroblasts to investigate BBB dysfunction in these diseases. The use of gene therapy to attempt rescue of monolayer integrity was successful in one patient line but unsuccessful in the following two lines tested. However, the data generated from the microarray study mean that more candidate genes could be identified in future to study alteration of BBB properties.

Finally, although efforts have been made here to compare the pre-symptomatic, symptomatic and late-stage motor neuron datasets of Ferraiuolo et al. (2007) to the corresponding astrocyte datasets, this has been done in an observational fashion. It would therefore be interesting to conduct a more thorough bioinformatic analysis of the two datasets to extract correlating networks of genes between the two cell-types. Corresponding efforts should also be made to compare the human SOD1-ALS motor neurons analysed by Kirby et al. (2011) to the human SOD1-ALS astrocytes used here. Such comparisons could be a powerful way of elucidating non-cell autonomous effects of astrocytes upon neurons and also of the signals that motor neurons are sending towards astrocytes. Finally, these datasets can be compared to a human C9ORF72-ALS astrocyte dataset already generated at the Sheffield Institute of Translation Neuroscience (SITraN) to elucidate sub-type specific mechanisms of disease.

7.5.1 ALS should be considered in the context of age

This study, in combination with data from pre-symptomatic $SOD1^{G93A}$ astrocytes (Ferraiuolo et al., 2011a), has provided an image of astrocyte behaviour at multiple different time-points of the disease process (Figure 7.1). However, due to the aggressive nature of the disease course in $SOD1^{G93A}$ mice, the late-stage of the disease was at 120 days, which is still relatively early in the mouse life. This ignores one of the main risk factors for ALS: age. The risk of ALS increases up to a peak risk at ~75 years old (Al-Chalabi and Hardiman, 2013), therefore it is important in future studies that the interactions of age and disease be studied more carefully. This could be done by using a more slowly-progressing mouse model such as the $SOD1^{G85R}$ model (Bruijn et al., 1997). Alternatively, a rapidly ageing mouse model, such as senescence accelerated mice (SAMs) (Shimada and Hasegawa-Ishii, 2011) could be crossed with an ALS mouse to study the interaction between the rapid ageing process and the ALS disease process. SAMs even come in different strains possessing different aspects of ageing, such as osteoporosis in SAMP6 mice or reduction of neuronal dendritic arbour and synaptic number in SAMP10 mice, meaning interaction of ALS with different aspects of ageing could be investigated. It would be interesting to study what processes in ageing lead to increased susceptibility to ALS, as this might reveal opportunities for preventative therapies. With reference to astrocytes, it is known that the expression of different

cellular markers changes with age in mice, suggesting that astrocytes undergo a phenotypic shift during the ageing process (Rodriguez et al., 2014). Also of note, the expression of inflammatory genes increases with age (Berchtold et al., 2008), and given the neuro-inflammation observed in ALS this could have an intensifying effect.

Specifically with regard to the BBB disruption seen in the human microarray study, ageing by itself is seen to lead to BBB breakdown (Marques et al., 2013). This provides a further reason why BBB disruption did not show up in the late-stage mouse array study. In addition, perhaps the *in vitro* BBB model used in the human study, in which fibroblasts were de-differentiated to a neural precursor cell, removed some of the age-related behaviour that these astrocytes might exhibit *in vivo*. In addition these cells were co-cultured with neonatal endothelia, and therefore this BBB model may not have accurately modelled the ageing neurovascular unit. Perhaps *in vivo* during ALS the combination of ageing and disrupted astrocyte-endothelial signalling leads to a greater disruption of the BBB than can be studied *in vitro*. Such questions could be answered if mouse models were created that combined the two phenomena.

At the end of a chromatid there is a stretch of non-coding DNA nucleotides known as a telomere, which protects the coding-DNA from damage. During replication, telomeres are not fully replicated and so become shortened with each cell division (Harley et al., 1990). Upon loss of telomere caps in human fibroblasts by expression of a truncated dominant negative form of the telomere capping factor TRF2, DNA damage occurs which leads to cell-cycle arrest and cellular senescence (d'Adda di Fagagna et al., 2003). Oxidative stress is shown to damage telomeres leading to senescence (Kurz et al., 2004), which is particularly interesting given that SOD1-ALS contains an oxidative stress component. In addition, lysosomal content of cells increases with senescence (Kurz et al., 2000), which is seen in the $SOD1^{G93A}$ astrocytes at symptomatic and late-stage disease in the current study. Finally, TGFβ secretion induces cell senescence in nearby cells in a paracrine fashion (Hubackova et al., 2012), and is increased in the human SOD1-ALS astrocytes in the current study. Therefore the following hypothesis has been formed about SOD1-ALS: SOD1-ALS is a disease caused by an accelerated ageing mechanism. Astrocytes would play a major part in this paradigm through oxidative stress of nearby cells, TGFβ secretion and an accelerated loss of supportive

function. Recently, telomere length has been found to be shorter in the leukocytes of sALS patients versus controls (De Felice et al., 2014). Future studies should investigate whether markers of ageing are increased in CNS cell-types in SOD1-ALS relative to controls and whether interference with key features of ageing astrocytes might prove beneficial.

7.6 Concluding remarks

In conclusion, this thesis presents the first study in which the gene expression of astrocytes has been mapped throughout the disease course in the $SOD1^{G93A}$ mouse model of ALS. This has identified common themes amongst the three disease stages, but also characteristics that change with disease progression. This could have powerful consequences upon future therapies, as the stage of disease will need to be taken into account so that the correct treatment is used for the phenotype of the cells being treated. In addition, astrocytes have been shown to interact with endothelia in human SOD1-ALS, possibly leading to BBB disruption. Lastly, a new hypothesis that SOD1-ALS contains an accelerated ageing mechanism has been formed, in which astrocytes could play a major part. These data highlight the myriad roles that astrocytes can play in disease and provide further evidence of ALS as a disease of more than just motor neurons.

8 References

Abbott, N. J., Ronnback, L. & Hansson, E. (2006) Astrocyte-endothelial interactions at the blood-brain barrier. *Nat Rev Neurosci,* 7**,** 41-53.

Aebischer, J., Cassina, P., Otsmane, B., Moumen, A., Seilhean, D., Meininger, V., Barbeito, L., Pettmann, B. & Raoul, C. (2011) IFNgamma triggers a LIGHT-dependent selective death of motoneurons contributing to the non-cell-autonomous effects of mutant SOD1. *Cell Death Differ,* 18**,** 754-68.

Affymetrix (2005) Gene Signal Estimates from Exon Arrays. Santa Clara,CA., Affymetrix.

Ajami, B., Bennett, J. L., Krieger, C., Tetzlaff, W. & Rossi, F. M. (2007) Local self-renewal can sustain CNS microglia maintenance and function throughout adult life. *Nat Neurosci,* 10**,** 1538-43.

Al-Chalabi, A. & Hardiman, O. (2013) The epidemiology of ALS: a conspiracy of genes, environment and time. *Nat Rev Neurol,* 9**,** 617-28.

Al-Saif, A., Al-Mohanna, F. & Bohlega, S. (2011) A mutation in sigma-1 receptor causes juvenile amyotrophic lateral sclerosis. *Ann Neurol,* 70**,** 913-9.

Alexianu, M. E., Kozovska, M. & Appel, S. H. (2001) Immune reactivity in a mouse model of familial ALS correlates with disease progression. *Neurology,* 57**,** 1282-9.

Allison, D. B., Cui, X., Page, G. P. & Sabripour, M. (2006) Microarray data analysis: from disarray to consolidation and consensus. *Nat Rev Genet,* 7**,** 55-65.

Almer, G., Vukosavic, S., Romero, N. & Przedborski, S. (1999) Inducible nitric oxide synthase up-regulation in a transgenic mouse model of familial amyotrophic lateral sclerosis. *J Neurochem,* 72**,** 2415-25.

Andersen, P. M., Nilsson, P., Ala-Hurula, V., Keranen, M. L., Tarvainen, I., Haltia, T., Nilsson, L., Binzer, M., Forsgren, L. & Marklund, S. L. (1995) Amyotrophic lateral sclerosis associated with homozygosity for an Asp90Ala mutation in CuZn-superoxide dismutase. *Nat Genet,* 10**,** 61-6.

Anderson, C. F. & Mosser, D. M. (2002) A novel phenotype for an activated macrophage: the type 2 activated macrophage. *J Leukoc Biol,* 72**,** 101-6.

Andjus, P. R., Bataveljic, D., Vanhoutte, G., Mitrecic, D., Pizzolante, F., Djogo, N., Nicaise, C., Gankam Kengne, F., Gangitano, C., Michetti, F., Van Der Linden, A., Pochet, R. & Bacic, G. (2009) In vivo morphological changes in animal models of amyotrophic lateral sclerosis and Alzheimer's-like disease: MRI approach. *Anat Rec (Hoboken),* 292**,** 1882-92.

Anneser, J. M., Cookson, M. R., Ince, P. G., Shaw, P. J. & Borasio, G. D. (2001) Glial cells of the spinal cord and subcortical white matter up-regulate neuronal nitric oxide synthase in sporadic amyotrophic lateral sclerosis. *Exp Neurol,* 171**,** 418-21.

Arai, T., Hasegawa, M., Akiyama, H., Ikeda, K., Nonaka, T., Mori, H., Mann, D., Tsuchiya, K., Yoshida, M., Hashizume, Y. & Oda, T. (2006) TDP-43 is a component of ubiquitin-positive tau-negative inclusions in frontotemporal lobar degeneration and amyotrophic lateral sclerosis. *Biochem Biophys Res Commun,* 351**,** 602-11.

Araque, A., Parpura, V., Sanzgiri, R. P. & Haydon, P. G. (1999) Tripartite synapses: glia, the unacknowledged partner. *Trends Neurosci,* 22**,** 208-15.

Argaw, A. T., Asp, L., Zhang, J., Navrazhina, K., Pham, T., Mariani, J. N., Mahase, S., Dutta, D. J., Seto, J., Kramer, E. G., Ferrara, N., Sofroniew, M. V. & John, G. R. (2012) Astrocyte-derived VEGF-A drives blood-brain barrier disruption in CNS inflammatory disease. *J Clin Invest,* 122**,** 2454-68.

Avossa, D., Grandolfo, M., Mazzarol, F., Zatta, M. & Ballerini, L. (2006) Early signs of motoneuron vulnerability in a disease model system: Characterization of transverse slice cultures of spinal cord isolated from embryonic ALS mice. *Neuroscience,* 138**,** 1179-1194.

Bak, L. K., Schousboe, A. & Waagepetersen, H. S. (2006) The glutamate/GABA-glutamine cycle: aspects of transport, neurotransmitter homeostasis and ammonia transfer. *J Neurochem,* 98**,** 641-53.

Bake, S., Friedman, J. A. & Sohrabji, F. (2009) Reproductive age-related changes in the blood brain barrier: expression of IgG and tight junction proteins. *Microvasc Res,* 78**,** 413-24.

Balbuena, P., Li, W. & Ehrich, M. (2010a) Assessments of tight junction proteins occludin, claudin 5 and scaffold proteins ZO1 and ZO2 in endothelial cells of the rat blood-brain barrier: cellular responses to neurotoxicants malathion and lead acetate. *Neurotoxicology,* 32**,** 58-67.

Balbuena, P., Li, W., Magnin-Bissel, G., Meldrum, J. B. & Ehrich, M. (2010b) Comparison of two blood-brain barrier in vitro systems: cytotoxicity and transfer assessments of malathion/oxon and lead acetate. *Toxicol Sci,* 114**,** 260-71.

Bannwarth, S., Ait-El-Mkadem, S., Chaussenot, A., Genin, E. C., Lacas-Gervais, S., Fragaki, K., Berg-Alonso, L., Kageyama, Y., Serre, V., Moore, D. G., Verschueren, A., Rouzier, C., Le Ber, I., Auge, G., Cochaud, C., Lespinasse, F., N'guyen, K., De Septenville, A., Brice, A., Yu-Wai-Man, P., Sesaki, H., Pouget, J. & Paquis-Flucklinger, V. (2014) A mitochondrial origin for frontotemporal dementia and amyotrophic lateral sclerosis through CHCHD10 involvement. *Brain,* 137**,** 2329-45.

Bataveljic, D., Nikolic, L., Milosevic, M., Todorovic, N. & Andjus, P. R. (2012) Changes in the astrocytic aquaporin-4 and inwardly rectifying potassium channel expression in the brain of the amyotrophic lateral sclerosis SOD1(G93A) rat model. *Glia,* 60**,** 1991-2003.

Beach, T. G. & Mcgeer, E. G. (1988) Lamina-specific arrangement of astrocytic gliosis and senile plaques in Alzheimer's disease visual cortex. *Brain Res,* 463**,** 357-61.

Beal, M. F., Ferrante, R. J., Browne, S. E., Matthews, R. T., Kowall, N. W. & Brown, R. H., Jr. (1997) Increased 3-nitrotyrosine in both sporadic and familial amyotrophic lateral sclerosis. *Ann Neurol,* 42**,** 644-54.

Beers, D. R., Henkel, J. S., Xiao, Q., Zhao, W., Wang, J., Yen, A. A., Siklos, L., Mckercher, S. R. & Appel, S. H. (2006) Wild-type microglia extend survival in PU.1 knockout mice with familial amyotrophic lateral sclerosis. *Proc Natl Acad Sci U S A,* 103**,** 16021-6.

Beers, D. R., Henkel, J. S., Zhao, W., Wang, J. & Appel, S. H. (2008) CD4+ T cells support glial neuroprotection, slow disease progression, and modify glial morphology in an animal model of inherited ALS. *Proc Natl Acad Sci U S A,* 105**,** 15558-63.

Beers, D. R., Zhao, W., Liao, B., Kano, O., Wang, J., Huang, A., Appel, S. H. & Henkel, J. S. (2011) Neuroinflammation modulates distinct regional and temporal clinical responses in ALS mice. *Brain Behav Immun,* 25**,** 1025-35.

Bellingham, M. C. (2011) A review of the neural mechanisms of action and clinical efficiency of riluzole in treating amyotrophic lateral sclerosis: what have we learned in the last decade? *CNS Neurosci Ther,* 17**,** 4-31.

Benkler, C., Ben-Zur, T., Barhum, Y. & Offen, D. (2013) Altered astrocytic response to activation in SOD1(G93A) mice and its implications on amyotrophic lateral sclerosis pathogenesis. *Glia,* 61**,** 312-26.

Berchtold, N. C., Cribbs, D. H., Coleman, P. D., Rogers, J., Head, E., Kim, R., Beach, T., Miller, C., Troncoso, J., Trojanowski, J. Q., Zielke, H. R. & Cotman, C. W. (2008) Gene expression changes in the course of normal brain aging are sexually dimorphic. *Proc Natl Acad Sci U S A,* 105**,** 15605-10.

Bergles, D. E., Roberts, J. D., Somogyi, P. & Jahr, C. E. (2000) Glutamatergic synapses on oligodendrocyte precursor cells in the hippocampus. *Nature,* 405**,** 187-91.

Bi, F., Huang, C., Tong, J., Qiu, G., Huang, B., Wu, Q., Li, F., Xu, Z., Bowser, R., Xia, X. G. & Zhou, H. (2013) Reactive astrocytes secrete lcn2 to promote neuron death. *Proc Natl Acad Sci U S A*.

Bilsland, L. G., Nirmalananthan, N., Yip, J., Greensmith, L. & Duchen, M. R. (2008) Expression of mutant SOD1 in astrocytes induces functional deficits in motoneuron mitochondria. *J Neurochem,* 107**,** 1271-83.

Bilsland, L. G., Sahai, E., Kelly, G., Golding, M., Greensmith, L. & Schiavo, G. (2010) Deficits in axonal transport precede ALS symptoms in vivo. *Proceedings of the National Academy of Sciences,* 107**,** 20523-20528.

Blackburn, D., Sargsyan, S., Monk, P. N. & Shaw, P. J. (2009) Astrocyte function and role in motor neuron disease: a future therapeutic target? *Glia,* 57**,** 1251-64.

Blackburn, D. J. (2010) The Role of Glial Cells in Motor Neuron Disease. *Academic Neurology Unit.* Sheffield, The University of Sheffield.

Boillee, S., Yamanaka, K., Lobsiger, C. S., Copeland, N. G., Jenkins, N. A., Kassiotis, G., Kollias, G. & Cleveland, D. W. (2006) Onset and progression in inherited ALS determined by motor neurons and microglia. *Science,* 312**,** 1389-92.

Bolstad, B. affyPLM: Methods for fitting probe-level models.

Bordet, T., Buisson, B., Michaud, M., Drouot, C., Galea, P., Delaage, P., Akentieva, N. P., Evers, A. S., Covey, D. F., Ostuni, M. A., Lacapere, J. J., Massaad, C., Schumacher, M., Steidl, E. M., Maux, D., Delaage, M., Henderson, C. E. & Pruss, R. M. (2007) Identification and characterization of cholest-4-en-3-one, oxime (TRO19622), a novel drug candidate for amyotrophic lateral sclerosis. *J Pharmacol Exp Ther,* 322**,** 709-20.

Brockington, A., Heath, P. R., Holden, H., Kasher, P., Bender, F. L., Claes, F., Lambrechts, D., Sendtner, M., Carmeliet, P. & Shaw, P. J. (2010) Downregulation of genes with a function in axon outgrowth and synapse formation in motor neurones of the VEGFdelta/delta mouse model of amyotrophic lateral sclerosis. *BMC Genomics,* 11**,** 203.

Brooks, B. R. (1994) El Escorial World Federation of Neurology criteria for the diagnosis of amyotrophic lateral sclerosis. Subcommittee on Motor Neuron Diseases/Amyotrophic Lateral Sclerosis of the World Federation of Neurology Research Group on Neuromuscular Diseases and the El Escorial "Clinical limits of amyotrophic lateral sclerosis" workshop contributors. *J Neurol Sci,* 124 Suppl**,** 96-107.

Brown, M. S. & Goldstein, J. L. (1997) The SREBP pathway: regulation of cholesterol metabolism by proteolysis of a membrane-bound transcription factor. *Cell,* 89**,** 331-40.

Bruijn, L. I., Becher, M. W., Lee, M. K., Anderson, K. L., Jenkins, N. A., Copeland, N. G., Sisodia, S. S., Rothstein, J. D., Borchelt, D. R., Price, D. L. & Cleveland, D. W. (1997) ALS-linked SOD1 mutant G85R mediates damage to astrocytes and promotes rapidly progressive disease with SOD1-containing inclusions. *Neuron,* 18**,** 327-38.

Bruinsma, I. B., De Jager, M., Carrano, A., Versleijen, A. A., Veerhuis, R., Boelens, W., Rozemuller, A. J., De Waal, R. M. & Verbeek, M. M. (2011) Small heat shock proteins induce a cerebral inflammatory reaction. *J Neurosci,* 31**,** 11992-2000.

Buffo, A., Rite, I., Tripathi, P., Lepier, A., Colak, D., Horn, A. P., Mori, T. & Gotz, M. (2008) Origin and progeny of reactive gliosis: A source of multipotent cells in the injured brain. *Proc Natl Acad Sci U S A,* 105**,** 3581-6.

Buratti, E. & Baralle, F. E. (2001) Characterization and functional implications of the RNA binding properties of nuclear factor TDP-43, a novel splicing regulator of CFTR exon 9. *J Biol Chem,* 276**,** 36337-43.

Burghes, A. H. M. & Beattie, C. E. (2009) Spinal muscular atrophy: why do low levels of survival motor neuron protein make motor neurons sick? *Nat Rev Neurosci,* 10**,** 597-609.

Bush, A. I. (2002) Is ALS caused by an altered oxidative activity of mutant superoxide dismutase? *Nat Neurosci,* 5**,** 919; author reply 919-20.

Butovsky, O., Siddiqui, S., Gabriely, G., Lanser, A. J., Dake, B., Murugaiyan, G., Doykan, C. E., Wu, P. M., Gali, R. R., Iyer, L. K., Lawson, R., Berry, J., Krichevsky, A. M., Cudkowicz, M. E. & Weiner, H. L. (2012) Modulating inflammatory monocytes with a unique microRNA gene signature ameliorates murine ALS. *The Journal of Clinical Investigation,* 122**,** 3063-3087.

Byrne, S., Elamin, M., Bede, P., Shatunov, A., Walsh, C., Corr, B., Heverin, M., Jordan, N., Kenna, K., Lynch, C., Mclaughlin, R. L., Iyer, P. M., O'brien, C., Phukan, J., Wynne, B., Bokde, A. L., Bradley, D. G., Pender, N., Al-Chalabi, A. & Hardiman, O. (2012) Cognitive and clinical characteristics of patients with amyotrophic lateral sclerosis carrying a C9orf72 repeat expansion: a population-based cohort study. *Lancet Neurology,* 11**,** 232-240.

Cabezas, R., Avila, M., Gonzalez, J., El-Bacha, R. S., Baez, E., Garcia-Segura, L. M., Jurado Coronel, J. C., Capani, F., Cardona-Gomez, G. P. & Barreto, G. E. (2014) Astrocytic modulation of blood brain barrier: perspectives on Parkinson's disease. *Front Cell Neurosci,* 8**,** 211.

Cahoy, J. D., Emery, B., Kaushal, A., Foo, L. C., Zamanian, J. L., Christopherson, K. S., Xing, Y., Lubischer, J. L., Krieg, P. A., Krupenko, S. A., Thompson, W. J. & Barres, B. A. (2008) A transcriptome database for astrocytes, neurons, and oligodendrocytes: a new resource for understanding brain development and function. *J Neurosci,* 28**,** 264-78.

Cai, J., Chen, Y., Cai, W. H., Hurlock, E. C., Wu, H., Kernie, S. G., Parada, L. F. & Lu, Q. R. (2007) A crucial role for Olig2 in white matter astrocyte development. *Development,* 134**,** 1887-99.

Carbone, M., Duty, S. & Rattray, M. (2012) Riluzole elevates GLT-1 activity and levels in striatal astrocytes. *Neurochem Int,* 60**,** 31-8.

Cassina, P., Cassina, A., Pehar, M., Castellanos, R., Gandelman, M., De Leon, A., Robinson, K. M., Mason, R. P., Beckman, J. S., Barbeito, L. & Radi, R. (2008) Mitochondrial dysfunction in SOD1G93A-bearing astrocytes promotes motor neuron degeneration: prevention by mitochondrial-targeted antioxidants. *J Neurosci,* 28**,** 4115-22.

Casula, M., Iyer, A. M., Spliet, W. G. M., Anink, J. J., Steentjes, K., Sta, M., Troost, D. & Aronica, E. (2011) Toll-like receptor signaling in amyotrophic lateral sclerosis spinal cord tissue. *Neuroscience,* 179**,** 233-243.

Cataldo, A. M., Hamilton, D. J., Barnett, J. L., Paskevich, P. A. & Nixon, R. A. (1996) Properties of the endosomal-lysosomal system in the human central nervous system: disturbances mark most neurons in populations at risk to degenerate in Alzheimer's disease. *J Neurosci,* 16**,** 186-99.

Cautain, B., Hill, R., De Pedro, N. & Link, W. (2014) Components and regulation of nuclear transport processes. *FEBS J*.

Chang, D. T., Honick, A. S. & Reynolds, I. J. (2006) Mitochondrial trafficking to synapses in cultured primary cortical neurons. *J Neurosci,* 26**,** 7035-45.

Chang, G. H., Barbaro, N. M. & Pieper, R. O. (2000) Phosphatidylserine-dependent phagocytosis of apoptotic glioma cells by normal human microglia, astrocytes, and glioma cells. *Neuro Oncol,* 2**,** 174-83.

Chang, Y., Kong, Q., Shan, X., Tian, G., Ilieva, H., Cleveland, D. W., Rothstein, J. D., Borchelt, D. R., Wong, P. C. & Lin, C. L. (2008) Messenger RNA oxidation occurs early in disease pathogenesis and promotes motor neuron degeneration in ALS. *PLoS One,* 3**,** e2849.

Chavez, J. C., Baranova, O., Lin, J. & Pichiule, P. (2006) The transcriptional activator hypoxia inducible factor 2 (HIF-2/EPAS-1) regulates the oxygen-dependent expression of erythropoietin in cortical astrocytes. *J Neurosci,* 26**,** 9471-81.

Chen, Y. Z., Bennett, C. L., Huynh, H. M., Blair, I. P., Puls, I., Irobi, J., Dierick, I., Abel, A., Kennerson, M. L., Rabin, B. A., Nicholson, G. A., Auer-Grumbach, M., Wagner, K., De Jonghe, P., Griffin, J. W., Fischbeck, K. H., Timmerman, V., Cornblath, D. R. & Chance, P. F. (2004) DNA/RNA helicase gene mutations in a form of juvenile amyotrophic lateral sclerosis (ALS4). *Am J Hum Genet,* 74**,** 1128-35.

Chiu, I. M., Chen, A., Zheng, Y., Kosaras, B., Tsiftsoglou, S. A., Vartanian, T. K., Brown, R. H., Jr. & Carroll, M. C. (2008) T lymphocytes potentiate endogenous neuroprotective inflammation in a mouse model of ALS. *Proc Natl Acad Sci U S A,* 105**,** 17913-8.

Chiu, I. M., Morimoto, E. T., Goodarzi, H., Liao, J. T., O'keeffe, S., Phatnani, H. P., Muratet, M., Carroll, M. C., Levy, S., Tavazoie, S., Myers, R. M. & Maniatis, T. (2013) A Neurodegeneration-Specific Gene-Expression Signature of Acutely Isolated Microglia from an Amyotrophic Lateral Sclerosis Mouse Model. *Cell Rep*.

Chow, C. Y., Landers, J. E., Bergren, S. K., Sapp, P. C., Grant, A. E., Jones, J. M., Everett, L., Lenk, G. M., Mckenna-Yasek, D. M., Weisman, L. S., Figlewicz, D., Brown, R. H. & Meisler, M. H. (2009) Deleterious variants of FIG4, a phosphoinositide phosphatase, in patients with ALS. *Am J Hum Genet,* 84**,** 85-8.

Christou, Y. A., Ohyama, K., Placzek, M., Monk, P. N. & Shaw, P. J. (2013) Wild-type but not mutant SOD1 transgenic astrocytes promote the efficient generation of

motor neuron progenitors from mouse embryonic stem cells. *BMC Neurosci,* 14**,** 126.

Clement, A. M., Nguyen, M. D., Roberts, E. A., Garcia, M. L., Boillee, S., Rule, M., Mcmahon, A. P., Doucette, W., Siwek, D., Ferrante, R. J., Brown, R. H., Jr., Julien, J. P., Goldstein, L. S. & Cleveland, D. W. (2003) Wild-type nonneuronal cells extend survival of SOD1 mutant motor neurons in ALS mice. *Science,* 302**,** 113-7.

Colton, C. A. & Gilbert, D. L. (1987) Production of superoxide anions by a CNS macrophage, the microglia. *FEBS Lett,* 223**,** 284-8.

Cooper-Knock, J., Jenkins, T. & Shaw, P. J. (2013) *Clinical and Molecular Aspects of Motor Neuron Disease*, Morgan and Claypool Life Sciences.

Cornell-Bell, A. H., Finkbeiner, S. M., Cooper, M. S. & Smith, S. J. (1990) Glutamate induces calcium waves in cultured astrocytes: long-range glial signaling. *Science,* 247**,** 470-3.

Cortes, C. J. & La Spada, A. R. (2014) The many faces of autophagy dysfunction in Huntington's disease: from mechanism to therapy. *Drug Discovery Today,* 19**,** 963-971.

Corti, S., Locatelli, F., Papadimitriou, D., Del Bo, R., Nizzardo, M., Nardini, M., Donadoni, C., Salani, S., Fortunato, F., Strazzer, S., Bresolin, N. & Comi, G. P. (2007) Neural stem cells LewisX+ CXCR4+ modify disease progression in an amyotrophic lateral sclerosis model. *Brain,* 130**,** 1289-305.

Costa, J., Swash, M. & De Carvalho, M. (2012) Awaji criteria for the diagnosis of amyotrophic lateral sclerosis:a systematic review. *Arch Neurol,* 69**,** 1410-6.

Cox, L. E., Ferraiuolo, L., Goodall, E. F., Heath, P. R., Higginbottom, A., Mortiboys, H., Hollinger, H. C., Hartley, J. A., Brockington, A., Burness, C. E., Morrison, K. E., Wharton, S. B., Grierson, A. J., Ince, P. G., Kirby, J. & Shaw, P. J. (2010) Mutations in CHMP2B in lower motor neuron predominant amyotrophic lateral sclerosis (ALS). *PLoS One,* 5**,** e9872.

Crosio, C., Valle, C., Casciati, A., Iaccarino, C. & Carri, M. T. (2011) Astroglial inhibition of NF-kappaB does not ameliorate disease onset and progression in a mouse model for amyotrophic lateral sclerosis (ALS). *PLoS One,* 6**,** e17187.

Cucullo, L., Hallene, K., Dini, G., Dal Toso, R. & Janigro, D. (2004) Glycerophosphoinositol and dexamethasone improve transendothelial electrical resistance in an in vitro study of the blood-brain barrier. *Brain Res,* 997**,** 147-51.

Cudkowicz, M. E., Mckenna-Yasek, D., Sapp, P. E., Chin, W., Geller, B., Hayden, D. L., Schoenfeld, D. A., Hosler, B. A., Horvitz, H. R. & Brown, R. H. (1997) Epidemiology of mutations in superoxide dismutase in amyotrophic lateral sclerosis. *Ann Neurol,* 41**,** 210-21.

Cudkowicz, M. E., Shefner, J. M., Schoenfeld, D. A., Zhang, H., Andreasson, K. I., Rothstein, J. D. & Drachman, D. B. (2006) Trial of celecoxib in amyotrophic lateral sclerosis. *Ann Neurol,* 60**,** 22-31.

Cutler, R. G., Pedersen, W. A., Camandola, S., Rothstein, J. D. & Mattson, M. P. (2002) Evidence that accumulation of ceramides and cholesterol esters mediates oxidative stress-induced death of motor neurons in amyotrophic lateral sclerosis. *Ann Neurol,* 52**,** 448-57.

D'adda Di Fagagna, F., Reaper, P. M., Clay-Farrace, L., Fiegler, H., Carr, P., Von Zglinicki, T., Saretzki, G., Carter, N. P. & Jackson, S. P. (2003) A DNA damage checkpoint response in telomere-initiated senescence. *Nature,* 426**,** 194-8.

Dangond, F., Hwang, D., Camelo, S., Pasinelli, P., Frosch, M. P., Stephanopoulos, G., Brown, R. H., Jr. & Gullans, S. R. (2004) Molecular signature of late-stage human ALS revealed by expression profiling of postmortem spinal cord gray matter. *Physiol Genomics,* 16**,** 229-39.

De Felice, B., Annunziata, A., Fiorentino, G., Manfellotto, F., D'alessandro, R., Marino, R., Borra, M. & Biffali, E. (2014) Telomerase expression in amyotrophic lateral sclerosis (ALS) patients. *J Hum Genet,* 59**,** 555-61.

De Oliveira, G. P., Alves, C. J. & Chadi, G. (2013) Early gene expression changes in spinal cord from SOD1(G93A) Amyotrophic Lateral Sclerosis animal model. *Front Cell Neurosci,* 7**,** 216.

De Vos, K. J., Chapman, A. L., Tennant, M. E., Manser, C., Tudor, E. L., Lau, K. F., Brownlees, J., Ackerley, S., Shaw, P. J., Mcloughlin, D. M., Shaw, C. E., Leigh, P. N., Miller, C. C. & Grierson, A. J. (2007) Familial amyotrophic lateral sclerosis-linked SOD1 mutants perturb fast axonal transport to reduce axonal mitochondria content. *Hum Mol Genet,* 16**,** 2720-8.

Dehay, B., Bove, J., Rodriguez-Muela, N., Perier, C., Recasens, A., Boya, P. & Vila, M. (2010) Pathogenic lysosomal depletion in Parkinson's disease. *J Neurosci,* 30**,** 12535-44.

Dejesus-Hernandez, M., Mackenzie, I. R., Boeve, B. F., Boxer, A. L., Baker, M., Rutherford, N. J., Nicholson, A. M., Finch, N. A., Flynn, H., Adamson, J., Kouri, N., Wojtas, A., Sengdy, P., Hsiung, G. Y., Karydas, A., Seeley, W. W., Josephs, K. A., Coppola, G., Geschwind, D. H., Wszolek, Z. K., Feldman, H., Knopman, D. S., Petersen, R. C., Miller, B. L., Dickson, D. W., Boylan, K. B., Graff-Radford, N. R. & Rademakers, R. (2011) Expanded GGGGCC hexanucleotide repeat in noncoding region of C9ORF72 causes chromosome 9p-linked FTD and ALS. *Neuron,* 72**,** 245-56.

Deng, H. X., Chen, W., Hong, S. T., Boycott, K. M., Gorrie, G. H., Siddique, N., Yang, Y., Fecto, F., Shi, Y., Zhai, H., Jiang, H., Hirano, M., Rampersaud, E., Jansen, G. H., Donkervoort, S., Bigio, E. H., Brooks, B. R., Ajroud, K., Sufit, R. L., Haines, J. L., Mugnaini, E., Pericak-Vance, M. A. & Siddique, T. (2011) Mutations in UBQLN2 cause dominant X-linked juvenile and adult-onset ALS and ALS/dementia. *Nature,* 477**,** 211-5.

Deng, H. X., Shi, Y., Furukawa, Y., Zhai, H., Fu, R., Liu, E., Gorrie, G. H., Khan, M. S., Hung, W. Y., Bigio, E. H., Lukas, T., Dal Canto, M. C., O'halloran, T. V. & Siddique, T. (2006) Conversion to the amyotrophic lateral sclerosis phenotype is associated with intermolecular linked insoluble aggregates of SOD1 in mitochondria. *Proc Natl Acad Sci U S A,* 103**,** 7142-7.

Di Giorgio, F. P., Boulting, G. L., Bobrowicz, S. & Eggan, K. C. (2008) Human embryonic stem cell-derived motor neurons are sensitive to the toxic effect of glial cells carrying an ALS-causing mutation. *Cell Stem Cell,* 3**,** 637-48.

Di Giorgio, F. P., Carrasco, M. A., Siao, M. C., Maniatis, T. & Eggan, K. (2007) Non-cell autonomous effect of glia on motor neurons in an embryonic stem cell-based ALS model. *Nat Neurosci,* 10**,** 608-14.

Diaz-Amarilla, P., Olivera-Bravo, S., Trias, E., Cragnolini, A., Martinez-Palma, L., Cassina, P., Beckman, J. & Barbeito, L. (2011) Phenotypically aberrant astrocytes that promote motoneuron damage in a model of inherited amyotrophic lateral sclerosis. *Proc Natl Acad Sci U S A,* 108**,** 18126-31.

Doyle, J. P., Dougherty, J. D., Heiman, M., Schmidt, E. F., Stevens, T. R., Ma, G., Bupp, S., Shrestha, P., Shah, R. D., Doughty, M. L., Gong, S., Greengard, P. & Heintz, N. (2008) Application of a translational profiling approach for the comparative analysis of CNS cell types. *Cell,* 135**,** 749-62.

Drachman, D. B., Frank, K., Dykes-Hoberg, M., Teismann, P., Almer, G., Przedborski, S. & Rothstein, J. D. (2002) Cyclooxygenase 2 inhibition protects motor neurons and prolongs survival in a transgenic mouse model of ALS. *Ann Neurol,* 52**,** 771-8.

Dringen, R. (2000) Metabolism and functions of glutathione in brain. *Prog Neurobiol,* 62**,** 649-71.

Drory, V. E., Birnbaum, M., Peleg, L., Goldman, B. & Korczyn, A. D. (2003) Hexosaminidase A deficiency is an uncommon cause of a syndrome mimicking amyotrophic lateral sclerosis. *Muscle Nerve,* 28**,** 109-12.

Du, Y., Ma, Z., Lin, S., Dodel, R. C., Gao, F., Bales, K. R., Triarhou, L. C., Chernet, E., Perry, K. W., Nelson, D. L., Luecke, S., Phebus, L. A., Bymaster, F. P. & Paul, S. M. (2001) Minocycline prevents nigrostriatal dopaminergic neurodegeneration in the MPTP model of Parkinson's disease. *Proc Natl Acad Sci U S A,* 98**,** 14669-74.

Duan, L.-J., Takeda, K. & Fong, G.-H. (2014) Hypoxia Inducible Factor-2Î± Regulates the Development of Retinal Astrocytic Network by Maintaining Adequate Supply of Astrocyte Progenitors. *PLoS One,* 9**,** e84736.

Duan, W., Li, X., Shi, J., Guo, Y., Li, Z. & Li, C. (2010) Mutant TAR DNA-binding protein-43 induces oxidative injury in motor neuron-like cell. *Neuroscience,* 169**,** 1621-9.

Duffy, L. M., Chapman, A. L., Shaw, P. J. & Grierson, A. J. (2011) Review: The role of mitochondria in the pathogenesis of amyotrophic lateral sclerosis. *Neuropathol Appl Neurobiol,* 37**,** 336-52.

Duke, D. C., Moran, L. B., Pearce, R. K. & Graeber, M. B. (2007) The medial and lateral substantia nigra in Parkinson's disease: mRNA profiles associated with higher brain tissue vulnerability. *Neurogenetics,* 8**,** 83-94.

Eijssen, L. M., Jaillard, M., Adriaens, M. E., Gaj, S., De Groot, P. J., Muller, M. & Evelo, C. T. (2013) User-friendly solutions for microarray quality control and pre-processing on ArrayAnalysis.org. *Nucleic Acids Res,* 41**,** W71-6.

Elden, A. C., Kim, H. J., Hart, M. P., Chen-Plotkin, A. S., Johnson, B. S., Fang, X., Armakola, M., Geser, F., Greene, R., Lu, M. M., Padmanabhan, A., Clay-Falcone, D., Mccluskey, L., Elman, L., Juhr, D., Gruber, P. J., Rub, U., Auburger, G., Trojanowski, J. Q., Lee, V. M., Van Deerlin, V. M., Bonini, N. M. & Gitler, A. D. (2010) Ataxin-2 intermediate-length polyglutamine expansions are associated with increased risk for ALS. *Nature,* 466**,** 1069-75.

Engelhardt, J. I., Soos, J., Obal, I., Vigh, L. & Siklos, L. (2005) Subcellular localization of IgG from the sera of ALS patients in the nervous system. *Acta Neurol Scand,* 112**,** 126-33.

Engelhardt, J. I., Tajti, J. & Appel, S. H. (1993) Lymphocytic infiltrates in the spinal cord in amyotrophic lateral sclerosis. *Arch Neurol,* 50**,** 30-6.

Escartin, C., Won, S. J., Malgorn, C., Auregan, G., Berman, A. E., Chen, P. C., Deglon, N., Johnson, J. A., Suh, S. W. & Swanson, R. A. (2011) Nuclear factor erythroid 2-related factor 2 facilitates neuronal glutathione synthesis by upregulating neuronal excitatory amino acid transporter 3 expression. *J Neurosci,* 31**,** 7392-401.

Faulkner, J. R., Herrmann, J. E., Woo, M. J., Tansey, K. E., Doan, N. B. & Sofroniew, M. V. (2004) Reactive astrocytes protect tissue and preserve function after spinal cord injury. *J Neurosci,* 24**,** 2143-55.

Fawcett, J. W. & Asher, R. A. (1999) The glial scar and central nervous system repair. *Brain Res Bull,* 49**,** 377-91.

Fehrenschild, D., Galli, U., Breiden, B., Bloch, W., Schettina, P., Brodesser, S., Michels, C., Gunschmann, C., Sandhoff, K., Niessen, C. M. & Niemann, C. (2012) TCF/Lef1-Mediated Control of Lipid Metabolism Regulates Skin Barrier Function. *J Invest Dermatol,* 132**,** 337-345.

Ferraiuolo, L., Heath, P. R., Holden, H., Kasher, P., Kirby, J. & Shaw, P. J. (2007) Microarray analysis of the cellular pathways involved in the adaptation to and progression of motor neuron injury in the SOD1 G93A mouse model of familial ALS. *J Neurosci,* 27**,** 9201-19.

Ferraiuolo, L., Higginbottom, A., Heath, P. R., Barber, S., Greenald, D., Kirby, J. & Shaw, P. J. (2011a) Dysregulation of astrocyte-motoneuron cross-talk in mutant superoxide dismutase 1-related amyotrophic lateral sclerosis. *Brain,* 134**,** 2627-41.

Ferraiuolo, L., Kirby, J., Grierson, A. J., Sendtner, M. & Shaw, P. J. (2011b) Molecular pathways of motor neuron injury in amyotrophic lateral sclerosis. *Nature Reviews Neurology,* 7**,** 616-630.

Ferrante, R. J., Browne, S. E., Shinobu, L. A., Bowling, A. C., Baik, M. J., Macgarvey, U., Kowall, N. W., Brown, R. H., Jr. & Beal, M. F. (1997) Evidence of increased oxidative damage in both sporadic and familial amyotrophic lateral sclerosis. *J Neurochem,* 69**,** 2064-74.

Finkelstein, A., Kunis, G., Seksenyan, A., Ronen, A., Berkutzki, T., Azoulay, D., Koronyo-Hamaoui, M. & Schwartz, M. (2011) Abnormal changes in NKT cells, the IGF-1 axis, and liver pathology in an animal model of ALS. *PLoS One,* 6**,** e22374.

Fischer, L. R., Culver, D. G., Tennant, P., Davis, A. A., Wang, M., Castellano-Sanchez, A., Khan, J., Polak, M. A. & Glass, J. D. (2004) Amyotrophic lateral sclerosis is a distal axonopathy: evidence in mice and man. *Exp Neurol,* 185**,** 232-40.

Fitzmaurice, P. S., Shaw, I. C., Kleiner, H. E., Miller, R. T., Monks, T. J., Lau, S. S., Mitchell, J. D. & Lynch, P. G. (1996) Evidence for DNA damage in amyotrophic lateral sclerosis. *Muscle Nerve,* 19**,** 797-8.

Fodor, S. P., Read, J. L., Pirrung, M. C., Stryer, L., Lu, A. T. & Solas, D. (1991) Light-directed, spatially addressable parallel chemical synthesis. *Science,* 251**,** 767-73.

Forsberg, K., Andersen, P. M., Marklund, S. L. & Brannstrom, T. (2011) Glial nuclear aggregates of superoxide dismutase-1 are regularly present in patients with amyotrophic lateral sclerosis. *Acta Neuropathol,* 121**,** 623-34.

Forsberg, K., Jonsson, P. A., Andersen, P. M., Bergemalm, D., Graffmo, K. S., Hultdin, M., Jacobsson, J., Rosquist, R., Marklund, S. L. & Brannstrom, T. (2010) Novel antibodies reveal inclusions containing non-native SOD1 in sporadic ALS patients. *PLoS One,* 5**,** e11552.

Foust, K. D., Nurre, E., Montgomery, C. L., Hernandez, A., Chan, C. M. & Kaspar, B. K. (2009) Intravascular AAV9 preferentially targets neonatal neurons and adult astrocytes. *Nat Biotechnol,* 27**,** 59-65.

Foust, K. D., Salazar, D. L., Likhite, S., Ferraiuolo, L., Ditsworth, D., Ilieva, H., Meyer, K., Schmelzer, L., Braun, L., Cleveland, D. W. & Kaspar, B. K. (2013) Therapeutic AAV9-mediated suppression of mutant SOD1 slows disease progression and extends survival in models of inherited ALS. *Mol Ther,* 21**,** 2148-59.

Frakes, A. E., Ferraiuolo, L., Haidet-Phillips, A. M., Schmelzer, L., Braun, L., Miranda, C. J., Ladner, K. J., Bevan, A. K., Foust, K. D., Godbout, J. P., Popovich, P. G., Guttridge, D. C. & Kaspar, B. K. (2014) Microglia induce motor neuron death via the classical NF-kappaB pathway in amyotrophic lateral sclerosis. *Neuron,* 81**,** 1009-23.

Frey, D., Schneider, C., Xu, L., Borg, J., Spooren, W. & Caroni, P. (2000) Early and selective loss of neuromuscular synapse subtypes with low sprouting competence in motoneuron diseases. *J Neurosci,* 20**,** 2534-42.

Fukada, Y., Yasui, K., Kitayama, M., Doi, K., Nakano, T., Watanabe, Y. & Nakashima, K. (2007) Gene expression analysis of the murine model of amyotrophic lateral sclerosis: studies of the Leu126delTT mutation in SOD1. *Brain Res,* 1160**,** 1-10.

Furman, J. L., Sama, D. M., Gant, J. C., Beckett, T. L., Murphy, M. P., Bachstetter, A. D., Van Eldik, L. J. & Norris, C. M. (2012) Targeting astrocytes ameliorates neurologic changes in a mouse model of Alzheimer's disease. *J Neurosci,* 32**,** 16129-40.

Garbuzova-Davis, S., Haller, E., Saporta, S., Kolomey, I., Nicosia, S. V. & Sanberg, P. R. (2007a) Ultrastructure of blood-brain barrier and blood-spinal cord barrier in SOD1 mice modeling ALS. *Brain Res,* 1157**,** 126-37.

Garbuzova-Davis, S., Hernandez-Ontiveros, D. G., Rodrigues, M. C., Haller, E., Frisina-Deyo, A., Mirtyl, S., Sallot, S., Saporta, S., Borlongan, C. V. & Sanberg, P. R. (2012) Impaired blood-brain/spinal cord barrier in ALS patients. *Brain Res,* 1469**,** 114-28.

Garbuzova-Davis, S., Saporta, S., Haller, E., Kolomey, I., Bennett, S. P., Potter, H. & Sanberg, P. R. (2007b) Evidence of compromised blood-spinal cord barrier in early and late symptomatic SOD1 mice modeling ALS. *PLoS One,* 2**,** e1205.

Gavard, J. & Gutkind, J. S. (2006) VEGF controls endothelial-cell permeability by promoting the [beta]-arrestin-dependent endocytosis of VE-cadherin. *Nat Cell Biol,* 8**,** 1223-1234.

Genda, E. N., Jackson, J. G., Sheldon, A. L., Locke, S. F., Greco, T. M., O'donnell, J. C., Spruce, L. A., Xiao, R., Guo, W., Putt, M., Seeholzer, S., Ischiropoulos, H. & Robinson, M. B. (2011) Co-compartmentalization of the Astroglial Glutamate Transporter, GLT-1, with Glycolytic Enzymes and Mitochondria. *J Neurosci,* 31**,** 18275-88.

Genevestigator.Com https://www.genevestigator.com/userdocs/manual/qc.html (12/08/2014)

Gentleman, R. C., Carey, V. J., Bates, D. M., Bolstad, B., Dettling, M., Dudoit, S., Ellis, B., Gautier, L., Ge, Y., Gentry, J., Hornik, K., Hothorn, T., Huber, W., Iacus, S., Irizarry, R., Leisch, F., Li, C., Maechler, M., Rossini, A. J., Sawitzki, G., Smith, C., Smyth, G., Tierney, L., Yang, J. Y. & Zhang, J. (2004) Bioconductor: open

software development for computational biology and bioinformatics. *Genome Biol,* 5**,** R80.

Giordana, M. T., Ferrero, P., Grifoni, S., Pellerino, A., Naldi, A. & Montuschi, A. (2011) Dementia and cognitive impairment in amyotrophic lateral sclerosis: a review. *Neurol Sci,* 32**,** 9-16.

Goldknopf, I. L., Sheta, E. A., Bryson, J., Folsom, B., Wilson, C., Duty, J., Yen, A. A. & Appel, S. H. (2006) Complement C3c and related protein biomarkers in amyotrophic lateral sclerosis and Parkinson's disease. *Biochem Biophys Res Commun,* 342**,** 1034-9.

Goldsworthy, S. M., Stockton, P. S., Trempus, C. S., Foley, J. F. & Maronpot, R. R. (1999) Effects of fixation on RNA extraction and amplification from laser capture microdissected tissue. *Mol Carcinog,* 25**,** 86-91.

Gong, Y. H., Parsadanian, A. S., Andreeva, A., Snider, W. D. & Elliott, J. L. (2000) Restricted expression of G86R Cu/Zn superoxide dismutase in astrocytes results in astrocytosis but does not cause motoneuron degeneration. *J Neurosci,* 20**,** 660-5.

Gonzalez-Mariscal, L., Tapia, R. & Chamorro, D. (2008) Crosstalk of tight junction components with signaling pathways. *Biochim Biophys Acta,* 1778**,** 729-56.

Gordon, P. H., Moore, D. H., Miller, R. G., Florence, J. M., Verheijde, J. L., Doorish, C., Hilton, J. F., Spitalny, G. M., Macarthur, R. B., Mitsumoto, H., Neville, H. E., Boylan, K., Mozaffar, T., Belsh, J. M., Ravits, J., Bedlack, R. S., Graves, M. C., Mccluskey, L. F., Barohn, R. J. & Tandan, R. (2007) Efficacy of minocycline in patients with amyotrophic lateral sclerosis: a phase III randomised trial. *Lancet Neurol,* 6**,** 1045-53.

Gordon, S. & Martinez, F. O. (2010) Alternative activation of macrophages: mechanism and functions. *Immunity,* 32**,** 593-604.

Gowing, G., Philips, T., Van Wijmeersch, B., Audet, J. N., Dewil, M., Van Den Bosch, L., Billiau, A. D., Robberecht, W. & Julien, J. P. (2008) Ablation of proliferating microglia does not affect motor neuron degeneration in amyotrophic lateral sclerosis caused by mutant superoxide dismutase. *J Neurosci,* 28**,** 10234-44.

Greenway, M. J., Andersen, P. M., Russ, C., Ennis, S., Cashman, S., Donaghy, C., Patterson, V., Swingler, R., Kieran, D., Prehn, J., Morrison, K. E., Green, A., Acharya, K. R., Brown, R. H., Jr. & Hardiman, O. (2006) ANG mutations segregate with familial and 'sporadic' amyotrophic lateral sclerosis. *Nat Genet,* 38**,** 411-3.

Gresham, D., Dunham, M. J. & Botstein, D. (2008) Comparing whole genomes using DNA microarrays. *Nat Rev Genet,* 9**,** 291-302.

Grewal, R. P., Morgan, T. E. & Finch, C. E. (1999) C1qB and clusterin mRNA increase in association with neurodegeneration in sporadic amyotrophic lateral sclerosis. *Neurosci Lett,* 271**,** 65-7.

Gruber, M., Mathew, L. K., Runge, A. C., Garcia, J. A. & Simon, M. C. (2010) EPAS1 Is Required for Spermatogenesis in the Postnatal Mouse Testis. *Biol Reprod,* 82**,** 1227-36.

Guo, H., Lai, L., Butchbach, M. E., Stockinger, M. P., Shan, X., Bishop, G. A. & Lin, C. L. (2003) Increased expression of the glial glutamate transporter EAAT2 modulates excitotoxicity and delays the onset but not the outcome of ALS in mice. *Hum Mol Genet,* 12**,** 2519-32.

Gurney, M. E., Pu, H., Chiu, A. Y., Dal Canto, M. C., Polchow, C. Y., Alexander, D. D., Caliendo, J., Hentati, A., Kwon, Y. W., Deng, H. X. & Et Al. (1994) Motor neuron degeneration in mice that express a human Cu,Zn superoxide dismutase mutation. *Science,* 264**,** 1772-5.

Haidet-Phillips, A. M., Gross, S. K., Williams, T., Tuteja, A., Sherman, A., Ko, M., Jeong, Y. H., Wong, P. C. & Maragakis, N. J. (2013) Altered astrocytic expression of TDP-43 does not influence motor neuron survival. *Exp Neurol,* 250**,** 250-9.

Haidet-Phillips, A. M., Hester, M. E., Miranda, C. J., Meyer, K., Braun, L., Frakes, A., Song, S., Likhite, S., Murtha, M. J., Foust, K. D., Rao, M., Eagle, A., Kammesheidt, A., Christensen, A., Mendell, J. R., Burghes, A. H. & Kaspar, B. K. (2011) Astrocytes from familial and sporadic ALS patients are toxic to motor neurons. *Nat Biotechnol,* 29**,** 824-8.

Han, X., Chen, M., Wang, F., Windrem, M., Wang, S., Shanz, S., Xu, Q., Oberheim, N. A., Bekar, L., Betstadt, S., Silva, A. J., Takano, T., Goldman, S. A. & Nedergaard, M. (2013) Forebrain engraftment by human glial progenitor cells enhances synaptic plasticity and learning in adult mice. *Cell Stem Cell,* 12**,** 342-53.

Hand, C. K., Khoris, J., Salachas, F., Gros-Louis, F., Lopes, A. A., Mayeux-Portas, V., Brewer, C. G., Brown, R. H., Jr., Meininger, V., Camu, W. & Rouleau, G. A. (2002) A novel locus for familial amyotrophic lateral sclerosis, on chromosome 18q. *Am J Hum Genet,* 70**,** 251-6.

Harley, C. B., Futcher, A. B. & Greider, C. W. (1990) Telomeres shorten during ageing of human fibroblasts. *Nature,* 345**,** 458-60.

Hart, P. J. (2006) Pathogenic superoxide dismutase structure, folding, aggregation and turnover. *Curr Opin Chem Biol,* 10**,** 131-8.

Hashioka, S., Klegeris, A., Schwab, C. & Mcgeer, P. L. (2009) Interferon-gamma-dependent cytotoxic activation of human astrocytes and astrocytoma cells. *Neurobiol Aging,* 30**,** 1924-35.

He, F. & Sun, Y. E. (2007) Glial cells more than support cells? *Int J Biochem Cell Biol,* 39**,** 661-5.

Hegedus, J., Putman, C. T. & Gordon, T. (2007) Time course of preferential motor unit loss in the SOD1 G93A mouse model of amyotrophic lateral sclerosis. *Neurobiol Dis,* 28**,** 154-64.

Henkel, J. S., Beers, D. R., Siklos, L. & Appel, S. H. (2006) The chemokine MCP-1 and the dendritic and myeloid cells it attracts are increased in the mSOD1 mouse model of ALS. *Mol Cell Neurosci,* 31**,** 427-37.

Henkel, J. S., Beers, D. R., Wen, S., Bowser, R. & Appel, S. H. (2009) Decreased mRNA expression of tight junction proteins in lumbar spinal cords of patients with ALS. *Neurology,* 72**,** 1614-6.

Henkel, J. S., Beers, D. R., Wen, S., Rivera, A. L., Toennis, K. M., Appel, J. E., Zhao, W., Moore, D. H., Powell, S. Z. & Appel, S. H. (2013) Regulatory T-lymphocytes mediate amyotrophic lateral sclerosis progression and survival. *EMBO Mol Med,* 5**,** 64-79.

Henkel, J. S., Engelhardt, J. I., Siklos, L., Simpson, E. P., Kim, S. H., Pan, T., Goodman, J. C., Siddique, T., Beers, D. R. & Appel, S. H. (2004) Presence of dendritic cells, MCP-1, and activated microglia/macrophages in amyotrophic lateral sclerosis spinal cord tissue. *Ann Neurol,* 55**,** 221-35.

Hensley, K., Abdel-Moaty, H., Hunter, J., Mhatre, M., Mou, S., Nguyen, K., Potapova, T., Pye, Q. N., Qi, M., Rice, H., Stewart, C., Stroukoff, K. & West, M. (2006) Primary glia expressing the G93A-SOD1 mutation present a neuroinflammatory phenotype and provide a cellular system for studies of glial inflammation. *J Neuroinflammation,* 3**,** 2.

Hensley, K., Fedynyshyn, J., Ferrell, S., Floyd, R. A., Gordon, B., Grammas, P., Hamdheydari, L., Mhatre, M., Mou, S., Pye, Q. N., Stewart, C., West, M., West, S. & Williamson, K. S. (2003) Message and protein-level elevation of tumor necrosis factor alpha (TNF alpha) and TNF alpha-modulating cytokines in spinal cords of the G93A-SOD1 mouse model for amyotrophic lateral sclerosis. *Neurobiol Dis,* 14**,** 74-80.

Heurich, B., El Idrissi, N. B., Donev, R. M., Petri, S., Claus, P., Neal, J., Morgan, B. P. & Ramaglia, V. (2011) Complement upregulation and activation on motor neurons and neuromuscular junction in the SOD1 G93A mouse model of familial amyotrophic lateral sclerosis. *J Neuroimmunol,* 235**,** 104-9.

Higgins, C. M., Jung, C., Ding, H. & Xu, Z. (2002) Mutant Cu, Zn superoxide dismutase that causes motoneuron degeneration is present in mitochondria in the CNS. *J Neurosci,* 22**,** RC215.

Hochstim, C., Deneen, B., Lukaszewicz, A., Zhou, Q. & Anderson, D. J. (2008) Identification of positionally distinct astrocyte subtypes whose identities are specified by a homeodomain code. *Cell,* 133**,** 510-22.

Howland, D. S., Liu, J., She, Y., Goad, B., Maragakis, N. J., Kim, B., Erickson, J., Kulik, J., Devito, L., Psaltis, G., Degennaro, L. J., Cleveland, D. W. & Rothstein, J. D. (2002) Focal loss of the glutamate transporter EAAT2 in a transgenic rat model of SOD1 mutant-mediated amyotrophic lateral sclerosis (ALS). *Proc Natl Acad Sci U S A,* 99**,** 1604-9.

Hruz, T., Laule, O., Szabo, G., Wessendorp, F., Bleuler, S., Oertle, L., Widmayer, P., Gruissem, W. & Zimmermann, P. (2008) Genevestigator v3: a reference expression database for the meta-analysis of transcriptomes. *Adv Bioinformatics,* 2008**,** 420747.

Huang, C., Tong, J., Bi, F., Zhou, H. & Xia, X. G. (2012) Mutant TDP-43 in motor neurons promotes the onset and progression of ALS in rats. *J Clin Invest,* 122**,** 107-18.

Hubackova, S., Krejcikova, K., Bartek, J. & Hodny, Z. (2012) IL1- and TGFbeta-Nox4 signaling, oxidative stress and DNA damage response are shared features of replicative, oncogene-induced, and drug-induced paracrine 'bystander senescence'. *Aging (Albany NY),* 4**,** 932-51.

Hukema, R. K., Riemslagh, F. W., Melhem, S., Van Der Linde, H. C., Severijnen, L., Edbauer, D., Maas, A., Charlet-Berguerand, N., Willemsen, R. & Van Swieten, J. C. (2014) A new inducible transgenic mouse model for C9orf72-associated GGGGCC repeat expansion supports a gain-of-function mechanism in C9orf72 associated ALS and FTD. *Acta Neuropathol Commun,* 2**,** 166.

Ince, P., Stout, N., Shaw, P., Slade, J., Hunziker, W., Heizmann, C. W. & Baimbridge, K. G. (1993) Parvalbumin and calbindin D-28k in the human motor system and in motor neuron disease. *Neuropathol Appl Neurobiol,* 19**,** 291-9.

Ince, P. G., Lowe, J. & Shaw, P. J. (1998a) Amyotrophic lateral sclerosis: current issues in classification, pathogenesis and molecular pathology. *Neuropathol Appl Neurobiol,* 24**,** 104-17.

Ince, P. G., Tomkins, J., Slade, J. Y., Thatcher, N. M. & Shaw, P. J. (1998b) Amyotrophic lateral sclerosis associated with genetic abnormalities in the gene encoding Cu/Zn superoxide dismutase: molecular pathology of five new cases, and comparison with previous reports and 73 sporadic cases of ALS. *J Neuropathol Exp Neurol,* 57**,** 895-904.

Inoue, J., Misawa, A., Tanaka, Y., Ichinose, S., Sugino, Y., Hosoi, H., Sugimoto, T., Imoto, I. & Inazawa, J. (2009) Lysosomal-associated protein multispanning transmembrane 5 gene (LAPTM5) is associated with spontaneous regression of neuroblastomas. *PLoS One,* 4**,** e7099.

Investigators, N. N.-P. (2006) A randomized, double-blind, futility clinical trial of creatine and minocycline in early Parkinson disease. *Neurology,* 66**,** 664-71.

Ishihara, H., Kubota, H., Lindberg, R. L., Leppert, D., Gloor, S. M., Errede, M., Virgintino, D., Fontana, A., Yonekawa, Y. & Frei, K. (2008) Endothelial cell barrier impairment induced by glioblastomas and transforming growth factor beta2 involves matrix metalloproteinases and tight junction proteins. *J Neuropathol Exp Neurol,* 67**,** 435-48.

Jayakumar, A. R., Tong, X. Y., Ospel, J. & Norenberg, M. D. (2012) Role of cerebral endothelial cells in the astrocyte swelling and brain edema associated with acute hepatic encephalopathy. *Neuroscience,* 218**,** 305-16.

Jiang, Y. M., Yamamoto, M., Kobayashi, Y., Yoshihara, T., Liang, Y., Terao, S., Takeuchi, H., Ishigaki, S., Katsuno, M., Adachi, H., Niwa, J., Tanaka, F., Doyu, M., Yoshida, M., Hashizume, Y. & Sobue, G. (2005) Gene expression profile of spinal motor neurons in sporadic amyotrophic lateral sclerosis. *Ann Neurol,* 57**,** 236-51.

Johnson, J. O., Mandrioli, J., Benatar, M., Abramzon, Y., Van Deerlin, V. M., Trojanowski, J. Q., Gibbs, J. R., Brunetti, M., Gronka, S., Wuu, J., Ding, J., Mccluskey, L., Martinez-Lage, M., Falcone, D., Hernandez, D. G., Arepalli, S., Chong, S., Schymick, J. C., Rothstein, J., Landi, F., Wang, Y. D., Calvo, A., Mora, G., Sabatelli, M., Monsurro, M. R., Battistini, S., Salvi, F., Spataro, R., Sola, P., Borghero, G., Galassi, G., Scholz, S. W., Taylor, J. P., Restagno, G., Chio, A. & Traynor, B. J. (2010) Exome sequencing reveals VCP mutations as a cause of familial ALS. *Neuron,* 68**,** 857-64.

Johnson, J. O., Pioro, E. P., Boehringer, A., Chia, R., Feit, H., Renton, A. E., Pliner, H. A., Abramzon, Y., Marangi, G., Winborn, B. J., Gibbs, J. R., Nalls, M. A., Morgan, S., Shoai, M., Hardy, J., Pittman, A., Orrell, R. W., Malaspina, A., Sidle, K. C., Fratta, P., Harms, M. B., Baloh, R. H., Pestronk, A., Weihl, C. C., Rogaeva, E., Zinman, L., Drory, V. E., Borghero, G., Mora, G., Calvo, A., Rothstein, J. D., Drepper, C., Sendtner, M., Singleton, A. B., Taylor, J. P., Cookson, M. R., Restagno, G., Sabatelli, M., Bowser, R., Chio, A. & Traynor, B. J. (2014) Mutations in the Matrin 3 gene cause familial amyotrophic lateral sclerosis. *Nat Neurosci,* 17**,** 664-6.

Jolkowska, J. & Witt, M. (2000) The EVI-1 gene--its role in pathogenesis of human leukemias. *Leuk Res,* 24**,** 553-8.

Jonsson, P. A., Graffmo, K. S., Brannstrom, T., Nilsson, P., Andersen, P. M. & Marklund, S. L. (2006) Motor neuron disease in mice expressing the wild type-like D90A mutant superoxide dismutase-1. *J Neuropathol Exp Neurol,* 65**,** 1126-36.

Jullien, D., Gorlich, D., Laemmli, U. K. & Adachi, Y. (1999) Nuclear import of RPA in Xenopus egg extracts requires a novel protein XRIPalpha but not importin alpha. *EMBO J,* 18**,** 4348-58.

Kabuta, T., Suzuki, Y. & Wada, K. (2006) Degradation of amyotrophic lateral sclerosis-linked mutant Cu,Zn-superoxide dismutase proteins by macroautophagy and the proteasome. *J Biol Chem,* 281**,** 30524-33.

Kang, S. H., Fukaya, M., Yang, J. K., Rothstein, J. D. & Bergles, D. E. (2010) NG2+ CNS glial progenitors remain committed to the oligodendrocyte lineage in postnatal life and following neurodegeneration. *Neuron,* 68**,** 668-81.

Kang, S. H., Li, Y., Fukaya, M., Lorenzini, I., Cleveland, D. W., Ostrow, L. W., Rothstein, J. D. & Bergles, D. E. (2013) Degeneration and impaired regeneration of gray matter oligodendrocytes in amyotrophic lateral sclerosis. *Nat Neurosci,* 16**,** 571-9.

Kaspar, B. K., Llado, J., Sherkat, N., Rothstein, J. D. & Gage, F. H. (2003) Retrograde viral delivery of IGF-1 prolongs survival in a mouse ALS model. *Science,* 301**,** 839-42.

Kegg http://www.genome.jp/kegg/

Kettenmann, H. & Ransom, B. R. (2005) *Neuroglia,* Oxford, Oxford University Press.

Kieran, D., Hafezparast, M., Bohnert, S., Dick, J. R., Martin, J., Schiavo, G., Fisher, E. M. & Greensmith, L. (2005) A mutation in dynein rescues axonal transport defects and extends the life span of ALS mice. *J Cell Biol,* 169**,** 561-7.

Kigerl, K. A., Gensel, J. C., Ankeny, D. P., Alexander, J. K., Donnelly, D. J. & Popovich, P. G. (2009) Identification of two distinct macrophage subsets with divergent effects causing either neurotoxicity or regeneration in the injured mouse spinal cord. *J Neurosci,* 29**,** 13435-44.

Kim, H. J., Kim, N. C., Wang, Y. D., Scarborough, E. A., Moore, J., Diaz, Z., Maclea, K. S., Freibaum, B., Li, S., Molliex, A., Kanagaraj, A. P., Carter, R., Boylan, K. B., Wojtas, A. M., Rademakers, R., Pinkus, J. L., Greenberg, S. A., Trojanowski, J. Q., Traynor, B. J., Smith, B. N., Topp, S., Gkazi, A. S., Miller, J., Shaw, C. E., Kottlors, M., Kirschner, J., Pestronk, A., Li, Y. R., Ford, A. F., Gitler, A. D., Benatar, M., King, O. D., Kimonis, V. E., Ross, E. D., Weihl, C. C., Shorter, J. & Taylor, J. P. (2013) Mutations in prion-like domains in hnRNPA2B1 and hnRNPA1 cause multisystem proteinopathy and ALS. *Nature,* 495**,** 467-73.

Kim, J., Efe, J. A., Zhu, S., Talantova, M., Yuan, X., Wang, S., Lipton, S. A., Zhang, K. & Ding, S. (2011) Direct reprogramming of mouse fibroblasts to neural progenitors. *Proc Natl Acad Sci U S A,* 108**,** 7838-43.

Kim, Y. J., Nakatomi, R., Akagi, T., Hashikawa, T. & Takahashi, R. (2005) Unsaturated fatty acids induce cytotoxic aggregate formation of amyotrophic lateral sclerosis-linked superoxide dismutase 1 mutants. *J Biol Chem,* 280**,** 21515-21.

Kinchen, J. M., Cabello, J., Klingele, D., Wong, K., Feichtinger, R., Schnabel, H., Schnabel, R. & Hengartner, M. O. (2005) Two pathways converge at CED-10 to mediate actin rearrangement and corpse removal in C. elegans. *Nature,* 434**,** 93-9.

King, A. E., Dickson, T. C., Blizzard, C. A., Foster, S. S., Chung, R. S., West, A. K., Chuah, M. I. & Vickers, J. C. (2007) Excitotoxicity mediated by non-NMDA receptors causes distal axonopathy in long-term cultured spinal motor neurons. *Eur J Neurosci,* 26**,** 2151-9.

Kirby, J., Halligan, E., Baptista, M. J., Allen, S., Heath, P. R., Holden, H., Barber, S. C., Loynes, C. A., Wood-Allum, C. A., Lunec, J. & Shaw, P. J. (2005) Mutant SOD1 alters the motor neuronal transcriptome: implications for familial ALS. *Brain,* 128**,** 1686-706.

Kirby, J., Ning, K., Ferraiuolo, L., Heath, P. R., Ismail, A., Kuo, S. W., Valori, C. F., Cox, L., Sharrack, B., Wharton, S. B., Ince, P. G., Shaw, P. J. & Azzouz, M. (2011) Phosphatase and tensin homologue/protein kinase B pathway linked to motor neuron survival in human superoxide dismutase 1-related amyotrophic lateral sclerosis. *Brain,* 134**,** 506-17.

Kobayashi, K., Hayashi, M., Nakano, H., Fukutani, Y., Sasaki, K., Shimazaki, M. & Koshino, Y. (2002) Apoptosis of astrocytes with enhanced lysosomal activity and oligodendrocytes in white matter lesions in Alzheimer's disease. *Neuropathol Appl Neurobiol,* 28**,** 238-51.

Kobayashi, M., Nakano, M., Atobe, Y., Kadota, T. & Funakoshi, K. (2011) Islet-1 expression in thoracic spinal motor neurons in prenatal mouse. *Int J Dev Neurosci,* 29**,** 749-56.

Kofuji, P. & Newman, E. A. (2004) Potassium buffering in the central nervous system. *Neuroscience,* 129**,** 1045-56.

Kraft, A. D., Johnson, D. A. & Johnson, J. A. (2004) Nuclear factor E2-related factor 2-dependent antioxidant response element activation by tert-butylhydroquinone and sulforaphane occurring preferentially in astrocytes conditions neurons against oxidative insult. *J Neurosci,* 24**,** 1101-12.

Krausgruber, T., Blazek, K., Smallie, T., Alzabin, S., Lockstone, H., Sahgal, N., Hussell, T., Feldmann, M. & Udalova, I. A. (2011) IRF5 promotes inflammatory macrophage polarization and TH1-TH17 responses. *Nat Immunol,* 12**,** 231-8.

Kriz, J., Nguyen, M. D. & Julien, J. P. (2002) Minocycline slows disease progression in a mouse model of amyotrophic lateral sclerosis. *Neurobiol Dis,* 10**,** 268-78.

Kruman, Ii, Pedersen, W. A., Springer, J. E. & Mattson, M. P. (1999) ALS-linked Cu/Zn-SOD mutation increases vulnerability of motor neurons to excitotoxicity by a mechanism involving increased oxidative stress and perturbed calcium homeostasis. *Exp Neurol,* 160**,** 28-39.

Kuhle, J., Lindberg, R. L., Regeniter, A., Mehling, M., Steck, A. J., Kappos, L. & Czaplinski, A. (2009) Increased levels of inflammatory chemokines in amyotrophic lateral sclerosis. *Eur J Neurol,* 16**,** 771-4.

Kurz, D. J., Decary, S., Hong, Y. & Erusalimsky, J. D. (2000) Senescence-associated (beta)-galactosidase reflects an increase in lysosomal mass during replicative ageing of human endothelial cells. *J Cell Sci,* 113 (Pt 20)**,** 3613-22.

Kurz, T., Leake, A., Von Zglinicki, T. & Brunk, U. T. (2004) Relocalized redox-active lysosomal iron is an important mediator of oxidative-stress-induced DNA damage. *Biochem J,* 378**,** 1039-45.

Kwiatkowski, T. J., Jr., Bosco, D. A., Leclerc, A. L., Tamrazian, E., Vanderburg, C. R., Russ, C., Davis, A., Gilchrist, J., Kasarskis, E. J., Munsat, T., Valdmanis, P., Rouleau, G. A., Hosler, B. A., Cortelli, P., De Jong, P. J., Yoshinaga, Y., Haines, J. L., Pericak-Vance, M. A., Yan, J., Ticozzi, N., Siddique, T., Mckenna-Yasek, D., Sapp, P. C., Horvitz, H. R., Landers, J. E. & Brown, R. H., Jr. (2009) Mutations in the FUS/TLS gene on chromosome 16 cause familial amyotrophic lateral sclerosis. *Science,* 323**,** 1205-8.

Lederer, C. W., Torrisi, A., Pantelidou, M., Santama, N. & Cavallaro, S. (2007) Pathways and genes differentially expressed in the motor cortex of patients with sporadic amyotrophic lateral sclerosis. *BMC Genomics,* 8**,** 26.

Lee, M., Schwab, C. & Mcgeer, P. L. (2011) Astrocytes are GABAergic cells that modulate microglial activity. *Glia,* 59**,** 152-65.

Lee, Y., Morrison, B. M., Li, Y., Lengacher, S., Farah, M. H., Hoffman, P. N., Liu, Y., Tsingalia, A., Jin, L., Zhang, P. W., Pellerin, L., Magistretti, P. J. & Rothstein, J. D. (2012) Oligodendroglia metabolically support axons and contribute to neurodegeneration. *Nature,* 487**,** 443-8.

Lefebvre, S., Burglen, L., Reboullet, S., Clermont, O., Burlet, P., Viollet, L., Benichou, B., Cruaud, C., Millasseau, P., Zeviani, M. & Et Al. (1995) Identification and characterization of a spinal muscular atrophy-determining gene. *Cell,* 80**,** 155-65.

Lehnardt, S., Lachance, C., Patrizi, S., Lefebvre, S., Follett, P. L., Jensen, F. E., Rosenberg, P. A., Volpe, J. J. & Vartanian, T. (2002) The toll-like receptor TLR4 is necessary for lipopolysaccharide-induced oligodendrocyte injury in the CNS. *J Neurosci,* 22**,** 2478-86.

Lehnardt, S., Schott, E., Trimbuch, T., Laubisch, D., Krueger, C., Wulczyn, G., Nitsch, R. & Weber, J. R. (2008) A vicious cycle involving release of heat shock protein 60 from injured cells and activation of toll-like receptor 4 mediates neurodegeneration in the CNS. *J Neurosci,* 28**,** 2320-31.

Leigh, P. N., Anderton, B. H., Dodson, A., Gallo, J. M., Swash, M. & Power, D. M. (1988) Ubiquitin deposits in anterior horn cells in motor neurone disease. *Neurosci Lett,* 93**,** 197-203.

Leonardi, A., Abbruzzese, G., Arata, L., Cocito, L. & Vische, M. (1984) Cerebrospinal fluid (CSF) findings in amyotrophic lateral sclerosis. *J Neurol,* 231**,** 75-8.

Leoni, G., Rattray, M. & Butt, A. M. (2009) NG2 cells differentiate into astrocytes in cerebellar slices. *Molecular and Cellular Neuroscience,* 42**,** 208-218.

Leoni, V. & Caccia, C. (2015) The impairment of cholesterol metabolism in Huntington disease. *Biochim Biophys Acta*.

Lepore, A. C., Rauck, B., Dejea, C., Pardo, A. C., Rao, M. S., Rothstein, J. D. & Maragakis, N. J. (2008) Focal transplantation-based astrocyte replacement is neuroprotective in a model of motor neuron disease. *Nat Neurosci,* 11**,** 1294-301.

Lewis, C. A., Solomon, J. N., Rossi, F. M. & Krieger, C. (2009) Bone marrow-derived cells in the central nervous system of a mouse model of amyotrophic lateral sclerosis are associated with blood vessels and express CX(3)CR1. *Glia,* 57**,** 1410-9.

Li, J., Huang, N. F., Zou, J., Laurent, T. J., Lee, J. C., Okogbaa, J., Cooke, J. P. & Ding, S. (2013) Conversion of human fibroblasts to functional endothelial cells by defined factors. *Arterioscler Thromb Vasc Biol,* 33**,** 1366-75.

Li, L. & Renier, G. (2007) Adipocyte-derived Lipoprotein Lipase Induces Macrophage Activation and Monocyte Adhesion: Role of Fatty Acids. *Obesity,* 15**,** 2595-2604.

Liang, W. S., Reiman, E. M., Valla, J., Dunckley, T., Beach, T. G., Grover, A., Niedzielko, T. L., Schneider, L. E., Mastroeni, D., Caselli, R., Kukull, W., Morris, J. C., Hulette, C. M., Schmechel, D., Rogers, J. & Stephan, D. A. (2008) Alzheimer's disease is

associated with reduced expression of energy metabolism genes in posterior cingulate neurons. *Proc Natl Acad Sci U S A,* 105**,** 4441-6.

Liao, B., Zhao, W., Beers, D. R., Henkel, J. S. & Appel, S. H. (2012) Transformation from a neuroprotective to a neurotoxic microglial phenotype in a mouse model of ALS. *Exp Neurol,* 237**,** 147-52.

Liao, X., Sharma, N., Kapadia, F., Zhou, G., Lu, Y., Hong, H., Paruchuri, K., Mahabeleshwar, G. H., Dalmas, E., Venteclef, N., Flask, C. A., Kim, J., Doreian, B. W., Lu, K. Q., Kaestner, K. H., Hamik, A., Clement, K. & Jain, M. K. (2011) Kruppel-like factor 4 regulates macrophage polarization. *J Clin Invest,* 121**,** 2736-49.

Ligon, L. A. & Steward, O. (2000) Movement of mitochondria in the axons and dendrites of cultured hippocampal neurons. *J Comp Neurol,* 427**,** 340-50.

Liodis, P., Denaxa, M., Grigoriou, M., Akufo-Addo, C., Yanagawa, Y. & Pachnis, V. (2007) Lhx6 activity is required for the normal migration and specification of cortical interneuron subtypes. *J Neurosci,* 27**,** 3078-89.

Litvak, V., Ramsey, S. A., Rust, A. G., Zak, D. E., Kennedy, K. A., Lampano, A. E., Nykter, M., Shmulevich, I. & Aderem, A. (2009) Function of C/EBPdelta in a regulatory circuit that discriminates between transient and persistent TLR4-induced signals. *Nat Immunol,* 10**,** 437-43.

Liu, J., Lillo, C., Jonsson, P. A., Vande Velde, C., Ward, C. M., Miller, T. M., Subramaniam, J. R., Rothstein, J. D., Marklund, S., Andersen, P. M., Brannstrom, T., Gredal, O., Wong, P. C., Williams, D. S. & Cleveland, D. W. (2004) Toxicity of familial ALS-linked SOD1 mutants from selective recruitment to spinal mitochondria. *Neuron,* 43**,** 5-17.

Liu, J. P., Tang, Y., Zhou, S., Toh, B. H., Mclean, C. & Li, H. (2010) Cholesterol involvement in the pathogenesis of neurodegenerative diseases. *Mol Cell Neurosci,* 43**,** 33-42.

Livak, K. J. & Schmittgen, T. D. (2001) Analysis of relative gene expression data using real-time quantitative PCR and the 2(-Delta Delta C(T)) Method. *Methods,* 25**,** 402-8.

Lobsiger, C. S., Boillee, S. & Cleveland, D. W. (2007) Toxicity from different SOD1 mutants dysregulates the complement system and the neuronal regenerative response in ALS motor neurons. *Proc Natl Acad Sci U S A,* 104**,** 7319-26.

Lobsiger, C. S., Boillee, S., Mcalonis-Downes, M., Khan, A. M., Feltri, M. L., Yamanaka, K. & Cleveland, D. W. (2009) Schwann cells expressing dismutase active mutant SOD1 unexpectedly slow disease progression in ALS mice. *Proc Natl Acad Sci U S A,* 106**,** 4465-70.

Lobsiger, C. S., Boillee, S., Pozniak, C., Khan, A. M., Mcalonis-Downes, M., Lewcock, J. W. & Cleveland, D. W. (2013) C1q induction and global complement pathway activation do not contribute to ALS toxicity in mutant SOD1 mice. *Proc Natl Acad Sci U S A,* 110**,** E4385-92.

Loov, C., Hillered, L., Ebendal, T. & Erlandsson, A. (2012) Engulfing astrocytes protect neurons from contact-induced apoptosis following injury. *PLoS One,* 7**,** e33090.

Lowe, J., Lennox, G., Jefferson, D., Morrell, K., Mcquire, D., Gray, T., Landon, M., Doherty, F. J. & Mayer, R. J. (1988) A filamentous inclusion body within anterior horn neurones in motor neurone disease defined by immunocytochemical localisation of ubiquitin. *Neurosci Lett,* 94**,** 203-10.

Lu, Q. R., Sun, T., Zhu, Z., Ma, N., Garcia, M., Stiles, C. D. & Rowitch, D. H. (2002) Common Developmental Requirement for Olig Function Indicates a Motor Neuron/Oligodendrocyte Connection. *Cell,* 109**,** 75-86.

Lujan, E., Chanda, S., Ahlenius, H., Sudhof, T. C. & Wernig, M. (2012) Direct conversion of mouse fibroblasts to self-renewing, tripotent neural precursor cells. *Proc Natl Acad Sci U S A,* 109**,** 2527-32.

Mackenzie, I. R., Bigio, E. H., Ince, P. G., Geser, F., Neumann, M., Cairns, N. J., Kwong, L. K., Forman, M. S., Ravits, J., Stewart, H., Eisen, A., Mcclusky, L., Kretzschmar, H. A., Monoranu, C. M., Highley, J. R., Kirby, J., Siddique, T., Shaw, P. J., Lee, V. M. & Trojanowski, J. Q. (2007) Pathological TDP-43 distinguishes sporadic amyotrophic lateral sclerosis from amyotrophic lateral sclerosis with SOD1 mutations. *Ann Neurol,* 61**,** 427-34.

Magnus, T., Carmen, J., Deleon, J., Xue, H., Pardo, A. C., Lepore, A. C., Mattson, M. P., Rao, M. S. & Maragakis, N. J. (2008) Adult glial precursor proliferation in mutant SOD1G93A mice. *Glia,* 56**,** 200-8.

Mahuran, D. J. (1995) Beta-hexosaminidase: biosynthesis and processing of the normal enzyme, and identification of mutations causing Jewish Tay-Sachs disease. *Clin Biochem,* 28**,** 101-6.

Mangia, S., Simpson, I. A., Vannucci, S. J. & Carruthers, A. (2009) The in vivo neuron-to-astrocyte lactate shuttle in human brain: evidence from modeling of measured lactate levels during visual stimulation. *J Neurochem,* 109 Suppl 1**,** 55-62.

Mantovani, A., Sica, A., Sozzani, S., Allavena, P., Vecchi, A. & Locati, M. (2004) The chemokine system in diverse forms of macrophage activation and polarization. *Trends Immunol,* 25**,** 677-86.

Mardis, E. R. (2008) Next-generation DNA sequencing methods. *Annu Rev Genomics Hum Genet,* 9**,** 387-402.

Marques, F., Sousa, J. C., Sousa, N. & Palha, J. A. (2013) Blood-brain-barriers in aging and in Alzheimer's disease. *Mol Neurodegener,* 8**,** 38.

Martin, M. G., Pfrieger, F. & Dotti, C. G. (2014) Cholesterol in brain disease: sometimes determinant and frequently implicated. *EMBO Rep,* 15**,** 1036-52.

Martínez-Estrada, O. M., Rodríguez-Millán, E., González-De Vicente, E., Reina, M., Vilaró, S. & Fabre, M. (2003) Erythropoietin protects the in vitro blood–brain barrier against VEGF-induced permeability. *European Journal of Neuroscience,* 18**,** 2538-2544.

Maruyama, H., Morino, H., Ito, H., Izumi, Y., Kato, H., Watanabe, Y., Kinoshita, Y., Kamada, M., Nodera, H., Suzuki, H., Komure, O., Matsuura, S., Kobatake, K., Morimoto, N., Abe, K., Suzuki, N., Aoki, M., Kawata, A., Hirai, T., Kato, T., Ogasawara, K., Hirano, A., Takumi, T., Kusaka, H., Hagiwara, K., Kaji, R. & Kawakami, H. (2010) Mutations of optineurin in amyotrophic lateral sclerosis. *Nature,* 465**,** 223-6.

Mattiazzi, M., D'aurelio, M., Gajewski, C. D., Martushova, K., Kiaei, M., Beal, M. F. & Manfredi, G. (2002) Mutated human SOD1 causes dysfunction of oxidative phosphorylation in mitochondria of transgenic mice. *J Biol Chem,* 277**,** 29626-33.

Matyash, V. & Kettenmann, H. (2010) Heterogeneity in astrocyte morphology and physiology. *Brain Res Rev,* 63**,** 2-10.

Mead, R. J., Bennett, E. J., Kennerley, A. J., Sharp, P., Sunyach, C., Kasher, P., Berwick, J., Pettmann, B., Battaglia, G., Azzouz, M., Grierson, A. & Shaw, P. J. (2011) Optimised and rapid pre-clinical screening in the SOD1(G93A) transgenic mouse model of amyotrophic lateral sclerosis (ALS). *PLoS One,* 6**,** e23244.

Meehan, C. F., Moldovan, M., Marklund, S. L., Graffmo, K. S., Nielsen, J. B. & Hultborn, H. (2010) Intrinsic properties of lumbar motor neurones in the adult G127insTGGG superoxide dismutase-1 mutant mouse in vivo: evidence for increased persistent inward currents. *Acta Physiol (Oxf),* 200**,** 361-76.

Meissner, F., Molawi, K. & Zychlinsky, A. (2010) Mutant superoxide dismutase 1-induced IL-1beta accelerates ALS pathogenesis. *Proc Natl Acad Sci U S A,* 107**,** 13046-50.

Meyer, K., Ferraiuolo, L., Miranda, C. J., Likhite, S., Mcelroy, S., Renusch, S., Ditsworth, D., Lagier-Tourenne, C., Smith, R. A., Ravits, J., Burghes, A. H., Shaw, P. J., Cleveland, D. W., Kolb, S. J. & Kaspar, B. K. (2013) Direct conversion of patient fibroblasts demonstrates non-cell autonomous toxicity of astrocytes to motor neurons in familial and sporadic ALS. *Proc Natl Acad Sci U S A,* 111**,** 829-32.

Mikita, J., Dubourdieu-Cassagno, N., Deloire, M. S., Vekris, A., Biran, M., Raffard, G., Brochet, B., Canron, M. H., Franconi, J. M., Boiziau, C. & Petry, K. G. (2011) Altered M1/M2 activation patterns of monocytes in severe relapsing experimental rat model of multiple sclerosis. Amelioration of clinical status by M2 activated monocyte administration. *Mult Scler,* 17**,** 2-15.

Mikulowska-Mennis, A., Taylor, T. B., Vishnu, P., Michie, S. A., Raja, R., Horner, N. & Kunitake, S. T. (2002) High-quality RNA from cells isolated by laser capture microdissection. *Biotechniques,* 33**,** 176-9.

Miller, C. J. Simpleaffy: very simple high level analysis of affymetrix data.

Miller, R. G., Mitchell, J. D., Lyon, M. & Moore, D. H. (2007) Riluzole for amyotrophic lateral sclerosis (ALS)/motor neuron disease (MND). *Cochrane Database Syst Rev***,** CD001447.

Miller, T. M., Kim, S. H., Yamanaka, K., Hester, M., Umapathi, P., Arnson, H., Rizo, L., Mendell, J. R., Gage, F. H., Cleveland, D. W. & Kaspar, B. K. (2006) Gene transfer demonstrates that muscle is not a primary target for non-cell-autonomous toxicity in familial amyotrophic lateral sclerosis. *Proc Natl Acad Sci U S A,* 103**,** 19546-51.

Miron, V. E., Boyd, A., Zhao, J. W., Yuen, T. J., Ruckh, J. M., Shadrach, J. L., Van Wijngaarden, P., Wagers, A. J., Williams, A., Franklin, R. J. & Ffrench-Constant, C. (2013) M2 microglia and macrophages drive oligodendrocyte differentiation during CNS remyelination. *Nat Neurosci*.

Miyazaki, K., Ohta, Y., Nagai, M., Morimoto, N., Kurata, T., Takehisa, Y., Ikeda, Y., Matsuura, T. & Abe, K. (2011) Disruption of neurovascular unit prior to motor neuron degeneration in amyotrophic lateral sclerosis. *J Neurosci Res,* 89**,** 718-28.

Mizielinska, S., Gronke, S., Niccoli, T., Ridler, C. E., Clayton, E. L., Devoy, A., Moens, T., Norona, F. E., Woollacott, I. O., Pietrzyk, J., Cleverley, K., Nicoll, A. J., Pickering-Brown, S., Dols, J., Cabecinha, M., Hendrich, O., Fratta, P., Fisher, E. M., Partridge, L. & Isaacs, A. M. (2014) C9orf72 repeat expansions cause neurodegeneration in Drosophila through arginine-rich proteins. *Science,* 345**,** 1192-4.

Mojsilovic-Petrovic, J., Nesic, M., Pen, A., Zhang, W. & Stanimirovic, D. (2004) Development of rapid staining protocols for laser-capture microdissection of brain vessels from human and rat coupled to gene expression analyses. *J Neurosci Methods,* 133**,** 39-48.

Mosser, D. M. (2003) The many faces of macrophage activation. *J Leukoc Biol,* 73**,** 209-12.

Muroyama, Y., Fujiwara, Y., Orkin, S. H. & Rowitch, D. H. (2005) Specification of astrocytes by bHLH protein SCL in a restricted region of the neural tube. *Nature,* 438**,** 360-3.

Nagai, M., Re, D. B., Nagata, T., Chalazonitis, A., Jessell, T. M., Wichterle, H. & Przedborski, S. (2007) Astrocytes expressing ALS-linked mutated SOD1 release factors selectively toxic to motor neurons. *Nat Neurosci,* 10**,** 615-22.

Nardinocchi, L., Puca, R., Sacchi, A., Rechavi, G., Givol, D. & D'orazi, G. (2009) Targeting hypoxia in cancer cells by restoring homeodomain interacting protein-kinase 2 and p53 activity and suppressing HIF-1alpha. *PLoS One,* 4**,** e6819.

Nardo, G., Iennaco, R., Fusi, N., Heath, P. R., Marino, M., Trolese, M. C., Ferraiuolo, L., Lawrence, N., Shaw, P. J. & Bendotti, C. (2013) Transcriptomic indices of fast and slow disease progression in two mouse models of amyotrophic lateral sclerosis. *Brain,* 136**,** 3305-32.

Neumann, H., Kotter, M. R. & Franklin, R. J. (2009) Debris clearance by microglia: an essential link between degeneration and regeneration. *Brain,* 132**,** 288-95.

Neumann, M., Kwong, L. K., Truax, A. C., Vanmassenhove, B., Kretzschmar, H. A., Van Deerlin, V. M., Clark, C. M., Grossman, M., Miller, B. L., Trojanowski, J. Q. & Lee, V. M. (2007) TDP-43-positive white matter pathology in frontotemporal lobar degeneration with ubiquitin-positive inclusions. *J Neuropathol Exp Neurol,* 66**,** 177-83.

Neumann, M., Sampathu, D. M., Kwong, L. K., Truax, A. C., Micsenyi, M. C., Chou, T. T., Bruce, J., Schuck, T., Grossman, M., Clark, C. M., Mccluskey, L. F., Miller, B. L., Masliah, E., Mackenzie, I. R., Feldman, H., Feiden, W., Kretzschmar, H. A., Trojanowski, J. Q. & Lee, V. M. (2006) Ubiquitinated TDP-43 in frontotemporal lobar degeneration and amyotrophic lateral sclerosis. *Science,* 314**,** 130-3.

Nicaise, C., Mitrecic, D., Demetter, P., De Decker, R., Authelet, M., Boom, A. & Pochet, R. (2009a) Impaired blood-brain and blood-spinal cord barriers in mutant SOD1-linked ALS rat. *Brain Res,* 1301**,** 152-62.

Nicaise, C., Soyfoo, M. S., Authelet, M., De Decker, R., Bataveljic, D., Delporte, C. & Pochet, R. (2009b) Aquaporin-4 Overexpression in Rat ALS Model. *The Anatomical Record: Advances in Integrative Anatomy and Evolutionary Biology,* 292**,** 207-213.

Niebroj-Dobosz, I., Rafalowska, J., Fidzianska, A., Gadamski, R. & Grieb, P. (2007) Myelin composition of spinal cord in a model of amyotrophic lateral sclerosis (ALS) in SOD1G93A transgenic rats. *Folia Neuropathol,* 45**,** 236-41.

Nishimura, A. L., Mitne-Neto, M., Silva, H. C., Richieri-Costa, A., Middleton, S., Cascio, D., Kok, F., Oliveira, J. R., Gillingwater, T., Webb, J., Skehel, P. & Zatz, M. (2004) A mutation in the vesicle-trafficking protein VAPB causes late-onset spinal muscular atrophy and amyotrophic lateral sclerosis. *Am J Hum Genet,* 75**,** 822-31.

Nishiyama, A., Komitova, M., Suzuki, R. & Zhu, X. (2009) Polydendrocytes (NG2 cells): multifunctional cells with lineage plasticity. *Nat Rev Neurosci,* 10**,** 9-22.

Norenberg, M. D. & Martinez-Hernandez, A. (1979) Fine structural localization of glutamine synthetase in astrocytes of rat brain. *Brain Res,* 161**,** 303-10.

Oberheim, N. A., Takano, T., Han, X., He, W., Lin, J. H., Wang, F., Xu, Q., Wyatt, J. D., Pilcher, W., Ojemann, J. G., Ransom, B. R., Goldman, S. A. & Nedergaard, M. (2009) Uniquely hominid features of adult human astrocytes. *J Neurosci,* 29**,** 3276-87.

Offen, D., Barhum, Y., Melamed, E., Embacher, N., Schindler, C. & Ransmayr, G. (2009) Spinal cord mRNA profile in patients with ALS: comparison with transgenic mice expressing the human SOD-1 mutant. *J Mol Neurosci,* 38**,** 85-93.

Okamoto, K., Mizuno, Y. & Fujita, Y. (2008) Bunina bodies in amyotrophic lateral sclerosis. *Neuropathology,* 28**,** 109-15.

Olson, J. K. & Miller, S. D. (2004) Microglia initiate central nervous system innate and adaptive immune responses through multiple TLRs. *J Immunol,* 173**,** 3916-24.

Orlacchio, A., Babalini, C., Borreca, A., Patrono, C., Massa, R., Basaran, S., Munhoz, R. P., Rogaeva, E. A., St George-Hyslop, P. H., Bernardi, G. & Kawarai, T. (2010) SPATACSIN mutations cause autosomal recessive juvenile amyotrophic lateral sclerosis. *Brain,* 133**,** 591-8.

Osada, T., Gu, Y. H., Kanazawa, M., Tsubota, Y., Hawkins, B. T., Spatz, M., Milner, R. & Del Zoppo, G. J. (2011) Interendothelial claudin-5 expression depends on cerebral endothelial cell-matrix adhesion by beta(1)-integrins. *J Cereb Blood Flow Metab,* 31**,** 1972-85.

Pan, L., Yoshii, Y., Otomo, A., Ogawa, H., Iwasaki, Y., Shang, H. F. & Hadano, S. (2012) Different human copper-zinc superoxide dismutase mutants, SOD1G93A and SOD1H46R, exert distinct harmful effects on gross phenotype in mice. *PLoS One,* 7**,** e33409.

Papadeas, S. T., Kraig, S. E., O'banion, C., Lepore, A. C. & Maragakis, N. J. (2011) Astrocytes carrying the superoxide dismutase 1 (SOD1G93A) mutation induce wild-type motor neuron degeneration in vivo. *Proc Natl Acad Sci U S A,* 108**,** 17803-8.

Parman, C., Halling, C. & Gentleman, R. affyQCReport: QC Report Generation for affyBatch objects.

Pasinelli, P., Belford, M. E., Lennon, N., Bacskai, B. J., Hyman, B. T., Trotti, D. & Brown, R. H., Jr. (2004) Amyotrophic lateral sclerosis-associated SOD1 mutant proteins bind and aggregate with Bcl-2 in spinal cord mitochondria. *Neuron,* 43**,** 19-30.

Pasinetti, G. M., Ungar, L. H., Lange, D. J., Yemul, S., Deng, H., Yuan, X., Brown, R. H., Cudkowicz, M. E., Newhall, K., Peskind, E., Marcus, S. & Ho, L. (2006) Identification of potential CSF biomarkers in ALS. *Neurology,* 66**,** 1218-22.

Patterson, T. A., Lobenhofer, E. K., Fulmer-Smentek, S. B., Collins, P. J., Chu, T. M., Bao, W., Fang, H., Kawasaki, E. S., Hager, J., Tikhonova, I. R., Walker, S. J., Zhang, L., Hurban, P., De Longueville, F., Fuscoe, J. C., Tong, W., Shi, L. & Wolfinger, R. D. (2006) Performance comparison of one-color and two-color platforms within the MicroArray Quality Control (MAQC) project. *Nat Biotechnol,* 24**,** 1140-50.

Pearson, R. D., Liu, X., Sanguinetti, G., Milo, M., Lawrence, N. D. & Rattray, M. (2009) puma: a Bioconductor package for propagating uncertainty in microarray analysis. *BMC Bioinformatics,* 10**,** 211.

Pedersen, W. A., Fu, W., Keller, J. N., Markesbery, W. R., Appel, S., Smith, R. G., Kasarskis, E. & Mattson, M. P. (1998) Protein modification by the lipid peroxidation product 4-hydroxynonenal in the spinal cords of amyotrophic lateral sclerosis patients. *Ann Neurol,* 44**,** 819-24.

Pellerin, L., Bouzier-Sore, A. K., Aubert, A., Serres, S., Merle, M., Costalat, R. & Magistretti, P. J. (2007) Activity-dependent regulation of energy metabolism by astrocytes: an update. *Glia,* 55**,** 1251-62.

Pellerin, L. & Magistretti, P. J. (1994) Glutamate uptake into astrocytes stimulates aerobic glycolysis: a mechanism coupling neuronal activity to glucose utilization. *Proc Natl Acad Sci U S A,* 91**,** 10625-9.

Perrin, F. E., Boisset, G., Docquier, M., Schaad, O., Descombes, P. & Kato, A. C. (2005) No widespread induction of cell death genes occurs in pure motoneurons in an amyotrophic lateral sclerosis mouse model. *Hum Mol Genet,* 14**,** 3309-20.

Phatnani, H. P., Guarnieri, P., Friedman, B. A., Carrasco, M. A., Muratet, M., O'keeffe, S., Nwakeze, C., Pauli-Behn, F., Newberry, K. M., Meadows, S. K., Tapia, J. C., Myers, R. M. & Maniatis, T. (2013) Intricate interplay between astrocytes and motor neurons in ALS. *Proc Natl Acad Sci U S A,* 110**,** E756-65.

Philips, T., Bento-Abreu, A., Nonneman, A., Haeck, W., Staats, K., Geelen, V., Hersmus, N., Kusters, B., Van Den Bosch, L., Van Damme, P., Richardson, W. D. & Robberecht, W. (2013) Oligodendrocyte dysfunction in the pathogenesis of amyotrophic lateral sclerosis. *Brain,* 136**,** 471-82.

Philips, T. & Rothstein, J. D. (2014) Glial cells in amyotrophic lateral sclerosis. *Exp Neurol,* 262PB**,** 111-120.

Pines, G., Danbolt, N. C., Bjoras, M., Zhang, Y., Bendahan, A., Eide, L., Koepsell, H., Storm-Mathisen, J., Seeberg, E. & Kanner, B. I. (1992) Cloning and expression of a rat brain L-glutamate transporter. *Nature,* 360**,** 464-7.

Poirier, J., Baccichet, A., Dea, D. & Gauthier, S. (1993) Cholesterol synthesis and lipoprotein reuptake during synaptic remodelling in hippocampus in adult rats. *Neuroscience,* 55**,** 81-90.

Pokrishevsky, E., Grad, L. I., Yousefi, M., Wang, J., Mackenzie, I. R. & Cashman, N. R. (2012) Aberrant localization of FUS and TDP43 is associated with misfolding of SOD1 in amyotrophic lateral sclerosis. *PLoS One,* 7**,** e35050.

Pollari, E., Savchenko, E., Jaronen, M., Kanninen, K., Malm, T., Wojciechowski, S., Ahtoniemi, T., Goldsteins, G., Giniatullina, R., Giniatullin, R., Koistinaho, J. & Magga, J. (2011) Granulocyte colony stimulating factor attenuates inflammation in a mouse model of amyotrophic lateral sclerosis. *J Neuroinflammation,* 8**,** 74.

Pramatarova, A., Laganiere, J., Roussel, J., Brisebois, K. & Rouleau, G. A. (2001) Neuron-specific expression of mutant superoxide dismutase 1 in transgenic mice does not lead to motor impairment. *J Neurosci,* 21**,** 3369-74.

R-Core-Team (2014) R: A Language and Environment for Statistical Computing. R Foundation for Statistical Computing.

Rabin, S. J., Kim, J. M. Â. H., Baughn, M., Libby, R. T., Kim, Y. J., Fan, Y., Libby, R. T., La Spada, A., Stone, B. & Ravits, J. (2010) Sporadic ALS has compartment-specific aberrant exon splicing and altered cellâ€“matrix adhesion biology. *Human Molecular Genetics,* 19**,** 313-328.

Raff, M. C., Fields, K. L., Hakomori, S. I., Mirsky, R., Pruss, R. M. & Winter, J. (1979) Cell-type-specific markers for distinguishing and studying neurons and the major classes of glial cells in culture. *Brain Res,* 174**,** 283-308.

Raman, R., Allen, S. P., Goodall, E. F., Kramer, S., Ponger, L. L., Heath, P. R., Milo, M., Hollinger, H. C., Walsh, T., Highley, J. R., Olpin, S., Mcdermott, C. J., Shaw, P. J. & Kirby, J. (2014) Gene expression signatures in motor neuron disease fibroblasts reveal dysregulation of metabolism, hypoxia-response and RNA processing functions. *Neuropathol Appl Neurobiol*.

Ramesh, T., Lyon, A. N., Pineda, R. H., Wang, C., Janssen, P. M., Canan, B. D., Burghes, A. H. & Beattie, C. E. (2010) A genetic model of amyotrophic lateral sclerosis in zebrafish displays phenotypic hallmarks of motoneuron disease. *Dis Model Mech,* 3**,** 652-62.

Ranganathan, S., Williams, E., Ganchev, P., Gopalakrishnan, V., Lacomis, D., Urbinelli, L., Newhall, K., Cudkowicz, M. E., Brown, R. H., Jr. & Bowser, R. (2005) Proteomic profiling of cerebrospinal fluid identifies biomarkers for amyotrophic lateral sclerosis. *J Neurochem,* 95**,** 1461-71.

Rao, S. D. & Weiss, J. H. (2004) Excitotoxic and oxidative cross-talk between motor neurons and glia in ALS pathogenesis. *Trends Neurosci,* 27**,** 17-23.

Reaume, A. G., Elliott, J. L., Hoffman, E. K., Kowall, N. W., Ferrante, R. J., Siwek, D. F., Wilcox, H. M., Flood, D. G., Beal, M. F., Brown, R. H., Jr., Scott, R. W. & Snider, W. D. (1996) Motor neurons in Cu/Zn superoxide dismutase-deficient mice develop normally but exhibit enhanced cell death after axonal injury. *Nat Genet,* 13**,** 43-7.

Regina, A., Morchoisne, S., Borson, N. D., Mccall, A. L., Drewes, L. R. & Roux, F. (2001) Factor(s) released by glucose-deprived astrocytes enhance glucose transporter expression and activity in rat brain endothelial cells. *Biochim Biophys Acta,* 1540**,** 233-42.

Renton, A. E., Majounie, E., Waite, A., Simon-Sanchez, J., Rollinson, S., Gibbs, J. R., Schymick, J. C., Laaksovirta, H., Van Swieten, J. C., Myllykangas, L., Kalimo, H., Paetau, A., Abramzon, Y., Remes, A. M., Kaganovich, A., Scholz, S. W., Duckworth, J., Ding, J., Harmer, D. W., Hernandez, D. G., Johnson, J. O., Mok, K., Ryten, M., Trabzuni, D., Guerreiro, R. J., Orrell, R. W., Neal, J., Murray, A., Pearson, J., Jansen, I. E., Sondervan, D., Seelaar, H., Blake, D., Young, K., Halliwell, N., Callister, J. B., Toulson, G., Richardson, A., Gerhard, A., Snowden, J., Mann, D., Neary, D., Nalls, M. A., Peuralinna, T., Jansson, L., Isoviita, V. M., Kaivorinne, A. L., Holtta-Vuori, M., Ikonen, E., Sulkava, R., Benatar, M., Wuu, J., Chio, A., Restagno, G., Borghero, G., Sabatelli, M., Heckerman, D., Rogaeva, E., Zinman, L., Rothstein, J. D., Sendtner, M., Drepper, C., Eichler, E. E., Alkan, C., Abdullaev, Z., Pack, S. D., Dutra, A., Pak, E., Hardy, J., Singleton, A., Williams, N. M., Heutink, P., Pickering-Brown, S., Morris, H. R., Tienari, P. J. & Traynor, B. J. (2011) A hexanucleotide repeat expansion in C9ORF72 is the cause of chromosome 9p21-linked ALS-FTD. *Neuron,* 72**,** 257-68.

Robertson, J., Sanelli, T., Xiao, S., Yang, W., Horne, P., Hammond, R., Pioro, E. P. & Strong, M. J. (2007) Lack of TDP-43 abnormalities in mutant SOD1 transgenic mice shows disparity with ALS. *Neurosci Lett,* 420**,** 128-32.

Rodriguez-Arellano, J. J., Parpura, V., Zorec, R. & Verkhratsky, A. (2015) Astrocytes in physiological aging and Alzheimer's disease. *Neuroscience*.

Rodriguez, J. J., Yeh, C. Y., Terzieva, S., Olabarria, M., Kulijewicz-Nawrot, M. & Verkhratsky, A. (2014) Complex and region-specific changes in astroglial markers in the aging brain. *Neurobiol Aging,* 35**,** 15-23.

Rosen, D. R., Siddique, T., Patterson, D., Figlewicz, D. A., Sapp, P., Hentati, A., Donaldson, D., Goto, J., O'regan, J. P., Deng, H. X. & Et Al. (1993) Mutations in Cu/Zn superoxide dismutase gene are associated with familial amyotrophic lateral sclerosis. *Nature,* 362**,** 59-62.

Rothstein, J. D., Dykes-Hoberg, M., Pardo, C. A., Bristol, L. A., Jin, L., Kuncl, R. W., Kanai, Y., Hediger, M. A., Wang, Y., Schielke, J. P. & Welty, D. F. (1996) Knockout of glutamate transporters reveals a major role for astroglial transport in excitotoxicity and clearance of glutamate. *Neuron,* 16**,** 675-86.

Rothstein, J. D., Patel, S., Regan, M. R., Haenggeli, C., Huang, Y. H., Bergles, D. E., Jin, L., Dykes Hoberg, M., Vidensky, S., Chung, D. S., Toan, S. V., Bruijn, L. I., Su, Z. Z., Gupta, P. & Fisher, P. B. (2005) Beta-lactam antibiotics offer neuroprotection by increasing glutamate transporter expression. *Nature,* 433**,** 73-7.

Rutkove, S. B. (2015) Clinical Measures of Disease Progression in Amyotrophic Lateral Sclerosis. *Neurotherapeutics*.

Sacino, A. N., Brooks, M., Mckinney, A. B., Thomas, M. A., Shaw, G., Golde, T. E. & Giasson, B. I. (2014) Brain injection of alpha-synuclein induces multiple proteinopathies, gliosis, and a neuronal injury marker. *J Neurosci,* 34**,** 12368-78.

Samantaray, S., Knaryan, V. H., Shields, D. C. & Banik, N. L. (2013) Critical role of calpain in spinal cord degeneration in Parkinson's disease. *J Neurochem,* 127**,** 880-90.

Sapp, P. C., Hosler, B. A., Mckenna-Yasek, D., Chin, W., Gann, A., Genise, H., Gorenstein, J., Huang, M., Sailer, W., Scheffler, M., Valesky, M., Haines, J. L., Pericak-Vance, M., Siddique, T., Horvitz, H. R. & Brown, R. H., Jr. (2003) Identification of two novel loci for dominantly inherited familial amyotrophic lateral sclerosis. *Am J Hum Genet,* 73**,** 397-403.

Sargsyan, S. A., Blackburn, D. J., Barber, S. C., Grosskreutz, J., De Vos, K. J., Monk, P. N. & Shaw, P. J. (2011) A comparison of in vitro properties of resting SOD1 transgenic microglia reveals evidence of reduced neuroprotective function. *BMC Neurosci,* 12**,** 91.

Sargsyan, S. A., Monk, P. N. & Shaw, P. J. (2005) Microglia as potential contributors to motor neuron injury in amyotrophic lateral sclerosis. *Glia,* 51**,** 241-53.

Sarlette, A., Krampfl, K., Grothe, C., Neuhoff, N., Dengler, R. & Petri, S. (2008) Nuclear erythroid 2-related factor 2-antioxidative response element signaling pathway in motor cortex and spinal cord in amyotrophic lateral sclerosis. *J Neuropathol Exp Neurol,* 67**,** 1055-62.

Sasaki, S., Shibata, N., Komori, T. & Iwata, M. (2000) iNOS and nitrotyrosine immunoreactivity in amyotrophic lateral sclerosis. *Neurosci Lett,* 291**,** 44-8.

Schena, M., Shalon, D., Davis, R. W. & Brown, P. O. (1995) Quantitative monitoring of gene expression patterns with a complementary DNA microarray. *Science,* 270**,** 467-70.

Schousboe, A., Sarup, A., Bak, L. K., Waagepetersen, H. S. & Larsson, O. M. (2004) Role of astrocytic transport processes in glutamatergic and GABAergic neurotransmission. *Neurochemistry International,* 45**,** 521-527.

Schroder, K., Hertzog, P. J., Ravasi, T. & Hume, D. A. (2004) Interferon-gamma: an overview of signals, mechanisms and functions. *J Leukoc Biol,* 75**,** 163-89.

Schubert, D., Soucek, T. & Blouw, B. (2009) The induction of HIF-1 reduces astrocyte activation by amyloid beta peptide. *Eur J Neurosci,* 29**,** 1323-34.

Sephton, C. F., Cenik, C., Kucukural, A., Dammer, E. B., Cenik, B., Han, Y., Dewey, C. M., Roth, F. P., Herz, J., Peng, J., Moore, M. J. & Yu, G. (2011) Identification of neuronal RNA targets of TDP-43-containing ribonucleoprotein complexes. *J Biol Chem,* 286**,** 1204-15.

Serio, A., Bilican, B., Barmada, S. J., Ando, D. M., Zhao, C., Siller, R., Burr, K., Haghi, G., Story, D., Nishimura, A. L., Carrasco, M. A., Phatnani, H. P., Shum, C., Wilmut, I., Maniatis, T., Shaw, C. E., Finkbeiner, S. & Chandran, S. (2013) Astrocyte pathology and the absence of non-cell autonomy in an induced pluripotent stem cell model of TDP-43 proteinopathy. *Proc Natl Acad Sci U S A,* 110**,** 4697-702.

Shaw, P. J., Ince, P. G., Falkous, G. & Mantle, D. (1995) Oxidative damage to protein in sporadic motor neuron disease spinal cord. *Ann Neurol,* 38**,** 691-5.

Shefner, J. M., Reaume, A. G., Flood, D. G., Scott, R. W., Kowall, N. W., Ferrante, R. J., Siwek, D. F., Upton-Rice, M. & Brown, R. H., Jr. (1999) Mice lacking cytosolic copper/zinc superoxide dismutase display a distinctive motor axonopathy. *Neurology,* 53**,** 1239-46.

Shih, A. Y., Johnson, D. A., Wong, G., Kraft, A. D., Jiang, L., Erb, H., Johnson, J. A. & Murphy, T. H. (2003) Coordinate regulation of glutathione biosynthesis and release by Nrf2-expressing glia potently protects neurons from oxidative stress. *J Neurosci,* 23**,** 3394-406.

Shimada, A. & Hasegawa-Ishii, S. (2011) Senescence-accelerated Mice (SAMs) as a Model for Brain Aging and Immunosenescence. *Aging Dis,* 2**,** 414-35.

Shinojima, T., Oya, M., Takayanagi, A., Mizuno, R., Shimizu, N. & Murai, M. (2007) Renal cancer cells lacking hypoxia inducible factor (HIF)-1alpha expression maintain vascular endothelial growth factor expression through HIF-2alpha. *Carcinogenesis,* 28**,** 529-36.

Simpson, I. A., Carruthers, A. & Vannucci, S. J. (2007) Supply and demand in cerebral energy metabolism: the role of nutrient transporters. *J Cereb Blood Flow Metab,* 27**,** 1766-91.

Simpson, J. E., Ince, P. G., Shaw, P. J., Heath, P. R., Raman, R., Garwood, C. J., Gelsthorpe, C., Baxter, L., Forster, G., Matthews, F. E., Brayne, C. & Wharton, S. B. (2011) Microarray analysis of the astrocyte transcriptome in the aging brain: relationship to Alzheimer's pathology and APOE genotype. *Neurobiol Aging,* 32**,** 1795-807.

Simpson, J. E., Wharton, S. B., Cooper, J., Gelsthorpe, C., Baxter, L., Forster, G., Shaw, P. J., Savva, G., Matthews, F. E., Brayne, C. & Ince, P. G. (2010) Alterations of the blood-brain barrier in cerebral white matter lesions in the ageing brain. *Neurosci Lett,* 486**,** 246-51.

Skibinski, G., Parkinson, N. J., Brown, J. M., Chakrabarti, L., Lloyd, S. L., Hummerich, H., Nielsen, J. E., Hodges, J. R., Spillantini, M. G., Thusgaard, T., Brandner, S., Brun, A., Rossor, M. N., Gade, A., Johannsen, P., Sorensen, S. A., Gydesen, S., Fisher, E. M. & Collinge, J. (2005) Mutations in the endosomal ESCRTIII-complex subunit CHMP2B in frontotemporal dementia. *Nat Genet,* 37**,** 806-8.

Sleigh, J. N., Barreiro-Iglesias, A., Oliver, P. L., Biba, A., Becker, T., Davies, K. E., Becker, C. G. & Talbot, K. (2014) Chondrolectin affects cell survival and neuronal outgrowth in in vitro and in vivo models of spinal muscular atrophy. *Hum Mol Genet,* 23**,** 855-69.

Sofroniew, M. V. (2009) Molecular dissection of reactive astrogliosis and glial scar formation. *Trends Neurosci,* 32**,** 638-47.

Spandidos, A., Wang, X., Wang, H., Dragnev, S., Thurber, T. & Seed, B. (2008) A comprehensive collection of experimentally validated primers for Polymerase Chain Reaction quantitation of murine transcript abundance. *BMC Genomics,* 9**,** 633.

Spandidos, A., Wang, X., Wang, H. & Seed, B. (2010) PrimerBank: a resource of human and mouse PCR primer pairs for gene expression detection and quantification. *Nucleic Acids Res,* 38**,** D792-9.

Sreedharan, J., Blair, I. P., Tripathi, V. B., Hu, X., Vance, C., Rogelj, B., Ackerley, S., Durnall, J. C., Williams, K. L., Buratti, E., Baralle, F., De Belleroche, J., Mitchell, J. D., Leigh, P. N., Al-Chalabi, A., Miller, C. C., Nicholson, G. & Shaw, C. E. (2008) TDP-43 mutations in familial and sporadic amyotrophic lateral sclerosis. *Science,* 319**,** 1668-72.

Sta, M., Sylva-Steenland, R. M., Casula, M., De Jong, J. M., Troost, D., Aronica, E. & Baas, F. (2011) Innate and adaptive immunity in amyotrophic lateral sclerosis: evidence of complement activation. *Neurobiol Dis,* 42**,** 211-20.

Stallings, N. R., Puttaparthi, K., Luther, C. M., Burns, D. K. & Elliott, J. L. (2010) Progressive motor weakness in transgenic mice expressing human TDP-43. *Neurobiol Dis,* 40**,** 404-14.

Stein, M., Keshav, S., Harris, N. & Gordon, S. (1992) Interleukin 4 potently enhances murine macrophage mannose receptor activity: a marker of alternative immunologic macrophage activation. *J Exp Med,* 176**,** 287-92.

Stevens, B., Allen, N. J., Vazquez, L. E., Howell, G. R., Christopherson, K. S., Nouri, N., Micheva, K. D., Mehalow, A. K., Huberman, A. D., Stafford, B., Sher, A., Litke, A. M., Lambris, J. D., Smith, S. J., John, S. W. & Barres, B. A. (2007) The classical complement cascade mediates CNS synapse elimination. *Cell,* 131**,** 1164-78.

Stollg, G. & Jander, S. (1999) The role of microglia and macrophages in the pathophysiology of the CNS. *Prog Neurobiol,* 58**,** 233-47.

Storck, T., Schulte, S., Hofmann, K. & Stoffel, W. (1992) Structure, expression, and functional analysis of a Na(+)-dependent glutamate/aspartate transporter from rat brain. *Proc Natl Acad Sci U S A,* 89**,** 10955-9.

Strittmatter, W. J., Saunders, A. M., Schmechel, D., Pericak-Vance, M., Enghild, J., Salvesen, G. S. & Roses, A. D. (1993) Apolipoprotein E: high-avidity binding to beta-amyloid and increased frequency of type 4 allele in late-onset familial Alzheimer disease. *Proc Natl Acad Sci U S A,* 90**,** 1977-81.

Sun, Z., Wu, T., Zhao, F., Lau, A., Birch, C. M. & Zhang, D. D. (2011) KPNA6 (Importin {alpha}7)-mediated nuclear import of Keap1 represses the Nrf2-dependent antioxidant response. *Mol Cell Biol,* 31**,** 1800-11.

Sutterwala, F. S., Noel, G. J., Clynes, R. & Mosser, D. M. (1997) Selective suppression of interleukin-12 induction after macrophage receptor ligation. *J Exp Med,* 185**,** 1977-85.

Sutterwala, F. S., Noel, G. J., Salgame, P. & Mosser, D. M. (1998) Reversal of proinflammatory responses by ligating the macrophage Fcgamma receptor type I. *J Exp Med,* 188**,** 217-22.

Swarup, V., Phaneuf, D., Bareil, C., Robertson, J., Rouleau, G. A., Kriz, J. & Julien, J. P. (2011) Pathological hallmarks of amyotrophic lateral sclerosis/frontotemporal lobar degeneration in transgenic mice produced with TDP-43 genomic fragments. *Brain,* 134**,** 2610-26.

Takahashi, Y., Fukuda, Y., Yoshimura, J., Toyoda, A., Kurppa, K., Moritoyo, H., Belzil, V. V., Dion, P. A., Higasa, K., Doi, K., Ishiura, H., Mitsui, J., Date, H., Ahsan, B., Matsukawa, T., Ichikawa, Y., Moritoyo, T., Ikoma, M., Hashimoto, T., Kimura, F., Murayama, S., Onodera, O., Nishizawa, M., Yoshida, M., Atsuta, N., Sobue, G., Fifita, J. A., Williams, K. L., Blair, I. P., Nicholson, G. A., Gonzalez-Perez, P., Brown, R. H., Jr., Nomoto, M., Elenius, K., Rouleau, G. A., Fujiyama, A., Morishita, S., Goto, J. & Tsuji, S. (2013) ERBB4 mutations that disrupt the neuregulin-ErbB4 pathway cause amyotrophic lateral sclerosis type 19. *Am J Hum Genet,* 93**,** 900-5.

Tateishi, T., Yamasaki, R., Tanaka, M., Matsushita, T., Kikuchi, H., Isobe, N., Ohyagi, Y. & Kira, J. (2010) CSF chemokine alterations related to the clinical course of amyotrophic lateral sclerosis. *J Neuroimmunol,* 222**,** 76-81.

Thomas, T., Thomas, G., Mclendon, C., Sutton, T. & Mullan, M. (1996) beta-Amyloid-mediated vasoactivity and vascular endothelial damage. *Nature,* 380**,** 168-71.

Tohgi, H., Abe, T., Yamazaki, K., Murata, T., Ishizaki, E. & Isobe, C. (1999) Remarkable increase in cerebrospinal fluid 3-nitrotyrosine in patients with sporadic amyotrophic lateral sclerosis. *Ann Neurol,* 46**,** 129-31.

Tong, J., Huang, C., Bi, F., Wu, Q., Huang, B., Liu, X., Li, F., Zhou, H. & Xia, X. G. (2013) Expression of ALS-linked TDP-43 mutant in astrocytes causes non-cell-autonomous motor neuron death in rats. *EMBO J,* 32**,** 1917-26.

Tong, X., Ao, Y., Faas, G. C., Nwaobi, S. E., Xu, J., Haustein, M. D., Anderson, M. A., Mody, I., Olsen, M. L., Sofroniew, M. V. & Khakh, B. S. (2014) Astrocyte Kir4.1 ion channel deficits contribute to neuronal dysfunction in Huntington's disease model mice. *Nat Neurosci,* 17**,** 694-703.

Trabzuni, D., Ryten, M., Walker, R., Smith, C., Imran, S., Ramasamy, A., Weale, M. E. & Hardy, J. (2011) Quality control parameters on a large dataset of regionally dissected human control brains for whole genome expression studies. *J Neurochem,* 119**,** 275-82.

Trias, E., Diaz-Amarilla, P., Olivera-Bravo, S., Isasi, E., Drechsel, D. A., Lopez, N., Bradford, C. S., Ireton, K. E., Beckman, J. S. & Barbeito, L. (2013) Phenotypic transition of microglia into astrocyte-like cells associated with disease onset in a model of inherited ALS. *Front Cell Neurosci,* 7**,** 274.

Trotter, J., Karram, K. & Nishiyama, A. (2010) NG2 cells: Properties, progeny and origin. *Brain Res Rev,* 63**,** 72-82.

Tsuboi, Y. & Yamada, T. (1994) Increased concentration of C4d complement protein in CSF in amyotrophic lateral sclerosis. *J Neurol Neurosurg Psychiatry,* 57**,** 859-61.

Tsuchiya, N., Ochiai, M., Nakashima, K., Ubagai, T., Sugimura, T. & Nakagama, H. (2007) SND1, a component of RNA-induced silencing complex, is up-regulated in human colon cancers and implicated in early stage colon carcinogenesis. *Cancer Res,* 67**,** 9568-76.

Turner, B. J. & Talbot, K. (2008) Transgenics, toxicity and therapeutics in rodent models of mutant SOD1-mediated familial ALS. *Prog Neurobiol,* 85**,** 94-134.

Ugbode, C. I., Hirst, W. D. & Rattray, M. (2014) Neuronal influences are necessary to produce mitochondrial co-localization with glutamate transporters in astrocytes. *J Neurochem,* 130**,** 668-77.

Umeda, K., Ikenouchi, J., Katahira-Tayama, S., Furuse, K., Sasaki, H., Nakayama, M., Matsui, T., Tsukita, S. & Furuse, M. (2006) ZO-1 and ZO-2 independently determine where claudins are polymerized in tight-junction strand formation. *Cell,* 126**,** 741-54.

Vaknin, I., Kunis, G., Miller, O., Butovsky, O., Bukshpan, S., Beers, D. R., Henkel, J. S., Yoles, E., Appel, S. H. & Schwartz, M. (2011) Excess circulating alternatively activated myeloid (M2) cells accelerate ALS progression while inhibiting experimental autoimmune encephalomyelitis. *PLoS One,* 6**,** e26921.

Valentine, J. S. & Hart, P. J. (2003) Misfolded CuZnSOD and amyotrophic lateral sclerosis. *Proc Natl Acad Sci U S A,* 100**,** 3617-22.

Van Beek, J., Elward, K. & Gasque, P. (2003) Activation of complement in the central nervous system: roles in neurodegeneration and neuroprotection. *Ann N Y Acad Sci,* 992**,** 56-71.

Van Damme, P., Bogaert, E., Dewil, M., Hersmus, N., Kiraly, D., Scheveneels, W., Bockx, I., Braeken, D., Verpoorten, N., Verhoeven, K., Timmerman, V., Herijgers, P., Callewaert, G., Carmeliet, P., Van Den Bosch, L. & Robberecht, W. (2007) Astrocytes regulate GluR2 expression in motor neurons and their vulnerability to excitotoxicity. *Proc Natl Acad Sci U S A,* 104**,** 14825-30.

Van Den Bosch, L., Tilkin, P., Lemmens, G. & Robberecht, W. (2002) Minocycline delays disease onset and mortality in a transgenic model of ALS. *Neuroreport,* 13**,** 1067-70.

Van Den Bosch, L., Van Damme, P., Bogaert, E. & Robberecht, W. (2006) The role of excitotoxicity in the pathogenesis of amyotrophic lateral sclerosis. *Biochim Biophys Acta,* 1762**,** 1068-82.

Vance, C., Rogelj, B., Hortobagyi, T., De Vos, K. J., Nishimura, A. L., Sreedharan, J., Hu, X., Smith, B., Ruddy, D., Wright, P., Ganesalingam, J., Williams, K. L., Tripathi, V., Al-Saraj, S., Al-Chalabi, A., Leigh, P. N., Blair, I. P., Nicholson, G., De Belleroche, J., Gallo, J. M., Miller, C. C. & Shaw, C. E. (2009) Mutations in FUS, an RNA processing protein, cause familial amyotrophic lateral sclerosis type 6. *Science,* 323**,** 1208-11.

Vande Velde, C., Miller, T. M., Cashman, N. R. & Cleveland, D. W. (2008) Selective association of misfolded ALS-linked mutant SOD1 with the cytoplasmic face of mitochondria. *Proc Natl Acad Sci U S A,* 105**,** 4022-7.

Vanier, M. T. (2014) Complex lipid trafficking in Niemann-Pick disease type C. *J Inherit Metab Dis*.

Vargas, M. R., Johnson, D. A., Sirkis, D. W., Messing, A. & Johnson, J. A. (2008a) Nrf2 activation in astrocytes protects against neurodegeneration in mouse models of familial amyotrophic lateral sclerosis. *J Neurosci,* 28**,** 13574-81.

Vargas, M. R., Pehar, M., Cassina, P., Martinez-Palma, L., Thompson, J. A., Beckman, J. S. & Barbeito, L. (2005) Fibroblast growth factor-1 induces heme oxygenase-1 via nuclear factor erythroid 2-related factor 2 (Nrf2) in spinal cord astrocytes: consequences for motor neuron survival. *J Biol Chem,* 280**,** 25571-9.

Vargas, M. R., Pehar, M., Diaz-Amarilla, P. J., Beckman, J. S. & Barbeito, L. (2008b) Transcriptional profile of primary astrocytes expressing ALS-linked mutant SOD1. *J Neurosci Res,* 86**,** 3515-25.

Verstraete, E., Biessels, G. J., Van Den Heuvel, M. P., Visser, F., Luijten, P. R. & Van Den Berg, L. H. (2010) No evidence of microbleeds in ALS patients at 7 Tesla MRI. *Amyotroph Lateral Scler,* 11**,** 555-7.

Virgin, H. W. & Levine, B. (2009) Autophagy genes in immunity. *Nat Immunol,* 10**,** 461-70.

Waller, R., Woodroofe, M. N., Francese, S., Heath, P. R., Wharton, S. B., Ince, P. G., Sharrack, B. & Simpson, J. E. (2012) Isolation of enriched glial populations from post-mortem human CNS material by immuno-laser capture microdissection. *J Neurosci Methods,* 208**,** 108-13.

Walsh, M. J., Cooper-Knock, J., Dodd, J. E., Stopford, M. J., Mihaylov, S. R., Kirby, J., Shaw, P. J. & Hautbergue, G. M. (2014) Decoding the pathophysiological mechanisms that underlie RNA dysregulation in neurodegenerative disorders: a review of the current state of the art. *Neuropathol Appl Neurobiol*.

Wang, J., Xu, G., Gonzales, V., Coonfield, M., Fromholt, D., Copeland, N. G., Jenkins, N. A. & Borchelt, D. R. (2002) Fibrillar inclusions and motor neuron degeneration in transgenic mice expressing superoxide dismutase 1 with a disrupted copper-binding site. *Neurobiol Dis,* 10**,** 128-38.

Wang, L., Gutmann, D. H. & Roos, R. P. (2011) Astrocyte loss of mutant SOD1 delays ALS disease onset and progression in G85R transgenic mice. *Hum Mol Genet,* 20**,** 286-93.

Wang, L., Sharma, K., Grisotti, G. & Roos, R. P. (2009) The effect of mutant SOD1 dismutase activity on non-cell autonomous degeneration in familial amyotrophic lateral sclerosis. *Neurobiol Dis,* 35**,** 234-40.

Wang, X. & Seed, B. (2003) A PCR primer bank for quantitative gene expression analysis. *Nucleic Acids Res,* 31**,** e154.

Welser-Alves, J. V., Crocker, S. J. & Milner, R. (2011) A dual role for microglia in promoting tissue inhibitor of metalloproteinase (TIMP) expression in glial cells in response to neuroinflammatory stimuli. *J Neuroinflammation,* 8**,** 61.

Whistler, T., Chiang, C. F., Lonergan, W., Hollier, M. & Unger, E. R. (2010) Implementation of exon arrays: alternative splicing during T-cell proliferation as determined by whole genome analysis. *BMC Genomics,* 11**,** 496.

Wichterle, H., Lieberam, I., Porter, J. A. & Jessell, T. M. (2002) Directed differentiation of embryonic stem cells into motor neurons. *Cell,* 110**,** 385-97.

Wiedemann, F. R., Manfredi, G., Mawrin, C., Beal, M. F. & Schon, E. A. (2002) Mitochondrial DNA and respiratory chain function in spinal cords of ALS patients. *J Neurochem,* 80**,** 616-25.

Wijesekera, L. C., Mathers, S., Talman, P., Galtrey, C., Parkinson, M. H., Ganesalingam, J., Willey, E., Ampong, M. A., Ellis, C. M., Shaw, C. E., Al-Chalabi, A. & Leigh, P. N. (2009) Natural history and clinical features of the flail arm and flail leg ALS variants. *Neurology,* 72**,** 1087-94.

Wilczak, N., De Vos, R. A. & De Keyser, J. (2003) Free insulin-like growth factor (IGF)-I and IGF binding proteins 2, 5, and 6 in spinal motor neurons in amyotrophic lateral sclerosis. *Lancet,* 361**,** 1007-11.

Williams, T. L., Day, N. C., Ince, P. G., Kamboj, R. K. & Shaw, P. J. (1997) Calcium-permeable alpha-amino-3-hydroxy-5-methyl-4-isoxazole propionic acid receptors: a molecular determinant of selective vulnerability in amyotrophic lateral sclerosis. *Ann Neurol,* 42**,** 200-7.

Williamson, T. L. & Cleveland, D. W. (1999) Slowing of axonal transport is a very early event in the toxicity of ALS-linked SOD1 mutants to motor neurons. *Nat Neurosci,* 2**,** 50-6.

Wilson, C., Pepper, S. D. & Miller, C. J. QC and Affymetrix Data. Patterson Institute for Cancer Research. Electronic documentation from *simpleaffy* v. 2.0.13 http://bioconductor.wustl.edu/bioc/vignettes/simpleaffy/inst/doc/QCandSimpleaffy.pdf.

Winkler, E. A., Sengillo, J. D., Sullivan, J. S., Henkel, J. S., Appel, S. H. & Zlokovic, B. V. (2013) Blood-spinal cord barrier breakdown and pericyte reductions in amyotrophic lateral sclerosis. *Acta Neuropathol,* 125**,** 111-20.

Wong, P. C., Pardo, C. A., Borchelt, D. R., Lee, M. K., Copeland, N. G., Jenkins, N. A., Sisodia, S. S., Cleveland, D. W. & Price, D. L. (1995) An adverse property of a familial ALS-linked SOD1 mutation causes motor neuron disease characterized by vacuolar degeneration of mitochondria. *Neuron,* 14**,** 1105-16.

Woodruff, T. M., Costantini, K. J., Crane, J. W., Atkin, J. D., Monk, P. N., Taylor, S. M. & Noakes, P. G. (2008) The complement factor C5a contributes to pathology in a rat model of amyotrophic lateral sclerosis. *J Immunol,* 181**,** 8727-34.

Wootz, H., Weber, E., Korhonen, L. & Lindholm, D. (2006) Altered distribution and levels of cathepsinD and cystatins in amyotrophic lateral sclerosis transgenic mice: possible roles in motor neuron survival. *Neuroscience,* 143**,** 419-30.

Wu, C. H., Fallini, C., Ticozzi, N., Keagle, P. J., Sapp, P. C., Piotrowska, K., Lowe, P., Koppers, M., Mckenna-Yasek, D., Baron, D. M., Kost, J. E., Gonzalez-Perez, P., Fox, A. D., Adams, J., Taroni, F., Tiloca, C., Leclerc, A. L., Chafe, S. C., Mangroo, D., Moore, M. J., Zitzewitz, J. A., Xu, Z. S., Van Den Berg, L. H., Glass, J. D., Siciliano, G., Cirulli, E. T., Goldstein, D. B., Salachas, F., Meininger, V., Rossoll, W., Ratti, A., Gellera, C., Bosco, D. A., Bassell, G. J., Silani, V., Drory, V. E., Brown, R. H., Jr. & Landers, J. E. (2012a) Mutations in the profilin 1 gene cause familial amyotrophic lateral sclerosis. *Nature,* 488**,** 499-503.

Wu, L. S., Cheng, W. C., Hou, S. C., Yan, Y. T., Jiang, S. T. & Shen, C. K. (2010) TDP-43, a neuro-pathosignature factor, is essential for early mouse embryogenesis. *Genesis,* 48**,** 56-62.

Wu, L. S., Cheng, W. C. & Shen, C. K. (2012b) Targeted depletion of TDP-43 expression in the spinal cord motor neurons leads to the development of amyotrophic lateral sclerosis-like phenotypes in mice. *J Biol Chem,* 287**,** 27335-44.

Wyss-Coray, T., Loike, J. D., Brionne, T. C., Lu, E., Anankov, R., Yan, F., Silverstein, S. C. & Husemann, J. (2003) Adult mouse astrocytes degrade amyloid-beta in vitro and in situ. *Nat Med,* 9**,** 453-7.

Xavier, A. L., Menezes, J. R., Goldman, S. A. & Nedergaard, M. (2014) Fine-tuning the central nervous system: microglial modelling of cells and synapses. *Philos Trans R Soc Lond B Biol Sci,* 369**,** 20130593.

Yamanaka, K., Boillee, S., Roberts, E. A., Garcia, M. L., Mcalonis-Downes, M., Mikse, O. R., Cleveland, D. W. & Goldstein, L. S. (2008a) Mutant SOD1 in cell types other

than motor neurons and oligodendrocytes accelerates onset of disease in ALS mice. *Proc Natl Acad Sci U S A,* 105**,** 7594-9.

Yamanaka, K., Chun, S. J., Boillee, S., Fujimori-Tonou, N., Yamashita, H., Gutmann, D. H., Takahashi, R., Misawa, H. & Cleveland, D. W. (2008b) Astrocytes as determinants of disease progression in inherited amyotrophic lateral sclerosis. *Nat Neurosci,* 11**,** 251-3.

Yang, Y., Hentati, A., Deng, H. X., Dabbagh, O., Sasaki, T., Hirano, M., Hung, W. Y., Ouahchi, K., Yan, J., Azim, A. C., Cole, N., Gascon, G., Yagmour, A., Ben-Hamida, M., Pericak-Vance, M., Hentati, F. & Siddique, T. (2001) The gene encoding alsin, a protein with three guanine-nucleotide exchange factor domains, is mutated in a form of recessive amyotrophic lateral sclerosis. *Nat Genet,* 29**,** 160-5.

Yao, B., La, L. B., Chen, Y. C., Chang, L. J. & Chan, E. K. (2012) Defining a new role of GW182 in maintaining miRNA stability. *EMBO Rep,* 13**,** 1102-8.

Yoo, J., Nichols, A., Mammen, J., Calvo, I., Song, J. C., Worrell, R. T., Matlin, K. & Matthews, J. B. (2003) Bryostatin-1 enhances barrier function in T84 epithelia through PKC-dependent regulation of tight junction proteins. *Am J Physiol Cell Physiol,* 285**,** C300-9.

Yoon, C. H., Rho, S. B., Kim, S. T., Kho, S., Park, J., Jang, I. S., Woo, S., Kim, S. S., Lee, J. H. & Lee, S. H. (2012) Crucial role of TSC-22 in preventing the proteasomal degradation of p53 in cervical cancer. *PLoS One,* 7**,** e42006.

Zhang, J. M., Wang, H. K., Ye, C. Q., Ge, W., Chen, Y., Jiang, Z. L., Wu, C. P., Poo, M. M. & Duan, S. (2003) ATP released by astrocytes mediates glutamatergic activity-dependent heterosynaptic suppression. *Neuron,* 40**,** 971-82.

Zhang, X., Zara, J., Siu, R. K., Ting, K. & Soo, C. (2010) The role of NELL-1, a growth factor associated with craniosynostosis, in promoting bone regeneration. *J Dent Res,* 89**,** 865-78.

Zhang, Y. & Barres, B. A. (2010) Astrocyte heterogeneity: an underappreciated topic in neurobiology. *Curr Opin Neurobiol,* 20**,** 588-94.

Zhang, Y., Chen, K., Sloan, S. A., Bennett, M. L., Scholze, A. R., O'keeffe, S., Phatnani, H. P., Guarnieri, P., Caneda, C., Ruderisch, N., Deng, S., Liddelow, S. A., Zhang, C., Daneman, R., Maniatis, T., Barres, B. A. & Wu, J. Q. (2014) An RNA-Sequencing Transcriptome and Splicing Database of Glia, Neurons, and Vascular Cells of the Cerebral Cortex. *The Journal of Neuroscience,* 34**,** 11929-11947.

Zhao, W., Beers, D. R., Henkel, J. S., Zhang, W., Urushitani, M., Julien, J. P. & Appel, S. H. (2010) Extracellular mutant SOD1 induces microglial-mediated motoneuron injury. *Glia,* 58**,** 231-43.

Zhao, W., Beers, D. R., Liao, B., Henkel, J. S. & Appel, S. H. (2012) Regulatory T lymphocytes from ALS mice suppress microglia and effector T lymphocytes through different cytokine-mediated mechanisms. *Neurobiol Dis,* 48**,** 418-28.

Zhao, W., Xie, W., Xiao, Q., Beers, D. R. & Appel, S. H. (2006) Protective effects of an anti-inflammatory cytokine, interleukin-4, on motoneuron toxicity induced by activated microglia. *J Neurochem,* 99**,** 1176-87.

Zhong, N. & Weisgraber, K. H. (2009) Understanding the basis for the association of apoE4 with Alzheimer's disease: opening the door for therapeutic approaches. *Curr Alzheimer Res,* 6**,** 415-8.

Zhong, Z., Deane, R., Ali, Z., Parisi, M., Shapovalov, Y., O'banion, M. K., Stojanovic, K., Sagare, A., Boillee, S., Cleveland, D. W. & Zlokovic, B. V. (2008) ALS-causing SOD1 mutants generate vascular changes prior to motor neuron degeneration. *Nat Neurosci,* 11**,** 420-2.

Zhong, Z., Ilieva, H., Hallagan, L., Bell, R., Singh, I., Paquette, N., Thiyagarajan, M., Deane, R., Fernandez, J. A., Lane, S., Zlokovic, A. B., Liu, T., Griffin, J. H., Chow, N., Castellino, F. J., Stojanovic, K., Cleveland, D. W. & Zlokovic, B. V. (2009) Activated protein C therapy slows ALS-like disease in mice by transcriptionally inhibiting SOD1 in motor neurons and microglia cells. *J Clin Invest,* 119**,** 3437-49.

9 Outputs

***Oral Presentations**:*

- The 23rd annual symposium of the Motor Neuron Disease Association (Chicago, 2012).
- The 12th annual meeting of the European Network for the Cure of Amyotrophic Lateral Sclerosis (ENCALS) (Leuven, Belgium 2014).
- The University of Sheffield Medical School Research Day 2014.

***Poster presentation**:*

- The 11th annual ENCALS meeting (Sheffield, U.K. 2013).

Publications

- *Manuscript submitted.* Baker et al. (2015) Lysosomal and phagocytic activity is increased in astrocytes during the progression of amyotrophic lateral sclerosis.
- *Manuscript in preparation.* Baker et al. (2015) Astrocytes from SOD1 and sporadic ALS patients influence the properties of co-cultured endothelia.